Inaugural dissertation

for

obtaining the doctoral degree

of the

Combined Faculty of Mathematics, Engineering and Natural Sciences

of the

Ruprecht - Karls – University

Heidelberg

Presented by

Siu Wang, Ng M.Sc.

born in Jinjiang, China

Oral examination: 14th October 2025

Identification of Modulators in Melanoma-T Cell Interaction

Referees:

Prof. Dr. Michael Boutros

Prof. Dr. Aurelio Teleman

1. Table of Contents

2. Declaration

I hereby declare that I have written the submitted dissertation “Identification of Modulators in Melanoma-T Cell Interaction” myself and in this process have not used any other sources than those indicated.

I hereby declare that I have not applied to be examined at any other institution, nor have I used the dissertation in this or any other form at any other institution as an examination paper, nor submitted it to any other faculty as a dissertation.

Ng, Siu Wang

3. Abstract

Despite advances in immunotherapy, melanoma remains challenging to treat, particularly in advanced stages where resistance to immune-based therapies frequently develops. Adoptive cell therapy, including chimeric antigen receptor (CAR) T cells, holds promise but has shown limited efficacy in melanoma.

In this dissertation, a genome-wide CRISPR/Cas9 screen composed of melanoma cells and CAR-T cells was established to systematically uncover genes that regulate melanoma cell susceptibility to T cell-mediated killing. Using this screening platform, I identified genetic determinants beyond classical immune evasion mechanisms like major histocompatibility complex downregulation or impaired interferon-γ signaling. The co-culture screen demonstrated high reproducibility and robustness, evidenced by consistent changes in sgRNA abundance and the recovery of known tumor-promoting and suppressive targets. I have identified key candidate genes, particularly those involved in oxidative phosphorylation, amino acid transport, NF-κB and mTOR signaling, and the mediator complex, highlighting alternative resistance mechanisms to T cell cytotoxicity. To refine target selection, I have conducted an additional A375 fitness screen to identify essential genes independent of T cell-mediated killing. This allowed for the exclusion of general fitness genes and the prioritization of candidates specifically relevant to immune evasion. I have discovered that CD98 (SLC3A2/SLC7A5) modulates melanoma resistance to T cell-secreted TRAIL, acting via suppression of apoptotic signaling rather than altering T cell activity or TRAIL receptor expression. Additionally, I have performed a meta-analysis across seven screening projects to confirm the technical and functional reliability of the Heidelberg CRISPR sgRNA library. Despite varying experimental contexts, the library maintained consistent sequencing quality and gene essentiality profiles, with most variability stemming from known technical or biological factors.

Altogether, this study provides new insight into tumor–immune interactions, uncovers potential therapeutic targets for overcoming TRAIL resistance in melanoma, and reinforces the HD sgRNA library as a robust tool for functional genomics.

4. Zusammenfassung

Trotz bedeutender Fortschritte in der Immuntherapie bleibt das Melanom insbesondere in fortgeschrittenen Stadien schwer behandelbar, da häufig Resistenzen gegenüber immunbasierten Therapien entstehen. Die adoptive Zelltherapie, einschließlich der Anwendung von chimären Antigenrezeptor (CAR)-T-Zellen, gilt als vielversprechender Ansatz, zeigt jedoch bislang nur eine begrenzte Wirksamkeit beim Melanom.

Im Rahmen dieser Dissertation wurde ein genomweiter CRISPR/Cas9-Screen etabliert, der Melanomzellen und CAR-T-Zellen kombiniert, um systematisch Gene zu identifizieren, die die Anfälligkeit von Melanomzellen gegenüber T-Zell-vermittelter Zytotoxizität regulieren. Mithilfe dieser Screening-Plattform konnten genetische Determinanten jenseits klassischer Immun-Evasionsmechanismen wie der Herunterregulierung des Haupthistokompatibilitätskomplexes oder gestörter Interferon-γ-Signalübertragung identifiziert werden. Der Ko-Kultur-Screen erwies sich als hochreproduzierbar und robust, was sich in konsistenten Veränderungen der sgRNA-Häufigkeiten sowie in der Identifikation bekannter tumorfördernder und tumorsuppressiver Zielgene widerspiegelt. Es konnten zentrale Kandidatengene identifiziert werden, insbesondere solche, die an der oxidativen Phosphorylierung, dem Aminosäuretransport, der NF-κB- und mTOR-Signalübertragung sowie dem Mediator-Komplex beteiligt sind. Diese Ergebnisse deuten auf alternative Resistenzmechanismen gegenüber der T-Zell-Zytotoxizität hin. Zur gezielteren Auswahl relevanter Gene wurde ein zusätzlicher Fitness-Screen mit der Melanomzelllinie A375 durchgeführt, um Gene zu identifizieren, die unabhängig von T-Zell-vermittelter Zytotoxizität essenziell sind. Dadurch konnten allgemeine Fitness-Gene ausgeschlossen und Kandidaten mit spezifischer Relevanz für Immun-Evasionsmechanismen priorisiert werden. Eine zentrale Entdeckung war die Rolle von CD98 (SLC3A2/SLC7A5) bei der Vermittlung von Resistenz gegenüber T-Zell-sezerniertem TRAIL. Der Mechanismus beruht auf der Unterdrückung apoptotischer Signalwege und nicht auf Veränderungen der T-Zell-Aktivität oder der Expression von TRAIL-Rezeptoren. Zusätzlich wurde eine Meta-Analyse über sieben unabhängige Screening-Projekte hinweg durchgeführt, um die technische und funktionelle Zuverlässigkeit der Heidelberger CRISPR-sgRNA-library zu evaluieren. Trotz unterschiedlicher experimenteller Kontexte zeigte die Bibliothek durchgehend eine hohe Sequenzierungsqualität und konsistente Gen-Essenzialitätsprofile. Die beobachteten Variabilitäten waren überwiegend auf bekannte technische oder biologische Faktoren zurückzuführen.

Insgesamt liefert diese Arbeit neue Einblicke in die komplexen Interaktionen zwischen Tumorzellen und dem Immunsystem, identifiziert potenzielle therapeutische Zielstrukturen zur Überwindung der TRAIL-Resistenz beim Melanom und bestätigt die HD-sgRNA-library als zuverlässiges Werkzeug für funktionelle Genomanalysen.

5. Introduction

Melanoma is one of the most aggressive and lethal skin malignancies, urging current research to understand treatment resistance and improve therapeutic strategies. While significant progress has been made in immunotherapy, notably with the success of ipilimumab and nivolumab combination therapy, many patients remain unresponsive or develop acquired resistance. Additionally, cellular immunotherapy has shown limited success in treating solid tumors like melanoma, underscoring the need for a deeper understanding of the factors affecting immunotherapy efficacy. To overcome these challenges, this project was initiated to establish a genome-wide CRISPR-mediated melanoma-CAR-T cell co-culture screening platform to identify gene targets involved in T cell-tumor cell interactions but are independent of the major histocompatibility complex (MHC)-antigen presentation machinery or interferon-γ (IFNγ) signaling. By uncovering alternative pathways that influence CAR-T cell efficacy, this study has the potential to contribute to the development of novel therapeutic strategies that enhance ACT effectiveness in solid tumors.

5.1. Cancer immunology

The immune system serves as a pivotal role in cancer prevention by a process known as immune surveillance, in which abnormal or mutated cells are identified and destroyed before they can proliferate uncontrollably. However, tumors can develop sophisticated strategies to evade immune detection, leading to cancer progression. The immune system is divided into innate and adaptive immunity, both of which play crucial roles in recognizing and eliminating tumor cells.

The innate immune system creates the frontline of defense against cancer formation, using non-specific mechanisms to detect and eliminate abnormal cells. Natural killer cells, for instance, directly kill tumor cells without prior sensitization. They recognize and target cells that lack MHC class I molecules, a common feature of transformed cells.

Macrophages and tumor-associated neutrophils can promote or suppress tumor growth according to their subtype polarization (Nagaraj et al., 2010; Overmeire et al., 2014). Dendritic cells represent a unique role in processing tumor-associated antigens and presenting them to T cells.

In contrast to the innate immune system, the adaptive immune system provides long-term, specific immunity against tumors through antigen recognition by T cells and B cells. $CD8^+$ Cytotoxic T cells recognize tumor antigens presented on MHC class I molecules and induce apoptosis in cancer cells by various tactics such as perforin and granzymes, alongside $CD4^+$ Helper T cells that secrete cytokines to activate other immune cells depending on their $T_h1/T_h2/$ regulatory subtypes. B lymphocytes, on the other side, produce antibodies that can recognize and bind tumor antigens, facilitating immune-mediated destruction via complement activation or antibody-dependent cellular cytotoxicity (Alberts et al., 2007). Understanding the components of the immune system involved in cancer immunity is essential for developing effective immunotherapies.

5.2. Recent development of Immunotherapies

Immunotherapy, also known as biological therapy, is defined as the treatment of disease by activating or suppressing the immune system, with a particular emphasis on cancer treatment. In recent years, significant advancements in immunotherapy, driven by a deeper understanding of cancer immunology and technological innovations have been witnessed. These rapidly emerging transformative approaches have overcome challenges present in traditional radiotherapy and chemotherapy in terms of efficacy for certain advanced or inoperable diseases. In advanced non-small cell lung cancer administration of pembrolizumab (anti-PD-1) monotherapy achieved 5-year overall survival (OS) rate of 31.9% as compared to 16.3% with chemotherapy (Reck et al., 2016). Other studies have also revealed that the combination treatment of Nivolumab (anti-PD-1) and Ipilimumab (anti-CTLA-4) achieved as high as 52% five-year survival

rates for malignant melanoma patient (Larkin et al., 2019) as compared to a median survival of less than one year with chemotherapy (Serrone et al., 2000).

The immune system naturally detects and destroys abnormal cells, a process often compromised in neoplastic tissue due to a wide variety of resistance strategies. Immunotherapy augments this capacity of the immune system through various approaches, such as immune checkpoint blockers (ICBs) including the above three antibodies, which block cell surface molecules like PD-1 and CTLA-4 on T cells to unleash their cytotoxicity against cancer cells, or chimeric antigen receptor (CAR) T-cell therapy, where T cells are genetically engineered to target specific cell surface tumor antigens. Cancer vaccines and oncolytic viruses, represent another facet, designed to stimulate immune recognition of tumor-specific antigens particularly with personalized neoantigen vaccines. A spectrum of available cancer immunotherapy methods, ranging from biologics administration to autologous transfer of T cells, has been summarized in Table 1 below.

The various techniques presented in Table 1 indicate that immunotherapy is in general a more targeted approach than traditional chemotherapy or radiotherapy. Immunotherapy aims at enhancing the effector function of immune cells that recognize antigens specific to cancer cells. The purpose of immunotherapeutic agents, including monoclonal antibodies, cancer vaccines and various autologous cell transfer (ACT) approaches, aims to condition and provoke the immune system for searching and elimination of cancer cells displaying unique and highly enriched surface markers.

Tisagenlecleucel and axicabtagene ciloleucel, being two of the successful examples of FDA approved immunotherapy for the treatment of acute lymphoblastic leukemia and diffuse large B-cell lymphoma respectively (Braendstrup et al., 2020), target the exceptionally high level of surface CD19 protein on malignant B cell population. The two types of engineered T cell products can thus induce an immune response towards malignant B cells exclusively. This treatment can therefore limit the risk of damaging stromal tissue or other healthy organs, which is an adverse effect often observed in patients who receive radiotherapy or chemotherapy.

Table 1. Working principle of available immunotherapies.

Antigen specificity	Method	Composition	Mechanism of action
Non-specific	Cytokine	Recombinant protein including interleukin-2/-10/-12; interferons, Granulocyte-macrophage colony-stimulating factor (GM-CSF) and granulocyte colony-stimulating factor (G-CSF) (Berraondo et al., 2019; Duggan et al., 2016; Mumm et al., 2011; Payne et al., 2014; Voest et al., 1995).	Stimulate proliferation of endogenous T cells or white blood cells that target tumor cells.
	Immune checkpoint blockers	monoclonal antibodies targeting molecules that primarily suppress T cell function, including Pembrolizumab for PD-L1, Nivolumab for PD-1 and Ipilimumab for CTLA-4 in treating gastric cancer, Lung cancer and melanoma (Bristol-Myers Squibb, 2021, 2024; Incyte Corporation, 2022).	Reducing the inhibition of endogenous T cell effector function.
	Oncolytic virus	Native or genetically modified virus capable of selectively infecting cancer cells. Seneca Valley Virus (SVV-001) in a recent trial has shown antitumor activity in small cell lung cancer (Rudin et al., 2011).	Direct destruction of cancer cell by oncolysis and inducing immunogenic cell death through the release of potential release of new tumor antigens.
Specific	Cancer treatment vaccines	Vaccine in various form to introduce the tumor-associated antigens that are enriched in tumor cells but not in stromal cells. Recent trial showed WT1 recombinant protein vaccination achieve remission in elderly AML patients (Kreutmair et al., 2022).	Allowing endogenous immune cells to recognize specific tumor cells.
	Monoclonal antibodies	Purified antibodies against specific cancer markers, such as Rituximab that targets CD20 in B-cell lymphomas and leukemias (Alduaij et al., 2011; Ginaldi et al., 1998).	Marking cancer cells for recognition and destruction by the immune system.
	Tumor infiltrating lymphocyte (TIL)	Purified and expanded T cells population from patient's tumor, with specificity on tumor antigen. This approach has been used in treating metastatic melanoma for 2 decades (Rosenberg et al., 2011a).	Transfer of T cells that recognize antigen specific cancer cells on certain MHC molecules.
	T cell receptor (TCR)-T cells	Over-expression of TCR on endogenous T cells that target selected cancer antigen. Afamitresgene autoleucel that targets MAGE-A4 was recently approved for the treatment of synovial sarcoma (D'Angelo et al., 2024).	Transfer of T cells that recognize antigen specific cancer cells on certain MHC molecules.
	Chimeric antigen receptor-T cells	Over-expression of CAR on endogenous T cells that target selected cancer antigen. CD19-targeted CAR T cells has been approved for various hematological cancer (Kochenderfer et al., 2012; Porter et al., 2011; M. Wang et al., 2020).	Transfer of engineered T cells that recognize cancer cells with specific surface protein, independent of MHC molecules.

Chemotherapy involves the systemic administration of cytotoxic drugs that largely target rapidly dividing cells, which includes not only cancer cells but also bone marrow, gastrointestinal epithelium, and hair follicles for instance. While radiotherapy exerts its therapeutic effect by delivering ionizing radiation to induce DNA damage and cell death, the radiation kills tumors cells alongside the surrounding normal tissues in an unavoidable manner. Damage to the healthy tissue, regardless of being localized or systemic, causes patients to experience a significantly compromised immune system, brain injury, heart disease, lung injury, and liver injury and more (Z. Zhang et al., 2022). The adverse effect can be both acute and chronic, marking it a painful process during and after the treatment for the patients. Even with comparable response rates for certain cancer types, radiotherapy or chemotherapy inevitably jeopardize the patient's quality of life. Further advancement in immunotherapy is needed not only for longer survival from cancerous diseases, but also for optimizing the quality of life during and after treatment.

5.3. Challenge of immunotherapy in solid tumor

Despite the clinical success of immunotherapy, the overall response rates vary significantly depending on the tumor microenvironment (TME), genetic mutations, and other intrinsic factors of malignancy. Solid tumors, encompassing cancers like melanoma, colorectal, lung, and breast cancer, present unique challenges for immunotherapy due to their complex TME. The TME is often immunosuppressive, characterized by hypoxia, nutrient starvation, and the presence of cells like regulatory T cells and myeloid-derived suppressor cells, which inhibit immune effector functions. This environment, along with inefficient trafficking and antigen heterogeneity, limits the effectiveness of immunotherapies compared to hematological malignancies (Abizanda-Campo et al., 2023).

The discrepancy in efficacy against leukemia and solid tumors becomes even more notable in the case of autologous cell transfer approaches that require the usage of TCR-

or CAR-T cells for treatment. CAR-T cell therapy has revolutionized treatment for several hematological malignancies. CD19 CAR-T cell therapy, especially for acute lymphoblastic leukemia, has high success rates, with over 80% of children achieving long-term remission (Ceolin et al., 2023), with 88% complete remission rate for follicular lymphoma treatment (Hirayama et al., 2019), and with 76% of diffuse large B-cell lymphoma or primary mediastinal B-cell lymphoma patients in complete remission (Cappell et al., 2020). While hematologic cancers have shown substantial sensitivity to CAR-T cell therapy, the similar approaches on solid tumors have yet to yield meaningful outcome. Clinical studies on TIL have reported objective response rates ranging from 30% to 50% only, with respective 3- and 5-year survival rates being 36% and 29% (Besser et al., 2010; Rosenberg et al., 2011b). A meta-analysis revealing that in some early trials, only 9.5% achieved partial remission and the overall remission rate is as low as 9% (Hou et al., 2019).

The evidence suggests that cell-based immunotherapy such as CAR-T cell therapy is effective for leukemias and lymphomas but not in solid tumors, whereas checkpoint inhibitors show promise for solid tumors such as melanoma, highlighting the need for a deeper understanding of tumor-immune interactions to account for the huge divergence in the outcome of treatment. Acquiring such information would be crucial to innovation of more targeted treatments on solid tumors, and diversification of the choice of therapeutic option for terminally ill patients.

5.4. Immunotherapy for melanoma

Melanoma is an aggressive form of skin cancer originating from melanocytes which are responsible for pigment production. It constitutes a smaller fraction of skin cancer cases and accounts for the majority of skin cancer-related deaths due to its propensity for rapid progression and metastasis. In the United States, the prevalent of melanoma increased from 99 in year 1990 to 138 in year 2019 per 100,000 individuals , with a mortality rate of 2.2 per 100,000 individuals remain unchanged (Aggarwal et al., 2021).

Survival rates for melanoma vary significantly based on the stage at diagnosis. Localized melanoma, confined to the primary site, boasts a 5-year relative survival rate exceeding 99%. However, once the neoplastic tissue starts to thicken and invade regional skin area, this rate drops to 70%. Further spreading of cancer cells to lymphatic system reduces the survival to approximately 40%. Eventually with distant metastasis throughout the body, the survival further declines to as low as 9.8% (Svedman et al., 2016).

Despite the recent success of Ipilimumab and nivolumab combination treatment in advance melanoma, almost half of all patients were either unresponsive to the treatment or have acquired resistance to the treatment. More unconventional therapeutic options need to be established to achieve in-depth eradication of malignant cells, particularly in cases of distal and unresectable metastasis of which the patients usually experience prognosis among all cancer types. The current limited treatment option further restricted the prognostic outcome and quality of life for this group of patients.

To address this issue, scientists could exploit the tumor mutational burden (TMB) of melanoma, which is one of the highest among all cancers. TMB quantifies the number of somatic mutations within a tumor's genome. The median TMB of melanoma reaches approximately 20 mutations/Mb as compared to median TMB of 3.6 mutations/Mb for all disease type surveyed from 100,000 human cancer genomes (Chalmers et al., 2017). Higher TMB often leads to the appearance of neo-antigens, which are novel peptides presented on tumor cells that the immune system can recognize. This increased neoantigen load can enhance the immunogenicity of the tumor, making it more susceptible to immune-mediated attacks (Chalmers et al., 2017). Another study reveals that TMB positively correlates with the effectiveness of pembrolizumab monotherapy on incurable solid tumor (Marabelle et al., 2020). This correlation is likely due to the expanded endogenous T cells ability to recognize a broader array of neo-antigens, thereby mounting a more robust anti-tumor response. This opens room for further development of immune-related treatment strategies that harness the high TMB status in melanoma cells to create more specific techniques with superior efficacy.

However, the relationship between TMB and ACT efficacy is complex. While a high TMB status can enhance tumor immunogenicity, it does not uniformly predict positive responses to all immunotherapies, especially in the field of ACT treatment on solid tumors. Factors such as the tumor microenvironment and the patient's immune status also critically influence therapeutic outcomes, suggesting a current knowledge gap prior to the establishment of a more effective and precise cell-based immunotherapy on solid tumor. Further investigations are needed to explain the discrepancy on the effectiveness after treatment between ACT and ICB, when the therapeutic outcome of both are ultimately driven T cells as effectors.

Melanoma serves as an appealing Target for rigorous examination concerning the relationship of ACT and solid tumor. Melanoma, being the most invasive skin disease, presents a constant demand for better treatment options. The high TMB status renders it a favorable target for the development of new ACT therapies, but factors that suppress their effectiveness should be closely examined. In this study the interaction between melanoma cells and T cells was utilized as the chassis for investigation. All the current ACT approaches are centered on T cells due to their primitive role in the immune system. T cells, being the final executioner in the adaptive immune response, perform clearance of cells that were infected by foreign particles such as viruses, and abnormal cells that present neo-antigens. Therefore, a close examination to discover new factors that enhance or reduce the cytotoxicity of T cells against melanoma cells was conducted.

5.5. Pooled genome-wide CRISPR/cas9-KO screens

CRISPR-Cas9 genome editing technology has revolutionized the way of studying functional genomics, enabling systematic and high-throughput interrogation of gene functions at an unprecedented scale. Among the various CRISPR-based approaches, genome-wide CRISPR-mediated pooled screens have emerged as a powerful tool for dissecting gene regulatory networks, identifying novel therapeutic targets, and delineating the molecular mechanisms for biological processes and diseases.

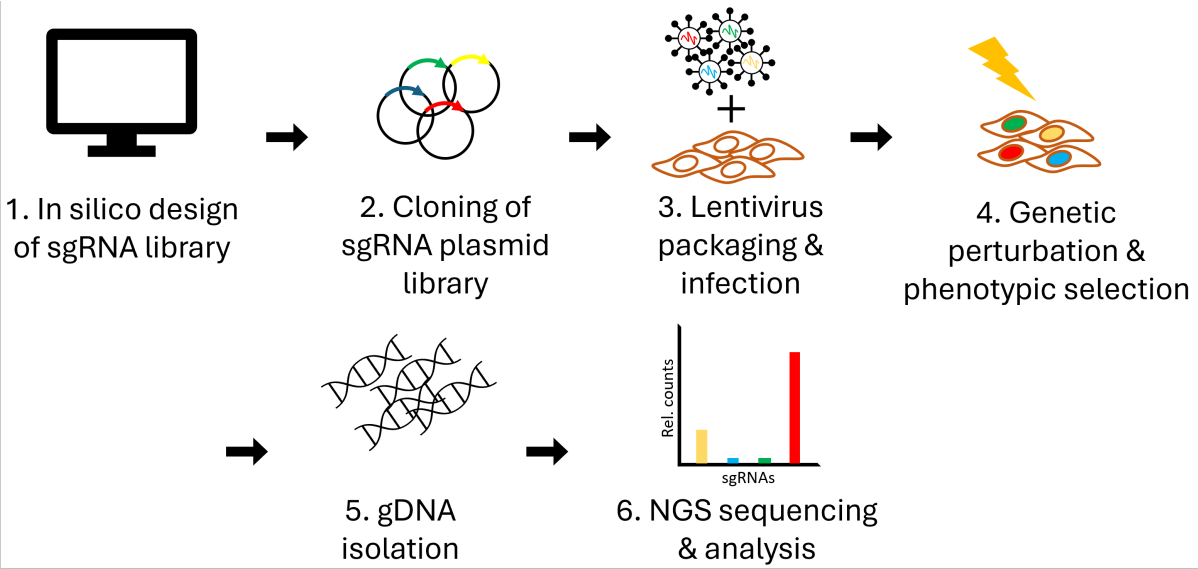

Figure 1. Schematic workflow of CRISPR-mediated pooled screen.

The screen starts with designing a suitable sgRNA according to the need of the study. The sgRNA library is cloned into plasmid vector for later packaging into lentivirus or retrovirus. The virus of sgRNA library is delivered to cells at low MOI. Transduced cells are then allowed time for gene edition. After treatment intervention and expansion, the gDNA will be harvested from the pool of cells. The gDNA will be processed with a series of steps to prepare for deep sequencing. The raw sequencing result is analyzed using MAGeCK package, and R scripts to compare the abundance of sgRNAs under different conditions.

Genome-wide CRISPR-mediated pooled screens rely on CRISPR-Cas9 technology to introduce targeted gene perturbations across the entire genome in a single experiment. These screens utilize large-scale single-guide RNA (sgRNA) libraries designed to target all genes in question at investigator's disposal, allowing for a comprehensive functional analysis. The pooled screening strategy involves transducing a population of cells with the sgRNA library at a low multiplicity of infection (MOI), ensuring that each cell receives only a single genetic perturbation. After a defined selection period based on a specific phenotype (e.g., drug resistance, proliferation, or differentiation), next-generation sequencing (NGS) is employed to quantify sgRNA representation, linking genetic perturbations to observed cellular responses (Figure 1). Knockout screens (CRISPR-KO), as the most adopted approach, use Cas9 to introduce

loss-of-function mutations. Fitness reflects how the absence of a gene at a given circumstance impacts cell viability or proliferation. On the contrary, activation screens (CRISPRa) use transcriptional activators to overexpress genes. Fitness indicates how increased gene expression affects cell behavior.

CRISPR-mediated pooled screens have been widely utilized across various biological domains, including identifying tumor suppressor genes, oncogenes, and drug resistance mechanisms in cancer research, discovering novel immune regulators and mechanisms of immune evasion in immunology, unraveling genetic contributors to neurodegenerative diseases and synaptic function in neuroscience, identifying host factors required for viral or bacterial infections in infectious Diseases, and last but not least, mapping genetic dependencies to facilitate the development of targeted therapies in drug discovery.

5.6. MHC molecules and IFNγ response

The immune system relies on the ability to recognize and eliminate foreign antigens, a process that is largely dependent on MHC molecules and antigen presentation pathways. These mechanisms are essential for initiating adaptive immune responses, particularly in the context of pathogen defense and tumor immunity. One key regulatory cytokine in this process is interferon-γ (IFNγ), which plays a central role in controlling antigen presentation and shaping immune responses.

MHC molecules are cell-surface glycoproteins that present antigenic peptides to T cells, enabling immune surveillance and activation of the adaptive immune system. In humans, MHC molecules are encoded by the highly polymorphic human leukocyte antigen (HLA) gene complex, and they are classified into two main classes. MHC Class I is found on almost all nucleated cells. It carries and displays cleaved peptides derived from endogenous proteins to $CD8^+$ cytotoxic T cells. This is important for the immune system to detect and eliminate virus-infected or malignant cells. MHC Class II instead presents exogenous peptides to $CD4^+$ helper T cells. It is mainly present on professional antigen-presenting cells (APCs) including B cells, dendritic cells, and macrophages. This

process is essential for orchestrating immune responses, including B cell activation and cytokine production.

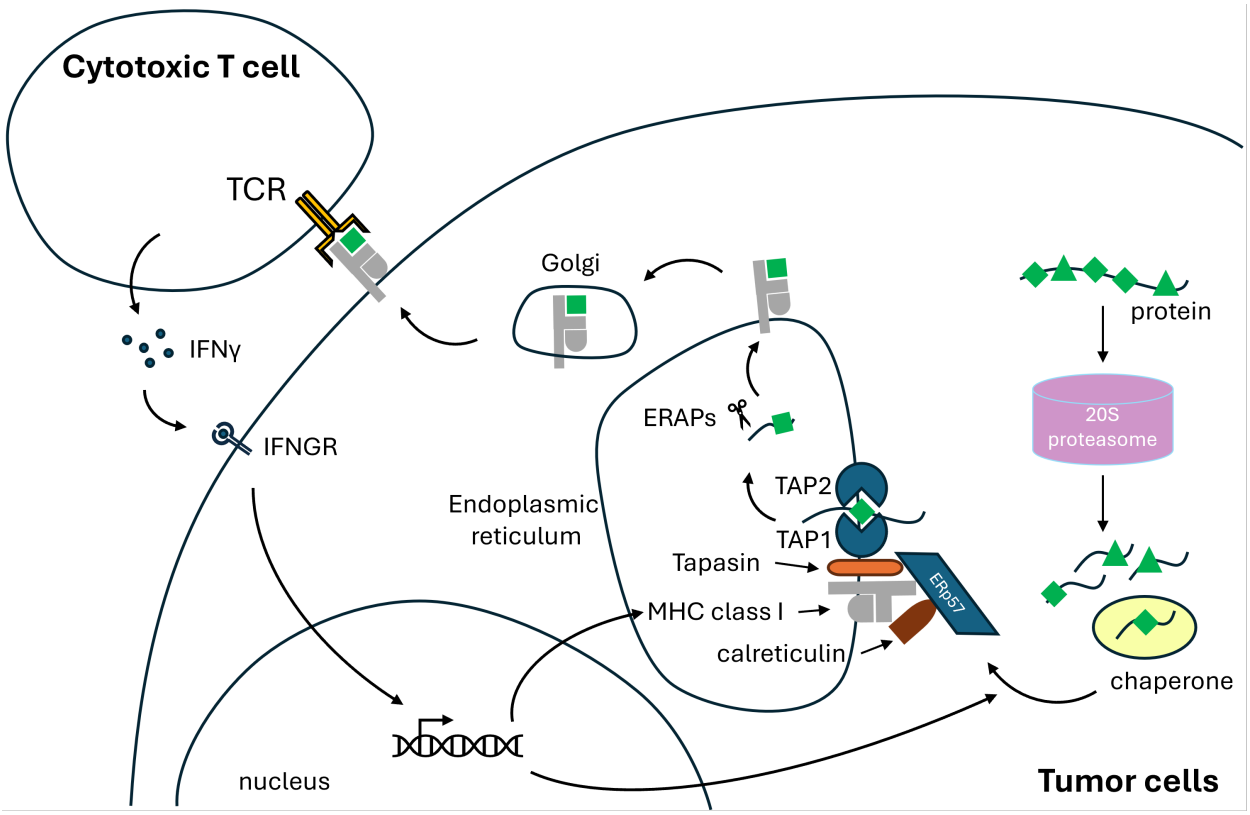

Figure 2. Antigen presentation by MHC class I molecules on tumor cells.

Proteins made within the cell (direct presentation) or released from endosomes (cross-presentation) undergo polyubiquitylation and are broken down by proteasomes. The resulting peptides are either the perfect length to bind MHC class I molecules or are longer precursors with extra amino acids at the N-terminus, which aminopeptidases can trim further. Chaperones in the cytoplasm stabilize these peptides to prevent their quick breakdown. TAP1 and TAP2, linked to newly forming MHC class I chains via tapasin, shuttle the peptides into the endoplasmic reticulum (ER), where ER aminopeptidases (ERAPs) may trim their N-terminal ends. When peptides bind tightly to the MHC class I heavy chain–β2-microglobulin (β2m) complex, it triggers final folding and release from the ER chaperone calreticulin, enabling the MHC class I molecule to leave the ER, travel through the Golgi, and reach the plasma membrane. The activation of interferon-γ receptor (IFNGR) up-regulates gene expression of components for antigen presentation.

A successful antigen presentation comprises of multiple stages in a meticulously controlled system (Figure 2). The process starts with proteolytic processing of

intracellular proteins by proteosome. The resulting peptides are transported into endoplasmic reticulum by the transporter associated with an antigen processing complex. Eventually, Peptides bind to MHC class I molecules, which are then transported to the cell surface for presentation to $CD8^+$ T cells (Groettrup et al., 2010).

IFNγ is a cytokine primarily produced by activated T cells and natural killer (NK) cells in response to infections or tumor formation. The IFNγ signaling pathway is mediated through the IFNγ receptor (IFNGR), which triggers the JAK-STAT pathway upon binding. This leads to the activation of interferon regulatory factors and signal transducer and activator of transcription 1 (STAT1), resulting in the transcription of genes involved in immune responses. This signaling event on tumor cells allows IFNγ to exert multiple immunomodulatory effects, including enhancing antigen presentation by upregulating MHC expression, inducing the production of proteasomal components that optimize antigen processing, activating macrophages and other immune cells to enhance pathogen clearance, and promoting T cell differentiation and function.

5.7. Recent discoveries from melanoma- T cell coculture screens

Prior to the commencement of this project, substantial effort has already been made by other research groups with similar interests to investigate the relationship between T cells and melanoma. These studies employed similar methodologies, including but not limited to CRISPR-based techniques.

In 2014, Zhou et al. conducted a pooled short hairpin RNA (shRNA) screen instead of a CRISPR-based approach. The shRNA library was transduced into mouse B16 melanoma cells which were subsequently selected by OT-I T cell in an *in vivo* mouse model. Their findings confirmed that the knockdown of *PPP2R2D* in melanoma suppressed T cell apoptosis, leading to enhanced tumor growth and increased cytokine release in the tumor microenvironment (Zhou et al., 2014).

In 2017, Patel et al. modified T cells to over-express NY-ESO-1 T cell receptor, which specifically detects NY-ESO-1 neo-antigen found exclusively in melanoma cells. Their screen pinpointed several loss-of-function (LOF) mutations in *APLNR*, which is prevalent in tumors that were refractory to immunotherapy, to be crucial to immune surveillance. They demonstrated that APLNR acts on JAK1 to modulate IFNγ responses in melanoma. The functional loss of APLNR reduces the effectiveness of ACT and ICB in mouse models (Patel et al., 2017).

That same year, another group conducted a CRISPR-mediated *in vivo* pooled screen using B16 melanoma cells. Relying on tumor vaccine, they were able to re-direct the T cell cytotoxicity towards the transplanted B16 cells carrying the sgRNA library. With this approach, they have discovered that protein tyrosine phosphatase, PTPN2, in tumor cells acts as a suppressor of immunotherapy effectiveness by reducing IFNγ-mediated effects on MHC presentation and growth inhibition (Manguso et al., 2017). Two years later, the same group of researchers continued validating gene candidates from their initial screen. In a follow-up publication, they have identified another important modulator of IFNγ response, whose presence constrained the ability of IFNγ to provoke apoptosis on melanoma cells (Ishizuka et al., 2019).

Taking a different perspective, another research group utilized the Pmel-1 CD T cell and OT-1 T in a CRISPR-mediated pool screen to select mouse B16F10 melanoma cells for loss-of-function mutations important for SWI/SNF chromatin remodeling complex in relation to immune response. They were able to confirm that loss of PBRM1 and ARID2, components of PBAF form of the SWI/SNF chromatin remodeling complex, restricts the chromatin accessibility for the IFNγ responsive genes in melanoma, resulting in a poor killing by T cells (Pan et al., 2018).

In 2019, a genome-wide CRISPR/Cas9 screen was conducted using MART-1 T cells and *IFNGR1*-knockout melanoma. The studies aimed to identify genes that render tumor cells more susceptible to T cell attacks under the circumstance that the IFNγ receptor was deficient. The gene *TRAF2* was validated as a key gene, with its deletion making

melanoma cells more vulnerable to T cell-mediated killing by altering downstream TNF signaling events (Vredevoogd et al., 2019).

Lastly, a group published a study involving a large-scale screen performed on a diverse set of mouse cell lines of different origins, including melanoma. Together with CL4 or OT-1 $CD8^+$ T cells, this study identified an essential set of genes and pathways that facilitate cancer cells to escape from killing by cytotoxic T cells. This involves the autophagy pathway as a conserved modulator for evasion of immune surveillance by cancer cells and revealed that this group of genes is required to defend against cytotoxicity induced by IFNγ or TNF (Lawson et al., 2020).

All studies mentioned above focused on melanoma cells in combination with a selective agent which is typically a T cell engineered to express T cell receptors targeting melanoma-specific antigens. It is noticeable that these studies prioritized investigating direct interactions between endogenous T cells and tumor cells, rather than indirect factors such as cytokines or immune checkpoint blockade, to simulate the dynamics of immunotherapy. This eventually led to the discovery of several novel regulators of direct immune response from cytotoxic T lymphocyte. However, this methodology also inherently limited the scope of findings, particularly in terms of primary mechanism of T cell recognition and killing. The issue will be further elaborated in the following sections.

It is conspicuous that most findings from recent melanoma-T cell studies inevitably lead to discovering novel modulators that are heavily related to IFNγ (Ishizuka et al., 2019; Lawson et al., 2020; Manguso et al., 2017; Pan et al., 2018; Patel et al., 2017; Zhou et al., 2014). In the majority of these studies, researchers employed either endogenous T cells or T cell engineered to express a conventional TCR with a specificity towards defined cancer-associated antigen as the selective agent acting on melanoma cell populations. The cytotoxic effector function of T cells is fundamentally dependent on the presentation of tumor antigens by MHC I molecules on melanoma cells. The immunomodulatory property of IFNγ essentially forms the bridge between T cells and tumor cells by up-regulating MHC expression, proteasomal cleavage of antigens and T cell differentiation. This cytokine-mediated upregulation of antigen presentation

increases the immunogenic visibility of melanoma cells, thereby promoting their recognition and elimination by T cells. Moreover, the interaction between T cells and antigen-presenting tumor cells can lead to further IFNγ secretion, creating a positive feedback loop that amplifies T cell-mediated cytotoxicity.

A disruption to the IFNγ signaling would render the T cell immune response futile and thus granting a better survival to melanoma cells. The phenotype of any gene that changes the behavior of the IFNγ response would clearly stands out from the rest and thus being highly enriched or depleted from the screen. However, having IFNγ response as the basis of the study confines the experimental outcome to a certain degree. Primarily, antigen presentation by MHC and IFNγ response would become a prerequisite for the entire selection mechanism of the screen to function. Any other gene candidate that also possess immunomodulatory function of cancer cell but not related to IFNγ can hardly be identified, such as the TRAF2 identified and validated by Vredevoogd et al. Other candidates that have weak influence on IFNγ signaling but modulates melanoma-T cell interact from another aspect might also be masked by the overwhelming phenotype of gene candidates that have strong connection to IFNγ signaling. Therefore, for furture studies to identify novel gene candidates that are not influenced by IFNγ signaling while regulate the interaction between melanoma and T cells, another screening strategy should be adopted to circumvent strong influence from IFNγ signaling from canonical immune responses.

5.8. Application of CAR in CRISPR-mediated screen

ACT technique offers an alternative perspective that do not primarily rely on IFNγ signaling or MHC class I-antigen presentation. ACT, as a powerful tool both in cancer immunotherapy and research, revolves around two major approaches, namely CAR and TCR. While both strategies leverage T cells to target and eliminate malignant cells, they differ significantly in their mechanisms of antigen recognition, signaling pathways, and therapeutic applications (Table 2).

Table 2.Key difference between CARs and TCRs.

Feature	CAR	TCR
Target recognition	Recognizes surface protein independent of MHC molecules.	Only recognizes peptide antigens presented by MHC molecules (MHC-restricted).
Antigen types	Targets proteins, carbohydrates, or glycolipids on the cell surface.	Limited to peptide fragments presented on MHC.
Receptor structure	Synthetic receptor combining an extracellular antigen-binding domain (from antibodies) and intracellular signaling domains.	Natural or engineered TCR heterodimers (α and β chains) interacting with MHC-peptide complexes.
Signaling mechanism	Built-in co-stimulatory domains (e.g., CD28, 4-1BB) for robust activation.	Requires accessory proteins (e.g., CD4, CD8, CD28) for co-stimulation.
Suitability for Tumors	Effective for surface-expressed antigens (e.g., CD19 in B cell malignancies).	Targets intracellular antigens, expanding the range of potential targets.
Immune evasion	Not affected by downregulation of MHC, as recognition is MHC-independent.	Susceptible to tumor immune evasion via MHC downregulation.
Clinical use	Widely used in hematologic cancers; less effective in solid tumors due to tumor microenvironment challenges.	Promising in both hematologic and solid tumors, but MHC restriction limits broad applicability.
Engineering complexity	Requires engineering of a single synthetic receptor.	Involves matching TCR specificity to MHC alleles and optimizing affinity for tumor antigens.

CARs are synthetic receptors designed to recognize specific surface antigens in an MHC-independent manner. Tumors often evade immune detection by downregulating MHC expression, a tactic that cripples TCRs since they rely on MHC to recognize antigens. CARs, being MHC-independent, are unaffected by this strategy and can still target and destroy cancer cells with reduced or absent MHC. This resilience against immune evasion gives CARs a critical advantage in treating tumors that employ such defenses, a common feature in many cancers. Moreover, the MHC-independent function of CAR permits the creation of new CARs that bind any epitopes across the cell surface including carbohydrates, or glycolipids given that an antibody is available to the corresponding epitopes. This allows development of novel cellular immunotherapy based on a new spectrum of target antigens. GD2 CAR, for instance, is a CAR that

targets on high level of disialoganglioside on neuroblastoma and melanoma (Straathof et al., 2020) .

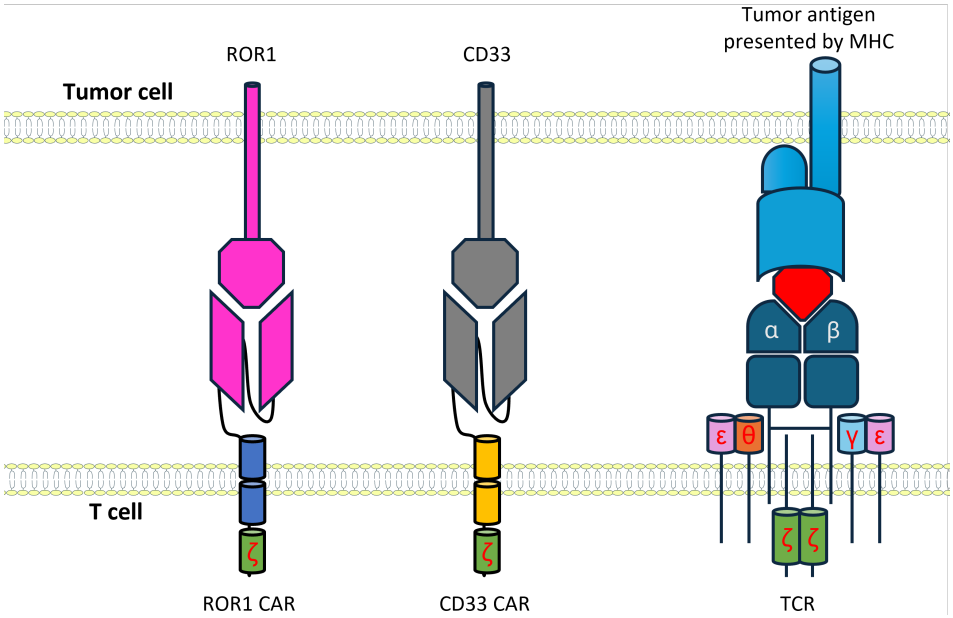

Figure 3. Structural difference between CAR and TCR.

A CAR features an extracellular antigen-binding site formed from the variable region of an antibody, connected by a linker sequence to an intracellular portion that includes a co-stimulatory domain and a CD3ζ signaling domain from the T cell receptor (TCR). Transgenic TCRs resemble natural TCRs but are modified with antigen-binding regions tailored to recognize a tumor-associated target. Unlike CARs, TCRs need co-stimulation from distinct receptors to fully activate T cells. CARs target antigens on the cell surface, while TCRs detect intracellular antigens displayed on major histocompatibility complex (MHC) molecules.

A CAR consists of an extracellular antigen-binding domain, which is also known as single chain variable region (Figure 3). This is typically derived from a monoclonal antibody of a different species, fused to intracellular signaling domains that activate T cell responses. A common choice of activation domain includes CD28, CD27, CD134 (OX40), and CD137 (4-1BB) (Kingwell, 2017). TCRs, in contrast, recognize processed versions of both surface and intracellular antigens presented on MHC molecules. TCR-based therapies rely on the natural antigen-processing machinery, allowing for the targeting of a wider spectrum of tumor-associated antigens, including those processed

from intracellular and surface-localized proteins. However, TCR therapy is limited by MHC restriction, meaning that treatment must be tailored to a patient's HLA type.

To solve the issue of biased candidate selection observed from other studies (section 5.7), an attempt was made to utilize the CAR-T cells instead of TCR-T cells as the model in the genome-wide screen and co-culture experiments. The decisive feature of CARs that render them preferable than TCRs is their way of detecting antigens associated with cancer. TCR requires the antigen to be cleaved by proteosome, loading onto MHC molecules and finally trafficked to the cell surface to be detected by T cells. As previously mentioned, such process is intricately connected to an intact IFNγ response, which present it as an unideal model for examining gene candidates independently of the MHC molecules. Consequently, CAR-T cells were chosen in this project as the model to study the connection between melanoma cells and T cells.

Genome-wide CRISPR-mediated pooled screens have significantly advanced our ability to investigate gene functions at a large scale, providing critical insights into complex biological systems and disease mechanisms. Therefore, in this project, a genome-wide pooled screen was adopted as a starting point to narrow down the directions of the research questions. With the use of a genome-wide sgRNA constructed and characterized by colleagues (Henkel et al., 2020), a melanoma-T cell co-culture screening platform was established to capture the genes that play a critical role in the interaction between these two cell types.

5.9. Objectives of this project

The advent of immunotherapy has replaced chemotherapy as the new standard first-line treatment for advanced melanoma. However, a significant fraction of patients still cannot benefit from this due to acquired resistance to the treatment or being unresponsive to it. Specifically, cellular immunotherapy has failed to show acceptable results in the treatment of solid tumors including melanoma, highlighting a need for deeper understanding of factors that influence the efficacy of such therapeutic strategy.

Genome-wide CRISPR-mediated pooled screens have significantly advanced our ability to investigate gene functions at a large scale, providing critical insights into complex biological systems and disease mechanisms. Therefore, in this project, my primary goal was to establish a genome-wide CRISPR-mediated melanoma-CAR-T cell co-culture screening platform for investigating MHC- and IFNγ-independent gene targets. With the use of the genome-wide Heidelberg CRISPR sgRNA library, a melanoma-T cell co-culture screening platform was to be established to capture the genes that play a critical role in the interaction between these two cell types. Gene functions crucial to immune evasion of melanoma cells or modulation of T cell cytotoxicity were to be identified from a LOF mutation perspective.

In addition, I sought to define the core set of essential genes to A375 melanoma with another gene dropout screen for the elimination of irrelevant candidates, that naturally confer growth disadvantages to A375 cells regardless of their influence on any immune response. Based on the information from the two screens, I aimed to obtain a list of gene candidates whose phenotype would be directly related to alteration of the T cell cytotoxicity or melanoma cell's susceptibility. By cross-referencing with publicly available datasets, I aimed to identify genes that are clinically relevant to the real-life patient's status. Finally, I aimed at validating novel gene candidates from the screen for further mechanistic insight with tailored experiments. My study aimed at providing insight into novel modulators of melanoma-T cell interaction.

Throughout my Ph.D. study, several collaboration opportunities have risen. I successfully accomplished several projects using the Heidelberg CRISPR library A and the CRISPR/Cas9 KO screening platform in different contexts. Considering the data generated from all these projects, I aimed to investigate the performance of the screening methodology with a meta-analysis to examine potential improvements or pitfalls when using the screening methods in the future.

6. Materials and Method

6.1. Materials

6.1.1. Chemicals and reagents

Table 3. List of chemicals and reagents used in this work.

Chemicals/reagents	Supplier	Catalog no.
0.5M EDTA, pH 8.0	Promega	V4231
0.5M Tris(2-carboxyethyl) phosphine hydrochloride	Sigma-Aldrich	646547-10X1ML
16% formaldehyde (W/V) methanol-free	Thermo Scientific	PIER28906
2-Mercaptoethanol	Sigma-Aldrich	63689-25ML-F
5× siRNA Buffer	Horizon Discovery	B-002000-UB100
6 x Loading Dye Solution	Life Technologies	R0611
7-Aminoactinomycin D (7-AAD)	BioLegend	420404
Accutase	Sigma	A6964-100ML
Acetic acid	Fisher Scientific	15642900
Agar	AppliChem	A0949,0500
Agarose NEEO	Carl Roth GmbH	2267.4
Annexin V Binding Buffer	BioLegend Europe BV	422201
Annexin V-FITC	Miltenyi Biotec	130-097-928
BCH	Biotechne	5027/50
BIS-Tris	Santa Cruz Biotechnology	sc-216088A
Blasticidin HCL	Invivogen	ant-bl-05
Bolt 4 to 12%, Bis-Tris, 1.0 mm, Mini Protein Gel, 15-well	Life Technologies	NW04125BOX
bovine serum albumin, Fraction V, Protease-free, low IgG	Serva	11948.01
Bromophenol Blue Sodium	Sigma	B5525-25G
Buffy coat from DRK Blutspendedienst	Blutspendedienst Baden-Württemberg - Hessen gGmbH	n/a
BX795	EnzoLifeScience GmbH	ENZ-CHM189-0005
Carbenicillin	AppliChem	A1491
Carboxyfluorescein succinimidyl ester	BioLegend Europe BV	423801
cOmplete, Mini phosSTOP	Roche	4906845001
cOmplete™, Mini Protease Inhibitor Cocktail	Roche	4693116001
D-(+)-Trehalose dihydrate	Sigma	T0167-10G
Dimethyl sulfoxide (DMSO)	Sigma	D8418-50ML

Chemicals/reagents	Supplier	Catalog no.
Dithiothreitol	AppliChem	A2948,0005
DNase I (RNase-Free)	New England Biolabs	M0303L
Dynabeads™ Human T-Activator CD3/CD28	Life Technologies	11131D
Chemicals/reagents	Supplier	Catalog no.
eBioscience 10X RBC Lysis Buffer (Multi-species)	Invitrogen	00-4300-54
eBioscience Intracellular Fixation & Permeabilization Buffer Set	Thermo Fisher Scientific	88-8824-00
Ethanol 99%	Sigma-Aldrich	14926
Fetal bovine serum (FBS)	Sigma-Aldrich	F7524-500 ML
Fixable Viability Dye eFluor 450	Invitrogen	65-0863-14
Gel Loading Dye, Purple (6X)	New England Biolabs	B7024 S
GeneRuler 1 kb DNA Ladder, ready-to-use	Life Technologies	SM0313
Gibco™ DMEM, High Glucose, L-Glutamine	Life Technologies GmbH	41965062
Gibco™ DPBS, no calcium, no magnesium	Life Technologies	14190250
Gibco™ IMDM	Life Technologies	21980065
Gibco™ MEM Amino Acids Solution (50X)	Life Technologies	11130036
Gibco™ Opti-MEM I Reduced Serum Medium	Life Technologies	31985047
Gibco™ PBS, pH 7.4-10	Life Technologies	10010056
Gibco™ RPMI 1640 Medium, no glutamine	Life Technologies	31870074
Gibco™ TrypLE Express Enzyme, no phenol red	Life Technologies	12604013
Gibco™ Trypsin-EDTA (0.25%), phenol red	Life Technologies	25200056
GlutaMAX Supplement	Life Technologies	35050038
Glycerol	Sigma	G5516-500ML
GolgiPlug™ Protein Transport Inhibitor (Containing Brefeldin A)	BD Biosciences	555029
Green CMFDA	Santa Cruz Biotechnology	sc-396581
Human Fas Ligand (soluble) Recombinant Protein	Life Technologies	310-03H-10UG
Human recombinant interferon gamma	Immunotools	11343534
Human Serum from human male AB plasma, USA origin, sterile filtered	Sigma-Aldrich	H4522-20ML
Human TRAIL (TNFSF10) (soluble) Recombinant Protein	Life Technologies	310-04-50UG
Human TruStain FcX™ (Fc Receptor Blocking Solution)	BioLegend Europe BV	422301
IL-2R alpha (CHO), soluble, rec. Human	PeproTech	200-02RC-250
Immobilon Western Chemiluminescent HRP Substrate	Merck Millipore	WBKLS0100
Immobilon-P, Porengröße 0,45 µm Rolle, 375 x 26,5 cm, PVDF-Membran	Merck Millipore	T831.1
jetOPTIMUS transfection reagent	Polyplus	101000051
JPH203	Hölzel Diagnostika	MOLN-M10188-10mg
Kapa HiFi HotStart ReadyMix	Roche	7958935001
L-690,330	Biotechne	0681/10

Chemicals/reagents	Supplier	Catalog no.
Lenti-X Concentrator	Takara Bio Inc	631231
LIVE/DEAD Fixable Violet Dead Cell Stain Kit, for 405 nm excitation	Life Technologies	L34964
Lymphoprep™	Stemcell	7811
Methanol	Sigma-Aldrich	32213
MHY1485	MedChem Express	MCE-HY-B0795-10MMX1ML
Molecular grade water DNase, Rnase free	GE Healthcare	10275262
Myricetin	Sigma-Aldrich	476275-25MG
N-Acetyl-L-cysteine	Sigma-Aldrich	A9165-5G
NutriFreez® D10 Cryopreservation Medium without Phenol Red	Sartorius A.G.	05-714-1B
PageRuler plus prestained protein ladder, 10 to 250 kDa	Thermo Fisher Scientific	26619
Pancoll human, Density: 1.077 g/ml	PAN Biotech	P04-60500
Polybrene	Sigma-Aldrich	TR-1003-G
Propan-2-ol	Honeywell	33539
Propidium iodide solution	Sigma	P4864-10ML
Puromycin, Dihydrochloride	Merck Millipore	5088380001
Q5 Hot Start High-Fidelity 2X Master Mix	New England Biolabs	M0494S
Quercetin,dihydrate	Sigma-Aldrich	551600-100MG-M
Quick CIP	New England Biolabs	M0525L
Quick Ligase	New England Biolabs	M2200S
Recombinant Human Interleukin-15 (rh IL-15)	Immunotools	11340153
Recombinant Human Interleukin-7 (rh IL-7)	Immunotools	11340073
Recombinant Human ROR1 Fc Chimera Protein, CF	R&D Systems	9490-RO-050
Recombinant Human TRAIL/APO 2 Ligand (rh TRAIL / CD253)	Life Technologies	310-04-50UG
Recombinant Human Tumor Necrosis Factor-alpha	Immunotools	11343015
Restore Western Blot Stripping Buffer	Life Technologies	21059
RIPA Lysis and Extraction Buffer	Life Technologies	89901
RNase A	Qiagen	19101
S.O.C. Medium	Thermo Fisher Scientific	15544034
Skim Milk Powder	Sigma	70166-500G
Small RNA ladder	Agilent	5067-1550
Sodium chloride	Sigma-Aldrich	31434-M
Sodium dodecyl sulfate	Sigma-Aldrich	75746-250G
Sybr Safe DNA Stain	Life Technologies	S33102
T4 Polynucleotide Kinase	Life Technologies	EK0032
Tigatuzumab	Selleck Chemicals	A2604-1mg
TransIT-LT1 transfection reagent	Mirus Bio	731-0029
Trizma® base	Sigma-Aldrich	T1503-1KG
Trypan blue solution	Sigma-Aldrich	T8154-20ML

Chemicals/reagents	Supplier	Catalog no.
TWEEN® 20	Sigma-Aldrich	P9416
V-9302	MedChem Express	V-9302-5mg
Vilazodone hydrochloride	MedChem Express	6202/10
Viobility™ Fixable Dyes 405/452	Miltenyi Biotec	130-109-816
X-VIVO 15 Serum-free Hematopoietic Cell Medium	Lonza	881027
Zombie Aqua™ Fixable Viability Kit	BioLegend Europe BV	423101

6.1.2. Consumables

Table 4. List of laboratory consumables use in this work.

Laboratory consumables	Supplier	Catalog no.
1000 µl TipOne® filter pipette tips (sterile)	Starlab	S1126-7710
8 Well PCR Tube Strips, 0.2 ml	Biozym	AF4TI-0792
96 well U-bottom plates	Greiner Bio-One	650185
Cell culture dish ;146 x 21mm	TPP	13714
Cell culture flask T225 225cm2 EasYFlask, 225 cm^2, CC, with filter cap	Fisher Scientific	10041542
Cell culture microplate, 96 WELL, PS, F-BODEN	Greiner Bio-One	655090
Combitips 10ml nonsterile	Eppendorf	12979
Combitips PLUS STERIL 5mL	Eppendorf	12627
Combitips® advanced 0,5 ml PCR clean	Eppendorf	106989782
Corning® CellBIND® Surface HYPERFlask® cell culture vessels	Sigma-Aldrich	CLS10030-4EA
CRYOTUBE 1.8 mL	Sigma-Aldrich	V7884-450EA
Deep well plate 96 well 1.2mL	Corning	732-2891
Deep well plate 96 well, 600µL, clear	Corning	736-0336
DNA LoBind Tubes; 1;5ml; PCR clean;	Eppendorf	525-0130
Easy Grip Disposable Polystyrene Sterile Bottles	Corning	10738212
Eppendorf® Protein LoBind microcentrifuge tubes 1.5 mL	Eppendorf	EP0030108116
Falcon® 3025 TC cell culture dish 150 mm	BD Falcon	12947
Falcon® 3136 TC-cell culture flask. 75CM^2 Filter	BD Falcon	14099
Falcon® 175cm2 Rectangular Straight Neck Cell Culture Flask with Vented Cap Case	BD Falcon	353112
Falcon® 25cm2 Rectangular Canted Neck Cell Culture Flask with Vented Cap Case	BD Falcon	1172715
Falcon® 5mL Round Bottom Polystyrene Test Tube, with Snap Cap, Sterile	BD Falcon	352058
Falcon® 875cm^2 Rectangular Straight Neck Cell Culture Multi-Flask, 5-layer with	BD Falcon	353144
Falcon® 96 Well Clear Round Bottom Not Treated Assay Plate, Nonsterile, 5/Pack, 50/Case	BD Falcon	353910
FINNTIPS FT 250 UNIVERSAL,	Thermo Labsystems	613-2597

Laboratory consumables	Supplier	Catalog no.
HS8151 Delta Cell Spreader	Fisher Scientific	11364035
Large Microflex XCEED Nitrile Gloves, Powder Free (1x250)	Starlab	13980
Laser Cryo-Babies(R) and Cryo-Tags(R), C	Sigma-Aldrich	L4164-1PAK
LUNA 2-Channel Cell Counting Slides	Logos Biosystems	L12002-LG
Medium Microflex XCEED Nitrile Gloves, Powder Free (1x250)	Starlab	13979
Multi-well plate for suspension cell culture 12 WELL, PS	Greiner Bio-One	665102
Nunc™ 50 mL Bioreactor Tube	Thermo Fisher Scientific	332260
OP Masks 3 layers	Meditrade	14887
pluriStrainer Mini 5 µm - 70 µm cell strainers	pluriSelect Life Science	43-10010-50, 43-50005-13, 43-10040-50, 43-10070-50
Polyallomer tubes 14 ml, 14x95 mm, thin walled (S)	Beranek Laborgeraete	5031
PS-multi-plate, 6 well	Greiner Bio-One	2506
SafeSeal reaction tube, 1.5 ml, PP	Sarstedt	72.706.500
SafeSeal reaction tube, 2 ml, PP	Sarstedt	72.695.500
SafeSeal SurPhob Spitzen,10 µl - 200 µl, sterile	Biozym	VT0200, VT0220, VT0240,
Scalpel FIG.21	Feather	13317
SepMate™-50 (IVD)	Stemcell	85450
Serological pipette 5 mL - 50 mL	Greiner Bio-One	14866, 14867, 14865, 14303
Stainless Steel Bent Tip Forceps, length: 130 mm,	Fisher Scientific	10366241
Suspension cultural bottle, 250 ml, PS, filter screw	Greiner Bio-One	658195
Suspension culture bottle, 50 ml, PS	Greiner Bio-One	C6731-200EA
15 mL and 50 mL tube, PP conical bottom	Greiner Bio-One	188261-N, 227261
X50 SYRINGE FILTER PES 33MM 0.45µm STR	Fisher Scientific	15216869

6.1.3. Standard kits

Table 5. list of standard kits used.

Kits	Supplier	Catalog no.
Agilent High Sensitivity DNA Kit	Agilent	5067-4626
DNA Standards 1-6 Illumina qPCR Library Quantification Kit	Roche	7960387001
EasySep™ Human $CD8^+$ T Cell Isolation Kit	Stemcell	17953
In-Fusion® Snap Assembly Master Mix	Takara	638948
NextSeq 500/550 Hi Output KT v2.5 (75 CYS)	Illumina	20024906
NucleoBond Xtra Maxi Plus kit for transfection-grade plasmid DNA	Macherey&Nagel	740414.10S

Kits	Supplier	Catalog no.
NucleoBond Xtra Midi Plus kit for transfection-grade plasmid DNA	Macherey&Nagel	740412.50
NucleoSpin Plasmid Transfection-grade, Mini kit for ultrapure plasmid DNA	Macherey&Nagel	740490.5
Pierce BCA Protein Assay Kit	Thermo Fisher Scientific	23227
QIAamp DNA Blood Maxi Kit (10x)	Qiagen	51192
Qiagen QIAquick PCR Purification Kit, 250rxn	Qiagen	12580
QIAquick Gel Extraction Kit	QIAGEN	28706X4
Qubit 1x dsDNA HS Assay Kit	Thermo Fisher	Q33230
RNeasy mini Kit	Qiagen	74106

6.1.4. Antibodies

Table 6. List of antibodies used in flow cytometry.

Antibodies	Conjugates	Dilution used	Supplier	Catalog no.
AffiniPure Goat Anti-Mouse IgG, $F(ab')_2$ fragment specific	Alexa Fluor® 647	1:100	Jackson	115-605-006
AffiniPure Goat Anti-Rabbit IgG, $F(ab')_2$ Fragment Specific	Alexa Fluor® 647	1:100	Jackson	111-605-006
AffiniPure Rabbit Anti-Human IgG, $F(ab')_2$ Fragment Specific	Alexa Fluor® 647	1:100	Jackson	309-005-006
anti-human CD107a Antibody	Brilliant Violet 785™	1:100	BioLegend	328643
anti-human CD151 Antibody	APC	1:50	BioLegend	350405
anti-human CD19 Antibody	FITC	1:40	BioLegend	302256
anti-human CD19 Antibody	n/a	1:40	Invitrogen	14-0199-82
anti-human CD223 Antibody	FITC	1:50	BioLegend	369307
anti-human CD261 Antibody	APC	1:50	BioLegend	307207
anti-human CD262 Antibody	n/a	1:50	BioLegend	307402
anti-human CD27 antibody	APC	1:50	BioLegend	986904
anti-human CD279 Antibody	APC	1:50	BioLegend	379207
anti-human CD279 Antibody	Brilliant Violet 421	1:50	BioLegend	329919
anti-human CD3	PerCP	1:25	BioLegend	300427
anti-human CD33 Antibody (P67.6)	FITC	1:40	BioLegend	366619
anti-human CD33 Antibody (WM-53)	n/a	1:40	Invitrogen	14-0338-82
anti-human CD366 Antibody	Brilliant Violet 421	1:50	BioLegend	345007
anti-human CD366 Antibody	PE/Cyanine7	1:50	BioLegend	345014
anti-human CD4 Antibody	FITC	1:25	BioLegend	300538
anti-human CD45RA Antibody	FITC	1:50	BioLegend	304105
anti-human CD45RA Antibody	PE	1:50	BioLegend	304108

Antibodies	Conjugates	Dilution used	Supplier	Catalog no.
anti-human CD45RO Antibody	FITC	1:50	BioLegend	304242
anti-human CD45RO Antibody	PE	1:50	BioLegend	304205
anti-human CD46 Antibody	APC	1:50	BioLegend	352405
anti-human CD69 Antibody	APC	1:50	BioLegend	310909
anti-human CD69 Antibody	Brilliant Violet 605	1:50	BioLegend	310937
anti-human CD8 Antibody	Alexa Fluor® 647	1:25	BioLegend	344726
anti-human CD8a Antibody	APC	1:25	BioLegend	301049
anti-human CD95 Antibody	n/a	1:50	BioLegend	684401
anti-human CD98 Antibody	n/a	1:50	BioLegend	315602
anti-Human CSPG4 antibody	Alexa Fluor® 647	1:25	BioLegend	562414
anti-human DcR1 Antibody	PE	1:40	BioLegend	307005
anti-human Ganglioside GD2	Alexa Fluor® 647	1:25	BioLegend	357317
anti-human ROR1 Antibody	Alexa Fluor® 647	1:25	BioLegend	357821
anti-human ROR1 MAb (Cl 1011919)	n/a	1:25	Biotechne	MAB20001-SP
anti-human TIGIT Antibody	Brilliant Violet 605	1:50	BioLegend	372711
anti-Human TRAILR4/TNFRSF10D Antibody	n/a	1:40	Biotechne	MAB633-SP
Mouse IgG1, κ Isotype Ctrl Antibody	APC	1:40	BioLegend	400119
Mouse IgG1, κ Isotype Ctrl Antibody	n/a	1:40	BioLegend	400101
Mouse IgG1, κ Isotype Ctrl Antibody	PE	1:40	BioLegend	400111
Mouse IgG2a kappa Isotype Control (eBM2a)	Alexa Fluor® 647	1:40	BioLegend	51-4724-81
Mouse IgG2b, κ Isotype Ctrl Antibody	n/a	1:40	BioLegend	400301

Table 7. List of antibodies used in Western blotting.

Antibodies	Dilution used	Supplier	Catalog no.
Anti IPMK Human MaxPab	1:1000	Tebu-Bio	157H00253430-D01P
Anti-4F2hc/SLC3A2 (D6O3P) Rabbit mAb	1:1000	Cell Signaling	13180S
Anti-Atg13 (E1Y9V) Rabbit mAb #13468	1:1000	Cell Signaling	13468T
Anti-beta-Actin (C4) HRP Antibody	1:5000	Santa Cruz Biotechnology	sc-47778 HRP
Anti-Caveolin-1 (D46G3) XP antibody	1:1000	Cell Signaling	3267
Anti-LaminB1-HRP antibody	1:5000	Abcam	ab194109
Anti-LAT1 Antibody	1:1000	Cell Signaling	5347S
Anti-mTOR antibody	1:1000	Cell Signaling	2983T
Anti-p70 S6 Kinase Antibody	1:1000	Cell Signaling	9202S
Anti-Phospho-Atg13 (Ser355) (E4D3T) Rabbit mAb	1:1000	Cell Signaling	46329S

Antibodies	Dilution used	Supplier	Catalog no.
Anti-Phospho-mTOR (Ser2448) Antibody (rabbit)	1:1000	Cell Signaling	2971S
Anti-Phospho-p70 S6 Kinase (Thr389/412) Antibody	1:1000	Hölzel Diagnostika	AF-AF3228-100ul
Peroxidase-AffiniPure Goat Anti-Mouse IgG (H+L)	1:10000	Jackson	JIM-115-035-003
Peroxidase-AffiniPure Goat Anti-Rabbit IgG (H+L)	1:10000	Jackson	JIM-111-035-003
StarBright Blue 520 Goat Anti-Mouse IgG	1:2000	Biorad	12005866
StarBright Blue 700 Goat Anti-Rabbit IgG	1:2000	Biorad	12004161

6.1.5. Bacterial strains

Table 8. Bacterial strains used in this study.

Bacterial strains	Supplier	Catalog no.	Genotype
One Shot Stbl3 Chemically Competent E. coli	Life Technologies	C737303	F–mcrB mrr hsdS20(rB–, mB–) recA13 supE44 ara-14 galK2 lacY1 proA2 rpsL20(StrR) xyl-5 λ–leu mtl-1
Stellar competent cells	Takara Bio Inc	636766	Genotype: F-, endA1, supE44, thi-1, recA1, relA1, gyrA96, phoA, Φ80d lacZΔ M15, Δ(lacZYA-argF) U169, Δ(mrr-hsdRMS-mcrBC), ΔmcrA, λ-

6.1.6. Cell lines and other cellular resources

Table 9. List of cellular resources used.

Cell type	Source	Features
A375	ATCC CRL-1619	Isolated from human malignant melanoma, displays epithelial morphology
WM793	Meenhard Herlyn (Wistar Institute, Philadelphia, USA)	isolated from vertical growth phase of a primary melanoma lesion
HEK293T	ATCC CRL-11268	Immortalized human embryonic kidney cells expressing the SV-40 for lentivirus production
A375-CD19-Cas9	This study	Modified from A375 to express CD19, Cas9 and blasticidin-resistance gene
A375-CD33-Cas9	This study	Modified from A375 to express CD33, Cas9 and blasticidin-resistance gene
A375-CD33-Cas9-sgSLC3A2_1	This study	Knocked out SLC3A2 gene from A375-CD33-Cas9
A375-CD33-Cas9-sgSLC3A2_3	This study	Knocked out SLC3A2 gene from A375-CD33-Cas9

Cell type	Source	Features
A375-CD33-Cas9-sgSLC7A5_1	This study	Knocked out SLC7A5 gene from A375-CD33-Cas9
A375-CD33-Cas9-sgSLC7A5_2	This study	Knocked out SLC7A5 gene from A375-CD33-Cas9
A375-Cas9	This study	Modified from A375 to express Cas9 and blasticidin-resistance gene
A375-Cas9-sgSLC3A2_1	This study	Knocked out SLC3A2 gene from A375-Cas9
A375-Cas9-sgSLC3A2_3	This study	Knocked out SLC3A2 gene from A375-Cas9
A375-Cas9-sgSLC7A5_1	This study	Knocked out SLC7A5 gene from A375-Cas9
A375-Cas9-sgSLC7A5_2	This study	Knocked out SLC7A5 gene from A375-Cas9
A375-ROR1 high-Cas9	This study	A375-Cas9 sorted for sub-population with high ROR1 expression
WM793-Cas9	This study	Modified from WM793 to express Cas9 and blasticidin-resistance gene
WM793-sgSLC3A2_1	This study	Knocked out SLC3A2 gene from WM793-Cas9
WM793-sgSLC3A2_3	This study	Knocked out SLC3A2 gene from WM793-Cas9
WM793-sgSLC7A5_1	This study	Knocked out SLC7A5 gene from WM793-Cas9
WM793-sgSLC7A5_2	This study	Knocked out SLC7A5 gene from WM793-Cas9
Primary human $CD8^+$ T cell	This study	Primary CD8 T cells isolated from buffy coat of healthy donors
Primary human $CD8^+$ T cell - CD19 CAR	This study	Primary CD8 T cells infected with lentivirus to express CD19 CAR
Primary human $CD8^+$ T cell - CD33 CAR	This study	Primary CD8 T cells infected with lentivirus to express CD33 CAR
Primary human $CD8^+$ T cell - CSPG4 CAR	This study	Primary CD8 T cells infected with lentivirus to express CSPG4 CAR
Primary human $CD8^+$ T cell - GD2 CAR	This study	Primary CD8 T cells infected with lentivirus to express GD2 CAR
Primary human $CD8^+$ T cell - ROR1 CAR	This study	Primary CD8 T cells infected with lentivirus to express ROR1 CAR

6.1.7. Buffers

Table 10. List of buffer formulation used in this study.

Buffer	Recipe
10X Annealing Buffer	Nuclease-free water 100 mM Tris-HCl (pH 7.5) 1 M NaCl 10 mM EDTA
TAE	DDH2O 40mM Tris base 20 mM acetic acid 1 mM EDTA
SDS running buffer	DDH2O

Buffer	Recipe
	190 mM glycine 25 mM Tris-HCl 0.1% SDS adjust to pH 8.3
TBS	DDH2O 50 mM Tris-HCl (pH 7.6) 150 mM NaCl
TBST	0.1% Tween-20 in TBS
Western blot blocking buffer	5% milk powder or 5% Bovine serum albumin TBST
protein lysis buffer	1x cOmplete phosSTOP tablet 1x cOmplete Protease Inhibitor Cocktail mini tablet per 10 mL of RIPA buffer
5 x Laemmli buffer	DDH2O 312.5 mM Tris-HCl, pH 6.8 50 % Glycerol 10 % SDS 10 % TCEP 0.1 % Bromphenol Blue 0.5 M DTT
MOPS buffer	DDH2O 50mM MOPS 50mM TRIZMA-Base 1mM EDTA 1% SDS
Ponceau S Solution	DDH2O 0.2 % Ponceau S 5 % Glacial Acetic Acid
LB medium	DDH2O 1 % Tryptone 1 % NaCl 0.5 % yeast extract
LB agar	1 l LB medium 15 g Agar
Tris-Glycine Transfer Buffer	DDH2O 25 mM Tris 192 mM Glycine 20% (v/v) methanol

6.1.8. Lab equipment and instruments

Table 11. list of lab equipment and instruments used in this work.

Equipment & instruments	Manufacturer
12-channel Transferpette 0.5 to 10 µl	Carl Roth GmbH
2100 Bioanalyzer	Agilent
BD FACSAria Fusion	Becton Dickinson
BD FACSCanto II	Becton Dickinson
BD LSRFortessa	Becton Dickinson
Berthold Mithras LB 940 Multimode Plate Reader	Berthold
Centrifuge 5425 R	Eppendorf
Centrifuge 5804 R	Eppendorf
Centrifuges 5415 R	Eppendorf
Centrifuges 5810 R	Eppendorf
ChemiDoc MP Imaging System	Biorad
EasyEights™ EasySep™ Magnet	Stemcell
Freezer -20 °C	Liebherr
Freezer -80 °C	Liebherr
Fridge 4 °C	Liebherr
Gel documentation E-Box VX2	Peqlab
InCell 6000 Microscope	GE
Incubator, with CO2 sensor	Binder
IncuCyte® Zoom	Essen BioScience Inc
Laminar flow hood/biosafety cabinet	Thermo Fisher Scientific
LightCycler® 480	Roche
Liquid nitrogen storage	Liebherr
Luna FL automated Cell Counter Fluorescence and Bright field	Logos Biosystems
Microscope EVOS FL	Thermo Fisher Scientific
Mini Blot Module	Thermo Fisher Scientific
Multidrop Combi+	Thermo Fisher Scientific
NanoDrop ND-1000 spectrophotometer	Peqlab
NextSeq 550 System	Illumnina
Optima LE-80K Ultracentrifuge	Beckman
Pipetboy	Integra
Precision scale 0,01 g - 500 g	Carl Roth GmbH
Shaking incubator	Infors AG
Stemi SV 6	Zeiss
Taylor Wharton™ K Series Cryogenic Storage System 24K	Taylor Wharton
Thermocycler Tadvanced	Analytikjena
Vortex Genie	Scientific Industries
Water bath	Julabo

6.1.9. Plasmids

Table 12. List of plasmids used in this work.

Plasmid	Source
HDCRISPRv1	(Henkel et al., 2020)
HDCRISPRv1-sgSLC3A2_1	this work
HDCRISPRv1-sgSLC3A2_3	this work
HDCRISPRv1-sgSLC7A5_1	this work
HDCRISPRv1-sgSLC7A5_2	this work
pSpCas9(BB)-2A-GFP (PX458)	addgene #48138
Lenti-Cas9-2A-Blast	addgene #73310
Lenti-EF1a-CD19-bGH pA-Cas9_T2A_Blast	this work
Lenti-EF1a-CD33-bGH pA-Cas9_T2A_Blast	this work
pENTR221-CD19	DKFZ Vector and Clone Repository
pENTR221-CD33	DKFZ Vector and Clone Repository
pLenti CMV/TO Puro DEST	addgene #17293
pLenti-EF1α-anti-CD19 CAR-PURO	this work
pLenti-EF1α-anti-CD33 CAR-PURO	this work
pLenti-EF1α-αCSPG4 CAR-PURO	this work
pLenti-EF1α-αGD2 CAR-PURO	this work
pLenti-EF1α-αROR1 CAR-T2A-eGFP-PURO	this work
pLKO.1 puro	addgene #8453
pMD2.G	addgene #12259
psPAX2	addgene #12260

6.1.10. Short-hairpin RNA (shRNA) & single-guide RNA (sgRNA)

Table 13. List of shRNA used in this work.

shRNA	Sequence (5' – 3')
shCTRL16	CCGGGCGCGATAGCGCTAATAATTTCTCGAGAAATTATTAGCGCTATCGCGCTTTTTaatt
shCTRL332	CCGGGCGCGATAGCGCTAATAATTTCTCGAGAAATTATTAGCGCTATCGCGCTTTTTaatt
shCSPG4_a	CCGGGACTTCATCTATGTGGACATACTCGAGTATGTCCACATAGATGAAGTCTTTTTTGaatt
shCSPG4_b	CCGGCTTTGCCACTGAGCCTTACAACTCGAGTTGTAAGGCTCAGTGGCAAAGTTTTTTGaatt
shGD3S_b	CCGGCCCATCTCTTTGCTATGACTACTCGAGTAGTCATAGCAAAGAGATGGGTTTTTGaatt
shGD3S_c	CCGGCAACACAAACTGGCTTAATAACTCGAGTTATTAAGCCAGTTTGTGTTGTTTTTTGaatt
shROR1_a	CCGGCTTTACTAGGAGACGCCAATACTCGAGTATTGGCGTCTCCTAGTAAAGTTTTTaatt
shROR1_b	CCGGGCACCGTCTATATGGAGTCTTCTCGAGAAGACTCCATATAGACGGTGCTTTTTaatt

Table 14. list of sgRNA used.

sgRNA	20nt target sequence (5' – 3')
sgPAXIP1_1	ACGGACAGAATCACCCAAGA
sgPAXIP1_2	GAGGTCAAGTATTACGCGGT
sgSLC7A5_1	GCTGTGGGTGGATCATGGAG
sgSLC7A5_2	TACAGCGGCCTCTTTGCCTA
sgPAGR1_2	TAGAGCCGCTGGATTTCGGA
sgPAGR1_3	ATAGAGCCGCTGGATTTCGG
sgATG9A_2	AGCAACCGCATCCTGTGGAT
sgATG9A_3	CTGCAGTCCCGCCTCAACCG
sgSLC3A2_1	GAGTAAGGTCCAGAATGACA
sgSLC3A2_3	AGAGCAGCAGCAGTGCCCAG
sgIPMK_3	CGTGCCCCTCTCGCATCAGG
sgIPMK_4	GGCCGGGCACATGTACGGGA
sgIPPK_1	AGAGCGCTCGGGGTTACCGA
sgIPPK_4	TTACCCTGAGTAGAGATCAA
sgITPK1_2	AGGCTCGTGAGCTCCATGAA
sgITPK1_3	AGGGAGCGGGTCCAGGACGA
sgPOLR2E_1	CATCACACGGGCTCTCATCG
sgPOLR2E_2	ATCGTTGTGGGCCACCAGCA
sgNONTARG_106	GTGACTAGACCCTTACGCGG
sgNONTARG_23	GATCGGCAGGTTACCTCTGA
sgKMT2A_2	CCATTTGCTACGCTACCGGC
sgKMT2A_4	CCACCCTGAGTGCCTTACCA
sgPTDSS1_3	CTGGACATCCTGTTGTGCAA
sgPTDSS1_4	TCCAGCAGAGACCGTAACTA
sgSLC25A26_2	GTGACCGCCAGACCCCATGC
sgSLC25A26_3	CATCTGAAGTGGTTAAGCAG
sgBCS1L_2	GGATGGTGTGGCTTCCACCG
sgBCS1L_4	GCAGAGCCTGGTACTCCTGG
sgMPI_3	TAGGGTGTGCCTGGATGGAC
sgMPI_4	GCCGGAAGCCACACAAGCCC
sgTA6L_1	TCATGAAGCACACCAAACGC
sgTA6L_3	AGTCCTCAACCGTCAGCTTC
sgTSC2_2	GATGACCAGAAGCCCCAGGA
sgTSC2_3	CAGCATCTCATACACACGCG
sgTAF5L_1	ATAGAAGGCATAGAAGCAGA
sgTAF5L_2	CACGTCAAGATGAATATGTA
sgTSC1_3	TATGCTTGTAAACACCTTGG
sgTSC1_4	ACTCCCATAGACCTGCCCTG
sgACVR1B_2	GGAAGCAGAGATATACCAGA
sgACVR1B_4	ACTGCAACAGGATCGACTTG

sgRNA	20nt target sequence (5’ – 3’)
sgNDC1_1	AGACACCACACAGCCAGACA
sgNDC1_4	CAGGCTATATTCCCAAAGCT
sgSEPTIN7_1	TTACCTTCAGCAACACCCCA
sgSEPTIN7_3	CTGGAGAATACAAATCTGTG
sgRPEL1_2	TTCGAAGGCTTTCTACCACA
sgRPEL1_4	GGGTGACCAAAGGTGATGTT
sgAAVS1_1	GCCTCTCCCCATTCAGACCC
sgAAVS1_2	GATGGAGCCAGAGAGGATCC
sgFADD_2	GCGCGTCGACGACTTCGAGG
sgFADD_3	TGACGTTAAATGCTGCACAC
sgTRAF2_1	CAGGAAGCGCCAGGAAGCTG
sgTRAF2_3	GGGGACCCTGAAAGAATACG
sgCASP8_2	CTCCTCCTCTTAGAACCTGC
sgCASP8_4	GGAACTTCAGACACCAGGCA
sgCD46_5	GAGTACAGCAGCAACACCA
sgCD46_3	GATCAGTAGCAATTTGGAG
sgCD151_6	CAGGTACTTGAGGCAAA
sgCD151_16	GCCACAGCCTACATCCTGG

6.1.11. Primers

Table 15. List of primers used.

Primers	sequence (5’ – 3’)
EF1a_CD19_F	GACGCGGGATCCCCACCATGCCACCTCCTCG
NotI_CD19_R	AGGTCTGAAGATCAGCGGCCCTACCTGGTGCTCCAGGTGC
EF1a_CD33_F	GACGCGGGATCCCCACCATGCCGCTGCTGC
NotI_CD33_R	AGGTCTGAAGATCAGCGGCCCTACTGGGTCCTGACCTCTGAGTATTCG
kz_EF1a_R	CATGGTGGGGATCCCGCGTCACGACACCT
NotI_EF1a_F	ACCGCACAGCAAGCGGCCGGGCAGAGCGCACATCGC
HMX2_bGH_F	CTAGATCTTGAGACAAATGGCTGTGCCTTCTAGTTGCCA
HMN2_bGH_R	AGGTCTGAAGATCAGCGGCCCCATAGAGCCCACCGCAT
CD3z_T2A_78_F	TGCAGGCCCTGCCTCCAAGAGGCAGTGGAGAGGGCAGAGGAAGTCTGCTAACAT GCGGTGACGTCGAGGAGAATCCTG
TLCV2_eGFP_R	GCGGCCGCCACTGTGCTGGATATCTTACTTGTACAGCTCGTCCATG

6.2. Methods

6.2.1. Transformation, bacterial culture, and plasmid extraction

Stellar competent cells were used for routine cloning of regular plasmids while Stbl3 competent cells were chosen specifically for cloning any lentiviral vector. The transformation of DNA into bacterial cells started with the frozen stock of competent cells on ice. 1–20 ng of plasmid DNA was added to 50 µL of competent cells and gently mix. The cells were incubated on ice for 15 minutes, then heat shocked at 42°C for exactly 45 seconds, followed by cooling for 2 minutes on ice. 450 µL of SOC medium was added to the mixture and incubate it at 37°C for 1 hour with shaking (~200 rpm). The cells were briefly spun down and retained only 100 µL of the medium. The cells were re-suspended in the remaining liquid and spread onto a LB agar plate with suitable antibiotics. The plates were then incubated at 37°C overnight.

For liquid bacterial culture, a single colony from the LB agar plate of bacteria was picked using a sterile pipette tip and inoculate into 3–5 mL of LB broth with appropriate antibiotics. The culture was incubated at 37°C with constant shaking (220 rpm) overnight. The freshly grown bacterial pellet was collected by centrifugation at 5000 rpm for 15 minutes. The plasmid DNA was then extracted from the bacteria using NucleoSpin Plasmid Mini kit according to manufacturer's instruction. The eluted plasmid DNA was quantified using NanoDrop ND-1000 spectrophotometer. For large-scale plasmid extraction, 50–200 mL of antibiotic-containing LB broth was inoculated using 1:100 dilution of the overnight culture as starter culture. the culture was Incubated at 37°C with shaking until the culture reaches OD600 of 0.6–0.8. Plasmid DNA was extracted from the collected bacterial culture using NucleoBond Xtra Maxi kit or midi kit instead.

6.2.2. Polymerase chain reaction.

DNA sequences were amplified for cloning using polymerase chain reaction (PCR). Primers containing restriction sites were used upstream and downstream of the DNA region of interest to enable sticky-end for ligations into the target backbone or homology regions for multiple component plasmid assembly using In-Fusion cloning kit. The PCR was performed using Q5® Hot Start High-Fidelity 2X Master Mix generally according to the following formula, with adjustment complying with manufacturer's recommendations:

Table 16. General PCR reaction recipe.

Reagents	Amount
Q5® Hot Start High-Fidelity 2X Master Mix	1x
Template DNA	10-200 ng
Forward primer	1.5 µM
Reverse primer	1.5 µM
ddH2O	up to 20 µL or 50 µL per reaction

Table 17. General thermocycler settings for PCR

Steps	Temperature and time	
Initial denaturation	98°C, 3 min	
Denaturation Annealing Elongation	98°C, 30 s 50-72°C, 10s/kb 72°C, 10s/kb	X25-30 cycles
Final elongation Hold	72°C, 2 min 4°C	

The annealing temperature of all primer pairs were predicted using NEB T_m calculator version 1.16.7 or Benchling T_m calculation function. The PCR products were enriched using NucleoSpin Gel and PCR Clean-up kit and examined by gel electrophoresis.

6.2.3. Agarose gel electrophoresis

1- 2% agarose was dissolved in 1x TAE buffer with appropriate heating. Prior to gel casting, the 1x SYBR Safe DNA Gel Stain was added to the warm gel solution (about 50°C). Upon solidification of the gel, it was transferred into Bio-Rad electrophoresis chamber and submerged in TAE buffer. DNA samples were mixed with 6x DNA loading dye and loaded to the wells of the gel. GeneRuler 1 kb DNA ladder or GeneRuler 100 bp DNA ladder were used as reference according to the target DNA size. Electrophoresis was conducted with 100V power supply for 30-60 min. DNA was detected under UV light at 366 nm wavelength.

6.2.4. DNA gel extraction

Chosen DNA fragments were excised from agarose gels on a blue-light illuminator platform and transferred to a reaction tube. DNA extraction from gel was performed with the QIAquick Gel Extraction Kit following the manufacturer's instructions. DNA was eluted with 35 µL nuclease-free water and the DNA concentration determined using NanoDrop 1000 Spectrophotometer.

6.2.5. Oligo annealing, restriction digest and ligation

To build sgRNA expression plasmid for individual gene knockout, complementary oligoes pairs underwent annealing procedures by combining 10 µM of each complementary oligoes in 1x annealing buffer. The mixture was then heated to 98°C, then cooled down at a rate of -1°C/min. The annealed oligos was later inserted into BfuAI-digested HDCRISPRv1 vector by quick ligation.

Plasmid DNA or DNA fragments were digested with desirable restriction endonuclease according to following set-up in general:

Table 18. General recipe for restriction enzyme digestion.

Components	Amount
DNA	1 µg
Compatible 10X NEBuffer	5 µl
Restriction Enzyme	1µl
Nuclease-free Water	to 50 µl

The reaction mixture was incubated at temperature and time ranges recommended for each enzyme. The digested DNA fragments were visualized by gel electrophoresis for confirmation or extracted from gel for further processing.

Purified digestion products were linked through DNA ligation. 50-200 ng of linearized backbone was mixed with a 3-fold molar excess of the insert, or the maximum available quantity if yields were low. The ligation reactions were carried out in a 20 µL volume containing 1x quick ligase buffer and 1U of quick ligase and incubated for 15 minutes at room temperature. Half of each ligation mixture was used to transform competent E. coli strains, following the procedure outlined in section 6.2.1.

6.2.6. Plasmid assembly

For the construction of Lenti-EF1a-CD19-bGH pA-Cas9_T2A_Blast and Lenti-EF1a-CD33-bGH pA-Cas9_T2A_Blast, CD19 and CD33 genes sequence were acquired from DKFZ Vector and Clone Repository in the form of pENTR221 plasmids. The CD19 and CD33 coding DNA sequences were amplified by PCR from the pENTR221 plasmids using EF1a_CD19_F/ EF1a_CD33_F and NotI_CD19_R/ NotI_CD33_R oligos (all primers refer to Table 15). EF1α promoter (by kz_EF1a_R and NotI_EF1a_F oligos) and bGH pA termination sequences were amplified from pSpCas9(BB)-2A-GFP (by HMX2_bGH_F and HMX2_bGH_R oligos). EF1α, CD19, CD33, and bGH pA were assembled in-frame into Lenti-Cas9-2A-Blast to produce final plasmids that harbors the

expression cassettes of Cas9-T2A-Blast together with either CD19 or CD33, using In-Fusion Cloning kits according to the manufacturer's instruction.

To build various CAR expressing plasmid, the coding DNA region of CAR were adopted from various studies:

Table 19. Source and structure of CAR variants used in this work.

CARs	Source	Structure
CD19 CAR	(Ying et al., 2019)	FMC63 scFv-CD8α hinge-CD28TM-4-1BB-CD3ζ
CD33 CAR	(Kenderian et al., 2015)	my96 scFv-IgG4 hinge-CD28TM-4-1BB-CD3ζ
CSPG4 CAR	(Geldres et al., 2014)	763.74 scFv-hinge CH_2CH_3 of IgG1- CD28TM-CD28-CD3ζ
GD_2 CAR	(Straathof et al., 2020)	K666 scFv-hinge CH_2CH_3 of IgG1- CD28TM-CD28-CD3ζ
ROR1 CAR	(Hudecek et al., 2013)	R12 scFv- CD28TM-CD28-CD3ζ

A homology region was attached to 5' and 3' ends of coding DNA sequence of the above CARs and the resulting DNA sequences were synthesized with the IDT gBlocks service. pLenti CMV/TO Puro DEST was digested by NdeI and EcoRV restriction enzymes and subsequently extracted for the larger fragment. The CAR DNA fragments were then inserted in-frame into the digested pLenti backbone along with a EF1α promoter using In-Fusion cloning kit to produce different pLenti-EF1α-CAR-PURO plasmids. For ROR1 CAR specifically, an additional GFP fragments with preceding T2A sequence and homology regions on both ends were cloned from pSpCas9(BB)-2A-GFP using CD3z_T2A_78_F and TLCV2_eGFP_R oligos. The GFP fragment alongside EF1α and ROR1 CAR fragments were fused with pLenti backbone to create the pLenti-EF1α-αROR1 CAR-T2A-eGFP-PURO using In-fusion cloning kits.

To produce the series of plasmid for sgRNA expression, HDCRISPRv1 plasmid was digested by BfuAI endonuclease. The large, linearized backbone was extracted after gel electrophoresis. "CACCG" nucleotides was added to the 5' of sgRNA forward sequence, at the same time, "AAAC" was added to the to the 5' of sgRNA reverse sequence. The modification gives the annealed oligos 2 overhangs that directly bind to the sticky ends of the linearized backbone of HDCRISPRv1, which was joined by simple ligation reaction.

6.2.7. Transfection and transduction

Plasmid transfection was performed using TransIT-LT1 Transfection Reagent for HEK293T and jetOPTIMUS transfection reagent for A375 cells. The general recipe for transfections of cells is as follows:

Table 20. Recipe Transduction mix for different culture vessels.

reagents	Amount in different culture vessels		
	15 cm dish	6-well plate	24-well plate
vector	20 µg	2.5 µg	0.5 µg
psPAX2	10.5 µg	1.3125 µg	0.2625 µg
pMD2.G	6.3 µg	0.7875 µg	0.157 µg
Opti-MEM	500 µL	250 µL	50 µL
TransIT-LT1	112.5 µL	7.5 µL	1.5 µL
Opti-MEM	500 µL	250 µL	50 µL

Table 21. Recipe of transfection mix using jetOPTIMUS

Reagents	1x reaction on 96 well microplate
vector	0.1 µg
dilution buffer	6.25 µL
jetOPTIMUS	0.11 µL
dilution buffer	6.25 µL

Cells were plated 24 hours before the transfection. The following day, the culture medium was refreshed after a single PBS wash. All reagents were equilibrated to room temperature prior to use. Plasmid DNA and transfection reagents were separately diluted in serum-reduced Opti-MEM medium. The two solutions were combined and mixed gently by inverting the tube. Mixtures were incubated for 15 minutes at room temperature and then added dropwise to the cells. Cells were collected 48 hours for downstream applications.

To perform transduction, it was necessary to package the lentivirus first with HEK293T cells. 10 million HEK293T cells were seeded onto each 15 cm dish on the first day. On the next day, psPAX2, pMD2.G, and the vector of interest were combined and transfected into HEK293 cells using the same procedure above for the 15 cm dish scale. On 24 hours post- transfection, the medium of the HEK293T cells was replaced with fresh complete IMDM medium. On 48 hours post-transfection. The supernatant of the HEK293T cells was collected and filtered through 0.45 μM PES filter. The filtered viral supernatant was concentrated either chemically with Lenti-x concentrator or physically by ultra-centrifugation.

For the Lenti-X concentrator, 3 parts of the viral supernatant were mixed with 1 part of the concentrator. The mixture was incubated overnight. On the next day, the mixture was centrifuged at 1500 x g for 45 min at 4°C. The resulting pellet was resuspended in PBS of 1/10 to 1/25 of original volume. As for ultra-centrifugation method, the viral supernatant was centrifuged at 96000 x g for 2 hours at 4°C. The virus pellet was resuspended in PBS of 1/50 of original volume. The enriched virus solution was aliquoted and store at -80°C until use.

To titrate the virus, 0.5 million cells of interest were seeded on each well of a 6-well plate and simultaneously mixed with different dilutions of virus solution in the presence of 8 μg/mL polybrene. The infected cells were allowed growth for 24 hours, followed by selection of corresponding antibiotic resistance. Puromycin (Puro) was used at 2 ug/mL whereas blasticidin (Blast) was used at 15 μg/mL. The selection period ranges from 2 to 7 days depending on the choice of antibiotics. Upon selection, the remaining viable cells were enumerated in all countable conditions. The viral titer was calculated in transforming units per mL (TU/mL) according to the following equation:

$$viral\ titer\ (TU/mL) = -\ln(1 - \frac{cell\ no.\ in\ the\ sample\ with\ Puro}{cell\ no.\ in\ the\ sample\ without\ Puro})$$

With the precise viral titer, melanoma cells were infected at a MOI of 1 in the presence of 8 μg/mL polybrene to establish corresponding cells lines, while T cells were specifically infected at a MOI of 50 without polybrene to produce different CAR-T cells.

6.2.8. Cell lines and culture

A375 (American Type Culture Collection, ATCC, CRL-1619) and human embryonic kidney cells HEK293T (ATCC CRL-11268) were acquired from ATCC before the commencement of this project. The human melanoma cell line WM793 was a gift to our group from Meenhard Herlyn (The Wistar Institute Melanoma Research Center, Philadelphia, USA), also before the start of this project. A375-CD19-Cas9 and A375-CD33-Cas9 were generated in this work by over-expression of Cas9 together with either CD19 or CD33 antigen. Clones have been isolated from two 2 lines, but the polyclonal population was also preserved with enrichment on respective antigens by FACS on top of blasticidin selection. WM793-Cas9 and A375-Cas9 were created using virus packaged from Lenti-Cas9-2A-Blast in this work. All the knockout cell lines were generated in-house from A375-Cas9 and WM793-Cas9 cells with or without CD33 over-expression, and the use of corresponding sgRNA expression plasmids. Primary human $CD8^+$ T cells were freshly isolated from buffy coats of healthy donors. The T cells were then infected with virus with different CAR expression sequences. The CAR-T cells produced were further enriched by sorting for high CAR populations.

All A375, WM793 and their derivative cell lines were maintained in DMEM medium + 10% FBS. HEK293T were maintained in IMDM + 10% FBS. At each expansion cycler, these cells were sub-cultured at 80%-90% confluency. These cells were detached from culture vessels by 0.25% Trypsin/EDTA solution after a PBS wash.

The primary T cells and newly generated CAR-T cells were cultured in X-VIVO 15 media supplemented with 5% human AB serum and 55 μM β-mercaptoethanol in non-TC treated vessels. The T cells were closely monitored and maintained at density not more than 3 million cell per mL medium. At each subculturing, The T samples were diluted to 0.5x10^6 cells/mL and replenished with 300 U/mL IL-2 and 3.12 μL ImmunoCult™ Human CD3/CD28 T Cell Activator for growth stimulation.

All cells used in this work were maintained in 37°C CO_2 incubator. The cells were cryo-preserved in NutriFreez D10 medium, by slowly cooling to -80°C, followed by transfer to liquid nitrogen tanks for long-term storage.

6.2.9. CD8+ T cell isolation, activation, and transduction

All T cells used in this work were isolated from buffy coat samples of healthy donors by negative immunoselection. Table 22 below lists all buffy coats used in this study.

To begin with, 10 mL of buffy coat was diluted with 2 parts of PBS. Then, 15 mL of Lymphoprep was transferred to SepMate tube, followed by addition of diluted buffy coat sample on top of the Lymphoprep in the tube. The tube was centrifuged at 1200 x g for 20 minutes at room temperature. The mononuclear cell layer was then removed from the tube and washed once with 40 mL PBS + 2% FBS. The cell pellet was resuspended in 2 mL of RBC lysis buffer and incubated at 4°C for 10 min. The processed peripheral blood mononuclear cells (PBMCs) were washed again with 10 mL PBS + 2% FBS. The PBMCs were negatively selected for $CD8^+$ T cells using EasySep™ Human $CD8^+$ T Cell Isolation Kit following manufacturer's instructions. 0.25 million isolated T cells in 0.5 mL of complete growth medium proceeded further to be activated. The fresh T cell samples were stained for CD3/CD4/CD8 with conjugated monoclonal antibodies and analyzed with BD LSRFortessa or FACSCanto II flow cytometers to determine the cell purity by enumerating the fraction of $CD8^+$ T cells.

For T activation, the CD3/CD28 Dynabeads were prepared according to manufacturer's instructions. The bead to cell ratio used was 1:1, resulting in 0.25 million being added to each T cells sample. In addition, 300 U/mL IL-2, 10 ng/mL IL-7 and 10 ng/mL IL-15 were also added to the T cell culture.

After incubating at 37°C for 24 hours, the cells were harvested and stripped clean of Dynabeads by magnetic separation. The viruses that contain different CAR expression sequences were added to the T cells at a MOI of 50. The infected T cells were allowed

to grow for 7 days before being examined for surface CAR expression using corresponding anti-F(ab')$_2$ antibody to the scFv's origin or by checking the endogenous GFP signals.

Table 22. List of buffy coat samples used in this work.

internal reference	sample ID	Blood type	Rh factor	Volume (mL)
D13	D70420907018	O-	-	25
D19	D70420292015	A+	+	45
D20	D70320129539	A+	+	50
D21	D70320962851	O+	+	50
D22	D70420910642	O-	-	50
D23	D70320962847	A+	+	50
D26	D70420396895	A+	+	50
D27	D70420398421	O+	+	25
D38	D70420131244	O+	+	50
D42	D70320245515	A+	+	50

6.2.10. Cas9-mediated knockout efficiency assay

To assess the Cas9 function in established cell lines, A375 -Cas9, A375-CD19-Cas9, A375-CD33-Cas9, and WM793-Cas9 were transduced with virus carrying sgCD46 and sgCD151 expression sequences. 24 hours after the infection, the cells were selected by PURO for 2 days and further expanded for a week afterwards. The cells were then stained with 1:40 dilution of APC-anti-human CD46 Antibody and APC-anti-human CD151 Antibody to examine the degree of gene knock out.

6.2.11. Cell proliferation assay

Live cell imaging with time-lapse was conducted to evaluate the proliferation abilities of melanoma cells using the IncuCyte ZOOM system paired with IncuCyte Basic Software. Specifically, melanoma cells were plated in clear flat-bottom 96-well plates in

300 µL of culture medium per well, with 3 technical replicates, and images were captured every 2 hours using a 10x objective. For the proliferation assessment, cell confluence was measured from 4 images per well. The cell confluence was used as a proxy for estimation of proliferation rate. The doubling time of cells were calculated as follows:

$$doubling\ time = \frac{Time * \ln 2}{\ln \frac{confluence\ at\ the\ beginning}{confluence\ at\ the\ end}}$$

6.2.12. T cell cytotoxicity assay

A confluency-based end point measurement was performed using the IncuCyte ZOOM system to assess CAR-T cells' cytotoxicity on A375 cells. The experiment started with seeding 10,000 cells of different A375 cell lines on clear flat bottom 96-well microplate with 250 µL of culture medium per well. 24 hours later control T cells or CAR-T cells were resuspended in complete DMEM growth medium and added onto the A375 cell culture at different Effector-to-target (E: T) ratio, ranging from 2:1 to 8:1. The T cells and A375 cells were co-cultured for 24 hours. The T cells were removed by washing with complete growth medium for 3 times at the end of the co-culture period. The confluency of A375 in each well was captured by the IncuCyte ZOOM system. The confluency was used as a proxy to estimate the percentage of specific lysis, which was calculated as follows:

$$\%\ specific\ lysis = 1 - (\frac{mean\ confluency\ of\ \ CAR - T\ cells\ coculrure}{mean\ confluency\ of\ \ control\ T\ cells\ coculrure})$$

6.2.13. Genome-wide CRISPR-mediated loss-of-function screens

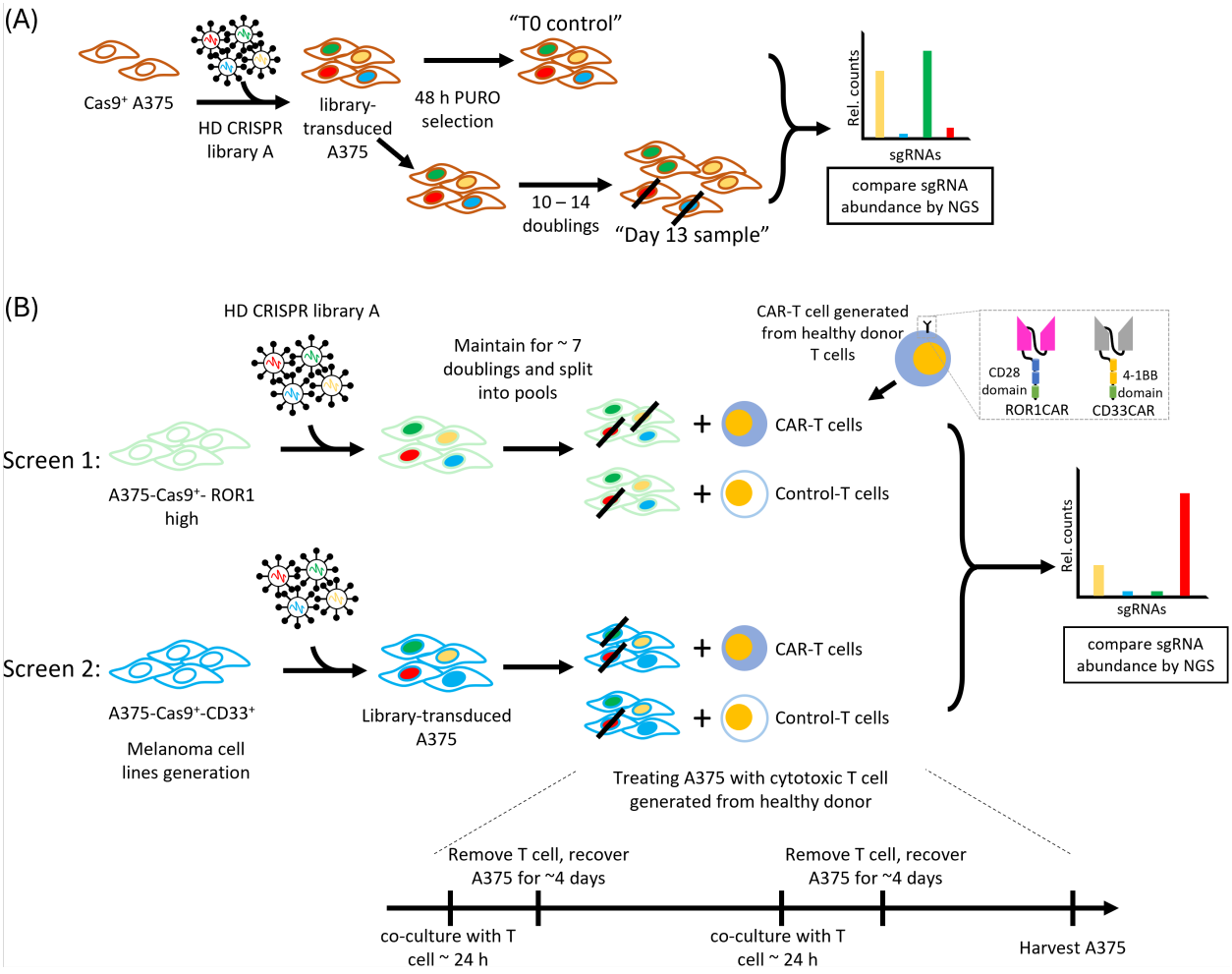

Figure 4. Design and Workflow of the CRISPR-mediated screens in this work.

Both screens started by transducing the genome-wide Heidelberg CRISPR sgRNA library A into A375 cells. (A) In A375 essential gene dropout screen immediately after Puro selection, a fraction of cells was harvested and designated as the "T0 control" sample. The remaining pool of cells continued to expand for several doublings until being collected as the "Day13 sample". Gene essentiality was inferred from comparing the sgRNA abundance at the 2 time points by deep sequencing. (B) As for A375-T cell co-culture screen, the infected A375 continued to expand for several doublings and split into several pools of cells, each to be treated by CAR-T cells or normal T cells generated from different donors. The T cells were removed after 24 hours of co-culture and A375 cells were allowed to recover for 4 days. The procedure was repeated once more before harvesting the sample for deep sequencing. Differential mutation fitness can be inferred from evaluating sgRNA abundance under different treatments.

Two different genome-wide CRISPR-mediated screens in which genes were perturbed by LOF mutations were implemented in this study. The set up and workflow of both types of screens were illustrated in Figure 4. The essential gene screen began with transducing A375 cell lines with the lentivirus packaged from Heidelberg CRISPR sgRNA library A at a MOI of 0.25 with 8 µg/mL of polybrene in the growth medium in 5-layer multi-flasks. The sgRNA library targets 18,913 genes using 74,987 sgRNAs with reported high on-target and low off-target activity based on phenotype in previously published screens (Henkel et al., 2020). 1 day after infection, the medium was replaced with complete growth medium containing 2 µg/mL Puro. 48 hours later, the medium was changed back to normal complete growth medium. A fraction of the transduced A375 cells was frozen as dry cell pellet at -20°C and designated as “day 0” samples. The culture continued to expand for several doublings until the A375 cells were harvested as “day 13” samples.

As for the co-culture screens, the transduced A375 cells proceeded with the same puro selection and expansion. A treatment scheme, in which control T cells and CAR-T cells prepared from different donors were added to the divided pooled of A375 cells at 0.5 or 1 effector-to-target (E:T) ratio. The treatment lasted for 24 hours before T cell being removed and the A375 recovered for 3 days. Then, the treatment scheme repeated once again.

All samples were eventually collected and frozen as dry cell pellet at -20°C. At any given time of the 2 experiments, including cell seeding, infection, post-Puro selection and sample collection, a minimum 300-fold coverage of the sgRNA library size was strictly maintained to minimize the loss of sgRNA representation.

6.2.14. library preparation and deep sequencing

gDNA of the previously collected screen samples was extracted with QIAamp DNA Blood Maxi Kit according to manufacturer’s instructions. The purified gDNA was further concentrated by ethanol precipitation. In brief, mix gDNA and absolute ethanol in 4:9

ratio (v/v) and add NaCl at a final concentration of 0.2 M. The well-mixed content was then centrifuged at 13,000 rpm for 15 minutes at 4°C. The supernatant was then aspirated, and 500 µL 70% ethanol was added to the pellet. The centrifugation was repeated once, followed by aspirating the supernatant. The pellet was air-dried and subsequently dissolved in nuclease free water at 1 µg/µL. The gDNA was quantified using Qubit dsDNA HS Assay Kit, following manufacturer's instructions.

PCR was performed using specific indexing primers (Table 23) to label the samples, which are listed in Table 23. Multiple reactions of the same sample were prepared to yield 100-fold coverage of the HD CRISPR sgRNA Library A. The number of reactions were adjusted according to the cell lines' genome size.

Table 23. List of Illumina primers for indexing sequencing samples.

Universal forward primer:	**5' – Primer Sequence [Universal adaptor – U6 promoter-spacer binding]– 3'**
F_TrueSq_HDCR_lib	aatgatacggcgaccaccgagatctacactctttccctacacgacgctcttccgatct tcttgtggaaaggacgaaacaccg
Reverse primer:	**5' – Primer Sequence [i7 adaptor – INDEX – spacer – plasmid binding] – 3'**
R1_Sq_HDCR_lib	caagcagaagacggcatacgagat **CGTGAT** gtgactggagttcagacgtgtgctcttccgatc tcttttaaaattgtggatgaatactgccattt
R2_Sq_HDCR_lib	caagcagaagacggcatacgagat **ACATCG** gtgactggagttcagacgtgtgctcttccgatc tcttttaaaattgtggatgaatactgccattt
R3_Sq_HDCR_lib	caagcagaagacggcatacgagat **GCCTAA** gtgactggagttcagacgtgtgctcttccgatc tcttttaaaattgtggatgaatactgccattt
R4_Sq_HDCR_lib	caagcagaagacggcatacgagat **TGGTCA** gtgactggagttcagacgtgtgctcttccgatc tcttttaaaattgtggatgaatactgccattt
R6_Sq_HDCR_lib	caagcagaagacggcatacgagat **ATTGGC** gtgactggagttcagacgtgtgctcttccgatc tcttttaaaattgtggatgaatactgccattt
R7_Sq_HDCR_lib	caagcagaagacggcatacgagat **GATCTG** gtgactggagttcagacgtgtgctcttccgatc tcttttaaaattgtggatgaatactgccattt
R8_Sq_HDCR_lib	caagcagaagacggcatacgagat **TCAAGT** gtgactggagttcagacgtgtgctcttccgatc tcttttaaaattgtggatgaatactgccattt
R9_Sq_HDCR_lib	caagcagaagacggcatacgagat **CTGATC** gtgactggagttcagacgtgtgctcttccgatc tcttttaaaattgtggatgaatactgccattt

R12_Sq_HDCR_lib	caagcagaagacggcatacgagat **TACAAG** gtgactggagttcagacgtgtgctcttccgatc tcttttaaaattgtggatgaatactgccattt
R13_Sq_HDCR_lib	caagcagaagacggcatacgagat **TTGACT** gtgactggagttcagacgtgtgctcttccgatc tcttttaaaattgtggatgaatactgccattt
R15_Sq_HDCR_lib	caagcagaagacggcatacgagat **TGACAT** gtgactggagttcagacgtgtgctcttccgatc tcttttaaaattgtggatgaatactgccattt
R23_Sq_HDCR_lib	caagcagaagacggcatacgagat **CCACTC** gtgactggagttcagacgtgtgctcttccgatc tcttttaaaattgtggatgaatactgccattt
R25_Sq_HDCR_lib	caagcagaagacggcatacgagat **ATCAGT** gtgactggagttcagacgtgtgctcttccgatc tcttttaaaattgtggatgaatactgccattt
R27_Sq_HDCR_lib	caagcagaagacggcatacgagat **AGGAAT** gtgactggagttcagacgtgtgctcttccgatc tcttttaaaattgtggatgaatactgccattt

Table 24. PCR recipe for amplifying sgRNA target sequence from NGS samples.

reagents	amount
2x Kapa HiFi HS RM	25 µL
10 µM Forward primer	1.5 µL
10 µM Reverse primer	1.5 µL
50 mM Mg2+	5 µL
Genomic DNA	For 2.5 µg per reaction
water	Up to 50 µL
Total	50 µL

Table 25. Thermocycler program for amplifying sgRNA target sequence from NGS samples.

Temperature (°C)	Duration	cycles
95°C	3 min	1
98°C	20 sec	30
68°C	15 sec	
72°C	15 sec	
72°C	1 min	1

PCR products were purified using the QiaQuick PCR purification kit according to the manufacturer's instruction. Gel electrophoresis of 2% agarose gel was then performed on the purified PCR products (section 6.2.3). The sharp DNA bands at roughly 300 bp were excised and then extracted for the DNA amplicons using the QiaQuick Gel

Extraction kit according to the manufacturer's instruction. The final DNA quantity was measured again with the Qubit instrument.

The purified DNA quality was further inspected using Agilent High Sensitivity DNA Kit paired with Bioanalyzer instrument according to manufacturer's instructions. On the electropherogram obtained Bioanalyzer, A sharp peek of DNA around size 297 bp represented a high quality of DNA, signaling the entry to subsequent deep sequencing process, otherwise the library preparation would have been discontinued, and samples would have been re-prepared. The DNA samples were then mixed at equimolar ratio, and the overall concentration was adjusted to 10 nM to create the multiplexed sequencing library.

The amount of adaptor sequence with Truseq I7 adaptor in the multiplexed library was measured using the KAPA library quantification kit to quantify the exact number of amplicons that can be sequenced. This provided an important metric for accurate dilution of the multiplexed library and subsequently the precise loading onto the Illumina flow cell. Together with the DNA Standards 1-6 for Illumina qPCR Library, multiple qPCR reactions, with technical triplicates and 2-fold dilutions of the multiplexed library, were prepared and run the reaction according to the following on a 384-well PCR plate:

Table 26. qPCR recipe and LightCycler program for quantifying readable amplicons.

Reagents		**Amount for 1 reaction**	
KAPA SYBR FAST qPCR Master Mix (2x) + Primer premix (10x)		12 µL	
water		4 µL	
DNA sample /Standard		4 µL	
Total		20 µL	
qPCR program			
initial activation / denaturation	95 °C	5 min	
Denaturation	95 °C	30 sec	35 cycles
Annealing/ extension / data acquisition	60 °C	45 sec	

Absolute quantitation method, against the 452 bp DNA Standard provided, was used for Cq value calculation, which were in turn used to plot the standard curve and estimate the sample concentration using the official data analysis template. The sequencing reaction was performed with NextSeq 500/550 Hi Output KT v2.5 (75 CYS), and a sequencing primer (SeqPrimer_HDCRISPR, CCGATCTTCTTGTGGAAAGGACGAAA-CACCG). The sequencing reaction was terminated after 20 cycles. Sequencing result was output as Fastq files containing 20-nt sgRNA sequence reads and corresponding index reads.

The raw data was processed using MAGeCK package to obtain the raw count of all sgRNA (Li et al., 2014). For the essential gene screen, the sgRNA counts were normalized and the sgRNA fold-change between sample and plasmid library was calculated. The sgRNA fold-change was used to classify genes into core-essential and non-essential categories using Bayesian analysis of gene essentiality (BAGEL) at 5% false discovery rate (FDR) (Hart & Moffat, 2016). For the co-culture screen, the mapped data was processed similarly to obtain the sgRNA fold-change. The data was subsequently processed further by calling the differential gene enrichment and the statistical significance of gene candidates using LIMMA package on R. Additional analysis including gene set enrichment analysis and gene ontology were performed using fgsea and clusterprofiler packages.

6.2.15. T cell degranulation assay

T cells were co-cultured with A375 cells at a 1:1 ratio on a 96-well U-bottom plate in total volume of 80 µL. BV785 anti-human CD107a Antibody was first diluted 1:10 in complete DMEM medium. 10 µL of the diluted antibody solution was added to all samples. The plate was spun at 300 rpm for 1 min, followed by incubation for 30 min in the 37°C CO_2 incubator. GolgiPlug was diluted 1:100 in complete DMEM medium added 10 µL to each sample without disturbing the pellet. The cells were then incubated for 4

hours at 37°C CO_2 incubator. After incubation, cells were collected, washed with PBS, and analyzed with a flow cytometer.

6.2.16. Annexin-V assay

Annexin-V assay was conducted to assess the extent of apoptosis and necrosis in melanoma cells after given a treatment. The cells were harvested, washed twice with cold PBS, and resuspended in 1X Annexin V binding buffer. Annexin V-FITC and propidium iodide were added according to the manufacturer's protocol and incubated at room temperature for 15 minutes in the dark. Samples were immediately analyzed by flow cytometry, and apoptotic cells were identified as Annexin-V+/PI− (early apoptosis) and Annexin-V+/PI+ (late apoptosis).

6.2.17. Drug/cytokine/conditioned medium treatments

The T cell-conditioned medium was obtained by co-culturing 5 million CAR-T cells with wild type A375 cells at a E:T ratio of 1:1 for 24 hours. The conditioned medium was clarified by centrifugation to remove T cells and cell debris. The chemical compounds were purchased from MedChemExpress or Selleckchem, while the cytokines were purchased from ImmunoTools.

The drug treatment started with seeding of melanoma cells in 96-well microplate for cytokine group and 24-well microplates. The drugs were added directly to the growth medium of the cells in accordance with the dosage specified in Table 27. In case of conditioned medium, the growth medium is completely replaced by the conditioned medium. The cells were then incubated for 2 days and then followed by an annexin-V assay, which refers to section 6.2.16, to assess the extent of A375 cell apoptosis.

Table 27. Dosage and function of drugs used in this study.

Reagent	Cat. No.	Solvent	EC50	Working conc.	Function
Rapamycin	BML-A275-0005	DMSO	1 nM	4 nM	inhibit mTOR, activate autophagy
MHY1485	MCE-HY-B0795	DMSO	10 μM	40 μM	activate mTOR, inhibit autophagy
JPH203	MOLN-M10188	DMSO	4.1 uM	30 uM	LAT1-inhibitor
V-9302	V-9302	water	9.6 uM	40 uM	LAT1-inhibitor
BCH	5027/50	water	0.1 mM	0.4 mM	activate mTOR, inhibit LAT1
TNF-α	11343015	water	2.5 ng/mL	10 ng/mL	induce apoptosis
IFN-γ	11343534	water	0.6 ng/mL	2.5 ng/mL	induce apoptosis
sFas Ligand	310-03H	water	10.0 ng/ml	40 ng/mL	induce apoptosis
TRAIL	310-04	water	5 ng/ml	20 ng/ml	induce apoptosis

6.2.18. Immunophenotyping

T cells or melanoma cells were harvested by centrifugation or accutase-mediated detachment. After collecting, the cells were washed twice with PBS. Then, the cells were stained in fluorophore-conjugated primary antibody solution (1:25 to 1:100 dilution) at 4°C for 30 minutes in the dark. After incubation, the cells were washed twice again with PBS and fixed in 4% paraformaldehyde and store at 4°C prior to being analyzed with a BD LSRFortessa flow cytometry.

6.2.19. Western blot

To obtain protein samples for analysis, the cells on 6-well plates were washed twice in 2mL ice-cold PBS. Complete lysis buffer was prepared by dissolving 1 tablet of cOmplete protease inhibitor cocktail and 1 tablet of cOmplete PhosSTOP in 10 mL of RIPA Lysis Buffer. 400 μL Complete Lysis Buffer was added onto the cells on each well. The cells were scraped off the culture plate completely using cell scrapers. The protein lysates by incubating with rotational motion at 4 °C for 20 min to ensure complete lysis, followed by clarification by centrifuging with 20000 x g force at 4°C.

Pierce bicinchonic acid Protein Assay Kit was used to determine protein concentrations according to the manufacturer's instructions. The absorbance at 562 nm was measured with a Mithras LB 940 Multimode Microplate Reader. Protein concentrations of each sample were then inferred from the standard curve calculated from BSA standards.

Sample proteins were denatured in 1x Laemmli buffer while heated to 95 °C for 5 minutes. 10 µg of denatured protein were loaded onto Bolt 4-12% Bis-Tris Plus Protein Gel. SDS-PAGE and MOPS buffer were used to separate proteins alongside a PageRuler Prestained Protein Ladder, running at 80 V for 10 minutes, then at 180 V for 32 minutes or until the blue loading dye exited the gel. Proteins were subsequently transferred to methanol-activated polyvinylidene difluoride membranes via wet blotting in the transfer buffer with 10% methanol for 60 minutes at 20 V. Transfer quality was visualized using Ponceau S solution.

After fully destaining the membranes in TBST, they were blocked with 5% skim milk/TBST or 5% BSA/TBST, according to different antibodies' requirement, for 30 minutes at room temperature. The membrane was then incubated with primary antibodies at 4 °C overnight or 1 hour at room temperature on a Roller Falcon Tube Mixer, followed by washing three times in TBST for 5 minutes each on a shaker. The blot is then incubated with horseradish peroxidase-conjugated antibodies for 1 hour at room temperature and washed again as described. All antibodies were diluted in 5% skim milk/TBST or 5% BSA/TBST. Membranes were then treated with enhanced chemiluminescence (ECL) substrates, and HRP-generated light signals were detected in BioRad ChemiDoc Imaging System.

6.2.20. Statistical analysis

Statistical analysis was conducted using GraphPad Prism v9 or R. Quantitative data was gathered from a minimum of three independent experiments and are expressed as mean ± standard deviation (sd) for each experiment unless specified otherwise.

Statistical significance was assessed with an unpaired, two-tailed Student's t-test, applying Welch's correction, when necessary, or ANOVA (Welch's ANOVA in case of unequal variance across samples) followed by a Tukey post-hoc test (Games-Howell *post hoc* test for Welch's ANOVA), as specified in the figure legends. In case of survival analysis, log-rank test was used to evaluate the difference between different patient cohorts. A p value below 0.05 was deemed statistically significant, with significance levels denoted as follows: ns ($p > 0.05$), * ($p < 0.05$), ** ($p < 0.01$), *** ($p < 0.001$), and **** ($p < 0.0001$).

7. Result

7.1. CRISPR fitness screen for gene essentiality

To identify essential genes in A375 which would result in cell death independent of immune cell treatment, I have conducted a whole-genome essential gene dropout screen as a starting point to define the core set of genes necessary to the survival of A375 melanoma cells and their derivative cell lines. Other researchers have already performed CRISPR screens for identifying gene essentiality in A375 (Hart et al., 2015). However, it was done using the TKO sgRNA library which has different composition from Heidelberg CRISPR sgRNA library. Therefore, the experiment was conducted to demonstrate the performance of Heidelberg CRISPR library in terms of fitness screens. LOF mutations on essential genes inherently cause A375 cells to gradually disappear from the pool of all mutations, so they were subsequently omitted from the final list of gene candidates obtained from the co-culture screen as they would cause the cell to vanish on its own regardless of T cells' presence, marking these mutations less relevant in this context. With this knowledge, I was able to focus exclusively on the candidates that cause significant phenotypic changes to T cell cytotoxicity or melanoma's defense mechanism.

7.1.1. Characterization of melanoma cells lines

To generate CAR-T cell targetable melanoma cell lines for the screens, the A375 wild-type cells were transduced to overexpress cas9 in conjunction with CD19 or CD33 proteins that later served as cell surface antigens to be detected by corresponding CAR-T cells. These 2 antigens were chosen based on the proven potent efficacy as exhibited by CD19-/CD33-CAR T cells on B-cell lymphomas and acute myeloid leukemia respectively (Kenderian et al., 2015; Ying et al., 2019).

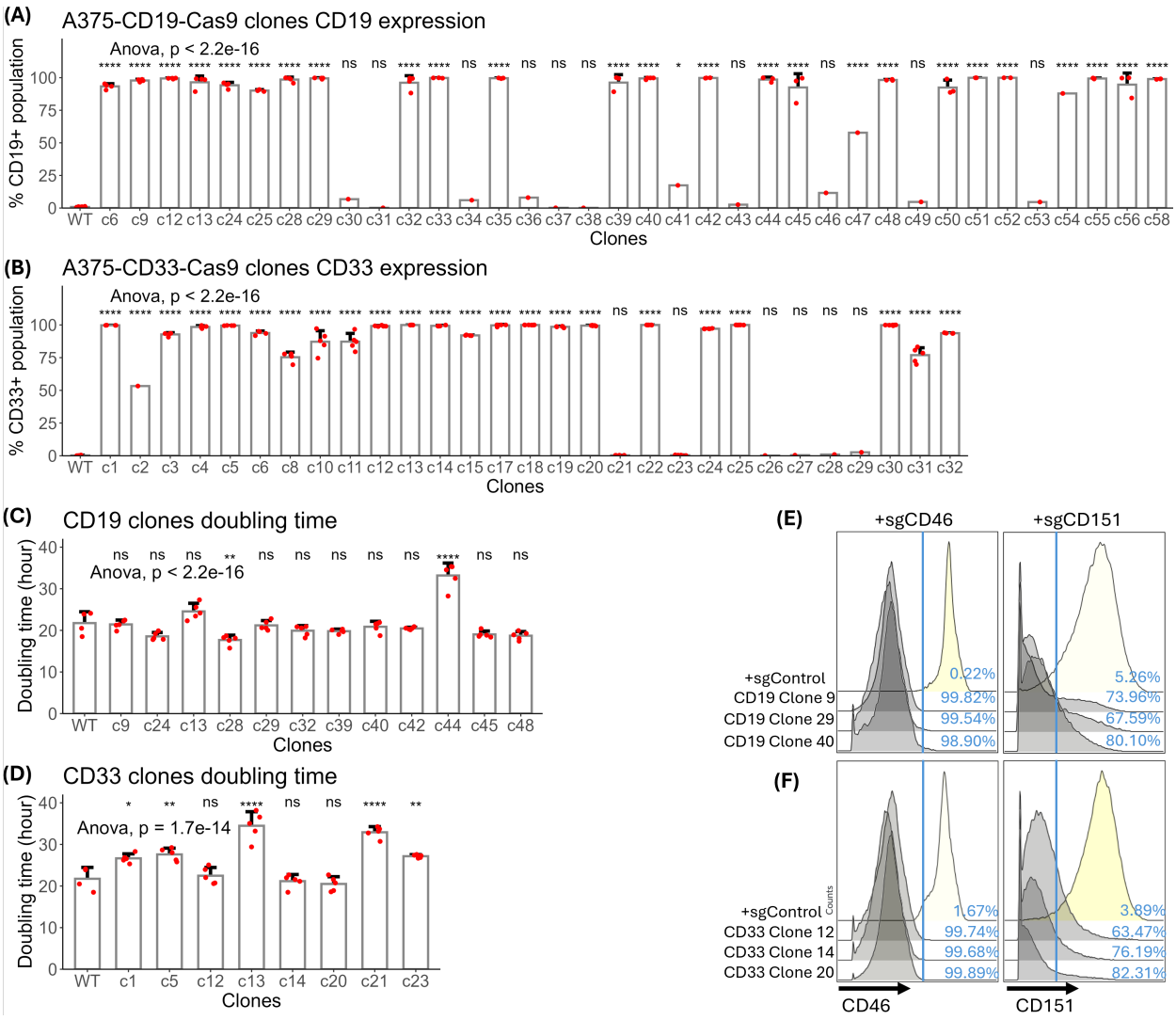

Figure 5. Antigen expression, Cas9 KO efficiency, and doubling time of A375 cell lines.

(A, B) CD19 or CD33 expression on isolated single-cell clones of respective cell lines. The WT A375 cells were infected by lentivirus and selected in 15 µg/mL Blasticidin for 2 weeks. The new cell lines were then FACS-sorted into 96-well plates at 0.5 cell/well. After expansion, the clones were fluorescently labeled for surface CD19 or CD33 expression. Red dots represent each replicate. The data is reported in mean ± sd. Statistical significance was computed from ANOVA, coupled with Tukey's tests. **(C, D)** Doubling time of selected A375 clone compared to that of WT cells. A375 cells were cultured on 96-well microplate and imaged in a time-lapse manner using IncuCyte Zoom system over the course of 5 days at a 2h interval. The captured cell confluency over time was converted into doubling time of cells as described in section 6.2.11. The data is reported in mean ± sd. Statistical significance was computed from ANOVA, coupled with Tukey's tests. **(E, F)** Cas9 editing efficiency of modified clones. Clones of A375-CD19/CD33-Cas9 cell lines were transduced to express CD46-/CD151-targeting sgRNAs or control sgRNAs. After selection in 2 µg/mL Puro selection for 48 hours, the A375 clones were stained for surface CD46 and CD151 protein and fixed in 4% PFA, before analyzing with a flow cytometer. Number represents the percentage of cells with a loss on CD46 and CD151 expression.

To ensure uniform detection of the surface antigen by CAR-T cells and Cas9 performance in the screens, homogeneous clones were isolated from the polyclonal population. Singlet cells from the $CD19^{high}$ or $CD33^{high}$ fractions of the infected cells lines were sorted by BD FACSAria Fusion flow cytometers into 96-well microplates at a density of 0.5 cell/well. 36 out of 60 CD19 clones survive while 32 out of 40 CD33 clones survived. The single-cell clones were stained for surface CD19/CD33 expression (Figure 5A&B). 12 CD19 clones and 8 CD33 clones were selected for their high surface marker expression.

To avoid survival bias, the A375 clones were then examined for their proliferation rate under the influence of the two transgenes (Figure 5C&D). The clones were imaged by IncuCyte Zoom system in the time-lapse mode. Cell confluency taken at each time point was converted into doubling time for each clone. Only those with similar doubling time to the wild type cells were included, thus lowering the chance of transgenes A375 cells altering the overall proliferation capacity.

Lastly, to confirm an intact Cas9 function, three clones from each cell line were further assessed by a surface CD46/CD151 KO assay. The Cas9-editing efficiency of the selected clones was approximated by the percentage of cell population underwent CD46 and CD151 KO. The selected clones exhibit almost complete KO with sgRNAs targeting CD46, whereas CD151 sgRNAs achieved KO for majority of cells (Figure 5E&F).

Based on the above quality, clone 9, 29, and 40 of A375-CD19-Cas9, and clone 12, 14, 20 of A375-CD33-Cas9 were included. The clones were separately combined to produce 2 polyclonal cells lines and screened as 2 populations.

7.1.2. Quality of the essential gene screen

The screening experiment was conducted as described in the method section 6.2.13 using the pseudo-bulk A375-CD19-Cas9 and A375-CD33-Cas9. In total, 2 replicates were performed for each cell line. The obtained reads were mapped, using MAGeCK

package, to the Heidelberg CRISPR sgRNA library to enumerate the counts each sgRNA across all samples. Quality control measures on the raw data were implemented to confirm the validity of the samples for further analysis. Table 28**Error! Reference source not found.** summarized the basic metrics of raw sgRNA data in all samples after sequencing read mapping.

Table 28. Basic metrics of sgRNA count distribution of dropout screen samples.

sample	10^{th} quantile	90^{th} quantile	Skew ratio	Zero-counts	Coverage
Plasmid library	242	1460	6.03	42	779
R1-T0d-CD19	103	1004	9.75	375	497
R1-T0d-CD33	81	836	10.3	475	410
R1-T13d-CD33	103	1888	18.3	585	864
R1-T13d-CD19	84	1835	21.8	1104	837
R2-T0d-CD19	23	838	36.4	808	379
R2-T0d-CD33	209	1384	6.62	747	721
R2-T13d-CD19	30	748	24.9	1294	341
R2-T13d-CD33	6	744	124	98	314

10^{th} quantile and 90^{th} quantile indicate the sgRNA counts at each quantile. The skew ratio, which is computed by dividing 90th quantile by 10^{th} quantile, provided a quick evaluation on irregularity or deviation from a normal distribution. Day 13 (T13d) samples in general were more skewed than day 0 control (T0d) samples, which met with the expectation that gene mutation altered cell fitness at later time points. The zero-counts were the sgRNA that had no reads mapped from the sequencing process. The zero-count pattern is also consistent with the skew ratio, as the loss of some sgRNA was exacerbated over time due to their essential nature to cell growth. Those sgRNA were thus removed from the pool. Of all samples, replicate 2 T0d of A375-CD19-Cas9 (skew ratio: 36.4) and replicate 2 T13d of A375-CD33-Cas9 (skew ratio: 124) apparently deviated from the rest, possibly due to over killing at Puro selection step that led to a loss of sgRNA representation.

Most of the samples have acquired sequencing coverage of 400 times the sgRNA library size, except for R2-T0d-CD19, R2-T13d-CD19 and R2-T13d-CD33 of which the coverage was 314x and 341x the library size. This is likely due to an over-estimation of DNA quantity at the library preparation steps, which caused less of these sample to be included and thus less to be sequenced. Despite the coverage being lower than expected, the sample is considered feasible for downstream analysis since no anomaly was found from the basic metrics.

The reproducibility between replicates was examined with the correlation plots. Overall, normalized read counts between replicates are highly reproducible, which is indicated by Pearson correlation coefficients (R) that ranged from 0.61 to 0.79 (Figure 6A), of which the statistical significance was indicated by a t-test. The reproducible readings suggest that the experimental procedures were performed appropriately without errors that could substantially impede the interpretation of the outcome.

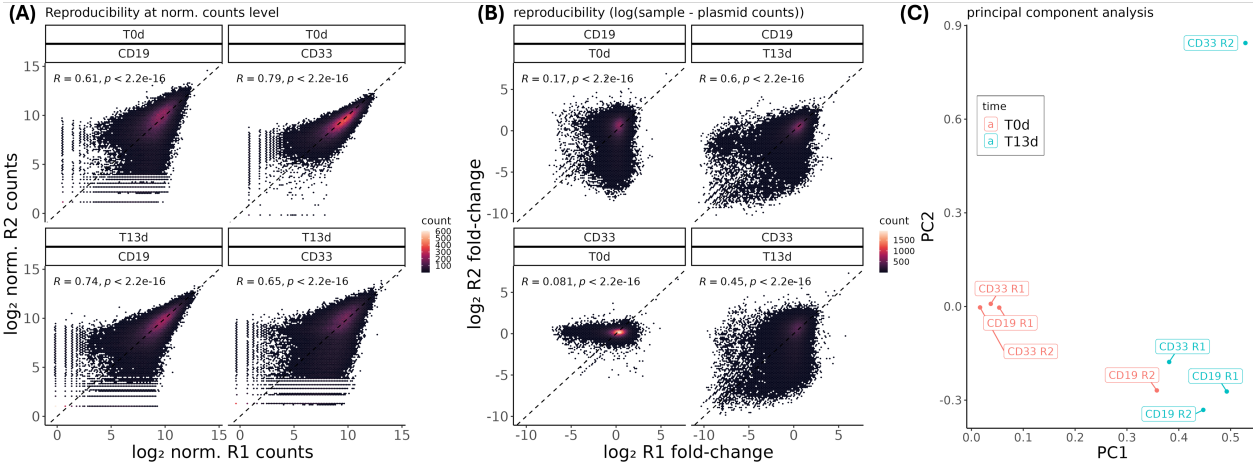

Figure 6. Dropout screen reproducibility and principal component analysis reveal high sample correlations.

Correlation plots for normalized sgRNA counts **(A)** and log scale fold-change of sgRNA counts between samples and plasmid library **(B)**. CD19 and CD33 represent A375-CD19-Cas9 and A375-CD33-Cas9 respectively. R refers to the Pearson correlation coefficient, supplemented with statistical significance calculated from T-tests. T0d denotes samples collected at time point zero, and T13d for samples at the end of the experiment. **(C)** PCA on sgRNA fold change using the first two principal components (PCs) as coordinate axes. The labels were colored based on the time of sample collection.

On the contrary, the correlation between replicates on the sgRNA fold change level is deemed as low to none, as indicated by R values close to 0 (Figure 6B left panel). This observation is, however, anticipated for T0d samples when their mutation was not given sufficient time to manifest a phenotype. The sgRNA fold-changes in this group of samples should center around 0 point as expected. As the experiment proceeded, the effect of LOF mutations began to deliver various growth effects on the A375 cells, causing the sgRNA representation to shift towards different directions. This was observed from the T13d samples (Figure 6B right panel). R values of 0.6 and 0.45, respective to the two A375 cell lines, signify a moderate to high correlation on the level of sgRNA fold-changes. A principal component analysis presents 2 major clusters for most samples corresponding to the time of sample harvest (Figure 6C). This clustering pattern further suggests that the sgRNA distribution of the samples are more similar within the same time of collection, regardless of the transgene expression, as explained by principal component 1.

7.1.3. Classification of gene mutation fitness

To profile the set of core-essential genes in A375 melanoma cell lines, I adopted the Bayesian analysis of gene essentiality (BAGEL) method (Hart & Moffat, 2016) for gene essentiality classifications. It has higher sensitivity in terms of detecting negatively selected genes target and is thus suitable for this screen. The classifier model is a supervised learning approach to be implemented together with a consensus set of reference essential and nonessential genes. The reference gene sets for the training of the classifiers and the essential genes of parental A375 cell line previously identified using TKO library were adopted from another study (Hart et al., 2014, 2015). The model outputs Bayes factors (BFs) as the final indicator of gene essentiality. Together with the individual sgRNA fold change obtained from my screen, I calculated with the classifier for the BFs of each gene in the CD19/CD33 over-expressing cells lines.

A higher BF score implies a greater certainty that a given genetic mutation reduces fitness. However, the score thereof does not indicate the degree of changes in a quantitative manner. The BF threshold had been set at 6 for the analysis based on literature (Hart et al., 2014, 2015), resulting in designation of 1721 genes to core-essential category for A375-CD19-Cas9 cells, and 1366 for A375-CD33-Cas9 cells. To assess the accuracy of the classifier model, I have computed the precision-recall (PR) curve and area-under-curve (AUC, Figure 7A). PR curve plots precision (positive predictive value) as a function of recall (true positive rate). At 5% FDR, there is a 95% probability of predicting a correct essential gene even when the classifier has already captured 90% or more of all true essential genes, suggesting the classifier performed accurately in the detection process. The AUC values (0.992 and 0.986 for the two cell lines respectively) also led to the same conclusion, when an AUC value of 1 is deemed as a flawless discernment. Using this classifier, I could confidently remove the essential genes from the candidate list in the subsequent co-culture screens to avoid the irrelevant hits.

The log scale fold-change of all genes across different samples were plotted on histogram (Figure 7B). The group of core-essential genes in both cell lines reduced significantly in abundance, despite the discrepancy in the degree of change between the two cell lines. I investigated the number of core-essential genes specific to or shared by the parental A375 cell line and the 2 derivative cell lines (Figure 7C). The diagram reveals that most essential genes found are still shared by all three cell lines, but significant differences were also observed where a large fraction of essential genes (463, equivalent to 27% of gene identified in parental line) were exclusive to the parental line. This might have been a consequence of different sgRNA libraries used in the two studies, hinting a substantial difference in the performance between TKO library and Heidelberg CRISPR sgRNA library. Another possibility would be in the difference incurred from the overexpression of CD19 or CD33 transgenes.

The correlation between different cell lines' BF value also confirms the observation which is shown in the 3 scatter plots (Figure 7D-F). When BFs of both A375-CD19-Cas9 and A375-CD33-Cas9 cell lines were compared to that of parental A375, the R value (0.6

to 0.64) is significantly lower than the R value (0.74) obtained from the comparison between A375-CD19-Cas9 and A375-CD33-Cas9. The observation supports the idea that there is a difference in the two sgRNA libraries led to a different definition of gene essentiality. Judging from the BFs correlation, the two new A375 cell lines are more related to each other than to the parental A375.

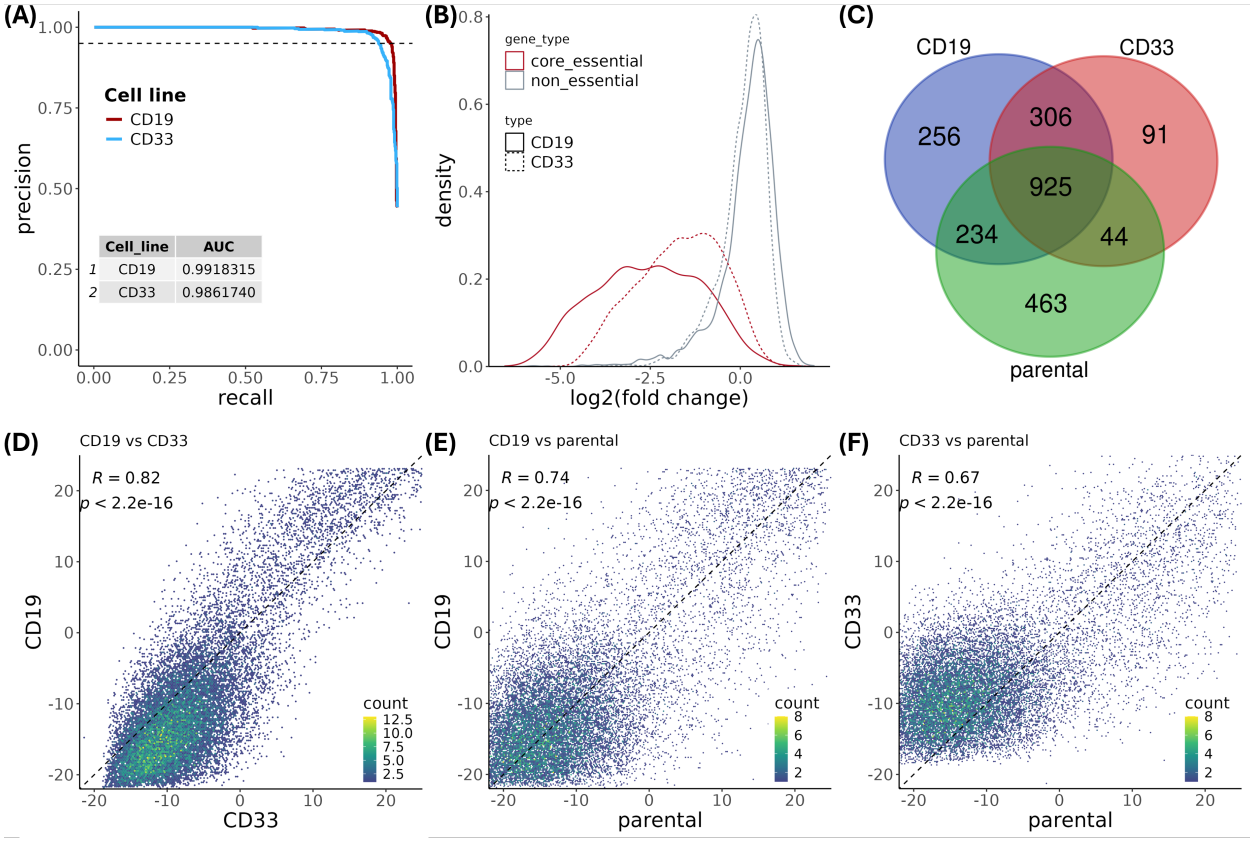

Figure 7. Essential gene classification by BAGEL and BFs correlation between parental A375 and derivatives.

(A) Precision recall curve plot for the two cell lines involved. Dashed line denotes 5% (FDR). Imbedded table contains AUC values for each cell line. **(B)** Histogram for the sgRNA fold-change distribution of core-essential genes and non-essential genes of A375-CD19-Cas9 (CD19) and A375-CD33-Cas9 (CD33). **(C)** Venn diagram displaying the number of identified core-essential genes that belong to each cell line, and overlapping regions denotes those shared between different cell lines. "Parental" represents the wild-type A375 screened using TKO library (Hart et al., 2015). **(D-F)** Plots for the correlation of BFs between cells lines. R equals the Pearson correlation coefficient, supplemented with statistical significance calculated from T-tests.

Between the two cell lines I prepared, 490 genes are exclusive to A375-CD19-Cas9 while there is only 91 to A375-CD33-Cas9, also indicating a large difference in the interaction between CD19/CD33 overexpression and sgRNA perturbations. Given that A375-CD19-Cas9 and A375-CD33-Cas9 were prepared from a combination of 3 clones each and 2 replicates were conducted for each, it is unlikely that the drastic increase in unique essential genes to CD19 cell line is due to specific CD19-Cas9 transgenes integrations or clonal effect. Considering the significantly higher mean fold-change on the non-essential genes in A375-CD19-Cas9 compared to that of A375-CD33-Cas9, the CD19 transgene apparently caused more alterations to A375 than CD33 does. In other words, the CD33 cell line is shown to be closer to the parental line. Therefore, A375-CD33-Cas9 was retained for the following screens while A375-CD19-Cas9 was discontinued.

7.2. Whole genome A375-CAR T cell co-culture screen

With the essential gene dropout screen, I have acquired knowledge on the characteristics of each newly developed cell line. The A375-CD33-Cas9 was chosen for its less transformed phenotype by the CD33 over expression. Hence, a co-culture screen using A375-CD33-Cas9 and CD33 CAR T cells was performed accordingly. However, the use of a single CAR-T cell targetable cell line could potentially cause artefacts due to overexpression of targets at non-physiological level. Therefore, an additional pair of antigen and CAR was included to expand the scope of the screen and to conduct the screen in a relatively native context where no overexpression of antigens was needed.

7.2.1. Selection of additional antigens for co-culture screen

In the field of solid tumor immunotherapy research, Chondroitin sulfate proteoglycan 4 (CSPG4), Tyrosine-protein kinase transmembrane receptor (ROR1), and disialoganglioside (GD2) surface antigens have been targets of interest for the

development of CAR-T cells therapy for various cancer types including brain, kidney, liver, and skin cancers (Sha et al., 2017). These surface antigens are notably popular in melanoma research for several reasons. They are either crucial to tumor growth or highly enriched on melanoma cells, making them favorable targets for CAR-T cells to target on, for a lower chance of antigen escape or a more tissue-specific T cell killing. Most importantly, CARs targeting these antigens had been established and tested in phase I study (Straathof et al., 2020) or pre-clinical models (Geldres et al., 2014; Hudecek et al., 2013), providing evidence on the effectiveness of selected CARs.

The Expression Public 24Q4 dataset provided important insight into the possible expression level of the three antigens on A375 cells (DepMap, 2023). As GD2 antigen is a glycolipid not directly produced by a gene, its surface abundance was approximated by the mRNA level of *ST8SIA1*, *ST3GAL5* and *B4GALNT1*, which are 3 primary enzymes responsible for the biosynthesis of GD2 (Sorokin et al., 2020). As compared to the mean expression of all Depmap cell lines, *CSPG4* and *BAGALNT1* in A375 express at a significant higher level, whereas the expression of *ROR1*, *ST8STA1* and *ST3GAL5* was on a par with the mean expression of all models (Figure 8A). In terms of absolute expression, a lower level is reported on *ROR1* and GD3 synthase (*ST8STA1*) in A375, while *CSPG4* and the rest of the two biosynthesis enzymes are reported to be highly expressed in A375.

To verify the expression of the 3 selected antigen on A375 cells, A375 WT cells were transiently transfected with a pool of two shRNAs targeting the corresponding genes. The result has shown that there was a loss of expression in all 3 antigens upon transfection of targeting shRNAs (Figure 8B), which indicates that A375 cells in fact express all 3 selected antigens, regardless of quantity. A low basal expression of GD2 and ROR1, and a high basal expression for CSPG4 has also confirmed the previously reported expression level by Depmap project. I therefore cloned CAR constructs that target the above 3 antigens to prepare CAR-T cells for a direct T cell cytotoxicity assay. This assay aims to indicate the feasibility of using these CARs and antigens in the subsequent co-culture screen.

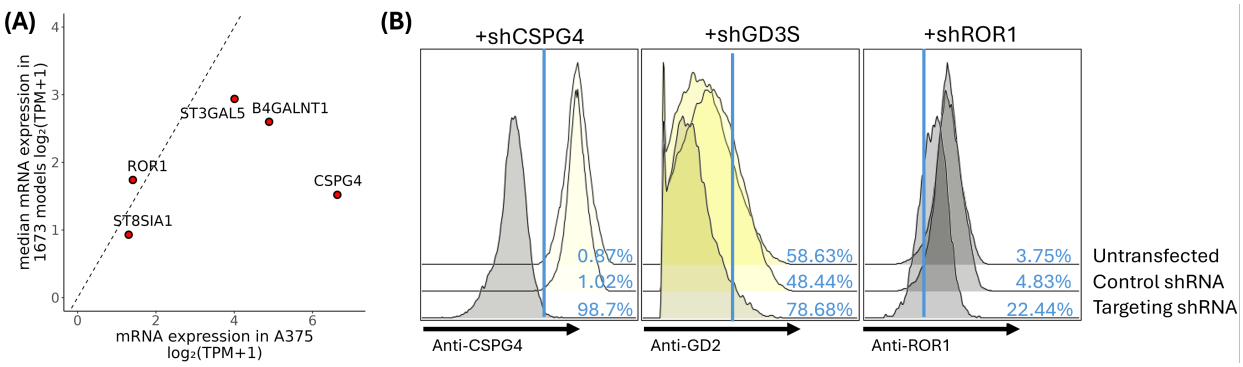

Figure 8. Reported expression level of additionally selected antigens were verified on A375.

(A) Scatter plot of mean mRNA expression of ROR1, CSPG4 and biosynthetic enzymes of GD2 adopted from the Expression Public 24Q4 set (DepMap, 2023). The expression level on A375 was plotted against the mean expression of all 1673 cell lines available in Depmap project. **(B)** Verification of the surface antigen expression by shRNA knockdown assay. WT A375 cells were transiently transfected with scrambles of plasmids of shRNA targeting the selected antigens or control shRNA. At 48-hour post-transfection, the A375 cells were labeled with corresponding antibodies, and analyzed in a flow cytometer. Numbers indicate the estimated size of population with a loss on CSPG4, GD2 or ROR1 expression.

7.2.2. CAR-T cells production and cytotoxicity against A375 cells

To prepare CAR-T cells for the screen, primary $CD8^+$ T cells were purified from buffy coat samples of multiple healthy donors by negative immunoselection to remove all PBMCs except $CD8^+$ T cells. Approximately 3 million $CD8^+$ T cells were reliably isolated from every 50 million PBMCs. The purity of T cells was immediately assessed by labeling their surface CD4 and CD8 protein and analyzed using a flow cytometer. For all 5 donors included in the co-culture screens, a purity between 93% to 98% of $CD8^+$ T cell population was achieved (Supp. Figure 1). The result was consistent across all donors. An unexpected enrichment of $CD4^+$ $CD8^+$ double positive T cells that constituted 1.44% to 5.26% of total $CD8^+$ T cells were also obtained in all donors. In general, a negligible amount of CD4+ T helper cells was present in the purified sample (<0.5%), and the cytotoxic T cell samples were considered purely $CD8^+$. The reason for the retention of some $CD4^+$ $CD8^+$ double positive T cells in the final sample could be explained by the inevitable inclusion of small fraction of duplet cells during gating procedures. The

enriched CD8 T cells population was then activated by CD3/CD28 stimulatory antibodies and IL-2 stimulation to initiate proliferation and later infected at a MOI of 50 by concentrated lentivirus solution. CD33 CAR-T cells were prepared from donors 19 and 20 T cells while ROR1 CAR T cells were from donors 21 to 23. The freshly prepared CAR-T cells were labeled with different anti-$F(ab')_2$ antibodies corresponding to their composition of scFv sequence – human $F(ab')_2$ for GD2 CAR, mouse $F(ab')_2$ for CD19 CAR or CD33 CAR, and CSPG4 CAR. ROR1 CAR was quantified by direct measurement the GFP signal in the cells.

The Majority of CD33 or GD2 CAR-T cells were positive for CAR expression after lentiviral infection, of which over 70% cells were detectable for CAR on the surface (Figure 9A). As for CD19, CSPG4 and ROR1 CAR-T cells, only about half of the population were expressing CAR, suggesting a difficulty in transforming primary T cells. The histogram revealed a bimodal distribution of CAR express for most of the cases, indicating a large subset of cells are more resistant to infection than the rest. This led to the obscure differentiation of the real CAR-T cell population, as the CAR^{low} subset overlaps significantly with the CAR^{-} population. Since approximately half or more of the CAR-T cell samples expressed CAR, these samples were directly used without further enrichment for downstream applications to avoid introducing stress to CAR-T cells.

To ensure the CAR-T cells were capable of efficiently targeting and eliminating A375 cells, the newly prepared samples were further tested an image-based T cell cytotoxicity assay. The CAR-T cells or control T cells were serially diluted distributed to different A375 cell lines to co-culture for a period. The T cells were removed afterwards and remaining A375 cells were imaged with the IncuCyte ZOOM system as an end-point measurement. A complete treatment scheme can be referred to section 6.2.12. The images were processed by IncuCyte ZOOM and converted into confluency from each condition. This value was in turn used to calculate the specific lysis caused by CAR-T cells, which is a numerical value commonly used for representing T cell cytotoxicity.

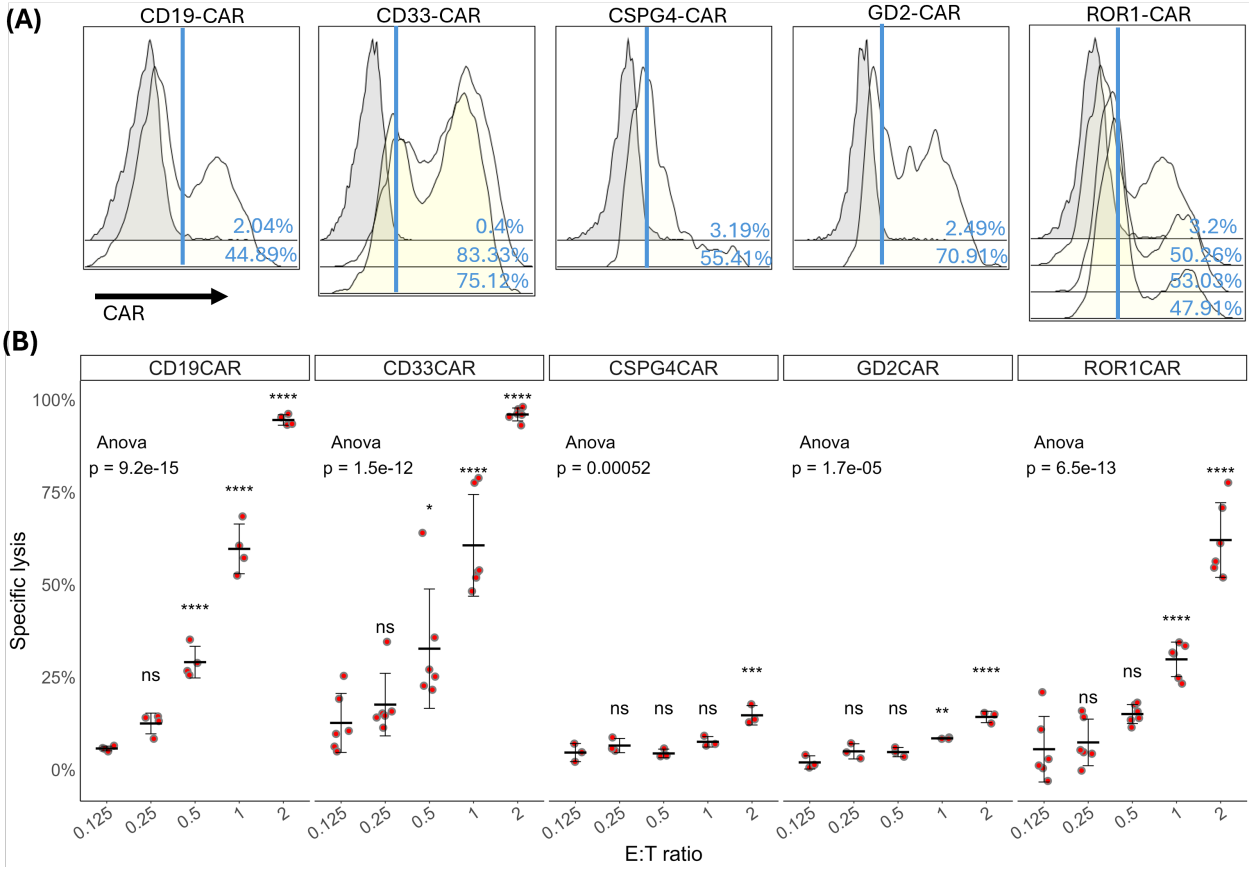

Figure 9. Selected CARs mediated T cell cytotoxicity against A375 cells.

(A) CAR expression on transduced T cells (yellow) as compared to control T cells (gray). Activated T cells were transduced at a MOI of 50 to overexpress different CARs. The CSPG4, CD19 and CD33 CARs were labeled by anti-mouse $F(ab')_2$ antibody, and GD2 CAR cells by anti-human $F(ab')_2$ antibody. The ROR1 CAR expression was quantified by the amount of GFP produced. Each yellow histogram represents a CAR-T cell sample prepared from one donor. Numbers indicate percentage of CAR^+ T cells. **(B)** Plots for CAR-T cells cytotoxicity against A375 cells. A375 were co-cultured with CAR-T cells at different effector-to-target ratio for 24 hours. T cells were removed prior to imaging A375 using IncuCyte ZOOM system. The confluency of A375 was converted into the percentage of specific lysis by T cells as described in section 6.2.12. Each red dot represents one replicate. The data is presented in mean ± SD. Statistical significance was computed from ANOVA, coupled with Tukey's test.

A melanoma-CAR-T cell co-culture experiment was conducted to measure the cytotoxicity of T cells as mediated by different CARs. Both CD19 and CD33 CARs exhibited potent killing efficiency on A375-CD19-Cas9 and A375-CD33-Cas9 respectively (Figure 9B). At dosages above 0.5:1 effector-to-target (E:T) ratio, they have shown significantly greater specific lysis on A375, as compared to 0.125:1 E:T ratio. They were both able to eradicate almost 100% of A375 from the culture when delivered in 2

times the A375 cell number in 24 hours or killing approximately 60% when given at the same number of cells as A375. This provided strong evidence on the effectiveness of these CAR on re-directing cytotoxic T lymphocytes effector function on $CD19^{+}$ or $CD33^{+}$ A375 cells. ROR1 CAR-T cells exhibited decent killing efficiency, despite being not as high as observed on CD33 CAR. At E:T ratio of 2, ROR1 CAR was able to mediate around 70% of A375 cells killing and roughly 30% at 1:1 ratio. This was likely because of the low basal expression or surface ROR1 as compared to higher level achieved by CD33 transgene (Figure 5D & Figure 8B). A375-Cas9 were then FACS sorted for $ROR1^{high}$ populations using the same gating threshold to ensure uniform recognition by ROR1 CAR-T cells. The resulting A375-$ROR1^{high}$-Cas9 cells were also tested for their Cas9 editing efficiency (Supp. Figure 2).

As for CSPG4 and GD2 CARs, they have failed to present an acceptable level of cytotoxicity against A375 for unsolved reasons. Only when A375 were treated at E:T ratio of 2, the CSPG4 and GD2 CARs only showed a statistically higher level of killing than the lowest dose. Nevertheless, both CARs achieved only around 20% at that dose, which is largely insufficient to be utilized in the screen. The reason behind the unsuccessful attempts could potentially be explained by a low inherent expression level on A375 and A375-specific post-translational modifications that mask the epitope. Due to the lack of CAR specific killing, GD2 and CSPG4 CARs were excluded for further experimentation.

To balance the T cell cytotoxicity to apply enough selective pressure on A375 cells to select for highly resistant mutation while not overkill to reduce sgRNA coverage, I had decided to use 50 % of A375 killing after 24 hours of CAR-T cells treatment as a threshold. This was used to maintain sgRNA coverage above 500 times the library size while and to allow sufficient recovery within 3 to 4 days of treatment. To achieve 30% to 50% of A375 cell killing after 24 hours, CD33 CAR-T cells were used at E:T of 0.5:1 and ROR1 CAR at 1:1 ratio.

7.2.3. Quality of the co-culture screen

Based on previous experiments, an experimental setup was established to perform the genome-wide CRISPR co-culture screen which includes A375-CD33-Cas9, A375-ROR^{high}-Cas9, and the corresponding CAR-T cells. Eventually 2 T cell samples (D19, D20) were included in the “CD33 CAR screen” and 3 samples (D21, D22, D23) in “ROR1 CAR screen”. Detailed timeline and procedures of experiment refers to section 6.2.13. T cell samples from different donors collapsed as experimental replicates for subsequent statistical analysis. With similar procedures as the dropout screen, all the reads from the deep sequencing were mapped to the sgRNA library to produce a count table of all sgRNAs across every sample using the MAGeCK package. The sgRNA counts were then normalized to the median sgRNA counts of a defined set of control sgRNAs. Hit calling was performed by fitting multiple linear regression models on the fold change of genes.

To assess the general quality of the screen result, the basic properties of the samples were determined (Table 29). Most samples acquired sufficient sequencing coverage of at least 300 times the sgRNA library size, except for one which is the control sample of D22 T cells. The slight deduction did not appear to affect the downstream analysis, which is indicated by a high correlation with D21 and D22 T cell in both control and CAR-T cell treated samples (Figure 10A, Supp. Figure 3). The clusters produced from PCA and hierarchical clusters from correlation matrix verified the observation (Figure 10A-C). D21, D22 and D23 control samples were grouped in the same cluster on the PCA plot, which were collected from the same experiment where ROR1 CAR was used. No abnormal readings were detected from the basic metrics (Table 29), and correlation matrices (Figure 10A&B)

A discrepancy between the samples prepared from CD33 CAR screen and ROR1 CAR screen was clearly shown by higher skew ratios and higher zero counts (Table 29). CD33 CAR samples have on average 4 time the number of sgRNA without any mapped reads from sequencing, indicate a rigorous depletion of certain genes over the course of experiment. The skew ratio of all samples from CD33 CAR experiments were similarly

shown to be higher, hinting towards a systematically more prominent change on sgRNA representation on CD33 CAR samples. The PCA result further provided evidence to the difference in the phenotype of the two CAR types, by grouping the samples into two well-separated clusters, one for each CAR type shown (Figure 10C).

Table 29. Basic metrics of sgRNA count distribution of co-culture screen samples.

sample	10th quantile	90th quantile	skew ratio	zero counts	coverage
D19_CAR	156	3975	25.5	2242	1800
D19_CTRL	82	2098	25.6	2326	958
D20_CAR	133	3362	25.3	2342	1530
D20_CTRL	171	4531	26.5	2488	2063
D21_CAR	82	908	11.1	550	444
D21_CTRL	150	1646	11	375	804
D22_CAR	75	825	11	478	403
D22_CTRL	52	592	11.4	505	288
D23_CAR	141	1558	11	470	764
D23_CTRL	166	1766	10.6	366	869

Overall, a high correlation between samples is observed, where a correlation test of all combinations resulted in all R values higher than 0.75 (Figure 10A). The matrix provides a comprehensive overview of correlations between all possible sample combinations regardless of being control-T cell treated, or CAR-T cell treated samples. This suggests a high reproducibility of the experimental procedures between the 2 types of CAR-T cell co-culture experiment, with no substantial technical errors observed between replicates introducing large deviations in the sgRNA representation. Consequently, a low inter-experimental variability was detected.

However, when analyzing on the reproducibility of sgRNA fold-change level between replicates, R values from 0.09 to 0.15 were indicated for replicates of ROR1 CAR screen (D21-D23) while 0.27 was revealed for CD33 CAR screen, all of which corresponds to weak correlations (Figure 10B, Supp. Figure 4). For sgRNA fold-change correlation calculated between the two screen, the general correlation approached zero, suggesting a disparity between the hit-selection outcome of the two screens (Figure 10B). The

phenomenon that highly correlated control and treatment samples yield poorly correlated fold-change values appears to be a common issue across similar experiments. This issue will be examined further in later chapters of this dissertation.

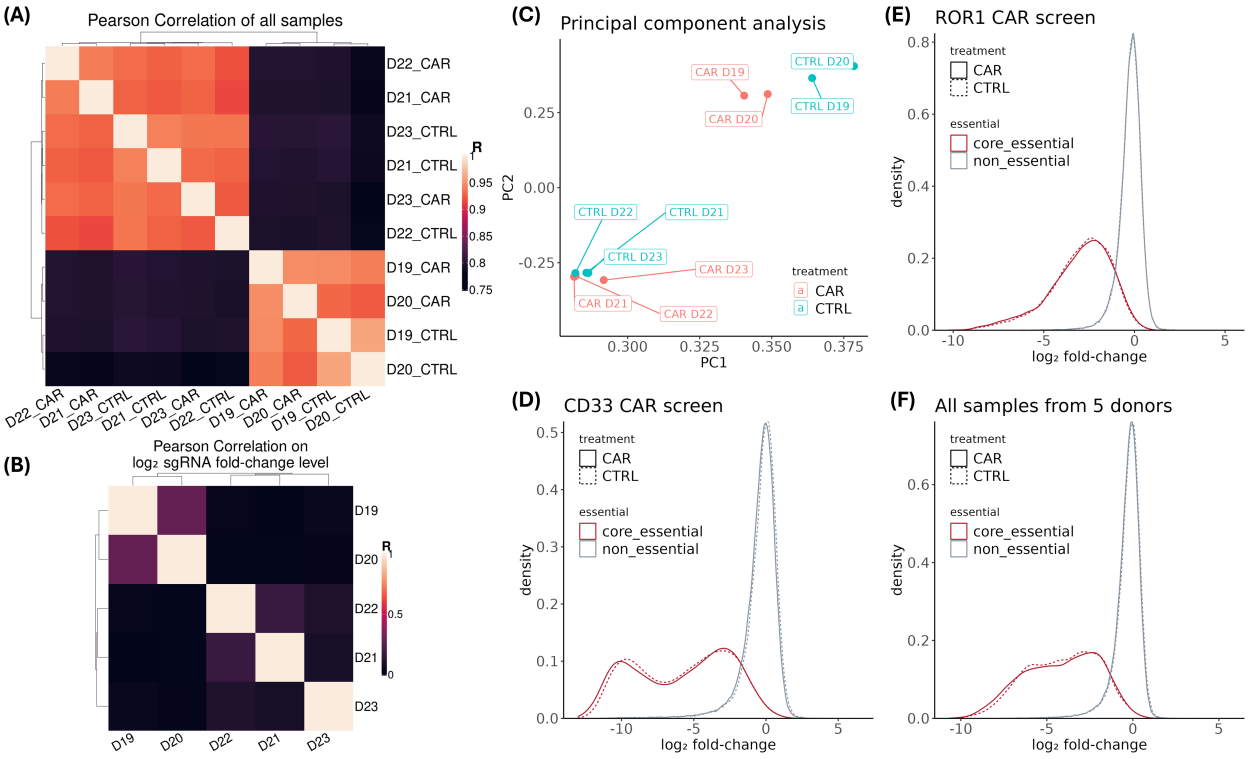

Figure 10. Gene essentiality, PCA and sample correlations revealed divergence between CD33 CAR-T cell and ROR1 CAR-T cell screens.

(A, B) Correlation matrices of normalized sgRNA count of control-T cell treated samples and CAR-T cell treated samples, and $\log_2$ fold-change level of sgRNA from all 5 screens. D19 to D23 denotes the identity of donors used to prepare T cells. The $\log_2$ fold-change of sgRNA refers to the difference between treated and control samples. R represents the Pearson correlation coefficient, of which the level is reflected on a color scale. All correlation shown have a *P<0.00001*. **(C)** PCA on the sgRNA fold change of all samples including control and treated samples, using the first 2 PCs as coordinate axes. The labels were colored based on the treatments. **(D, E, F)** Histograms of essential gene sgRNA fold-change in co-culture screens using CD33 CAR, ROR1 CAR or combined result. The sgRNA $\log_2$ fold-change of all samples is computed by subtracting Plasmid counts from Sample counts. The histograms were colored according to gene essentiality, and line type is changed according to treatment.

Additional observations support the existence of divergence between the two screens. When comparing all control T cell samples or all CAR T cell samples within the same

CAR experiment, the R values exceeded 0.9, which refers to a very high degree of correlation consistent with widely accepted research consensus. The R values dropped below 0.81 whenever D21 and D22 samples were compared with the other samples, which is one grade lower in term of degree of correlation (Figure 10A)., hinting a minor difference exists between the samples between the 2 co-culture experiments. Same observations were made from the PCA where the samples, regardless of sample types, appeared in 2 distinct clusters (Figure 10C) corresponding to each CAR-T cell co-culture experiments. The observation suggested that the difference between the experiments likely stemmed partially from the usage of the two types of CARs.

To further explore the issue in the context of functional genetics, the phenotype of gene essentiality in each sample was studied using the list of essential genes identified from the previous screen (Figure 10D-F). From a holistic perspective, the performance of the previously classified essential genes aligned well with expectations, where majority of these genes exhibited a significant depletion over the course of the experiments, whereas the non-essential genes remained largely stable without significant fold-change. The differential fitness was evidently conserved across different treatments within the same experiment, indicating that the treatment of CAR-T cells or normal T cells did not broadly affect proliferative phenotypes of all genes, demonstrating the robustness of the gene essentiality classification.

Despite a decrease in abundance of essential genes (red histograms) in both screens, a clear inconsistency in the distribution of these gene was also observed between CD33 CAR samples and ROR1 CAR samples (Figure 10D&E). Specifically, essential genes were depleted in 2 distinct patterns when perturbed. A subset of mutated essential genes presented a substantially stronger depletion effect in CD33 CAR screen, resulting in a bimodal distribution of the sgRNA fold-change of essential genes (Figure 10D, Supp. Figure 3). In contrast, the ROR1 CAR screen samples exhibited a skewed distribution, suggesting a less pronounced impact on essential gene depletion (Figure 10E).

To further analyze the influence from the type of CAR on the behavior of the essential genes, I have performed a Welch ANOVA was using CAR type and gene essentiality as

independent variables on the data grouped by gene essentiality and treatments (Supp. Table 2), assuming unequal variance of the data groups involved. A Games-Howell *post hoc* test was conducted to compare all possible pairwise comparison within treatment, CAR type and gene essentiality groups. The statistical analysis revealed a significant difference between the 2 screens across all grouping parameters. In core-essential genes groups (both CAR-T cell treated or control-T cell treated samples), a statistically significant mean $\log_2$ fold-change difference was observed between the two screens by different CARs, confirming the trends observed in Figure 10D&E. Contrarily, a significant difference was also detected between non-essential gene groups in CAR-T cell treated and control-T cell treated samples, with an estimated difference of 5.9% and 13.84% respectively. This estimation is notably higher than the 5.4% difference observed between the non-essential genes of CAR-T cells treated and control-T cells treated samples within the CD33 CAR screen, or the undetectable difference between the non-essential genes of CAR and control samples in the ROR1 CAR screen.

Experimental variations introduced from procedures including cell culture or cell passaging would not be sufficient to simultaneously alter the phenotype of a specific group of genes. The observed changes in both essential and non-essential genes signify that factors beyond technical variability contribute to these discrepancies. The most plausible explanation is that the difference in genetic background largely between the 2 A375 cell lines drive the divergence in essential gene phenotype. This was deduced from the behavior of the control-T cell treated samples. These samples principally functioned as untreated controls since normal T cells were not able to detect and kill A375 cells within the timeframe of each treatment in the screen. Despite A375 being neither target nor killed by control-T cells, a clear disparity between the control samples of the 2 screens were observed, suggesting that the A375-CD33-Cas9 and A375-ROR1^{high}-Cas9 exhibit diverging cellular response to essential genes perturbation. As a result, the genetic phenotypes of essential genes and candidate hits to be identified from the screen were likely to behave differently in each cell lines. Therefore, the most appropriate approach for downstream analysis is to analyze each screen independently to interpret context-specific effects accurately.

7.2.4. Inference of differential gene presence

To analyze which genes conferred A375 resistance or sensitivity against T cell cytotoxicity, I first normalized and transformed the raw sgRNA counts into log scale. The fold-change of sgRNA was computed by subtracting the read count of control samples from that of CAR-T cell treated samples. Multiple sgRNA fold-changes of the same underlying gene collapsed as data points for statistical calculation. The statistical significance of each gene was calculated by fitting a linear model and thus determining the differential expression between each gene and a defined set of control housekeeping genes. Empirical Bayes smoothing was applied to the standard error and p-value were adjusted for multiple comparison by Benjamini-Hochberg correction.

An FDR cutoff of 0.3 was applied to the gene list for marking genes of significance (Figure 11A&B). Gene significance was ranked based on the enrichment of sgRNA of the corresponding LOF mutation in the screens, and gene mutations that conferred melanoma cells with different attributes were categorized accordingly. Genes with qualified FDR and a negative fold-change were designated as “sensitizing”, and those with positive fold-change as “resistant”. Initially, 349 and 390 genes were included as candidates (resistant and sensitizing mutations combined) for CD33 CAR and ROR1 CAR screens respectively (Supp. Table 3 & Supp. Table 4). After filtering core-essential genes of A375, the resulting lists of genes contain 215 and 234 candidates in respective to the two CARs. Some of the hits with strongest phenotypes are illustrated for both screens (Figure 11C&D).

To evaluate the validity of the hit selection rationale, I first identified differentially expressed genes from the two screens that have existing validation data by KEGG pathway analysis. Two distinct classes of genes exhibiting strong phenotypes across both screens were observed (Figure 11E&F). One group matches twelve out of 137 genes in the KEGG Apoptosis pathway ($p = 0.011$; Supp. Figure 5), while the other one

matches 20 out of 169 genes in KEGG Autophagy Animal pathway (p = 0.00018; Supp. Figure 6).

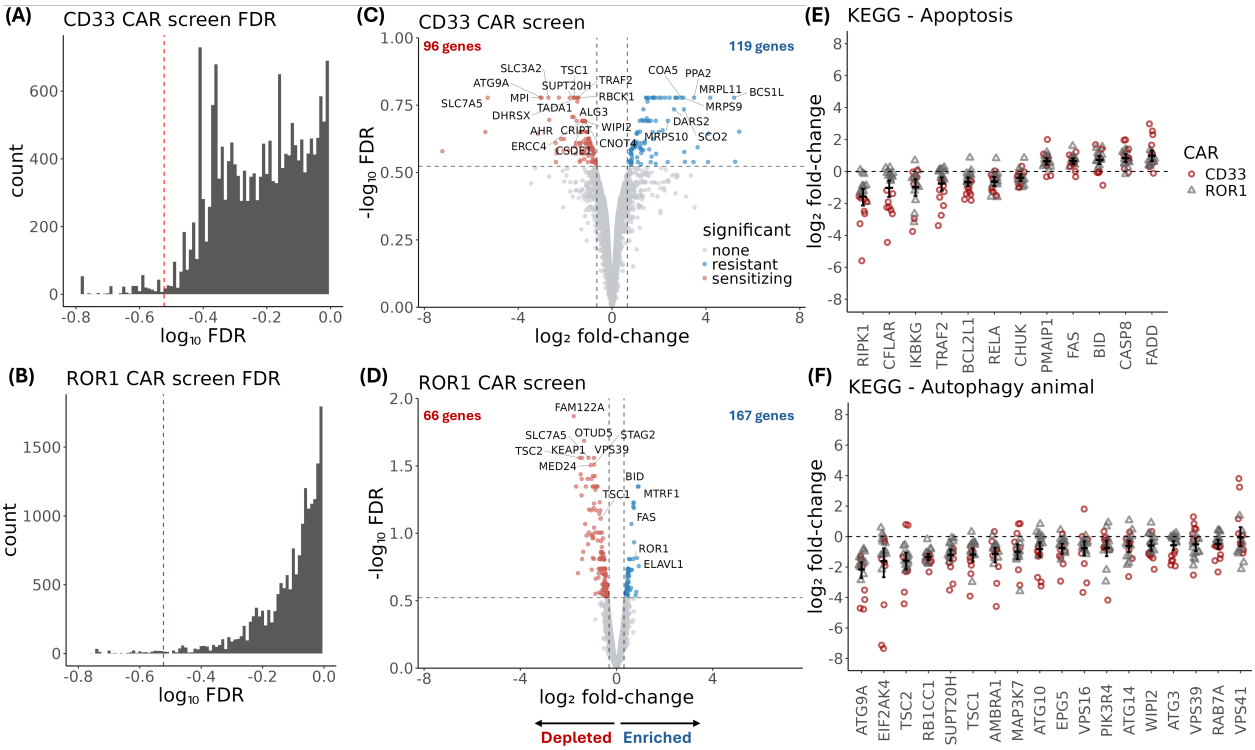

Figure 11. Hit calling of co-culture screens recapitulated established regulator genes of immune interaction.

(A, B) Distribution of FDR of each gene from respective screens. FDR represents the adjusted P value by Benjamini-Hochberg correction. Dashed line indicates the FDR threshold applied for the hit calling. **(C, D)** Volcano plots for displaying the range of P value and mean fold-change of every gene. Examples of candidates were labeled, excluding essential genes. Sensitizing (red) or resistant (blue) mutants were categorized based on "depleted" or "enriched" sgRNA. Dashed lines refer to the p value and level of fold-change at which the genes were assigned significance in respective screens. **(E, F)** Selection of hits that recapitulate findings from existing reports. The displayed hits were enriched in respective KEGG pathways. Each point represents the fold-change of one sgRNA from each replicate of each screen. The data is reported in mean ± 95% CI.

PMAIP1, BID, CASP8 and FADD are well characterized molecular components that have conserved roles as positive regulators or signal receptor in intrinsic or extrinsic apoptotic pathways. FAS is a transmembrane protein of the TNF receptor superfamily that initiates the extrinsic apoptotic pathway when bound by its cognate ligand, FasL.

Upon binding of FasL expressed on T cells, it forms death-inducing signaling complex (DISC) that recruits FADD and activates CASP8, which subsequently activate proapoptotic BID, triggering a cascade of events that leads to cell death (Chinnaiyan et al., 1995; Jost et al., 2009; Luo et al., 1998; Shu et al., 1997). In addition, PMAIP1, another pro-apoptotic member of the BCL-2 family within the BH3-only subfamily, promotes apoptosis by inhibiting anti-apoptotic BCL-2 family members and unleash function of CASP9 as part of the apoptotic signaling cascade (Oda et al., 2000). Inducing LOF on these achieved more than 100% increase in terms of sgRNA enrichment on average as compared to non-targeting controls, which renders the cells with respective LOF more resistant to the CAR-T cells attack. On the contrary, CFLAR, also known as c-FLIP, is an anti-apoptotic protein functions primarily by deterring CASP8 from associating with DISC, and thus inhibiting the activation of CASP8 and the downstream caspase cascade (Irmler et al., 1997). A LOF mutation in CFLAR during the screening experiment lifted the inhibition on CASP8 and hence sensitizing the cell towards death signals from T cells, resulting in approximately 1.5-fold decrease in sgRNA enrichment (Figure 11E).

PTPN2 (Figure 11E) has been verified to confer resistance to melanoma from an *in vivo* screen as discussed earlier in section 5.7. In two earlier studies, PTPN2 was found to dephosphorylate JAK1 and STAT1 to suppress their signaling transduction function (Kleppe et al., 2010, 2011). The absence of functional JAK1 and STAT1 abolish the type I and type II interferon signaling, which in turn allow the cancer to evade from the harmful effect of interferon molecules. Therefore, when LOF mutation was introduced to PTPN2, the interferon signaling pathway was rescued and allowed the stimulation of apoptosis by different interferon molecules (Manguso et al., 2017). TRAF2 was identified in the screen with similar phenotype (Figure 11E). A recent discovery, as mentioned in section 5.7, has demonstrated that in TNF signaling pathway of melanoma, the presence of TRAF2 deters TNFα signals from instigating RIPK1-dependent cell death (Vredevoogd et al., 2019). With the ablation of TRAF2 expression, the TNFα signals are transduced to promote apoptosis to a higher extent. These observations are in line with my results

where sgRNAs targeting TRAF2 were depleted upon CAR-T exposure indicating sensitization.

Evidence from a recent study support that autophagy is a conserved process utilized by melanoma to escape immune surveillance from cytotoxic T lymphocytes (Lawson et al., 2020). Researchers were able to elevate the T cell cytotoxicity by pharmacologically and genetically abolishing the autophagy function in melanoma cells. A large class of genes has been identified as sensitizing mutations in both screens (Figure 11F) and are annotated to animal autophagy pathway on KEGG (Supp. Figure 6). Of the selected hits, ATG3, ATG9A, ATG10 and ATG14 are shared by the study. All selected hits in Figure 11F were illustrated as positive mediators of autophagy. Consequently, when the group of genes was perturbed by the sgRNA library, they manifested as sensitizers of A375 against CAR-T cells attack.

The hits mentioned above exhibited sensitizers or resistors phenotypes in agreement with existing findings, indicating a correct performance of the screening method in resolving gene functions. Therefore, other hits identified from the screens with statistical significance were evidently relevant to the context of melanoma-CAR-T cell interaction, with indications on the underlying gene functions. Further mechanistic studies were designed and conducted according to the displayed phenotype of the candidates.

7.2.5. Classification of gene candidates by functional annotation

As several targets from both screens showed consistent phenotype to existing findings, one can confidently explore other candidates for potential regulators of melanoma-T cell interaction. A subsequent step in the analysis is to shortlist the most context-relevant candidates. The gene list was first ranked based on the average fold-change and inspected for potential functional clusters in terms of biological processes, molecular functions, and complex cellular components. DAVID functional annotation application provided by NIH (Huang et al., 2009; Sherman et al., 2022) was used to perform pathway enrichments and gene ontology (GO) enrichment analysis. The

candidates were annotated primarily to biological terms available in GO Database (Ashburner et al., 2000), KEGG Pathway Database (Kanehisa, 2019), Biocarta Pathways Dataset (Nishimura, 2001) and Reactome Pathway Database (Griss et al., 2020).

Candidates from each screen were connected to distinctive functional clusters as indicated by DAVID, which differentiate the scope of hits enriched from each screen on different perspectives (Figure 12A). Genes from CD33 CAR-T cell screens were predominantly annotated to signatures including mitochondrial assembly and function, as well as involvement in oxidative phosphorylation (OXPHOS), which account for more than one third of input genes. Reactive oxygen species (ROS) production may be increased in case of natural gene mutation and used as a defense mechanism against T cells. It has been proposed that T cells require a balanced level of ROS to efficiently execute theirs effector function (Cemerski et al., 2002; Kamiński et al., 2012; Sena et al., 2013). An insufficient level of ROS renders T cells inactivated whereas a high dose induces T cell apoptosis. It is possible that the perturbed OXPHOS genes may have turned on a metabolic switch to increase ROS production for fending off T cells as well as abolishing the potential apoptosis initiation.

As for ROR1 CAR-T cell screen, a third of hits were clustered in signatures concerning signaling network including and IL-17 signaling, TNF signaling, and Toll-like receptor signaling pathways (Figure 12A), all of which use NF-κB signaling as part of their signaling transduction axis (Kawai & Akira, 2007; T. Liu et al., 2017; Monin & Gaffen, 2018). NF-κB regulates the survival of melanoma upon reception of different cytokines (Karin & Greten, 2005), and melanoma cells hijacked the machinery to up-regulate transcription of numerous anti-apoptotic genes including inhibitor of apoptosis proteins, and TNFAIP3 which are BCL-2 family members. The difference between the functional clusters from the two screens hints a potential difference in the function of the two CARs in mediating the effector cells to eliminate melanoma cells as well as a potential involvement of CD33 transgene in altering the interaction.

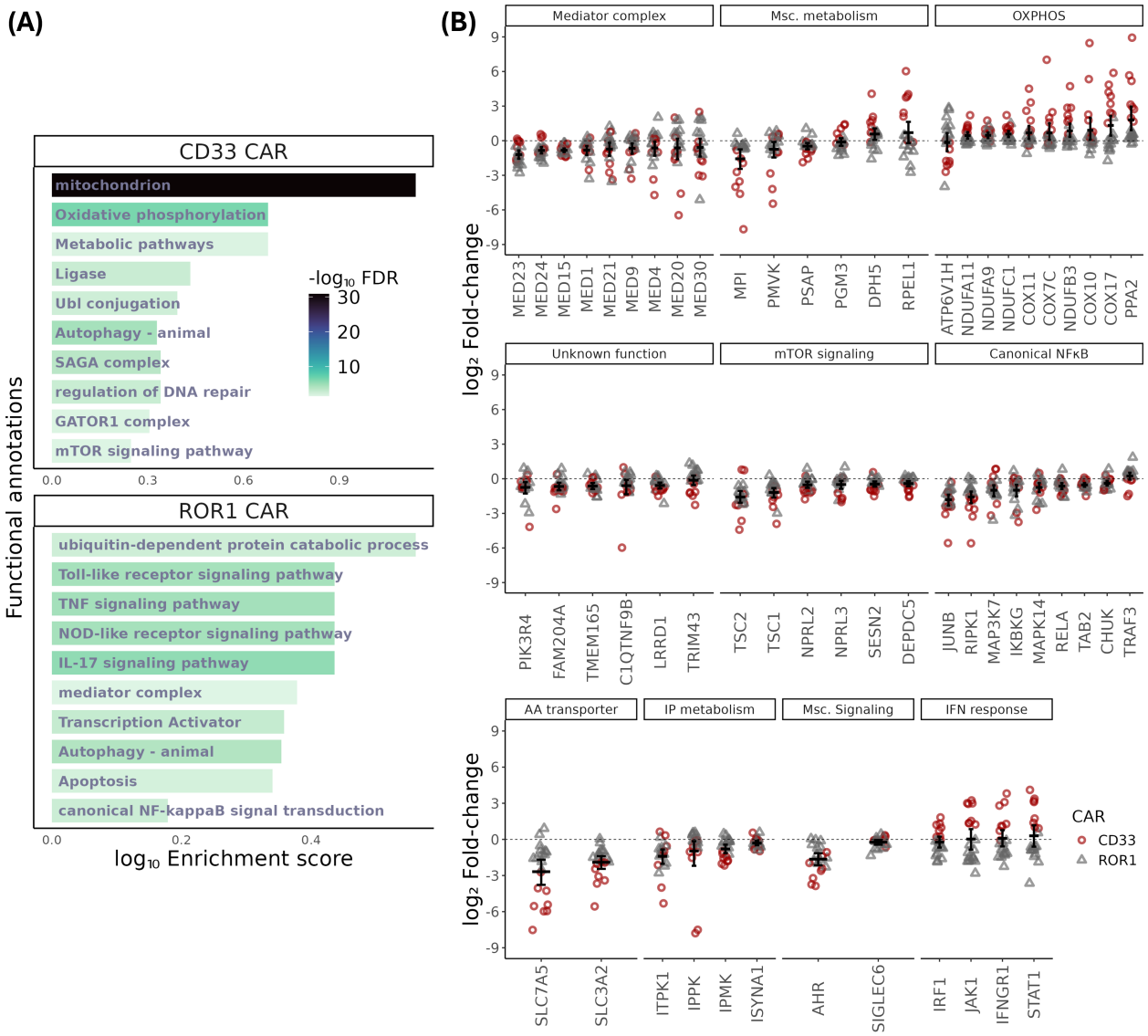

Figure 12. Functional clustering reveals biological processes implicated in melanoma-T cell interactions.

(A) Functional clustering of all screen hits below 0.3 FDR conducted using DAVID. Selected biological terms annotated from GO enrichment or pathways from KEGG pathway enrichment analysis were plotted respectively to each screen. Bars were colored according to the statistical significance level. **(B)** Log_2 fold-change of sgRNA of gene candidates from selected functional clusters. Each point represents the fold-change of one sgRNA from each replicate of each screen. Shapes designate the screen each point originated. The data is presented as mean ± 95% CI.

The actual performance of individual sgRNA of relevant genes from clusters including transcriptional control (mediator complex), OXPHOS, mTOR signaling and NF-κB

signaling pathways are summarized in Figure 12B. In addition to the large functional clusters stated, few smaller classes of genes were specifically included for their prominent sensitizing phenotypes exhibited. The clusters include an amino acid (AA) transporter, inositol phosphate (IP) metabolic enzymes, two signaling components and some unique metabolic enzymes. Another six candidates without functional characterization also displayed moderate to strong phenotypes in the screen, representing potentially novel mechanistic targets in the field of melanoma research. Most identified gene clusters manifested their phenotype by depleting cells during the screens except for most of the mitochondrial/OXPHOS-related genes. This is also a general observation from the two screens as there are more sensitizing mutations being identified than resistant mutations. The trend indicates that the co-culture screening platform has a propensity for detecting negative selected targets, which suffered a loss of representation in the mass cell population.

Perturbations to the SLC3A2/SLC7A5 AA transporter, IP metabolic enzymes, OXPHOS, and the selected members of metabolic enzymes resulted in the highest fold-change of A375 cell numbers (Figure 12B). Mean fold-change of sgRNA for AA transporter (log_2FC: -2.35), IP metabolic enzymes (log_2FC: -0.865), OXPHOS (log_2FC: 0.758), and several selected metabolism-related genes (log_2FC: -0.93 to 0.387) was recorded. This suggests a substantial contribution from metabolic regulation in the melanoma-T cell interaction, especially when the fold-change is consistent across the screens. A metabolic reprogramming of cancer cells is often described as one of the hallmarks of cancer to foster an immunosuppressive micro-environment (Biswas, 2015). Specific amino acid requirement, IP metabolites, ATP and ROS might collectively contribute to meet certain biosynthetic demands or to minimize the damage in response to the effector function of T cells.

mTOR activation has previously been linked to the malignant progression of melanoma (Karbowniczek et al., 2008). In these experiments I identify several genes in the mTOR pathway which sensitize A375 towards CAR-T cell mediated killing (log2FC: -0.845). This suggests a potential immunomodulatory role for some of the components on this pathway in melanoma cells.

A large class of mediator complex subunits also exhibited strong phenotypic changes (log_2FC: -0.771) upon genetic perturbation, suggesting a potential complex transcriptional control on the melanoma cells during immunosurveillance. It has been reported that a simultaneous loss of *MED1* and *MED24* promotes breast carcinoma by up-regulating E2F1 and cyclin D1 that accelerate cell cycles. Another study has also shown that *MED23* promotes growth and tumorigenicity of lung cancer with active Ras signaling. A potential connection to the expression of a specific set of genes that could protect melanoma from T cell attack can be postulated. However, the relationship between specific mediator complex subunits and melanoma progression remains understudied.

7.2.6. Clinical relevance of candidate genes

To determine candidates that may serve as potential druggable target or whether they are linked to melanoma progression in patients, the list of hits was examined for their characteristics in clinical samples. Patient data were acquired from The Cancer Genome Atlas Program (TCGA) and the cBio Cancer Genomics Portal (cBioPortal) (Cerami et al., 2012; Gao et al., 2013; de Bruijn et al., 2023). A curated dataset comprised of 647 patients from 4 studies was used for subsequent mRNA expression assessment, survival analysis and cytolytic activity analysis (Snyder et al., 2014; Van Allen et al., 2015; Reynolds et al., 2017; D. Liu et al., 2019). To avoid artefacts created only in experimental settings, the gene candidates were anticipated to be expressed consistently and moderately in melanoma patient's sample, conducive to certain prognostic outcome, and displaying an influence on T cells activity in melanoma samples.

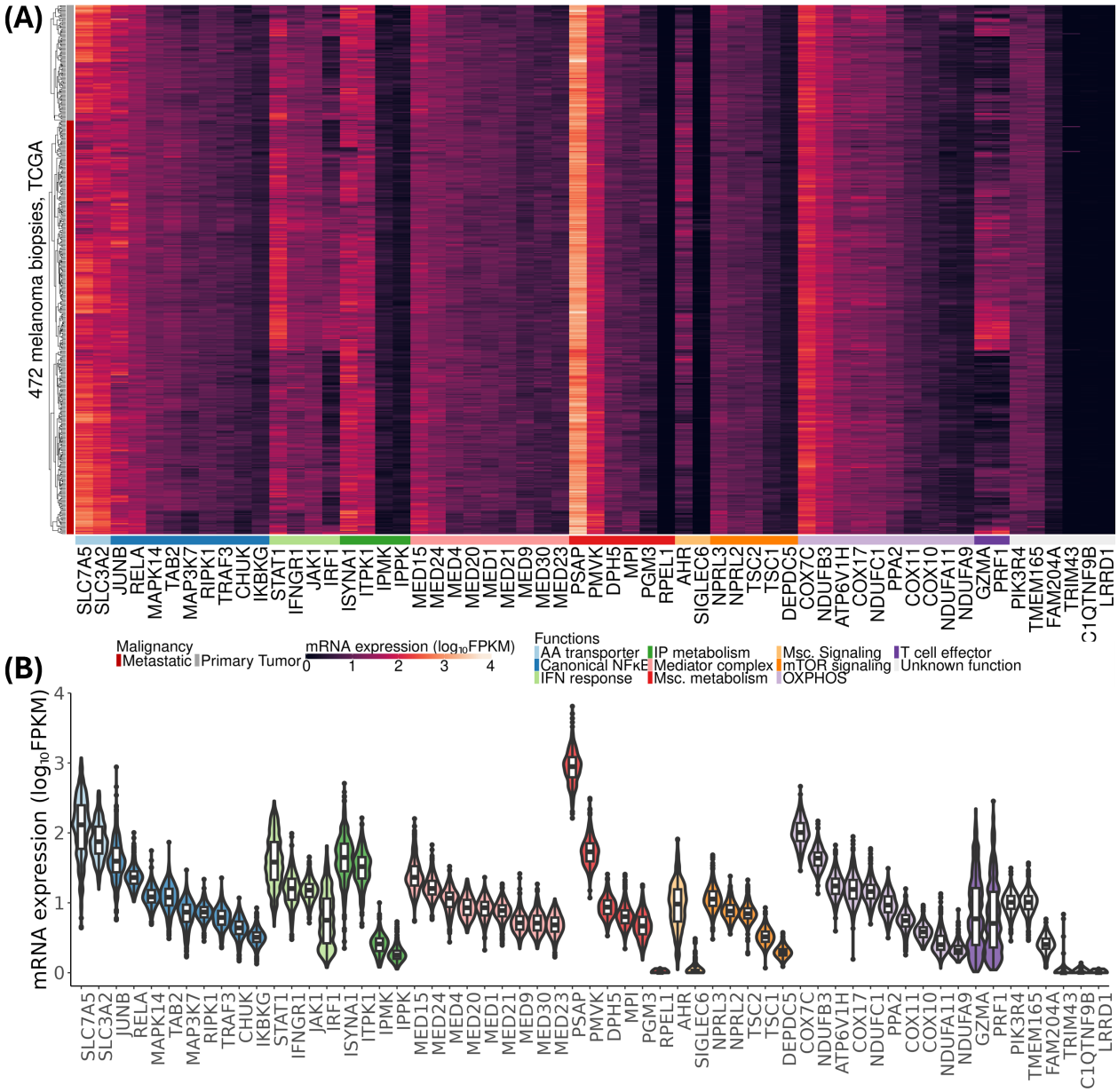

Figure 13. TCGA dataset reveals high and consistent mRNA expression of candidate genes in melanoma patients.

(A) Heatmap constructed from the relative mRNA expression level of top screen hits and the RNAseq data of 472 melanoma patients acquired from TCGA database. The dataset included both primary tumors and metastatic disease which are highlighted in different colors. Columns and rows were clustered by Ward D2 method. **(B)** violin plot and box plot represent the distribution of the mRNA expression of genes of TCGA patient samples. The area was colored according to the assigned functional annotations.

As summarized in the heatmap, the TCGA dataset reveals differentially regulated mRNA expressions of the selected candidate genes (Figure 13A). Most screen candidates have a uniform and moderate expression level across the patient's samples, which is indicated by their narrow interquartile range (4.52 FPKM on average) of the mRNA expression. A range of 1.78 to 17.4 FPKM of median mRNA expression of the selected hits was reported for most genes, with a few exceptions of highly expressed genes that reached beyond 50 FPKM. No statistically significant difference was found between the two disease stages as indicated by a two-sample t-test ($p= 0.73$). The majority of members of the same functional annotations were not closely clustered under the same hierarchical node while exhibiting different median expression levels of up to 25-fold difference, suggesting a disproportionate involvement between members for some pathways.

The *PSAP* gene, part of glycosphingolipids metabolism, was revealed to have the highest mRNA expression in the patient's data, with a median expression of 885 FKPM (Figure 13B). Similarly, *SLC3A2* (74.8 FPKM) and *SLC7A5* (130 FPKM) are reported to have the second highest mRNA expression in patient's samples as compared to other candidates. *JUNB* (39.4 FPKM) and *RELA* (23 FPKM) from the canonical NF-κB signaling, and *ISYNA1* (44.6 FPKM) and *ITPK1* (32.9 FPKM) of IP metabolism were also substantially expressed in patient samples. The consistently high expression of these genes across patient samples was in line with the reduced cell fitness mediated by LOF mutations in the co-culture screens. The same was observed from mediator complex subunits and mTOR signaling pathway which were reported to be commonly detected among patients. A key component in mTOR signaling, *TSC1* (3.26 FPKM), as a part of the TSC1-TSC2 mTORC1 inhibition complex, was poorly expressed in patients and hinted a possible mTOR activation mechanism to promote melanoma growth. Not all candidates assigned to OXPHOS category were expressed in patient samples uniformly (5.57 to 101 FKPM). The disparity in expression level signifies a disproportionate importance between the OXPHOS candidates.

The expression of components on the IFNγ response pathway were commonly detected across patients (5.08 to 38.2 FPKM). However, the moderate to high

expression in melanoma samples contradicts the general idea that IFNγ response downregulation serves as the defense mechanism against T cells cytotoxicity. Furthermore, a general correlation of these genes with the expression of granzyme (*GZMA*) and perforin-1 (*PRF1*) can be observed conspicuously from the clustering pattern on the heatmap (Figure 13A). This suggests a possibility of T cell being the source of the mRNA expression rather than melanoma tissue. The expressions of *GZMA* and *PRF1* are highly specific to hemopoietic cell types including T cells as shown in a consensus expression dataset of RNAseq of healthy tissue (Fagerberg et al., 2014; Lizio et al., 2019; Lonsdale et al., 2013; Uhlén et al., 2015). The mRNA transcript of these two genes was almost certainly captured from the TILs within the melanoma biopsy and, therefore, it is also possible that the sequencing reads from the endogenous expression of IFNγ signaling components were masked by that of TILs in the same manner.

The mRNA expression level in patient samples alone may not demonstrate the direct link between screen candidates and melanoma progression. Therefore, I have examined the overall survival of melanoma patients with the stratification on mRNA expression levels of each gene. The patients were segregated into high-expression and low-expression cohorts at 25^{th} and 75 quantiles of mRNA expression quantified within the same study. Kaplan-Meier survival curves were then plotted to illustrate the diverging clinical outcomes of different cohorts (Figure 14).

Substantial evidence was reported for genes from several clusters, including mediator complex subunits, AA transporter, IP metabolism, OXPHOS and mTOR signaling significantly influenced the prognostic outcome of melanoma patients (Figure 14, Supp. Table 5). The median overall survival time of melanoma patients was significantly prolonged in the low expression cohorts of *SLC3A2* (43.9 months), *SLC7A5* (18.4 months), and *ISYNA1* (49.2 months), whereas the survival was significantly lower in the high expression cohorts of MED15 (-35.7 months), MED20 (-22.2 months), *PIK3R4* (-25 months), *DEPDC5* (-17.2 months) and *NPRL3* (-15.7 months) as compared to the moderate expression cohorts. The prognosis in these high or low cohorts are in accordance with observations from the co-culture screens, in which the LOF mutations of *SLC3A2*, *SLC7A5* and *ISYNA1* caused cell depletion while those of *MED15*, *MED20*,

PIK3R4, *DEPDC5* and *NPRL3* led to cell enrichment. On the other side of the spectrum, a low expression of *COX17* of the OXPHOS process may associate with a poor prognosis of melanoma patients (-23.2 months). Based on the worse survival in high expression cohorts and sensitizing phenotype of the mutants observed in the screens, I hypothesize that *SLC3A2*, *SLC7A5*, *ISYNA1*, *MED15*, *MED20*, *PIK3R4*, *DEPDC5* and *NPRL3* could be potential resistant genes against T cells cytotoxicity when unperturbed. In the opposite, *COX17* could be a potential sensitizing genes. A summary of gene function inference is presented in Supp. Figure 8.

In contrast to the screen phenotypes, the low cohorts of *PGM3*, *PSAP* and *MED23* were 21.7, 26.7 and 28.6 months lower than the high expression cohorts respectively, whereas a decrease in *COX10* expression associated with better prognosis for melanoma patients (44 months). The clinical data supports that the unperturbed gene expressions of *PGM3*, *PSAP* and *MED23* serve a protective role for melanoma cells against T cells cytotoxicity, and *COX10* may serve as a sensitizer instead.

Selected candidates of the canonical NF-κB signaling pathway generally constituted a detrimental effect on the survival of melanoma patients with both upregulated and downregulated expressions. A range of 10.1 to 50.8 month decrease in median over survival time in both high and low expression cohorts was observed when compared to the moderate expression cohorts. The effect is most prominently exhibited by *CHUK*, *JUNB* and *MAP3K7* genes. The result in part agrees with the phenotype observed from the co-culture screen where they uniformly reduced the cell fitness when perturbed. However, clinical data showed a decline in melanoma patients' survival whenever the mRNA expression level deviated from the median expression. The observation suggests that an equilibrium of NF-κB signaling would seemingly need to be maintained by these gene candidates for an extended survival of melanoma patients.

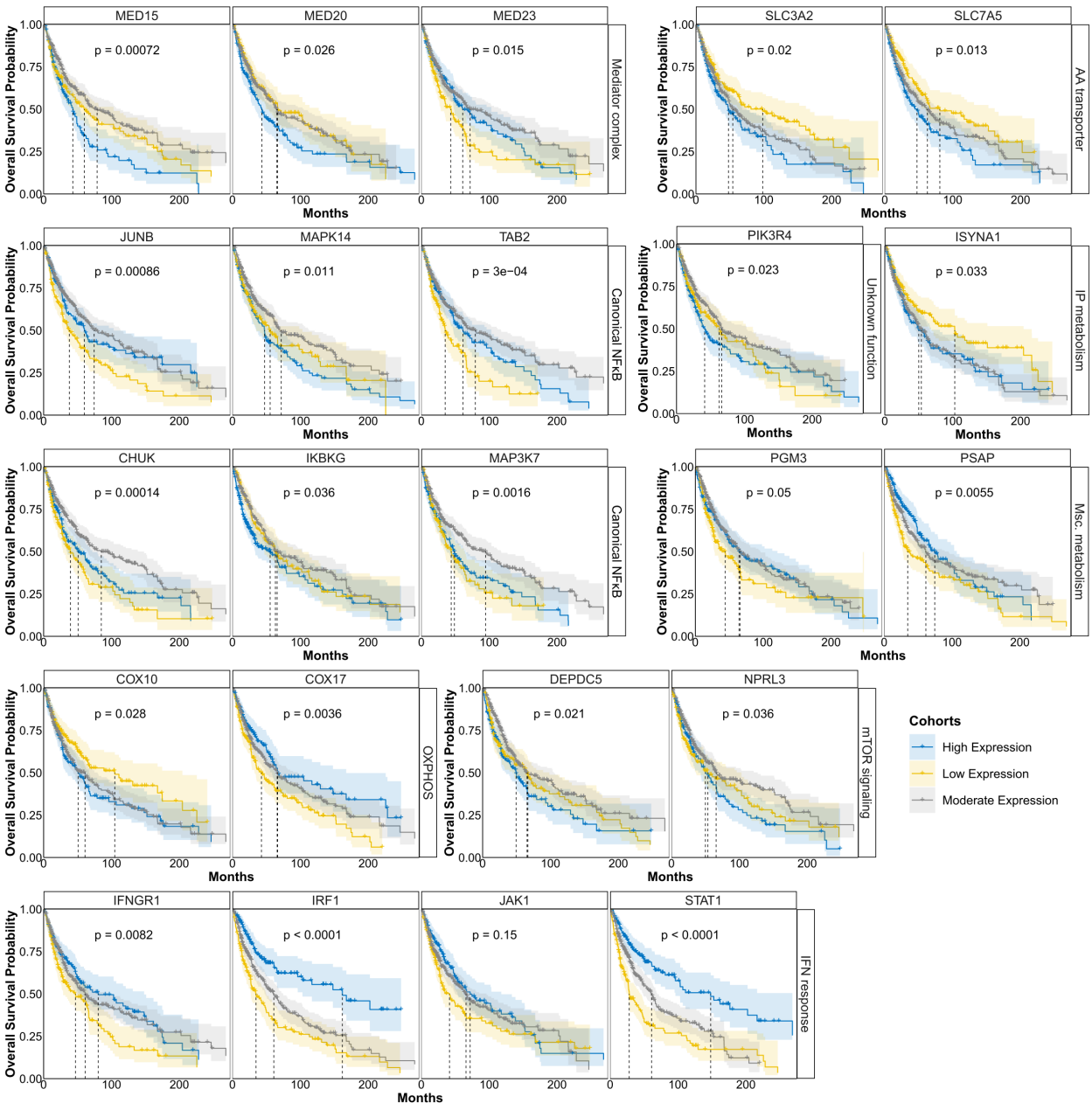

Figure 14. Gene candidates significantly altered the prognostic outcome of melanoma patients.

Kaplan-Meier curves are plotted for overall survival probability of melanoma patients that expressed different mRNA levels of selected gene candidates. 631 cutaneous and metastatic melanoma patients from 4 separate studies were included in the survival analysis. Patients were stratified into 3 mRNA expression cohorts at 25th and 75th quantiles of mRNA expression level within the same study. Each low or high expression cohort contains approximately 165 patients, and moderate cohort 320 patients. Statistical significance was evaluated by log-rank test. Shaded area specifies the 95% CI and dashed lines indicate the median survival time.

PGM3, and gene candidates annotated to IFNγ response on the other hands, exhibited divergent phenotypes in CD33 CAR-T cell screen and ROR1 CAR-T cell screen. However, these genes were only found to significantly incur a reduction in melanoma patients' overall survival when the expression was downregulated. A 14.3 to 32.9 month decrease in median survival time was reported from the combined dataset. The high expression of *IRF1* and *STAT1* further improved the survival time considerably by 87 to 101 months, highlighting the essentiality of IFNγ response in elimination of melanoma cells by T cells. The clinical importance of IFNγ signaling indicates that the result from CD33 CAR-T cell would be in better accordance with the patient's actual condition.

15 genes related to mediator complex, AA transporter, IP metabolism, mTOR signaling, OXPHOS and NF-κB signaling presented conforming expression level from clinical data and matching sensitizing/resistant phenotype in the screen.

To evaluate the direct association of T cells activity in the melanoma samples to different genetic contexts, a cytolytic activity analysis was conducted In parallel to survival analysis (Figure 15). A study has proposed to determine cytotoxic T lymphocyte activity from the melanoma biopsy (Rooney et al., 2015). The T cell cytolytic activity was reported as a score derived from the geometric mean mRNA expression of *GZMA* and *PRF1* genes from the bulk RNAseq of melanoma samples. The researchers further demonstrated that the *GZMA* and *PRF1* expressions are restricted to the infiltrating T cells inside the resected melanoma tissue and can thus be used to estimate the extent of T cell killing. In general, a higher cytolytic score implies stronger $CD8^+$ T cell cytotoxicity.

In a subset of the clinical data containing 88 patients, the cytolytic scores showed a significantly weak to moderate inverse correlation with the mRNA expression of *SLC3A2* (R: -0.37), *SLC7A5* (R: -0.22), ISYNA1 (R: -0.23), and PIK3R4 (R: -0.23) (Figure 15). Alternatively, the expression level of COX17 was weakly and positively correlated with the cytolytic score (R: 0.29). The directions of correlation shown in all the five genes aligned appropriately with the expectation based on the phenotype observed from

survival data and screen results. The result provided circumstantial evidence to these gene candidates' potential participation in modulating melanoma-T cell interaction.

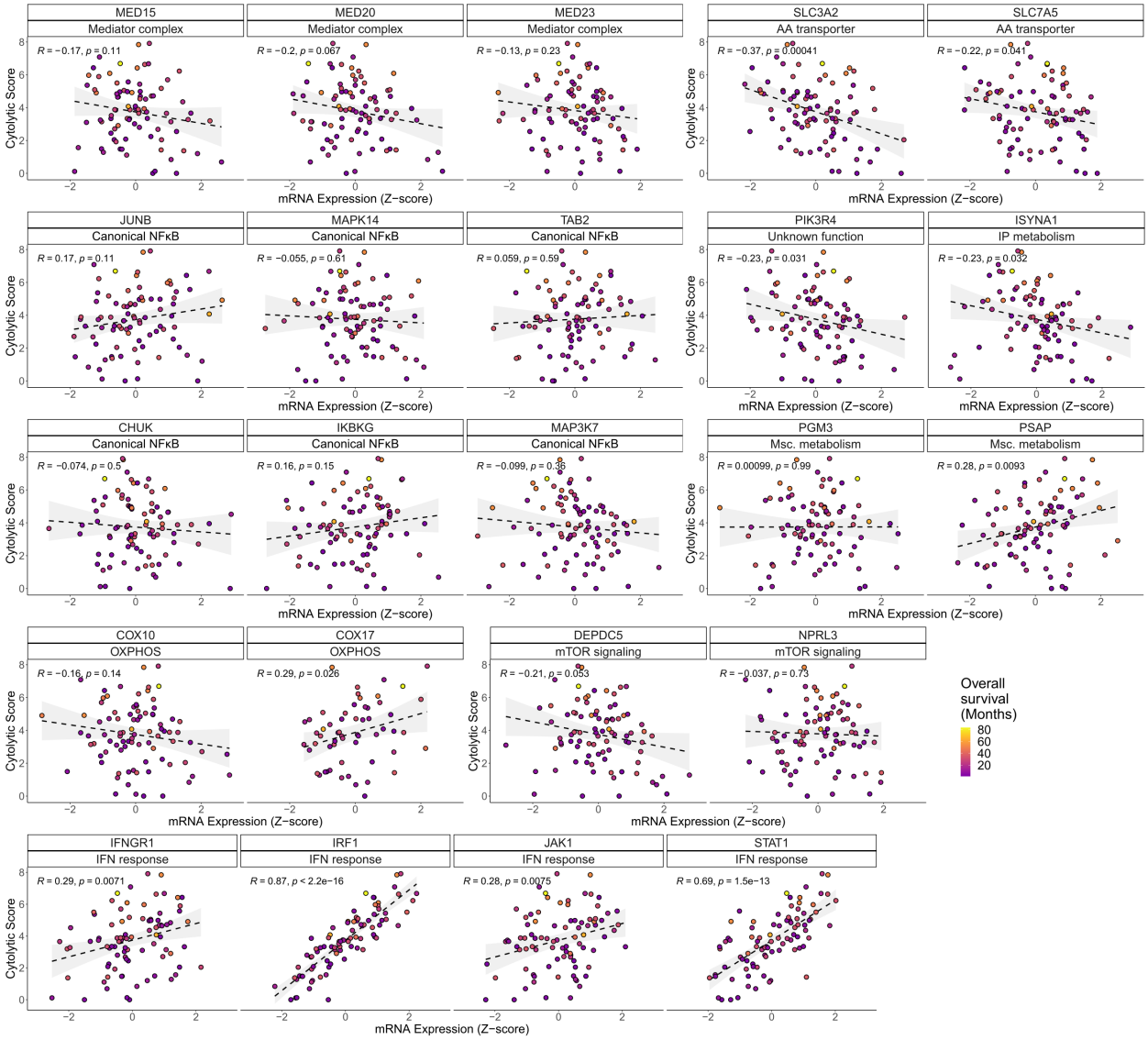

Figure 15. mRNA expression of gene candidates exhibits significant correlation with T cell cytolytic activity.

Scatter plots for the correlation between mRNA expression of gene candidates and the cytolytic score. The score is measured from the log-transformed geometric mean of GZMA and PRF1 mRNA expressions from the same patient sample. Z-score of the mRNA expression was used for axis. 88 metastatic melanoma samples were included in the analysis. A linear model was fitted to the data of each gene candidates (dashed line) and the shaded area depicts 95% CI. R value denotes the Pearson correlation coefficient.

Similarly, all genes assigned to IFN response, including *IFNGR1* (R: 0.29), *IRF1* (R: 0.87), *JAK1* (R: 0.28) and *STAT1* (0.69), exhibited a significantly weak to strong correlation with their mRNA expression, which were in line with overall survival data of melanoma patients. This supports their strong connection to the T cell effector function. The observation is coherent with existing findings in which IFNγ promotes activation, expansion, and differentiation of cytotoxic T lymphocytes (Badovinac et al., 2000; Whitmire et al., 2005; Curtsinger et al., 2012; Bhat et al., 2017). However, the findings also disagree with the phenotype of IFNγ pathway shown in ROR1 CAR T cells screen where the LOF mutation served as resistant mechanism against CAR-T cells. The underlying cause remained unsolved. In addition to the above genes, *PSAP* showed a positive correlation (R: 0.28) with the T cell function, confirming the survival data but not the screen result. This nonetheless suggests a possible involvement of *PSAP* in sensitizing melanoma cells.

Contrarywise, there was insufficient evidence to show a correlation between the expression of three other clusters of genes, including mediator complex, NF-κB signaling and mTOR signaling, and cytolytic score. Hence, their potential roles in modulating T cell cytotoxicity were not indicated. Their protective effect on melanoma cells or the survival benefit to patients were likely manifested through other cellular processes.

Despite being melanoma-intrinsic factors, *SLC3A2*, *SLC7A5*, *ISYNA1*, *PIK3R4* and *COX17* among other candidates eventually showed differential fitness in the screen, a significant influence on patient's survival and a correlation with T cell activity. Sufficient evidence was collected to suggest a potential immunomodulatory role for these cancer-intrinsic factors, which will be shortlisted for further examination for underlying mechanistic insight. Taking the protein localization and the lack of knowledge of these gene in the field of cancer immunity into account, the first two candidate to be functionally validated were *SLC3A2* and *SLC7A5*. The *SLC3A2* and *SLC7A5* are localized to plasma membrane of melanoma cells, which provides a possibility to directly interact with surface proteins on CD8+ T cells and hence influence their actions.

7.3. Validation of SLC3A2/SLC7A5 mutations as melanoma-intrinsic modulator against T cell cytotoxicity

SLC3A2 (CD98 heavy chain) is a type II transmembrane glycoprotein that forms heterodimers with SLC7A5 (L-type amino acid transporter 1) to create sodium-independent amino acid transporters (Supp. Figure 9), also collectively named CD98 complex. The transporter facilitates the uptake of large neutral amino acids (LNAA), such as leucine, isoleucine, valine, phenylalanine, tyrosine, tryptophan, methionine, and histidine. These amino acids are essential for protein synthesis and activating signaling pathways like mTOR, which are critical for cell growth and proliferation. Beyond transport, CD98 plays a significant role in integrin signaling, augmenting pathways like mTOR, PI3K/AKT, and MAPK, which are critical for cell adhesion, migration, and survival, as highlighted in CD98 as a prognostic biomarker and target for cancer treatment. This dual role in amino acid transport and signaling makes CD98 a multifunctional protein in cellular processes (Prasad et al., 1999; Yan et al., 2021).

7.3.1. CD98 expression on melanoma did not alter activation, senescence, and exhaustion of T cells.

SLC3A2 and *SLC7A5* were selected as two major screen hits for further investigation due to their potent enhancement of T cell cytotoxicity in the screen, and their clinical relevance as discussed in the last section. Also, the membrane-localization of the transporter provided a possibility of direct interaction with certain proteins on T cells to alter T cell effector function. Alternatively, T cells could enter senescence or exhaustion by themselves due to events triggered by the LNAA uptake function of the transporter on melanoma in the local environment. Therefore, I started the validation experiment by hypothesizing that T cell functions were suppressed in the presence of SLC3A2 and SLC7A5 (also referred to as CD98 to denote the complex transporter complex).

To prepare cell lines for assessing T cell cytotoxicity in the presence and absence of CD98, I have established stable KO cell lines of both *SLC3A2* and *SLC7A5* by lentiviral infection. The A375-CD33-Cas9 and A375-Cas9 cell lines were separately transduced to overexpress sgRNA. Two sgRNAs were used per gene (sgSLC3A2_1, sgSLC3A2_3, sgSLC7A5_1, and sgSLC7A5_2). The resulting KO efficiency was verified by western blotting (Figure 16A). The use of sgRNA targeting *SLC3A2* and *SLC7A5* yielded almost complete KO as shown on the blot and left a faint trail of residue. It is also worth noting that the expression of sgSLC7A5 simultaneously abolished the expression of SLC3A2 on protein level, and the sgSLC3A2 also drastically reduced the expression of SLC7A5 protein. Upon inspection of genome binding of the above four sgRNAs, it was found that no predicted off-target binding site was within the coding DNA sequences of the two genes, suggesting that the absence of SLC7A5 and SLC3A2 might have destabilized each other on protein level.

To validate the original findings from the screen, I performed a TRAIL treatment assay and a T cell cytotoxicity assay different *SLC3A2* and *SLC7A5* KO lines. Different A375 cell lines were treated with TRAIL and examined for CASP3 and CASP8 activity by western blotting (Figure 16A). The result showed a significant upregulation of cleaved product of caspase-3 was observed in SLC3A2/SLC7A5 KO cells. The elevated cleavage activity of caspase-3 indicates a higher extent of apoptosis in the absence of SLC3A2/SLC7A5 on molecular level. Alternatively, CD33 CAR-T cells were co-cultured with A375 cells at a E:T ratio of 0.5:1 for 24 hours. Annexin-V staining was performed afterwards to measure apoptotic and necrotic A375 cell populations as a result of the cytotoxicity of T cells. The result showed that the A375 expressing sgSLC3A2_3, sgSLC7A5_1, and sgSLC7A5_2 have a significantly increased level of apoptotic population, confirming the phenotype of the CD98 KO on A375 observed from the co-culture screens (Figure 16B).

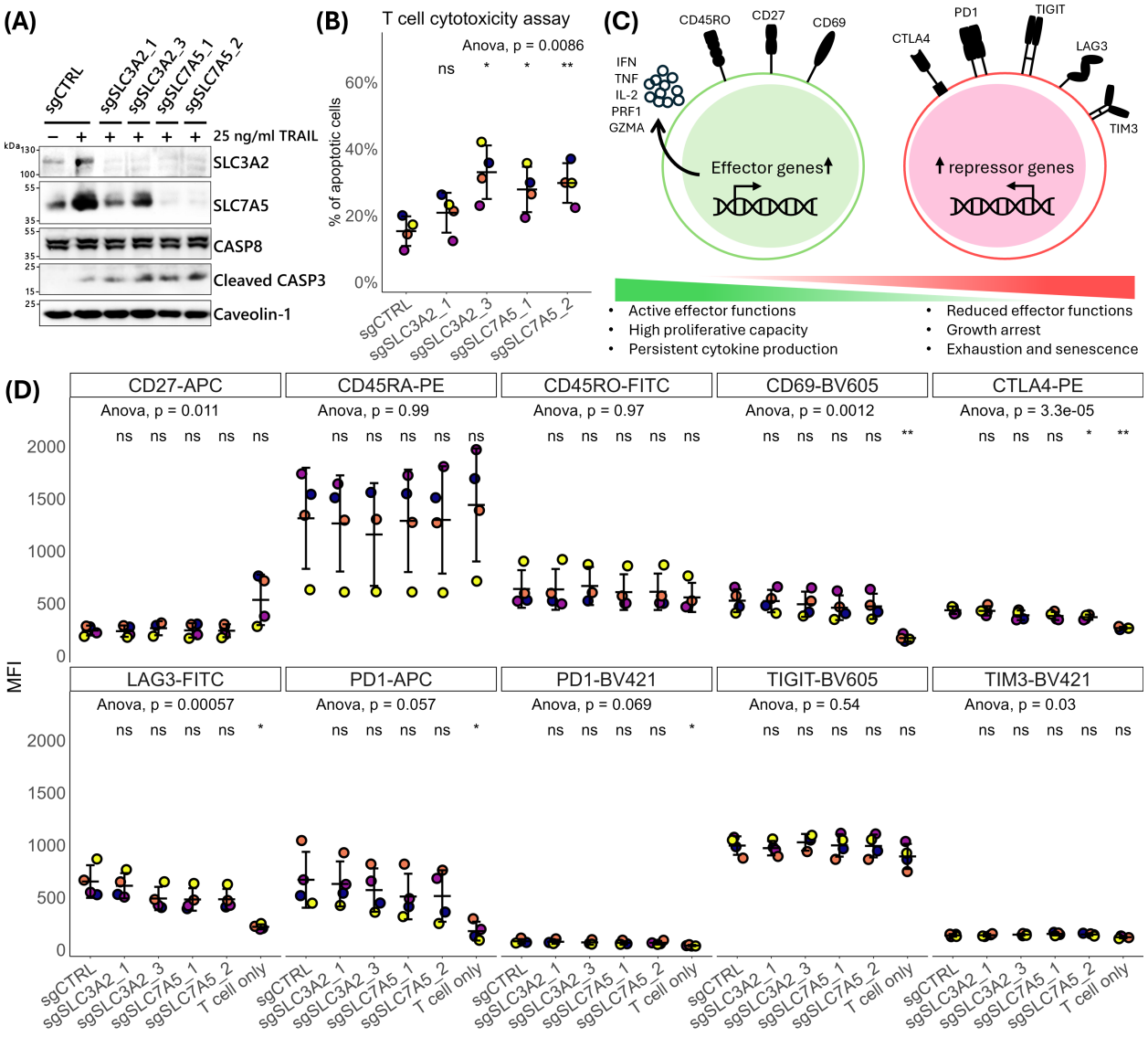

Figure 16. *SLC3A2*/*SLC7A5* did not differentially impact T cell activation, senescence, or exhaustion.

(A) KO verification of SLC3A2 and SLC7A5 genes, and effect of TRAIL treatment on A375 cells' caspase activity. A375-CD33-Cas9 were transduced to overexpress sgRNAs targeting SLC3A2 and SLC7A5. The established lines were treated with 25 ng/mL TRAIL for 48 h prior to analysis by western blotting. Caveolin-1 serves as loading control. **(B)** Annexin-V-based cytotoxicity assay of T cell on A375 cells. T cells and different A375 cell lines were co-cultured for 24 hour prior to analysis. **(C)** Graphical summary of established immune checkpoint molecules that indicate T cell activation, senescence, or exhaustion. The preferential expression of respective markers at activated and suppressed states are illustrated. **(D)** Immunophenotyping of CD33 CAR-T cells by a selected panel of markers after co-culturing with different lines of A375-CD33-Cas9 for 24 hours. The cells were stained with fluorophore-conjugated antibodies and analyzed by flow cytometry. T cell population was specifically gated by CD8 expression. "T cells only" sample refers to samples without A375 co-culture. All statistical significance in **(B & C)** were computed using ANOVA, couple with pairwise T tests. All data points were colored according to donors. The data were reported as mean ± sd.

To test the hypothesis that CD98 directly inhibitor T cell effector function, I have investigated the potential markers that could indicate the state of cytotoxic T cells. Figure 16C provided a graphical summary of well-established immune checkpoint molecules present on cytotoxic T cells. To be specific, a loss of CD27 and CD28 expression and a concurrent upregulation of CD57, KLRG1 serve as indications to the entry of senescent state by T cells (Strioga et al., 2011; Ahn et al., 2018). Alternatively, a relatively high expression of multiple inhibitory receptors on $CD8^+$ T cells, including PD-1, TIM-3, LAG-3, TIGIT, and CTLA-4, would be a sign of the cytotoxic T cell being dysfunctional or exhausted (Crespo et al., 2013), independent of a transient elevation of expression after antigen detection. Additional markers including CD45RA, CD69, and CD45RO assists the identification of naïve population, early activation and differentiated subset of T cells respectively (Clement, 1992; Mueller & Mackay, 2016). A selection of these markers was included to profile the state of T cells after co-culturing with different A375 cells.

To profile the expression of selected immune checkpoint molecules on T cells that are potentially affected by A375, CD33 CAR-T cells were co-culture with A375 for 24 hours. Both A375 and T cells were harvested at the end of the co-culture and stained together by different fluorescently labeled primary antibodies. The change in marker expression upon co-culture partly conforms with existing studies (Figure 16D). An upregulation of CD69 and PD1 was observed when comparing “T cell only” and co-culture conditions. The increase in the two marker is a sign of early T cell activation upon detecting A375 cells. Also, the transient upregulation of inhibitory receptors including LAG-3, and CTLA-4 was observed upon antigen activation, which is in line with established findings (Waldman et al., 2020). However, the observation also suggests that the T cells effector function was mostly suppressed to equal extent by different A375 cell lines upon co-culture. Except for the CTLA-4 marker, a slight but significant decrease in the percentage of cells expressing CTLA4 was detected only in A375 expressing sgSLC7A5_2, but it is not enough to explain the change observed in the screen and in the assay (Figure 16B). An insignificant difference was also observed from the expressions of CD27, CD45RA and CD45RO. Overall, the result did not reveal significant differences in most markers

assayed when comparing the KO cell line to WT cell lines, indicating the expression of SLC3A2/SLC7A5 in melanoma did not interfere with the effector function of T cells.

7.3.2. Loss of CD98 sensitized melanoma against T cell secreted TRAIL molecules.

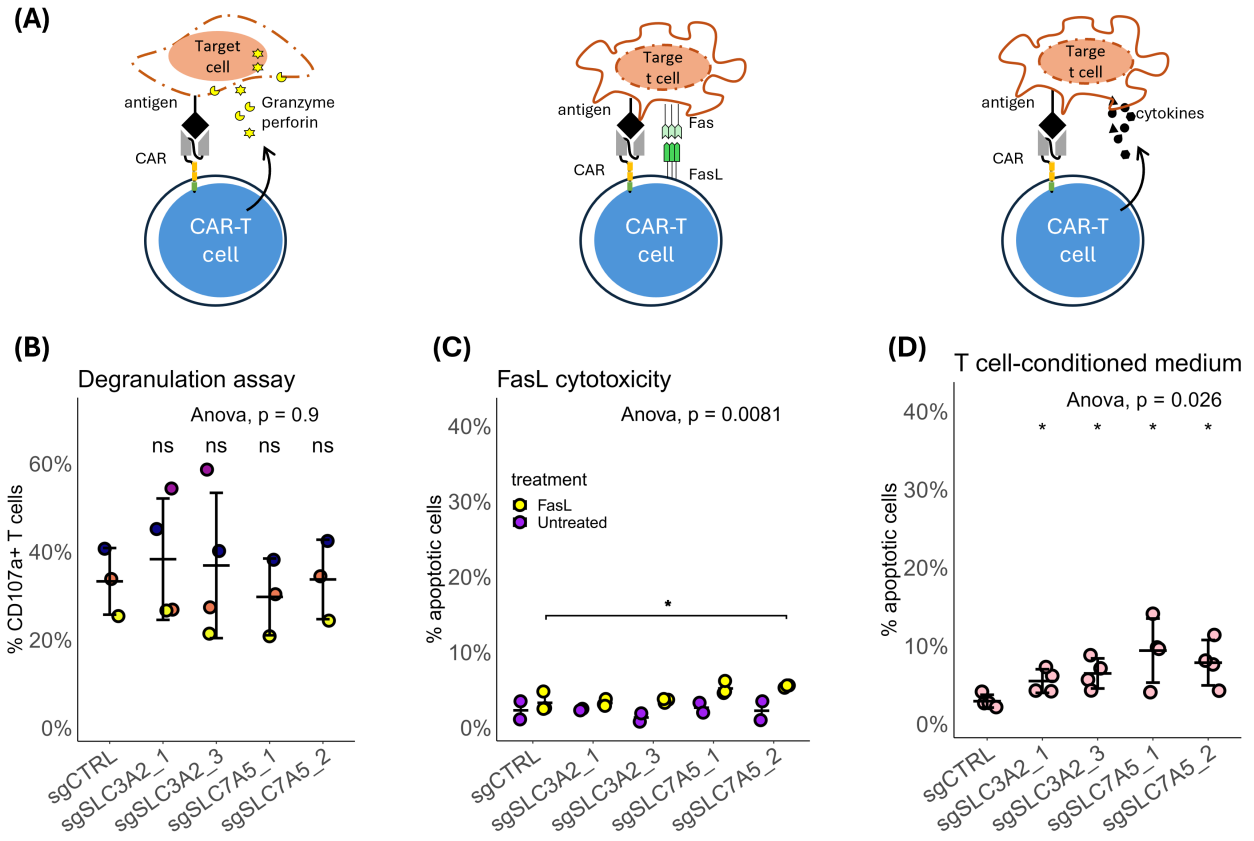

Figure 17. SLC3A2/SLC7A5 KO cell line were sensitive secreted factors of T cells.

(A) Graphical illustration of T cells' modes of killing. T cells primarily release granzyme and perforin to destroy target cells. Alternatively, T cells facilitate the binding of FasL to target cell's Fas (FasL receptor) or secrete cytokine to trigger apoptosis. **(B, C)** T cells were co-cultured with A375 cell lines (E:T = 1:1) for 4 h or treated with 40 ng/mL soluble FasL for 48 hours. Annexin V assay was performed to evaluate cell death in each condition. **(D)** T cell-conditioned medium was prepared from co-culturing CAR-T cells and WT A375. Afterwards, different A375 cell lines were cultured in the combined conditioned medium for 24 hours. Annexin V assay was performed to evaluate cell death in each condition. All statistical significance in (B-D) were

computed using ANOVA, couple with pairwise T tests. The data were reported as mean ± SD. Data points in **(B)** were colored according to donors while each data point in **(C & D)** denotes a replicate.

As the loss of CD98 protein in melanoma cells did not directly alter the T cell state upon cu-culturing, another aspect to examine would be which specific effector functions of T cell were differentially perceived by different A375 cell lines. There are three main methods of how T cells execute their function (Figure 17A). Their predominant effector function is by releasing granzyme and perforin which compromise the target cell membrane and cause apoptosis by activating caspase activity. Alternatively, T cells use membrane-bound FasL to trigger FAS-dependent apoptosis on cancers or secreting various cytotoxic cytokines in proximity to the target cells to induce similar apoptotic responses.

CD107a is an integral membrane protein present in the cytolytic granules that contains granzymes and perforin. After CAR activation, the contents of cytolytic granules are released into the immune synapse while exposing the CD107a. therefore, a transient increase in surface CD107a level can be used as a marker for T cell degranulation (Betts & Koup, 2004). Initially a CD107a degranulation assay was performed to confirm any discrepancies in the degree of granzyme and perforin release by labeling surface CD107a after A375-T cell co-culture. No significant difference in the extent of T cell degranulation was detected from the *SLC3A2*/*SLC7A5* KO cell lines as compared to the WT A375 (Figure 17B).

Next, I analyzed whether the FasL treatment may differentially cause apoptosis in A375 cells. There was generally no difference between the KO cells and the WT cells in the treated group, except for A375 expressing sgSLC7A5_2 that increased the apoptotic population by 2.2% (Figure 17C), suggesting FasL is not likely the major factor to cause the sensitivity against T cells. Lastly, to test the sensitivity in the secreted factors of T cells, T cell-conditioned medium was prepared by co-culturing only WT A375 and T cells for 24 hours. Different A375 cell lines were then cultured in clarified conditioned medium for 24 hours. The result showed that the conditioned medium caused a uniform increase

in the percentage of apoptotic cells across different KO cell lines as compared to the WT cells (Figure 17D), which raised up to 10% of apoptotic cell population. The treatment indicates certain components in the secretome of T cells were responsible for the heightened death of *SLC3A2*/*SLC7A5* KO cells.

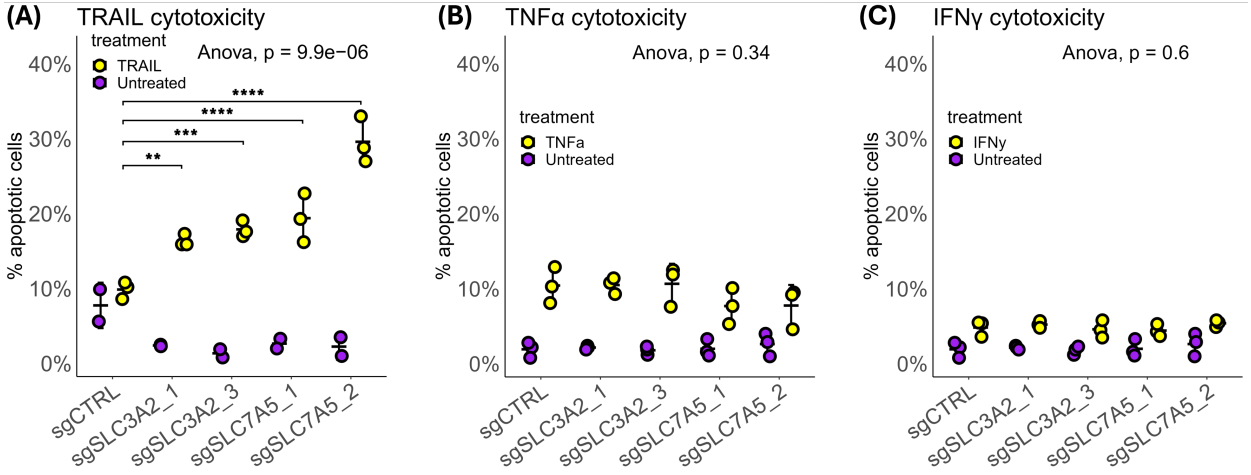

Figure 18. SLC3A2/SLC7A5 KO sensitize A375 to T cell cytotoxicity through TRAIL signaling

Different A375 cell lines were cultured in complete growth medium supplemented with indicated with different common cytokines of T cells, including 25 ng/mL TRAIL **(A)**, 2.5 ng/mL IFNγ **(B)**or 10 ng/mL TNFα **(C)** for 48 hours. After incubation, the cells were harvested and stained for annexin-v to evaluate the percentage of apoptotic cells. All statistical significance were computed using ANOVA, couple with pairwise T tests. The data were reported as mean ± SD. Each data point denotes a replicate.

To determine which factors secreted by T cell were causing the increased sensitivity in A375, different A375 cell lines were treated with a selection of cytokines that are commonly released during T cell immune response. The result reveal that among TRAIL, IFNγ and TNFα, only TRAIL caused a significant increase in the apoptotic A375 population when comparing the WT cell to KO cells in treatment group. An 8% to 20% increase in percentage of apoptotic cells were observed when KO cell lines were treated with 25 ng/mL TRAIL molecules (Figure 18). The result indicates that at least the TRAIL signaling pathway in A375 was responsible for a higher sensitivity against T cell

cytotoxicity in the absence CD98 and suggest that endogenous expression of the transporters inhibited TRAIL-induced apoptosis.

7.3.3. Determining the mechanism of TRAIL signaling responsible for the increased sensitivity

To determine through which axis TRAIL increases CAR T mediated Killing in A375 cells, I have first hypothesized that the surface expression of TRAIL receptors was downregulated by the CD98 proteins. There are several protein entities known to bind TRAIL at high affinity (Figure 19A). TRAIL receptor 1 (TRAIL-R1) and TRAIL receptor 2 (TRAIL-R2) bind incoming TRAIL molecules to initiate a cascade of downstream events for apoptosis. Decoy receptor 1 (DcR1) and decoy receptor 2 (DcR2), on the other hand, do not have functional death domains to initiate the apoptotic response in A375, but serve to compete with TRAIL-R1 and TRAIL-R2 for TRAIL. Osteoprotegerin (OPG) is a secreted protein of cancer cells that contains a similar motif with TRAIL R1 and R2 to compete for TRAIL (S. Wang & El-Deiry, 2003).

Using flow cytometry to measure cell surface levels of different TRAIL receptors on A375 cells under different KO conditions, the result did not reveal any difference in the expression of the selected TRAIL receptors between WT A375 and the *SLC3A2*/*SLC7A5* KO cell lines, indicating no regulation on the TRAIL receptor expression was inflicted by the presence of CD98 (Figure 19C).

I have then hypothesized that the LNAA uptake function of CD98 is connected to the TRAIL sensitivity. To suppress the function of the transporter while retaining the endogenous expression, SLC7A5 inhibitors including BCH and JPH203 were applied to WT A375 to test for the connection between the functionality and the TRAIL sensitivity. When the WT A375 cells were treated with BCH or JPH203 on top of TRAIL, contradicting outcomes were observed. BCH suppressed the expression of caspase-8 and the cleavage of caspase-3 while cleaved caspase-3 was highly upregulated,

indicating diverging responses mediated by the two drugs (Figure 19B). It is not clear whether one of the drug was associated with unknown off-target effect on A375, or whether this is the phenotype on TRAIL signaling. Therefore, it remains inconclusive whether the LNAA uptake function of CD98 is linked to TRAIL sensitivity and further experimentation using additional inhibitors or nutrient-depletion medium might be required to verify the hypothesis.

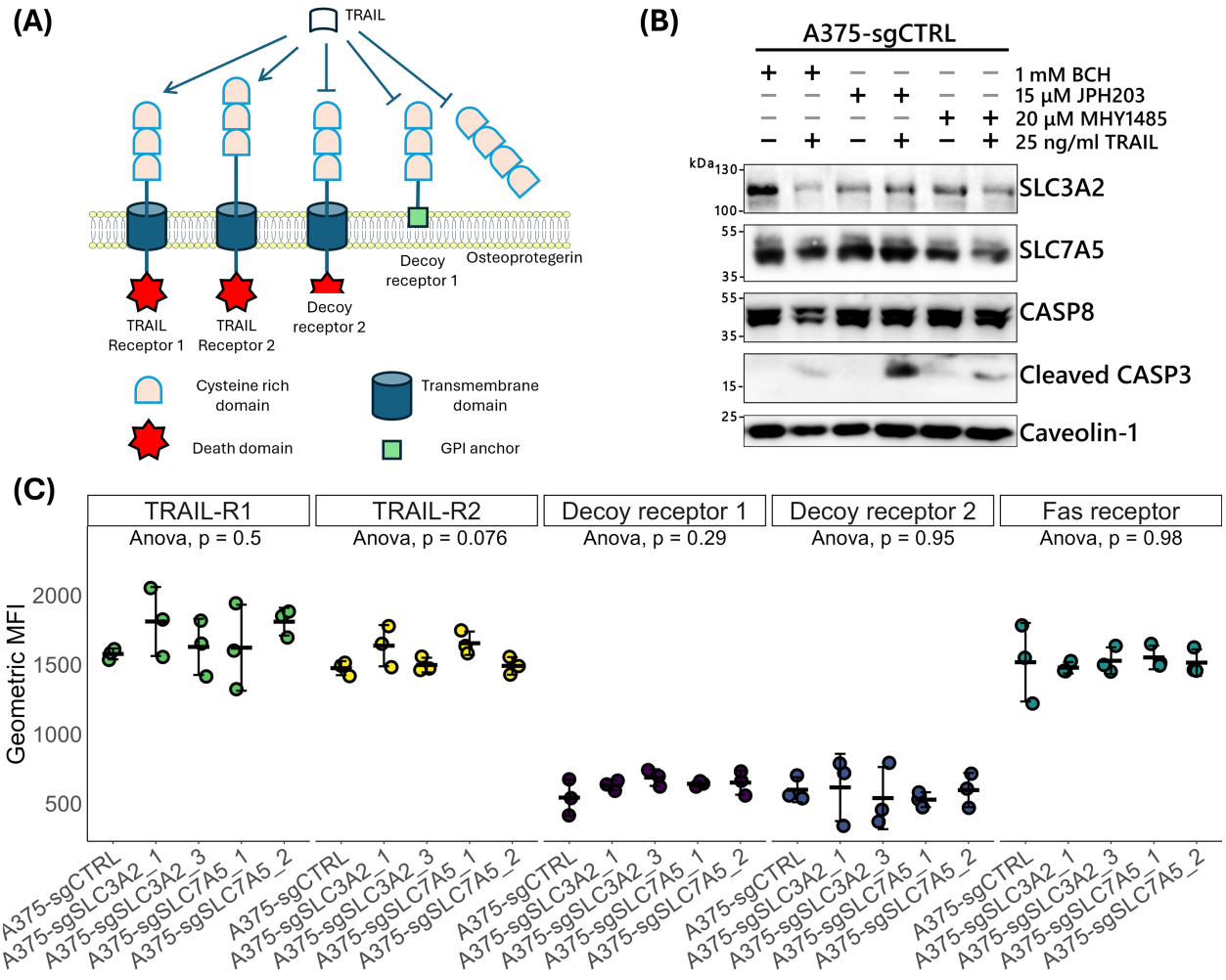

Figure 19. TRAIL receptors expression was not affected by SLC3A2/SLC7A5.

(A) Graphical summary of the variety and characteristics of TRAIL receptors. TRAIL-R1 and TRAIL-R2 bind TRAIL molecules and initiate apoptosis in cancer cells. Decoy receptors 1 and 2, and Osteoprotegerin compete with TRAIL-R1, TRAIL-R2 for TRAIL, but lack functional death domain to initiate apoptosis. **(B)** SLC7A5 inhibition on WT A375 cells. The WT A375 cells were treated with 1 mM BCH or 15 µM JPH203 for 24h, and then another 24 hours with 25 ng/mL TRAIL. The cells were harvested and analyzed on western blots. **(C)** Expression profile of

various death receptors on different A375 cell lines measured in geometric mean fluorescence intensity (MFI). All statistical significance were computed using ANOVA, couple with pairwise T tests. The data were reported as mean ± SD. Each data point denotes a replicate.

In the previous TRAIL treatment assay on different CD98-KO cells, the expressions of both SLC3A2 and SLC7A5 were notably upregulated upon TRAIL treatment (Figure 16A). however, the upregulation was abolished in the presence of SLC7A5 inhibitors, namely BCH and JPH203 (Figure 19B). While the implication of inhibited upregulation of CD98 remains unclear, I postulate that the expression of CD98 and TRAIL signaling activation might be synergistic, and a potential positive feedback loop would be present, driven by the LNAA uptake function of CD98.

7.4. Meta-analysis of Heidelberg CRISPR sgRNA library performance

The Heidelberg CRISPR sgRNA library (also referred to as HD sgRNA library) was previously constructed, cloned into the HDCRISPRv1 vector, and originally used in a HAP1 cells fitness screen by colleagues (Henkel et al., 2020). It has been successfully implemented in the melanoma-CAR-T cell screen for identifying modulators in the interaction between the two cell types and in the fitness screen to identify core essential genes of A375 cells. During my doctoral study, I also used the same sgRNA library on different occasions to address research questions pursued through several collaborative projects. In this section, I present the result of a meta-analysis on all past projects to examine the performance of HD sgRNA library and the general screening technique under different settings.

In total, 52 samples were collected from 7 projects. The sequencing result of the original plasmid sample was included as a reference for original sgRNA count distribution. A summary of the experimental designs, objectives and cell lines of the projects is presented in Table 30. The same workflow applied to all experiments as the

fitness screens and the co-culture screens for procedures including lentivirus packaging, infection, and cell pool expansion, and the last part of the screen, which is the cell harvesting, gDNA extraction, sequencing library preparation, deep sequencing method and bioinformatic analysis, as described in the method section 6.2.14. All cells were cultured for 7 days post-transduction and prior to additional treatments. The accountable difference between projects was the use of project-specific selection agents for exerting selective pressure onto the pool of perturbed, for instance, the use of T cells on A375 cells, or the application of ionizing radiation on SW480 cells. An exception was made for KinProLa project in which no selection agent was applied to the RKO cells. The RKOs were engineered to over-express KinProLa protein which can be labeled with fluorescent substrate in proportion to the intracellular PKA activities. Therefore, the selection was based on the colorimetric signal emitted by the KinProLa protein upon gene perturbation and labeling using a flow cytometer.

Table 30. All screening projects using Heidelberg sgRNA library

Time	Experiment	Cell line	Objective	Screen design
2018 Oct	Heidelberg sgRNA library plasmid preparation	n/a	Construct and clone sgRNA library into HDCRISPRv1 vector	n/a
2020 Jan	Baseline screen	A375-CD19/CD33	To identify core essential genes	Viability dropout of perturbed A375 cells
2021 Mar	CD8 T Cells Cytotoxicity	A375 + ROR1 CAR-T cells	To identify regulators of melanoma-T cell interaction	perturbed A375 cells selected by ROR1 CAR T cells
2021 Apr	NK Cells Cytotoxicity	A375 + NK cells	To identify regulators of melanoma-NK cell interaction	perturbed A375 cells selected by NK cells
2021 Sep	Colorectal Cancer Cell irradiation	SW480	To examine resistance mechanism arose after irradiation treatment	Viability dropout of perturbed SW480 cells after irradiation
2021 Nov	CD8 T Cells Cytotoxicity	A375 + CD33 CAR-T cells	To identify regulators of melanoma-T cell interaction	perturbed A375 cells selected by CD33 CAR T cells
2023 Nov	KinProLa protein	RKO	To identify regulators of PKA activity using KinProLa engineered protein	Perturbed RKO cells sorted by FACS according to KinProLa signals
2023 Dec	GD T Cells Cytotoxicity	A375 + GD T cells	To identify regulators of melanoma- GD T cell interaction	perturbed A375 cells selected by GD T cells

7.4.1. Sequencing sample quality

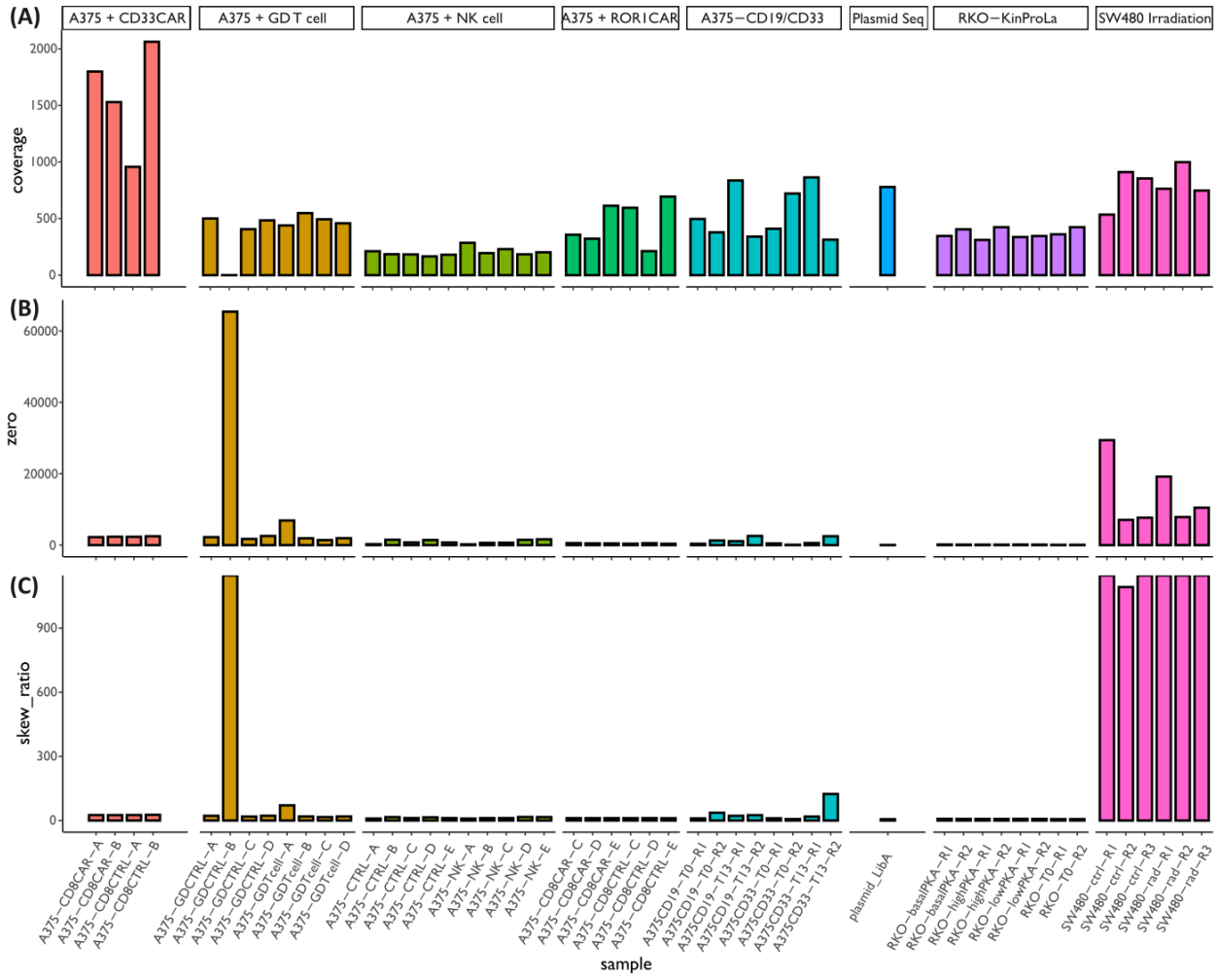

Figure 20. Coverage, zero counts and distribution skew ratio of all samples.

(A) The sequencing coverage of each samples expressed as the summation of all sgRNA counts divided by the library size. **(B)** The number of sgRNA without any detectable read from the sequencing procedure. **(C)** The skew ratio of each sample that is calculated from dividing sgRNA at 10th quantile by that of 90th quantile.

To examine if the use of HD sgRNA library may cause any anomalies in the raw sequencing data, the samples were checked for basic metrics derived from the raw data.

Most samples achieve at least 500-fold library size coverage which is a standard level for proper library representation, except for the samples from “NK Cells Cytotoxicity” project, and A375-GDCTRL-B sample from the “GD T Cells Cytotoxicity” project (Figure 20). For samples of “NK Cells Cytotoxicity” project, they achieved approximately 250x to 300x coverage, whereas the A375-GDCTRL-B was barely detected (coverage < 1x). The samples of “NK Cells Cytotoxicity” project yield lower coverage most likely due to insufficient sequencing kit used, in which overcrowding sample exceeded the capacity of the Nextseq550 kit. However, the lowered coverage of these samples apparently did not affect the sgRNA distribution which is reflected in the number of undetectable sgRNA and the distribution skewness, as well as in the similar histogram to the plasmid seq sample (Figure 20 & Figure 21). On the contrary, A375-GDCTRL-B showed a loss of 87% of the sgRNA library, and consequently an incalculable skew ratio. This was due to a technical error that caused the loss of most of the samples during sequencing library preparation as recorded in laboratory log.

For the rest of the qualified samples, no anomaly was identified as most of the sgRNA zero counts are below 10% of the library size and the skew ratios are below 50. A slightly left skewness distribution was observed for all samples, which is similar to the one generated from plasmid sample (Figure 21). This suggests the library representation in most samples was retained after all experimental procedures. Except for the six samples in “Colorectal Cancer Cell irradiation” project which have lost more than 20% of sgRNA library and have abnormal sgRNA count distribution as seen from their skew ratio and the erratic distribution. One possible cause would be the abnormal cell status occurred during the sample preparation before radiation treatment, which is traceable from the laboratory record. A small part of SW480 cells was observed to be irregularly enlarged and undergo apoptosis, which could have affected the phenotype of the cells in the culture. Similar cell status was not observed elsewhere.

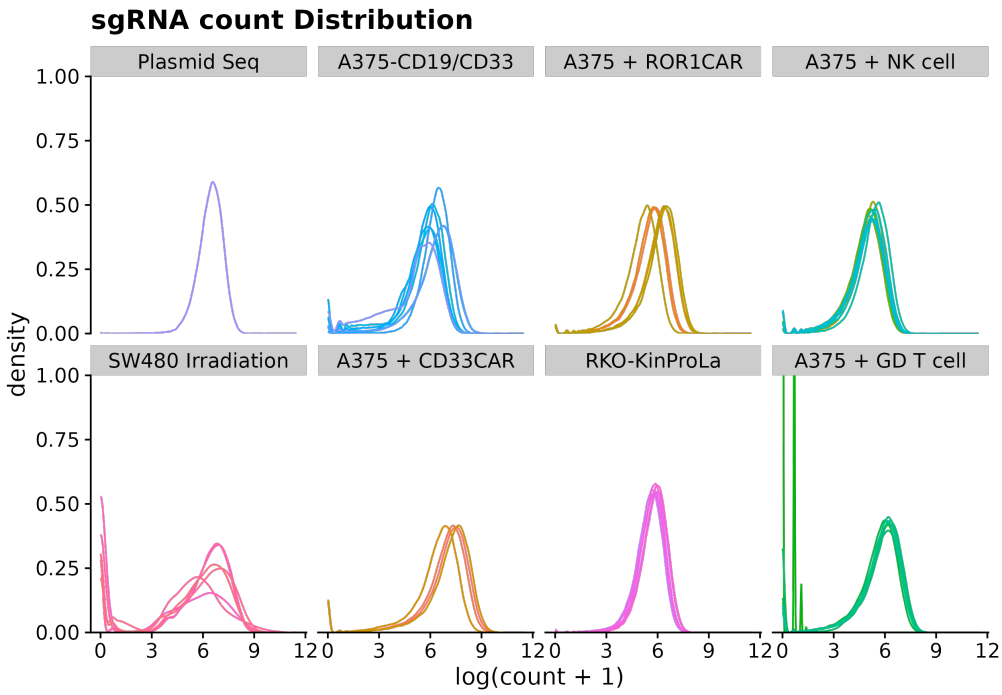

Figure 21. Normalized and log-transformed sgRNA count distribution.

Each sgRNA count was enumerated using MAGeCK package from raw sequencing data. All samples were first normalized according to the median control sgRNA counts and then were transformed into log10 scale. Samples were grouped by the project origins.

Overall, the use of HD sgRNA library did not yield irregular sequencing results, except for a few samples caused by known experimental errors. When the HD sgRNA library and the same preparation procedures were used, the sgRNA distribution for most sample remains closely comparable to the plasmid library even when different selective agents or conditions were applied, suggesting a consistent sequencing result. The sustained sgRNA distribution observed from the samples of the “NK Cells Cytotoxicity” project implied a larger margin of error from experimental procedures than expected, as a lower sequencing coverage did not seem to impose irregularities on the distribution of sgRNA counts.

7.4.2. Stability of sgRNA library over time

The plasmid sample of the original sgRNA library was constructed and cloned in 2018 and was stored at -20°C in Tris-EDTA buffer. The same plasmid sample has been used in all subsequent projects for fresh lentivirus preparation at the start of each project and subsequent infection. To examine the stability of the same HD sgRNA library sample over time, the plasmid samples were compared in a chronological manner (Figure 22A). Overall, a slight shift in the modes of distribution toward the negative side was observed over time. To assess the change of the library in a detailed manner, the distributions of sgRNA count were inspected in terms of the spread of distribution, which is measured in standard deviation, and average counts.

The result revealed a significantly weak and inverse correlation for both the spread and the mean count of distribution, with a Pearson correlation coefficient of -0.35 (Figure 22B&C). The observation suggests that the variability of sgRNA plasmids within the sample was reduced and the sgRNA plasmids could be depleted unevenly over time. However, it is also possible that the outcome was an artefact of the sequencing process or preparation.

To rule out such possibilities, the spread and mean counts of the distribution were compared also to other factors. A significantly strong correlation was found between the sequencing coverage and both the spread (R=0.65) and mean counts (R=0.67) of the distribution (Figure 22D&E). The opposing observation implies a higher sgRNA variability can be obtained and the distribution would remain comparable to the original plasmid sample, when a higher sequencing coverage is used. As the association is stronger with coverage than with the time of experimentation, the change in sgRNA distribution might be largely attributed to the discrepancies in sample preparation. To verify the hypothesis, one would need to test the original sgRNA plasmid sample at different time points in the future and at different sequencing coverage. Furthermore, whether the change in the distribution may affect the result interpretation will be explored in subsequent sections.

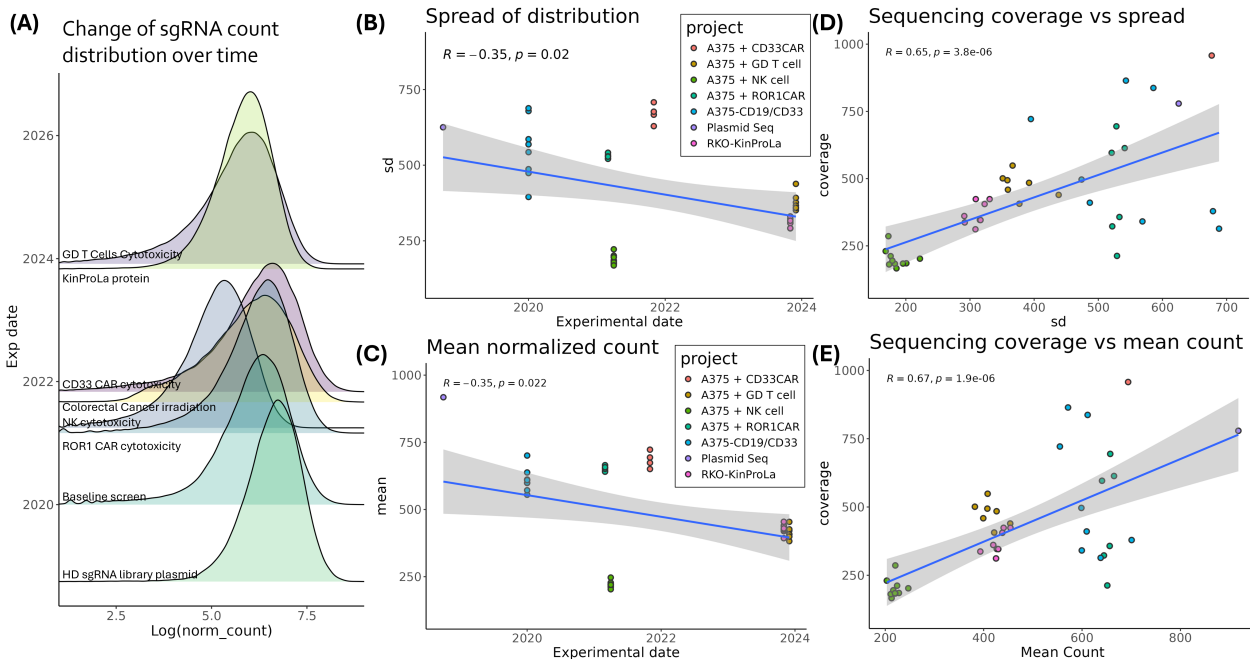

Figure 22. Change of normalized sgRNA count distribution over time.

(A) Histogram revealing the change of sgRNA count distribution from different projects. Each histogram represents the summation of normalized sgRNA count of all samples originated from a project. The histogram (B) & (C) scatter plots for the change of spread or mean of sgRNA count distribution of each sample over time. The spread of distribution was measured in stand deviation (sd). A375-GDCTRL-B and samples from SW480 irradiation project were excluded due to compromised library representation. R denotes Pearson's correlation coefficient. Blue line and shaded area represent the linear model fitted and 95% CI.

7.4.3. Reproducibility of screening results

Reproducibility serves as another quality control metric to gauge the inter-experimental variability of the HD sgRNA library. The reproducibility of screening results using the HD sgRNA library was assessed on 3 different levels which are the normalized counts, sgRNA fold-changes of all genes, and gene candidate fold-changes. The former directly correlates with raw sequencing data which concerns the technical variability, whereas the other two explain address the consistency in the candidate selection.

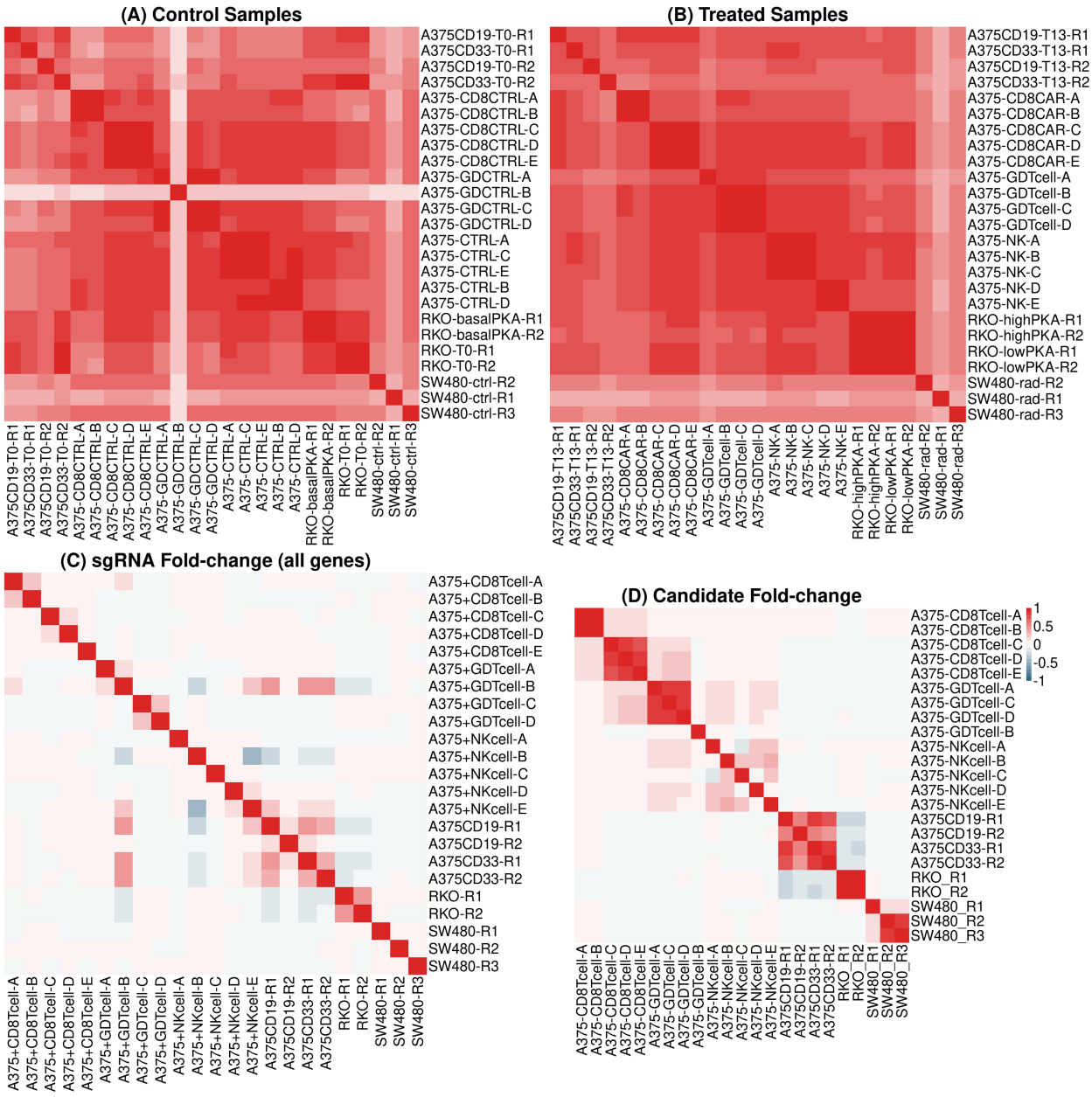

Figure 23. Correlation matrix of all samples in meta-analysis.

Pearson correlations of the normalized sgRNA counts were calculated for all control **(A)** and treated **(B)** samples. **(C)** The normalized sgRNA counts were converted to sgRNA fold-change by subtracting the count of sgRNA in control samples from that of treated sample, followed by log transformation. The sgRNA fold-change of all samples were then plotted into a correlation matrix. **(D)** The correlation of the fold-change of candidates selected from each screen. The color scale at the bottom panel on the right side represents R value and applies to all 4 plots.

When comparing all control or treated samples with each other, the samples in general display very high degree of reproducibility as indicated by R values of 0.7 or higher for fitness screen and R values of 0.88 or higher for all other samples (Figure 23A&B). Except for A375-GDCTRL-B and six SW480 samples, these samples show a significantly lower correlation with other replicates (R: 0.17 – 0.32), possibly due to the technical errors or cellular irregularities occurred during preparation. the reproducibility did not seem to be affected by the type of treatment or other cell screening method, which includes the use of different immune cell types as selective agents and FACS-based screening. The result indicates a high degree of consistency in the library representation when using the HD sgRNA library.

As for the reproducibility on sgRNA fold change level, all samples show a significantly lowered degree of agreement (R: 0.08 to 0.48) between replicates (Figure 23C). This is attributed to the fact that a majority of gene perturbations do not manifest in phenotypic changes towards the given source of stimulus. After subtracting the phenotype of ctrl group from that of treatment group, the fold change of most genes stochastically fluctuates at zero-fold-changes. As a result, most data points amassed at the zero coordinates and no trend can be evidently measured. This effect disappeared once all background genes were excluded, leaving only gene candidates identified from each screen. A very high correlation between the replicates in almost all screens is observed again, as indicated by R values ranging from 0.81 to 0.94 (Figure 23D), which signifies a consistency in hit selection strategies across projects.

Similarly, a moderate degree of similarity between replicates can be observed from PCA of sgRNA fold changes, in which only 2 loose clusters of samples can be found (Figure 24). While overlooking the abnormal A375-GDTcell-B and SW480 samples, other samples can be roughly segregated into 2 groups. One group is represented by samples from the A375 fitness screen, highlighting a difference in samples underwent additional steps in cells selection. Regardless of immune cells treatment or FACS-sorting, both procedures introduce an additional level of stress to the cells than spontaneous viability dropout and hence results in 2 clusters of samples.

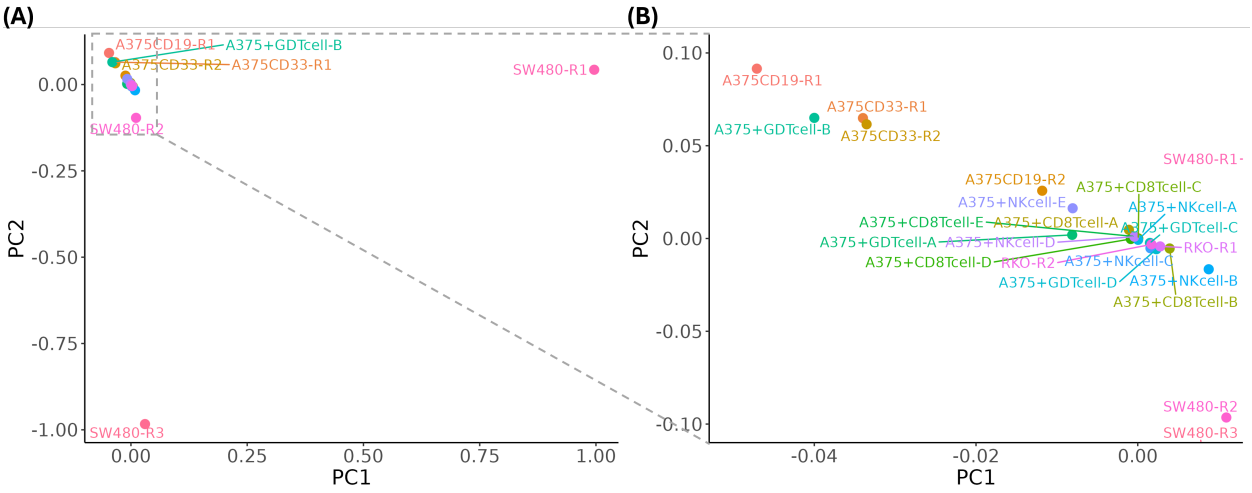

Figure 24. Two clusters of samples revealed by principal component analysis.

(A) Plot of the first two principal components from the PCA of normalized sgRNA counts of all samples. **(B)** The magnified region of the left panel as depicted by the gray box.

7.4.4. Performance in functional annotation

Lastly, to evaluate the performance of HD sgRNA library from a functional perspective, I assessed the precision of candidate selection across different screening projects. Given the limited availability of validated functional genomics data for the respective cell lines, it is currently not feasible to comprehensively review the functional relevance of each candidates from all individual screens. Instead, publicly available gene essentiality data for the A375 melanoma cell line (Hart et al., 2014) were leveraged in this meta-analysis in similar manner as described in section 7.1.3. Using this dataset as a reference, I examined the consistency in classification of A375 essential genes under the influence of different immune effector cell types.

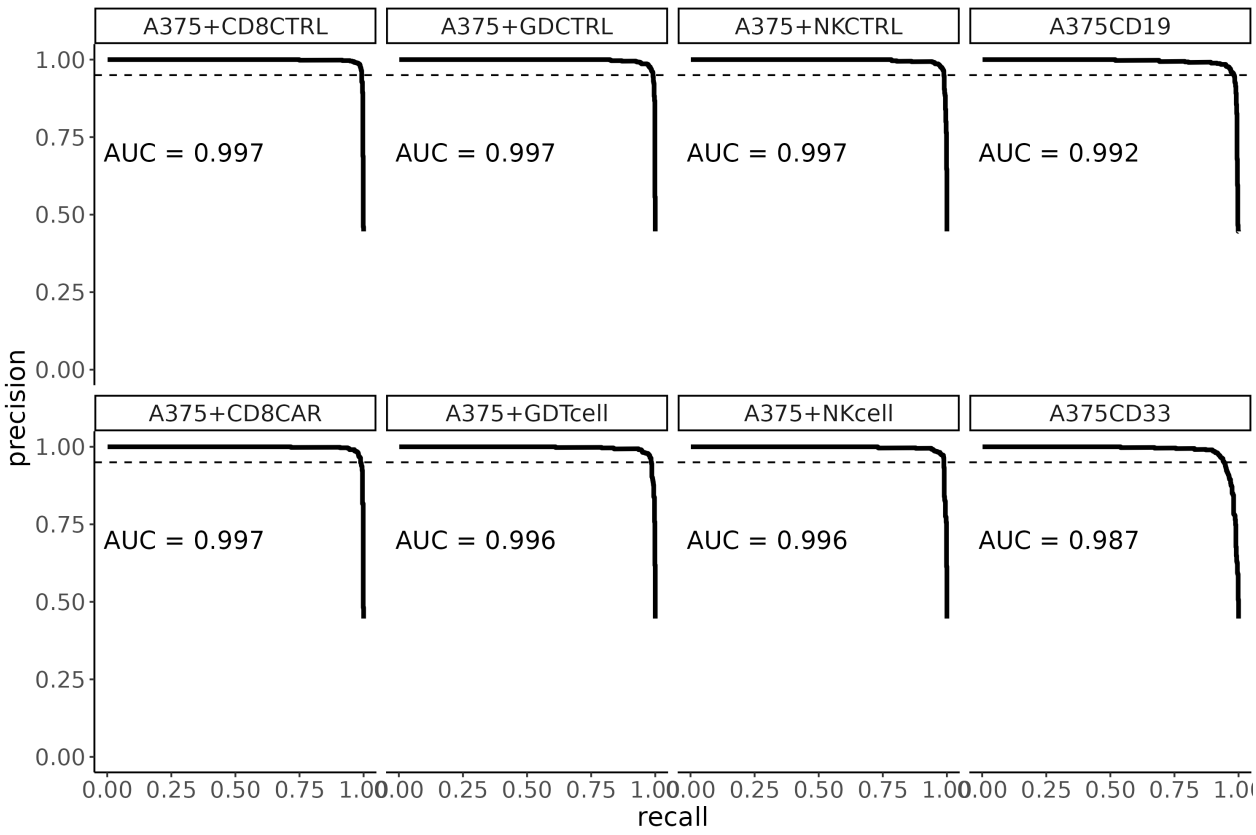

Figure 25. Precision-recall curve for classification of essential genes in A375 samples.

The precision-recall curve was plotted to evaluate the performance of core-essential genes for all samples that used A375 cell lines in the experiment under different treatments. The corresponding AUC values were calculated to quantify the overall accuracy of the model to select essential genes. The horizontal dashed line represents 95% FDR.

In the following analysis, all samples were compared directly with the sequencing result of the original sgRNA library for calculation of fold-changes due to time-zero samples not included in most of the experimental schemes. The sequencing reads from the original sequence library may represent the sample collected immediately after library transduction. The gene essentiality was analyzed again using BAGEL package to obtain the BF score for each gene in different conditions. Any gene with a BF score of 6 or above was designated as an essential gene. To determine the performance of the classifier model in each project, a PR curve was created for every control or immune cell-treated sample individually. PR curves plot precision as a function of recall. A slower

decline in the curve implies a lower probability of capturing false positive targets as more true positives are identified. Based on the curves generated, the classifier models of all eight samples suffer minimal reduction in the precision as more essential genes are being captured (Figure 25). The underlying AUC values from each curve (0.98 or higher) also indicate an exceptional performance of the model, as an AUC value of 0.9 or above is widely accepted as a sign for an excellent classifier, indicating a high reliability of the outcome. In terms of the true positive rate of essential genes, there was minimal influence from the presence of immune cells, the specific type of immune cell treatment, the execution time, and the operator of the experiment, on the identification of essential genes using the HD sgRNA library and the corresponding protocol. In other words, the use of HD sgRNA library and the corresponding protocol unlikely alters the precision of essential gene selection.

A graphic summary has clearly demonstrated an extensive dropout of essential genes at the end of each experiment regardless of the sample types, compared to the non-essential genes (Figure 26A). A total of 2816 unique essential genes were identified from all samples, and an average depletion of -4.835 $\log_2$FC was observed. The number of essential genes identified across the samples in immune cell cytotoxicity projects remains relatively consistent, ranging from 1896 to 2199 genes (Supp. Table 6), which is higher than those identified from A375-CD19/CD33 in baseline screen (1718 & 1372 genes). The control samples in immune cell screens are comprised of WT non-targeting $CD8^+$ T cells in $CD8^+$ T cell screen, and untreated samples in both GD T cell screen and NK cell screen. It is observed that A375CD19 and A375CD33 samples have lower numbers of essential genes identified than the control samples in immune cell screens despite the fact they received lower selective pressure. The difference might be explained by less frequent cell passaging and slightly shorter length of culture duration (3 days less) in baseline screen, which caused weaker manifestation of genes that are crucial to cell adhesion or proliferation.

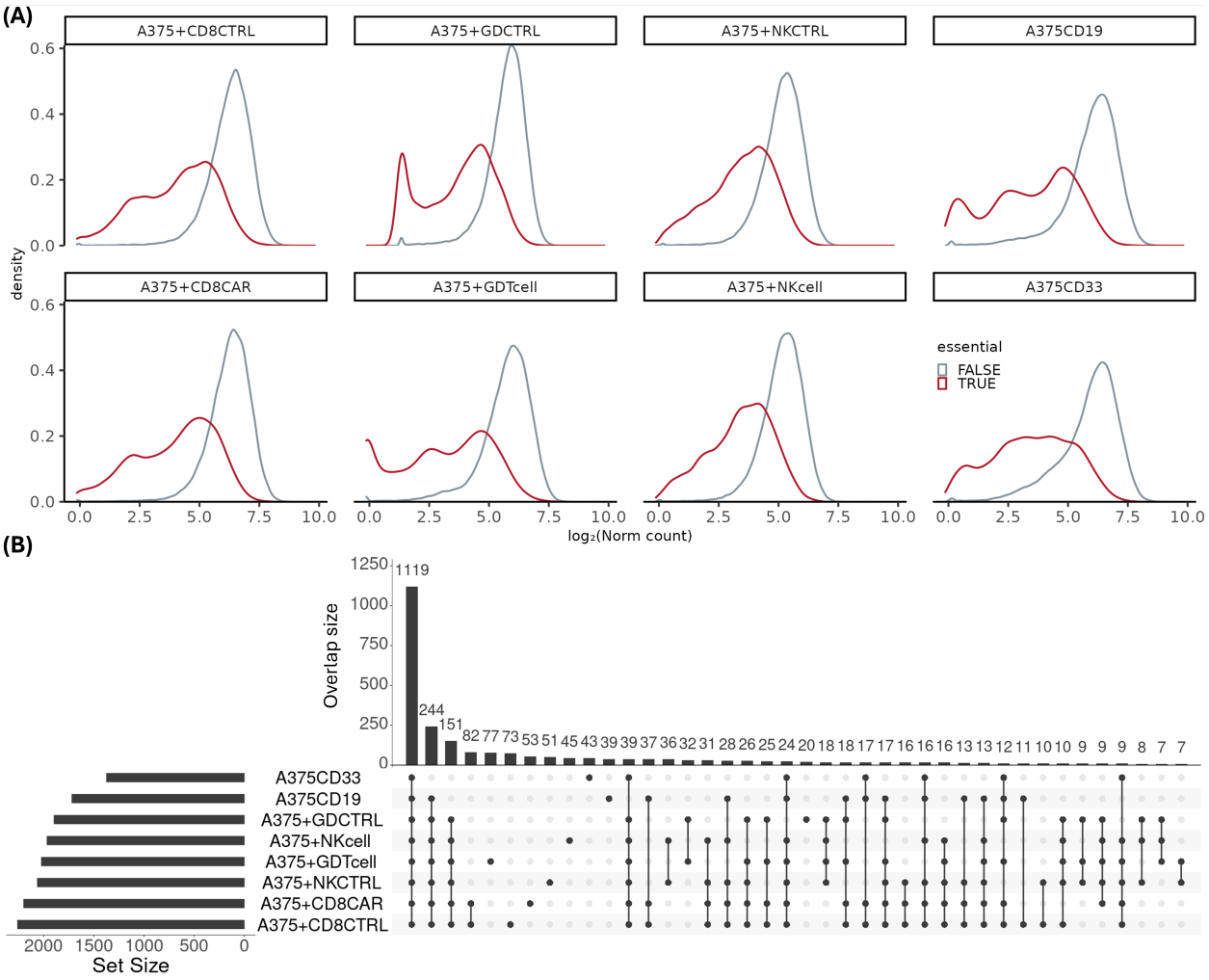

Figure 26. sgRNA fold-change and overlaps of essential genes in different experiments.

(A) The overlayed histograms consist of the distribution of both essential genes (red) and non-essential genes (grey) classified under each condition. The fold-changes were calculated by subtracting the counts of sgRNA of each sample from that of sgRNA library sample. A BF>6 was used for defining essential genes. The CTRL sample of CD8CAR screen consisted of WT CD8 T cells and A375, whereas the CTRL sample of GDT cell screen and NK cell screen were untreated. A375CD19/A375CD33 were also not treated **(B)** UpSet plot for indicating numbers of overlapping essential genes between each sample. The number above each bar represents the number of essential genes simultaneously shared among samples indicated by black dots linked by black lines beneath. Single black dots denote the number of essential genes unique to the corresponding samples.

To further investigate the disparities in gene essentiality across treatment conditions, I have created an UpSet plot to examine the overlap of essential genes among samples (Figure 26B). Approximately 1188 genes identified are directly shared between A375CD19 and A375CD33 samples, which constitute 70% to 86% of essential genes

respectively. As for immune cell cytotoxicity screens, 1514 genes were found common to the six samples, accounting for 70% to 80% genes identified. Among the remaining genes, a large majority were shared by 3 or more samples in a non-systematic pattern. More importantly, the number of essential genes uniquely identified to each sample (as indicated by single black dots) ranged only from 20 to 73, representing less than 3% of essential genes identified per sample. The observation is consistent with inherent biological variations in such experiment. This also point to the fact that It is unrealistic to capture the same set of essential genes across different experiments.

When accounting the actual fold-change of essential genes, there was an approximate 20% fluctuation in the magnitude of depletion observed in T cell-treated samples (-3.79 & -3.7 $\log_2$ fold-change) compared to other conditions (-4.22 to -5.09 $\log_2$ fold-change; Supp. Table 6). This suggests that certain treatments exert as a modest influence on the gene phenotype, which is independent of the classifier model's precision. In other words, the classifier model can precisely identify essential genes but not show the exact gene manifestation. Regardless of the weaker depletion of essential genes in $CD8^+$ T cell-treated samples, the use of HD sgRNA library still enabled the identification of comparable number of essential genes for the downstream analysis.

In terms of intra-experimental variability, the difference between the immune cell-treated and control samples were insignificant, which is indicated by a high percentage of overlapping essential genes fold-changes in $CD8^+$ T cell screen (87.4%, 1923 genes), GD T cell screen (92.2%, 1749 genes), and NK cell screen (89.6% ,1761 genes; Figure 26B & Supp. Table 6). Although discrepancy may occur as the result an additional layer of selective pressure exerted by immune cells in a co-culture setting. The effect is apparently not as profound as that incurred by a different cell culture scheme as discussed above.

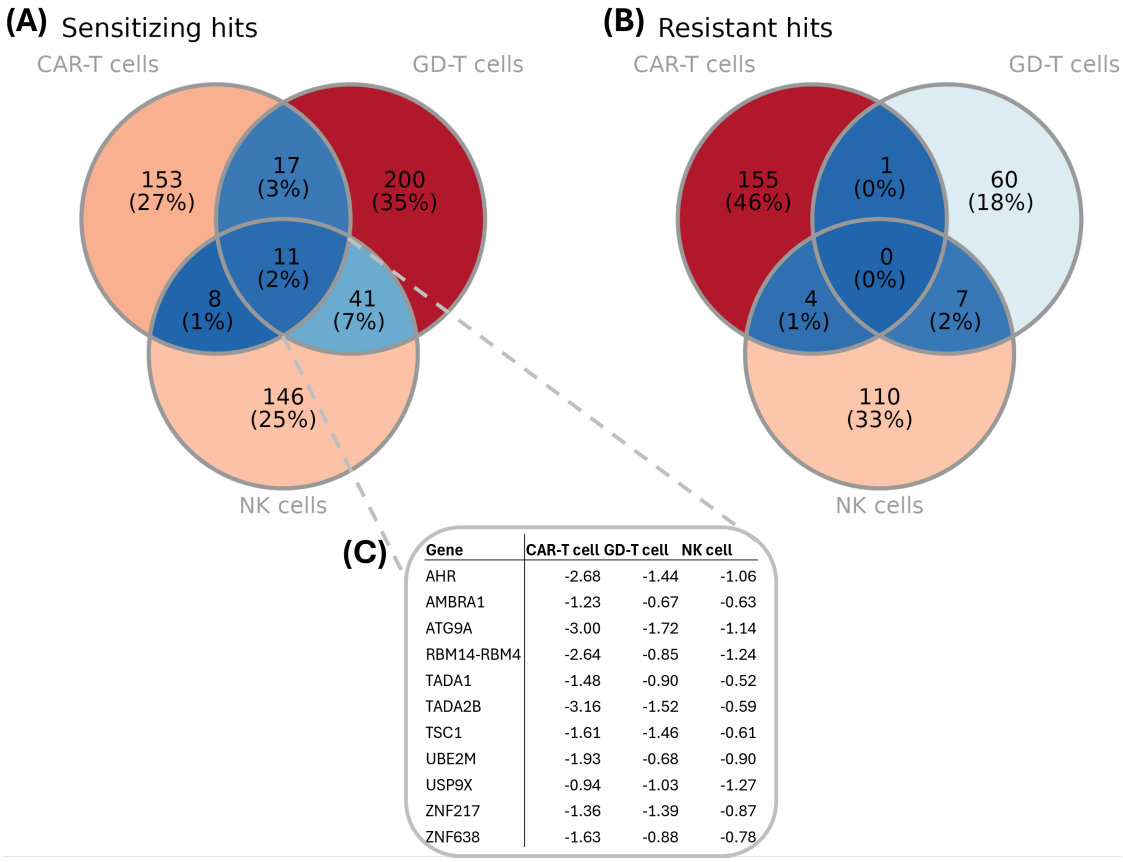

Gene	CAR-T cell	GD-T cell	NK cell
AHR	-2.68	-1.44	-1.06
AMBRA1	-1.23	-0.67	-0.63
ATG9A	-3.00	-1.72	-1.14
RBM14-RBM4	-2.64	-0.85	-1.24
TADA1	-1.48	-0.90	-0.52
TADA2B	-3.16	-1.52	-0.59
TSC1	-1.61	-1.46	-0.61
UBE2M	-1.93	-0.68	-0.90
USP9X	-0.94	-1.03	-1.27
ZNF217	-1.36	-1.39	-0.87
ZNF638	-1.63	-0.88	-0.78

Figure 27. Gene candidates identified from different immune cell treatments.

(A, B) Venn diagrams indicate the overlaps of potential regulators of immune cell cytotoxicity between different immune cell types. The hits were separated into sensitizing and resistant classes. The percentage represents the fraction of genes from all 3 screens combined. **(C)** fold-changes of 11 sensitizing gene shared by all 3 screens.

Contrary to the high consistency observed in essential gene classification, the identification of candidate modulators of immune cell function from the three different cytotoxicity screens have shown great disparities (Figure 27A&B). From each screen, I have included approximately 300 top ranked candidates with the lowest FDR for further analysis. Only 11 sensitizing hits (2%) were common to all three immune cell types, whereas no resistant hit shared across different screens. The vast majority of hits were unique to each screen, of which 499 genes (87%) in the sensitizing category and 248 genes (97%) in the resistant category were exclusive to a single immune effector type. The observation aligns well with expectations as the difference between the three

immune cell types are extensively studied. These immune effectors differ significantly in antigen recognition, cytokine secretion profiles, activation mechanisms, and memory formation (Kaech & Cui, 2012; Silva-Santos et al., 2019; Vivier et al., 2011). The use of the HD sgRNA library thus enabled the differentiation of context-specific regulators of immune effector function. Despite the large disparity between the screens, the presence of the 11 common genes suggests that certain cellular processes may be conserved across different immune effectors in mediating melanoma cells elimination. These 11 genes warrant further examination to clarify the functional relevance in diverse immune cell contexts.

The result indicates that inherent biological variation and variability from experimental design exists across different contexts, which is beyond the influence of HD sgRNA library. The use of HD sgRNA library does not introduce substantial technical variability within comparable experimental settings.

8. Discussion

8.1. CRISPR screen identified regulators of melanoma susceptibility to CAR-T cell-mediated killing independent of IFNγ signaling and antigen presentation.

Extensive efforts have been made to elucidate the molecular basis of T cell–melanoma interactions. Multiple high-throughput genetic screening approaches, such as *in vitro* shRNA screens (Zhou et al., 2014), *in vitro* CRISPR screen (Pan et al., 2018; Patel et al., 2017; Vredevoogd et al., 2019; Lawson et al., 2020), and *in vivo* CRISPR screen (Manguso et al., 2017; Ishizuka et al., 2019), have consistently identified genes that regulate melanoma susceptibility to T cells, primarily through pathways related to MHC class I antigen presentation and IFNγ signaling. This recurrent finding can be largely attributed to the use of engineered or antigen-specific TCR-T cells in these studies, which inherently depend on intact MHC class I presentation on tumor cells and a successful IFNγ response from the tumor cells to initiate an immune response. As a result, genes involved in the antigen processing and presentation machinery (e.g., *IFNGR1, IFNGR2, JAK1, STAT1, TAP1, TAP2, B2M, TAPBP, H2-K1*) are frequently enriched, as seen in pathway enrichment and GO term analyses in those studies. However, these pathways are not directly relevant to emerging T cell-based therapies such as chimeric antigen receptor (CAR) T cells, which recognize tumor antigens in an MHC-independent manner. The overrepresentation of MHC- and IFNγ-related genes may obscure the contribution of other tumor-intrinsic factors that affect sensitivity to T cell-mediated killing.

To fill in the gap in this field of study, I developed a genome-wide CRISPR/Cas9 screening platform using a co-culture system of melanoma cells and CAR-T cells. This approach allowed for the unbiased identification of genes that modulate tumor susceptibility to CAR-T cell-mediated cytotoxicity, independent of MHC class I and IFNγ signaling. The screen successfully uncovered both previously known and novel immune

evasion regulators. Combining the result of melanoma-T cell co-culture screen and A375 gene essentiality screen, the core-essential genes identified were filtered from final list of candidate prior to further analysis. The selection of candidates that naturally confer survival disadvantages to A375 independent of T cells was thus avoided.

Notably, hits were enriched in diverse cellular processes and pathways, including the mediator complex, OXPHOS, NF-κB signaling, mTOR signaling, and inositol phosphate metabolism (Figure 12). In contrast to TCR-T cell screens summarized in section 5.7, an over-representation of IFNγ-related genes or antigen presentation pathway was no longer observed when CAR-T cells instead of TCR-T cells were used in my screens. However, four core members (*IRF1*, *IFNGR1*, *JAK1*, and *STAT1*) of IFNγ response were still identified as candidates (Figure 12B). This finding is most likely attributed to their role in inducing DNA damage rather than up-regulating MHC class I antigen presentation as CAR-T cell cytotoxicity does not depend on antigen processing presentation by melanoma cells. The findings signify the versatility of IFNγ as a tool for T cell to eliminate target cells.

By cross-referencing TCGA and cBioPortal data, the expression of several candidates was found to be in line with the expression in melanoma biopsy, the overall survival, and the cytolytic activity derived from T cell markers.

Differential mRNA expression levels across melanoma patient samples reveal that most screen hits exhibit uniform and moderate expression (Figure 13). Notably, PSAP, SLC3A2 and SLC7A5 (885, 74.8 and 130 FPKM) were three of the highest expressed genes shown in patient samples. Genes from the canonical NF-κB pathway (*JUNB*, *RELA*) and the inositol phosphate (IP) metabolism pathway (*ISYNA1*, *ITPK1*) also demonstrated substantial expression across patient samples. These consistently high expression levels align with the in vitro screen results, where LOF mutations in these genes led to marked depletion of melanoma cell fitness, suggesting that their unperturbed expression supports tumor survival under immune attack.

Survival analysis further supports the functional relevance of several candidate genes (Figure 14). The lower expression of *SLC3A2*, *SLC7A5* was associated with prolonged

overall survival, whereas the higher expression of *MED15*, *MED20*, *PIK3R4*, *DEPDC5*, and *NPRL3* correlated with poorer outcomes. These trends align well with the *in vitro* screens where LOF mutations in *SLC3A2*, *SLC7A5*, and *ISYNA1* sensitized melanoma cells to T cell-mediated killing, while LOF in the latter group conferred resistance. Such concordance strengthens the hypothesis that these metabolic and signaling regulators play important roles in dampening T cell cytotoxicity when unperturbed.

Correlations with cytolytic scores further emphasize these genes' potential roles in modulating tumor–immune interactions (Figure 15). Negative correlations between *SLC3A2*, *SLC7A5*, *ISYNA1*, and *PIK3R4* expression and cytolytic activity, as well as a positive correlation for *COX17*, reinforce their hypothesized roles as immune evasion and sensitization factors, respectively.

Taken together, these findings suggest that several highly expressed, screen-validated genes, particularly *SLC3A2*, *SLC7A5*, may act as tumor-intrinsic resistance factors against T cell cytotoxicity. This screening design led to the identification and validation of *SLC3A2* and *SLC7A5*, which are components of the CD98 amino acid transporter complex, as novel regulators of tumor resistance to CAR-T cell-mediated killing. In addition to CD98, genes involved in autophagy and apoptosis, which have previously been implicated in melanoma resistance to T cell cytotoxicity, were also identified.

8.2. CD98 promotes TRAIL resistance in melanoma.

Initial validation experiments demonstrated that A375 melanoma cells exhibited increased susceptibility to T cell-mediated killing upon loss of either SLC3A2 or SLC7A5 which are key components of the CD98 transporter complex (Figure 16B). Analysis of a panel of T cell surface markers, including CD27, CD45RA, CD45RO, CD69, CTLA-4, LAG3, PD-1, TIGIT, and TIM-3, showed no significant differences in T cell activation or exhaustion status when co-cultured with A375 cells expressing or lacking CD98

components (Figure 16D). These results suggest that the altered cytotoxic response was not due to changes in T cell functionality.

To elucidate the mechanism by which CD98 modulates melanoma susceptibility to T cell cytotoxicity, further assays were conducted to assess melanoma responses to specific T cell effector functions. These included T cell degranulation assays and stimulation with FasL and various pro-inflammatory cytokines. Notably, the absence of CD98 significantly enhanced melanoma sensitivity to TRAIL receptor-mediated signaling (Figure 17 & Figure 18), resulting in a marked increase in apoptosis. These findings suggest that endogenous CD98 expression contributes to TRAIL resistance in melanoma cells, thereby impairing the efficacy of CAR-T cell-mediated cytotoxicity.

The observed link between CD98 and TRAIL signaling in melanoma has not been well characterized in existing studies, highlighting a novel mechanism of immune resistance that is independent of antigen presentation or IFN-γ signaling. To investigate further, I propose several strategies for delineating the role of CD98 in modulating TRAIL sensitivity in melanoma.

To assess whether the transporter function of SLC3A2/SLC7A5 influences TRAIL responses, transcriptomic or proteomic profiling could be performed on CD98-deficient cells treated with TRAIL. Additionally, quantitative PCR targeting a selected panel of genes potentially regulated by CD98 function may clarify specific mRNA level changes. These targets could include secondary messengers within the TRAIL-induced apoptotic pathway or transcriptional regulators such as mediator complex subunits identified in the co-culture screen (Figure 12). A comparative transcriptomic analysis of CD98-deficient versus wild-type cells may directly reveal differentially expressed gene clusters. However, existing literature suggests that key regulatory steps in TRAIL-induced apoptosis often occur at the post-translational level. Modifications such as glycosylation of TRAIL-R1/TRAIL-R2 (Dufour et al., 2017), ubiquitination and cleavage of caspases (Shin et al., 2005; Bellail et al., 2012), or proteasomal degradation (Hellwig et al., 2022) can critically affect receptor stability, DISC formation, and caspase activation. Investigating these post-translational modifications would require co-

immunoprecipitation combined with targeted immunoblotting or high-throughput approaches such as mass spectrometry.

To test whether the LNAA transport function of CD98 is crucial for TRAIL sensitivity, small-molecule inhibitors can be employed to block the function of SLC7A5 while not disrupting the structure of either SLC3A2 or SLC7A5. Initial experiments with JPH203 and BCH yielded conflicting results (Figure 19B). This may be due to off-target effects, as BCH has lower specificity and also inhibits other system L transporters such as SLC7A8 (Segawa et al., 1999). Therefore, more specific SLC7A5 inhibitors should be tested to minimize off-target effects. An appropriate TRAIL-only control group should also be included for proper comparison for the same experiment. Alternatively, monoclonal antibodies targeting the CD98 heavy chain may offer greater specificity while comparably inhibit the function of CD98. Notably, researchers have developed monoclonal antibodies that significantly reduce CD98 transporter activity to levels comparable to BCH treatment, providing a promising alternative approach for this scientific question (Hayes et al., 2015). This antibody could be used in place of the inhibitor for better specificity.

For *in vivo* validation, xenograft alongside immunocompromised mouse models could be used to verify the role of SLC3A2/SLC7A5 in regulating TRAIL sensitivity under physiological conditions. My co-culture screen was conducted entirely *in vitro*, which did not account for the effects of the TME and other immune cell types. Taking these factor into account, mouse models with T cell deficiency (for instance nude mouse, SCID mouse or NOD/SCID mouse) can be implanted with murine melanoma cells lacking *SLC3A2*/*SLC7A5* expressions. Once tumors are established, mice can be treated with engineered CAR-T cells targeting the grafted cells. Subsequently, the degree of tumor outgrowth, T cell infiltration, change in T cell functional status, and overall survival of mice can be monitored. Co-treatment with TRAIL and SLC7A5 inhibitors such as JPH203 in the absence of CAR-T cells on the grafted mice could further clarify whether targeting nutrient transport enhances TRAIL-induced apoptosis *in vivo*. Alternatively, an *in vivo* screen could be established using the same mouse models and CAR-T cells preparations. However, given the challenges in scaling up the experimental size in an in vivo condition, a more practical approach would be to implant tumor cells transduced

with a focus library targeting TRAIL-related genes rather than using a genome-wide library. The outgrowth of tumors after CAR-T cell treatment can be analyzed by deep-sequencing to identify genetic perturbations that modulate TRAIL sensitivity. Together, these strategies are critical for assessing the translational potential of TRAIL-sensitizing interventions identified *in vitro*.

8.3. Potential crosstalk between CD98 and pro-survival pathways strengthening TRAIL resistance

Although the link between CD98 and TRAIL resistance in melanoma remains largely unexplored, several studies have proposed mechanisms by which melanoma cells might evade TRAIL-mediated apoptosis. Notably, activation of the NF-κB signaling pathway has been shown to be crucial for the proper functioning of TRAIL receptor (TRAIL-R1, TRAIL-R2) signaling in various malignancies (Chaudhary et al., 1997; Hu et al., 1999; Mayo & Baldwin, 2000). Upon TRAIL engagement, the adaptor protein, namely TRADD recruit RIP and TRAF2, which activates the IKK complex, leading to the nuclear translocation of NF-κB. Once in the nucleus, NF-κB can upregulate a range of anti-apoptotic genes, including XIAP, cIAP1, cIAP2, BFL-1/A1, BCL-XL, and TNFAIP3 (Khoshnan et al., 2000; C.-Y. Wang et al., 1998; Zong et al., 1999; S. Q. Zhang et al., 2000), thereby promoting cell survival.

These findings suggest that suppression of NF-κB activity, via proteasome inhibitors or the overexpression of degradation-resistant IκBα mutants, may restore TRAIL sensitivity in tumor cells. Indeed, such interventions have been shown to enhance TRAIL-induced apoptosis in leukemia and melanoma models (Jeremias et al., 1998; Franco et al., 2001). However, the potential role of CD98 in modulating NF-κB activation and TRAIL resistance in melanoma has yet to be addressed.

In addition to NF-κB, other pro-survival signaling pathways, such as ERK1/2 and Akt (PKB), have also been implicated in conferring resistance to TRAIL-induced apoptosis,

possibly through their roles in the MAPK cascade (Boucher et al., 2000; Villunger et al., 2000; Schubert & Duronio, 2001; Tran et al., 2001). Although the precise mechanisms remain incompletely defined, these pathways represent additional potential points of interaction with CD98 function. Future studies aimed at dissecting the influence of CD98 on these signaling components may yield valuable insights into mechanisms of TRAIL resistance in melanoma.

The mTOR signaling pathway represents another key regulatory axis that may be linked to CD98 function and TRAIL sensitivity. The CD98 heterodimeric complex (comprising SLC3A2 and SLC7A5) functions as a bidirectional transporter for several amino acids. Notably, the coupled export of L-glutamine and import of L-leucine has been shown to maximally activate mTORC1 signaling via phosphorylation of S6K1 (Nicklin et al., 2009). In contrast, siRNA-mediated knockdown of either SLC3A2 or SLC7A5 results in reduced phosphorylation of S6K1 and impaired dissociation of 4EBP1 from the eIF4E cap complex, indicating a critical role for CD98-mediated amino acid transport in mTORC1 activation. mTOR signaling has been widely implicated in supporting proliferation and survival in various malignancies (Karbowniczek et al., 2008), suggesting that CD98 may help melanoma cells evade apoptosis through modulation of this pathway.

Consistent with this hypothesis, previous studies have shown that inhibition of mTOR using rapamycin sensitizes glioblastoma multiforme cells to TRAIL-induced apoptosis (Panner et al., 2005). Whether a similar mechanism operates in melanoma remains to be determined. The data shown in Figure 19B, are inconclusive regarding the direct involvement of CD98 in modulating mTOR signaling or TRAIL sensitivity. Therefore, expanding the panel of SLC7A5 and mTOR inhibitors would be important to clarify the role of transporter function in this context and to delineate the mechanistic relationship between CD98 and TRAIL signaling. Additionally, further investigation is warranted to determine whether melanoma cells preferentially uptake specific amino acids via CD98 that may influence mTOR activity or apoptotic resistance. This could be addressed through nutrient depletion assays or stable isotope labeling by amino acids (SILAC) in cell culture, coupled with mass spectrometry, to profile differential amino acid uptake and

utilization. These experiments would provide critical insight into the functional relevance of CD98-mediated transport in melanoma biology and TRAIL responsiveness.

In addition to the aforementioned biological processes, I hypothesized that CD98 may exert regulatory effects on components of the TRAIL signaling pathway or its downstream gene targets. To explore this, the expression levels of four known TRAIL receptors were assessed in the presence and absence of CD98 (Figure 19C). The analysis revealed no statistically significant differences in receptor expression across the tested cell lines. However, to comprehensively evaluate the influence of CD98 on the TRAIL signaling cascade, further investigation is warranted. This includes examining the expression and activation status of additional signaling components downstream of TRAIL, which can be assessed using western blotting or quantitative PCR.

8.4. Transition from *in vitro* to *in vivo* genome-wide screens

Based on the design of the co-culture screen, the focus of this study was limited to tumor-intrinsic factors that influence how melanoma cells respond to immune effector mechanisms. The melanoma-T cell interactions observed from this screen occur primarily in a direct manner, meaning that any changes on melanoma would most likely only interfere with the cell itself and any T cell in proximity. Accordingly, downstream validation experiments were conducted mainly on melanoma cells. As a result, potential influence from other cellular components in a TME, surrounding molecular composition, as well as changes on CAR-T cell cannot be evaluated. For example, the design of cytokine treatment assays (Figure 18) assumed that differences in melanoma cell sensitivity were driven solely due to intrinsic signaling events within melanoma cells. However, T cells can dynamically modulate their phenotype in response to changes in tumor cells. For instance, expression levels of surface-bound FasL on $CD8^+$ T cells have been shown to vary under different physiological contexts, potentially influencing the outcome of Fas-FasL signaling (Shustov et al., 1998; Tinhofer et al., 1998). Additionally, other components in TME, such as tumor-associated macrophages that inhibits T cell effector function by

PD-L1 stimulation were also neglected in this screen (Santarpia & Karachaliou, 2015), was not capture in this screen. Similarly, Similarly, the immunosuppressive effect of CTLA-4 expression on regulatory T cells, a key mechanism of suppressing cytotoxic T cell activity, is absent in the *in vitro* co-culture setup (Krummel & Allison, 1995). Moreover, chemotactic interactions are also overlooked. Melanoma can secrete CCL28 to recuit regulatory T cells to the TME, which in turn inhibit $CD8^+$ T cell function (Harlin et al., 2009; Sarkar et al., 2021).

Since the stated components are beyond the scope of an *in vitro* screen, the current methodology was restricted to regulators that act directly on melanoma cells and T cells in direct contact. To investigate melanoma–immune interactions, an *in vivo* screen would be needed to mimic a more comprehensively and physiologically relevant conditions in melanoma patients.

However, *in vivo* CRISPR screening poses significant challenges. *In vitro* genome-wide CRISPR screens can be scaled relatively easily, in which tens of thousands of sgRNAs can be delivered to large cell populations grown in culture under controlled conditions, maintaining high library coverage and high reproducibility. by contrast, *in vivo* models are logistically and technically challenging when it comes to maintaining sufficient representation for a large sgRNA library. Specifically, the size of the experiment is limited by the finite amount of tumor cells that can be grafted into a mouse, usually at $1x10^6$ to $5x10^6$ per mouse injected. A recent study used 30 mice per replicates to achieve enough coverage of a 95000-sgRNA library (Feng et al., 2024). Other recently published articles for *in vivo* screening also implemented a similar scale of experimental setup (X. Wang et al., 2021; Scheidmann et al., 2022; Lane-Reticker et al., 2023). Considering the amount of mice and the maintenance, the cost would be considerably higher than those of *in vitro* screens. In addition to the cost, *in vivo* screens are also affected from bottlenecking effects caused by selective pressure of different tissue niches or microenvironmental conditions (for instance nutrient deficiency and hypoxia). Such factors can lead to uneven clonal outgrowth and eventually stochastic loss of sgRNA representation at different targeted tissues. This makes it challenging to attribute sgRNA enrichment and depletion to actual gene function rather than random drift.

Given the hurdles of *in vivo* screens, it might not be cost-effective for me to directly switch into genome-wide *in vivo* screens. Instead, a more targeted approach using a more focused sgRNA library against TRAIL apoptotic pathway-related genes or *SLC3A2*/*SLC7A5*-related genes will be more practical for further validation experiments. However, if the logistical and technical barriers can be overcome in the future, comprehensive in vivo screens would enable a more systematic interrogation of gene functions in a physiologically relevant context.

8.5. Challenges in selecting representative models for melanoma

The successful implementation of genome-wide screen and the subsequent validation experiments demonstrates the robustness of the platform in identifying gene candidates involved in melanoma susceptibility to T cell-mediated cytotoxicity. However, inherent limitations in the current screening strategy arise, particularly from the restricted repertoire of CARs applicable to melanoma. This constraint is reflected in the necessity to employ artificial cell models, such as melanoma cells engineered to overexpress CD33 or enriched for ROR1^{high} population, neither of which fully recapitulates native melanoma biology.

CD33 is not naturally expressed at significant level in melanoma cells (DepMap, 2023). Its inclusion as a CAR target in this screen was based on prior evidence of its ability to mediate strong T cell cytotoxicity in high-expressing target cells (Kenderian et al., 2015), rather than its relevance to melanoma. Similarly, although ROR1 was detectable in melanoma, clinical samples indicate varying expression levels across tumor samples, which limits its utility as a robust and specific CAR target. Therefore, the use of these two antigens in the screening procedures may skew the screening results and limit their translational relevance.

One major concern is the potential for antigen overexpression to create artificial genetic dependencies. Overexpression of CD33 or CD19, for example, may introduce unanticipated changes in cell physiology that influence screening outcomes. I have observed this phenomenon when comparing A375-CD19-Cas9 and A375-CD33-Cas9 cells by Welch ANOVA. The result notably revealed that antigen overexpression significantly affects sgRNA fold-change distributions in both essential and non-essential gene categories (Supp. Table 1). Specifically, the Games-Howell post hoc test indicated that non-essential genes in the A375-CD19-Cas9 line exhibited significantly higher mean fold-change values than in A375-CD33-Cas9 (p: $6.7x10^{-11}$), and a 95% confidence interval (CI) of true difference that did not span zero point further support this effect. A general increase in proliferation capacity is thus concluded. Additionally, nearly 650 essential genes were exclusive to either CD19- or CD33-expressing cell lines, pointing to newly acquired gene dependencies driven by antigen overexpression (Figure 7C). However, I adopted the CD33 CAR developed for acute myeloid leukemia because no suitable, validated CAR target was readily available for melanoma at the commencement of this study.

These issues highlight the inadequacy of currently available CAR targets for faithfully modeling melanoma. For hematologic malignancies, specific surface markers such as CD19 is highly expressed in large B-cell lymphoma or multiple myeloma but not in other tissue (Kochenderfer et al., 2012; Munshi et al., 2021). The Most melanoma-associated antigens identified to date, including gp100, MART-1, tyrosinase, and NY-ESO-1, are intracellular and presented as peptides via MHC molecules (Lupetti et al., 1998; Zeng et al., 2000; Lennerz et al., 2005; Johnson et al., 2009), making them accessible to TCR-based therapies but not to conventional CARs, which recognize intact surface proteins. While some surface targets have been explored, such as GD2, CSPG4, Her2, and B7-H3. These antigens are not exclusive to melanoma cells and are variably expressed across tumors, increasing the risk of collateral damage to normal tissues.

The efficacy of CAR also directly influences screening outcomes, which is not systematically evaluated. For instance, CD33 CAR induced stronger selective pressure than ROR1 CAR, as shown by a broader range of gene fold-changes and superior killing

efficiency at comparable E:T ratios. At 0.5:1 E:T ratio, CD33 CAR induced up to 50% cell death within 24 hours, compared to a maximum of 30% by ROR1 CAR at 1:1 ratio (Figure 9C&D). This differential pressure likely accounts for the more pronounced sgRNA fold-change distributions observed in the CD33 screen, as weaker resistance phenotypes may have been masked under stronger cytotoxic stress. However, whether this effect emerges from a different CAR-antigen affinity, the structure of CAR, or the chosen E:T ratio needs further investigation to specify

Taken together, these findings underscore challenges in the application of CAR-based screening strategies for melanoma, due to the lack of surface antigens with high tumor specificity and functional relevance. In future studies, it will be essential to establish more representative melanoma models that avoid artificial antigen overexpression. The identification of endogenous CAR-accessible markers unique to melanoma would enable unbiased experimental systems and more reliable hit identification.

8.6. Consistency and Functional evaluation of Heidelberg CRISPR sgRNA library

The availability of Heidelberg CRISPR sgRNA library has enabled the completion of multiple screening across projects diverse biological contexts. In this study, I analyzed 52 samples from 7 independent projects to evaluate the library's performance, focusing on its impact on sequencing quality, reproducibility, and functional output in terms of gene essentiality.

HD sgRNA library is not observed to cause irregularities in raw sequencing data. With few exceptions with known technical errors, most samples achieved ≥500× library coverage, less than 10% zero-count sgRNAs and skew ratios similar to the original library. The metrics reveal no impact in the sequencing result introduced by the HD sgRNA library. Importantly, the HD sgRNA library maintained consistent performance across time. A longitudinal comparison showed only a mild leftward shift in sgRNA

distribution. While weak inverse correlations were observed between experimental time and both the distribution spread and mean counts (R: -0.35), stronger positive correlations were found with sequencing coverage (R: 0.65–0.67). This suggests that variation in sgRNA distributions is more attributable to differences in sequencing depth than degradation of the plasmid library over time.

sgRNA read counts obtained from HD sgRNA library remain reproducible across replicates. At the normalized count level, most samples demonstrated high reproducibility (R: >0.7) for viability screens and for other conditions (R: >0.88). Reproducibility was consistently high across treatment types, immune cell modalities, and screening methods, confirming reliable library representation. In contrast, sgRNA fold-change reproducibility was lower (R: 0.08 to 0.48), since most gene perturbations do not result in measurable phenotypic shifts. The stochastic biological variation becomes greater than true signal, and thus obscure correlated patterns across replicates. Despite this, PCA reveal similarity between replicates on sgRNA fold-change level.

Application of HD sgRNA library in different screen results in precise and consistent identification of essential genes. Essentiality data from the A375 melanoma cell line (Hart et al., 2014) served as a benchmark to assess the library's performance across different immune effector conditions. PR curve analysis demonstrated high precision across all samples, with AUC values ≥0.98. These results indicate strong classifier performance and suggest that immune treatment, operator differences, and technical variability did not compromise the precision of the model. Further analysis showed a substantial dropout of essential genes in all conditions. The number of essential genes identified across immune cytotoxicity screens ranged from 1896 to 2199, exceeding those identified in baseline CD19 and CD33 screens (1718 and 1372, respectively). These differences were likely attributed to different experimental designs in culture duration or passaging. Approximately 70–80% of essential genes were shared across samples in immune cytotoxicity projects, while 70–86% for those in baseline screen. Unique essential genes accounted for less than 5% in each sample. Intra-experimental comparisons between treated and control samples in immune cytotoxicity screens

revealed a high similarity in essential gene identification (87.4% to 92.2%), supporting that the HD sgRNA library performs consistently even under co-culture with immune cells. This reproducibility aligns with expected biological variability and supports the robustness of the library.

In summary, the HD sgRNA library demonstrated consistent sequencing quality across projects and timepoints. Observed anomalies were largely linked to identifiable experimental issues rather than intrinsic flaws in the library or its preparation protocol. The library also supports precise and reproducible essential gene identification across diverse screening contexts, with minimal technical variability introduced by experimental complexity or immune cell pressure, given that a similar experimental context and procedures could be maintained.

8.7. Conclusion

In this dissertation, a genome-wide CRISPR/Cas9-mediated screen was adopted to investigate the genetic landscape governing the interaction between melanoma cells and engineered T cells. By establishing a co-culture platform that mimics cytotoxic T lymphocyte pressure *in vitro*, I identified genes that modulate tumor cell susceptibility to T cell-mediated killing beyond classical immune evasion mechanisms such as MHC downregulation or IFNγ signaling disruption, as well as attempting to fill the critical gap in ACT effectiveness against solid tumors.

The results confirmed the robustness and reproducibility of the screening approach, as demonstrated by high intra-screen correlations, consistent essential gene depletion patterns, and successful recapitulation of established target known for their tumor promoting and inhibitory effect. Differential gene fitness analyses between experimental screens suggested significant influence from the genetic background of melanoma cells, which were eliminated from final hits list for precise identification of novel and relevant targets. Notably, multiple candidate genes emerged—many of which are associated with oxidative phosphorylation, NF-κB signaling, mTOR signaling, mediator complex, and

metabolic pathways. These findings shed light on alternative routes by which melanoma cells might resist T cell cytotoxicity, potentially offering novel targets for future immunotherapeutic strategies in addition to existing findings centered on IFNγ signaling.

From an in-depth analysis, I have validated CD98 as the novel gene target that modulates melanoma susceptibility against T cell-secreted TRAIL molecules. Further experiments on CD98 revealed that the modulatory effect was achieved through suppression of TRAIL signaling pathways among other apoptotic pathways, rather than influencing T cell effector functions. It has also been demonstrated in this study that the loss of SLC3A2/SLC7A5 did not change TRAIL receptor expression. However, a more extensive inquiry into the genetic regulation of TRAIL signaling components, functional implications of CD98 on TRAIL signaling and potential crosstalk with NF-κB signaling and mTOR signaling for a complete mechanistic elucidation. While this study used established cell lines, evaluating candidate genes in patient-derived cells or *in vivo* models could provide insight into their potential translational value. Insights from this screen may eventually inform hypotheses about combination therapies that could be tested in preclinical models, though further work is needed before clinical implications can be drawn.

Through a meta-analysis on HD sgRNA library, I evaluated its performance across multiple downstream applications. The findings demonstrate that the library delivers consistent sequencing quality and supports precise, reproducible identification of essential genes across diverse screening contexts. Minimal technical variability was observed, even under complex experimental conditions such as immune cell co-culture. Most inconsistencies were traceable to known technical errors, biological variation, or differences in experimental design. My thesis highlights the robustness and consistency of the HD sgRNA library as a tool for functional genomic screening.

Despite the successful identification of relevant regulators, currently, a major bottleneck in applying CAR technologies to melanoma lies in the limited availability of surface antigens that exhibit both high tumor specificity and functional significance. It will be crucial to develop more physiologically relevant melanoma models that do not rely on

artificial antigen overexpression. The discovery of melanoma-specific surface markers accessible to CAR recognition would enable more accurate experimental systems and facilitate reliable identification of functionally relevant gene targets.

Overall, my study contributes to a better understanding of the complex molecular factors involved in T cell–tumor interactions and offers a foundation for more targeted investigations into TRAIL resistance mechanisms in melanoma.

9. Supplementary information

Supp. Table 1. Welch ANOVA test on effect of antigen overexpression on grouped samples from the dropout screen.

Welch ANOVA, using cell line as variable, grouped by gene essentiality

Essentiality	.y.	n	statistic	DFn	DFd	p
core_essential	log2fc	5320	110.66	1	5306	1.3E-25
non_essential	log2fc	6712	42.7	1	6681	6.8E-11

Games-Howell *post hoc* test

Essentiality	.y.	group1	group2	n1	n2	estimate	CI low	CI high	p.adj	p.adj.signif
core_essential	log2fc	CD19	CD33	2660	2660	0.657	0.535	0.780	0	****
non_essential	log2fc	CD19	CD33	3356	3356	-0.173	-0.224	-0.121	6.7E-11	****

Legends:

CD19 = A375-CD19-Cas9 CD33= A375- CD33-Cas9

Supp. Table 2. Welch ANOVA test for effect of CAR type on grouped samples from the co-culture screen.

Welch ANOVA, using CAR type as variable, grouped by gene essentiality and treatment

Treatment	Essentiality	.y.	n	statistic	DFn	DFd	p
CAR	core_essential	log2fc	11940	3270	1	9026	0.0E+00
CAR	non_essential	log2fc	130336	1129	1	98567	5.0E-246
CTRL	core_essential	log2fc	11940	3369	1	9024	0.0E+00
CTRL	non_essential	log2fc	130336	233	1	95656	1.5E-52

Games-Howell *post hoc* test

group1	group2	n1	n2	estimate	CI low	CI high	p.adj	p.adj.signif
CD33: CAR: core_essential	CD33: CAR: non_essential	5970	65168	5.415	5.282	5.548	0.00E+00	****
CD33: CAR: core_essential	CD33: CTRL: core_essential	5970	5970	0.102	-0.082	0.286	6.97E-01	ns
CD33: CAR: core_essential	CD33: CTRL: non_essential	5970	65168	5.512	5.379	5.645	0.00E+00	****
CD33: CAR: core_essential	ROR1: CAR: core_essential	5970	5970	2.820	2.670	2.969	0.00E+00	****
CD33: CAR: core_essential	ROR1: CAR: non_essential	5970	65168	5.596	5.464	5.729	0.00E+00	****
CD33: CAR: core_essential	ROR1: CTRL: core_essential	5970	5970	2.861	2.713	3.009	5.67E-12	****
CD33: CAR: core_essential	ROR1: CTRL: non_essential	5970	65168	5.596	5.464	5.729	4.74E-13	****

group1	group2	n1	n2	estimate	CI low	CI high	p.adj	p.adj.signif
CD33: CAR: non_essential	CD33: CTRL: core_essential	65168	5970	-5.313	-5.441	-5.184	0.00E+00	****
CD33: CAR: non_essential	CD33: CTRL: non_essential	65168	65168	0.097	0.076	0.118	0.00E+00	****
CD33: CAR: non_essential	ROR1: CAR: core_essential	65168	5970	-2.595	-2.666	-2.524	0.00E+00	****
CD33: CAR: non_essential	ROR1: CAR: non_essential	65168	65168	0.182	0.165	0.198	0.00E+00	****
CD33: CAR: non_essential	ROR1: CTRL: core_essential	65168	5970	-2.554	-2.622	-2.485	0.00E+00	****
CD33: CAR: non_essential	ROR1: CTRL: non_essential	65168	65168	0.181	0.165	0.198	0.00E+00	****
CD33: CTRL: core_essential	CD33: CTRL: non_essential	5970	65168	5.410	5.281	5.538	0.00E+00	****
CD33: CTRL: core_essential	ROR1: CAR: core_essential	5970	5970	2.717	2.572	2.863	0.00E+00	****
CD33: CTRL: core_essential	ROR1: CAR: non_essential	5970	65168	5.494	5.366	5.622	0.00E+00	****
CD33: CTRL: core_essential	ROR1: CTRL: core_essential	5970	5970	2.759	2.615	2.903	0.00E+00	****
CD33: CTRL: core_essential	ROR1: CTRL: non_essential	5970	65168	5.494	5.366	5.622	0.00E+00	****
CD33: CTRL: non_essential	ROR1: CAR: core_essential	65168	5970	-2.693	-2.764	-2.621	0.00E+00	****
CD33: CTRL: non_essential	ROR1: CAR: non_essential	65168	65168	0.084	0.068	0.101	0.00E+00	****
CD33: CTRL: non_essential	ROR1: CTRL: core_essential	65168	5970	-2.651	-2.720	-2.582	0.00E+00	****
CD33: CTRL: non_essential	ROR1: CTRL: non_essential	65168	65168	0.084	0.068	0.101	0.00E+00	****
ROR1: CAR: core_essential	ROR1: CAR: non_essential	5970	65168	2.777	2.707	2.847	3.62E-12	****
ROR1: CAR: core_essential	ROR1: CTRL: core_essential	5970	5970	0.042	-0.055	0.138	8.96E-01	ns
ROR1: CAR: core_essential	ROR1: CTRL: non_essential	5970	65168	2.777	2.707	2.847	0.00E+00	****
ROR1: CAR: non_essential	ROR1: CTRL: core_essential	65168	5970	-2.735	-2.803	-2.668	0.00E+00	****
ROR1: CAR: non_essential	ROR1: CTRL: non_essential	65168	65168	0.000	-0.011	0.010	1.00E+00	ns
ROR1: CTRL: core_essential	ROR1: CTRL: non_essential	5970	65168	2.735	2.668	2.803	0.00E+00	****

Legends:

CD33 = CD33 CAR screen samples

CAR = CAR-T cells treated samples

ROR1= ROR1 CAR screen samples

CTRL = CTRL -T cells treated samples

Supp. Table 3. Candidates of CD33 CAR screen.

Gene Name	D19	D20	p-val	tstat	FDR	Mean FC	Type	BF	Essential
RPUSD4	4.39	6.45	0.001	9.69	0.22	5.42	resistant	3.61	FALSE
TFB1M	3.69	6.80	0.005	6.27	0.29	5.24	resistant	-3.31	FALSE
BCS1L	4.72	5.68	0.000	18.66	0.17	5.20	resistant	7.01	FALSE
HDAC3	3.19	5.30	0.003	7.41	0.26	4.24	resistant	16.46	TRUE
MRPL11	4.55	3.82	0.000	18.54	0.17	4.18	resistant	-0.31	FALSE
G6PD	4.93	3.27	0.001	9.01	0.23	4.10	resistant	-1.89	FALSE
LIG3	2.87	5.31	0.005	6.21	0.29	4.09	resistant	-0.44	FALSE
COX17	2.76	4.53	0.003	7.52	0.25	3.64	resistant	4.30	FALSE
PPA2	3.96	3.03	0.000	12.82	0.17	3.49	resistant	2.49	FALSE
COX6B1	2.65	4.30	0.003	7.66	0.25	3.47	resistant	7.10	TRUE
COA7	2.45	4.49	0.005	6.25	0.29	3.47	resistant	1.36	FALSE
SUPV3L1	3.65	2.98	0.000	15.62	0.17	3.32	resistant	12.18	TRUE
MAPK1	2.53	3.70	0.001	9.43	0.22	3.12	resistant	14.32	TRUE
COA6	2.20	4.01	0.005	6.28	0.29	3.10	resistant	3.85	FALSE
RPEL1	2.26	3.89	0.004	6.87	0.27	3.08	resistant	1.75	FALSE
SCO2	2.62	3.50	0.001	11.71	0.18	3.06	resistant	-3.79	FALSE
MRPS9	3.19	2.88	0.000	21.76	0.17	3.04	resistant	-2.66	FALSE
VARS2	2.42	3.58	0.001	9.14	0.22	3.00	resistant	8.03	TRUE
COA5	2.63	3.27	0.000	14.48	0.17	2.95	resistant	2.91	FALSE
TRIT1	2.63	2.97	0.000	19.27	0.17	2.80	resistant	-1.86	FALSE
SLC25A3	2.36	3.23	0.001	10.85	0.20	2.79	resistant	14.64	TRUE
UQCRC2	2.01	3.51	0.004	6.62	0.27	2.76	resistant	8.30	TRUE
WARS2	2.46	3.00	0.000	14.90	0.17	2.73	resistant	-4.07	FALSE
ASNS	2.16	3.25	0.002	8.68	0.24	2.71	resistant	7.40	TRUE
COX15	2.07	3.33	0.003	7.61	0.25	2.70	resistant	6.11	TRUE
CTNNBL1	1.89	3.51	0.006	6.07	0.30	2.70	resistant	13.80	TRUE
SLC25A26	2.56	2.83	0.000	20.14	0.17	2.69	resistant	2.05	FALSE
DARS2	2.27	3.00	0.001	11.75	0.18	2.63	resistant	-1.78	FALSE
MRP63	3.20	2.04	0.002	7.95	0.25	2.62	resistant	NA	NA
PTCD3	2.30	2.87	0.000	13.69	0.17	2.59	resistant	5.78	TRUE
ZBTB11	1.95	3.22	0.003	7.29	0.26	2.58	resistant	11.50	TRUE
TPI1	2.29	2.83	0.000	14.02	0.17	2.56	resistant	14.28	TRUE
MRPS18B	2.38	2.65	0.000	18.74	0.17	2.51	resistant	0.71	TRUE
DR1	2.29	2.72	0.000	15.53	0.17	2.51	resistant	11.93	TRUE
TRAPPC5	2.38	2.59	0.000	19.75	0.17	2.48	resistant	13.61	TRUE
CARS2	2.31	2.59	0.000	18.09	0.17	2.45	resistant	-5.50	FALSE
MRPS10	1.99	2.76	0.001	10.21	0.20	2.38	resistant	5.35	FALSE
ISCA2	1.68	3.06	0.005	6.18	0.29	2.37	resistant	-0.52	FALSE
LARS2	2.32	2.21	0.000	19.49	0.17	2.27	resistant	1.86	FALSE
COX6C	2.31	2.07	0.000	16.87	0.17	2.19	resistant	4.85	TRUE
MRPS18A	2.50	1.80	0.001	9.79	0.22	2.15	resistant	0.93	FALSE
ERAL1	1.92	2.30	0.000	13.88	0.17	2.11	resistant	-5.95	FALSE
SRP9	2.25	1.79	0.001	12.17	0.17	2.02	resistant	17.82	TRUE
CYB5B	2.00	1.99	0.000	17.69	0.17	2.00	resistant	0.02	FALSE

Gene Name	D19	D20	p-val	tstat	FDR	Mean FC	Type	BF	Essential
FASTKD5	1.65	2.34	0.001	9.23	0.22	1.99	resistant	-4.56	FALSE
ATL2	1.87	2.12	0.000	15.21	0.17	1.99	resistant	11.73	TRUE
MBTPS1	1.74	2.13	0.000	12.57	0.17	1.94	resistant	9.01	TRUE
NR2C2AP	1.40	2.43	0.004	6.48	0.28	1.92	resistant	10.37	TRUE
RRS1	1.85	1.98	0.000	16.20	0.17	1.91	resistant	15.07	TRUE
NDUFB3	1.39	2.36	0.004	6.69	0.27	1.87	resistant	2.43	FALSE
MRPL52	1.59	2.13	0.001	10.21	0.20	1.86	resistant	-6.88	FALSE
COQ4	1.33	2.39	0.005	6.10	0.29	1.86	resistant	-1.19	FALSE
MRPL13	1.71	2.00	0.000	13.63	0.17	1.85	resistant	1.45	FALSE
ELAVL1	1.70	1.84	0.000	14.88	0.17	1.77	resistant	4.84	FALSE
PTDSS1	1.83	1.69	0.000	14.77	0.17	1.76	resistant	-12.47	FALSE
MRPS27	1.43	2.06	0.002	8.68	0.24	1.75	resistant	3.92	FALSE
POLRMT	1.76	1.73	0.000	15.38	0.17	1.74	resistant	3.00	FALSE
OPA1	1.45	2.01	0.001	9.22	0.22	1.73	resistant	6.05	FALSE
PITRM1	1.65	1.79	0.000	14.51	0.17	1.72	resistant	-15.76	FALSE
MRPS12	1.50	1.94	0.001	10.57	0.20	1.72	resistant	8.49	TRUE
ABHD11	1.44	1.95	0.001	9.60	0.22	1.70	resistant	6.87	TRUE
COX11	1.25	2.12	0.004	6.58	0.28	1.69	resistant	-1.55	FALSE
SF3A2	1.73	1.61	0.000	14.29	0.17	1.67	resistant	15.01	TRUE
TUFM	1.86	1.44	0.001	10.36	0.20	1.65	resistant	5.20	FALSE
DPH6	1.19	2.10	0.005	6.18	0.29	1.64	resistant	-6.03	FALSE
SCAP	1.29	1.98	0.003	7.55	0.25	1.64	resistant	11.26	TRUE
ATP5E	1.69	1.49	0.000	12.69	0.17	1.59	resistant	8.26	TRUE
GTPBP10	1.23	1.94	0.003	7.22	0.26	1.58	resistant	-10.11	FALSE
MRPS2	1.59	1.58	0.000	14.00	0.17	1.58	resistant	7.14	FALSE
TUBD1	1.37	1.73	0.001	10.50	0.20	1.55	resistant	1.60	FALSE
SAE1	1.22	1.88	0.003	7.41	0.26	1.55	resistant	18.76	TRUE
OXSM	1.42	1.64	0.001	12.00	0.18	1.53	resistant	8.09	TRUE
IBA57	1.34	1.71	0.001	10.24	0.20	1.52	resistant	-3.40	FALSE
MCAT	1.43	1.60	0.000	12.47	0.17	1.51	resistant	-0.99	FALSE
MRPL32	1.41	1.60	0.001	12.24	0.17	1.51	resistant	4.00	FALSE
MRPS6	1.35	1.60	0.001	11.24	0.20	1.47	resistant	-5.30	FALSE
USP14	1.47	1.46	0.000	12.97	0.17	1.47	resistant	-8.46	FALSE
RANBP1	1.35	1.56	0.001	11.61	0.19	1.46	resistant	7.66	TRUE
MRPL39	1.42	1.47	0.000	12.75	0.17	1.45	resistant	5.66	FALSE
DYNLL1	1.05	1.82	0.005	6.13	0.29	1.44	resistant	10.73	TRUE
PARS2	1.28	1.59	0.001	10.24	0.20	1.43	resistant	4.10	FALSE
EGLN1	1.65	1.21	0.002	8.78	0.24	1.43	resistant	8.96	TRUE
TIMM22	1.61	1.22	0.001	9.16	0.22	1.41	resistant	9.21	TRUE
TEFM	1.17	1.64	0.002	8.31	0.24	1.40	resistant	1.63	FALSE
ZBTB17	1.29	1.52	0.001	10.89	0.20	1.40	resistant	9.51	TRUE
MRPS35	1.64	1.14	0.002	7.94	0.25	1.39	resistant	8.53	FALSE
MECR	1.35	1.32	0.001	11.80	0.18	1.33	resistant	-0.56	FALSE
KIF2A	1.62	1.04	0.003	7.01	0.26	1.33	resistant	-2.04	FALSE
KDSR	1.43	1.23	0.001	10.65	0.20	1.33	resistant	8.72	TRUE
DPH5	1.41	1.24	0.001	10.92	0.20	1.33	resistant	-5.70	FALSE

Gene Name	D19	D20	p-val	tstat	FDR	Mean FC	Type	BF	Essential
AGAP4	1.56	1.06	0.003	7.49	0.26	1.31	resistant	20.57	TRUE
ATP5F1	1.24	1.32	0.001	11.10	0.20	1.28	resistant	3.58	FALSE
COX7C	1.06	1.45	0.002	8.20	0.25	1.26	resistant	3.53	FALSE
COX10	1.00	1.51	0.003	7.13	0.26	1.26	resistant	-2.14	FALSE
GTPBP6	0.97	1.51	0.004	6.82	0.27	1.24	resistant	-8.81	FALSE
UQCC1	0.99	1.49	0.003	7.10	0.26	1.24	resistant	3.25	FALSE
MRPL17	0.92	1.55	0.005	6.08	0.29	1.23	resistant	0.04	FALSE
NDUFS2	1.00	1.40	0.002	7.71	0.25	1.20	resistant	1.29	FALSE
ATP5L	1.10	1.28	0.001	9.67	0.22	1.19	resistant	0.58	FALSE
MRPS33	0.97	1.40	0.003	7.40	0.26	1.18	resistant	-2.00	FALSE
SEPHS1	1.20	1.16	0.001	10.41	0.20	1.18	resistant	-5.32	FALSE
POP1	1.13	1.22	0.001	10.22	0.20	1.18	resistant	13.61	TRUE
CDK6	1.04	1.31	0.002	8.74	0.24	1.17	resistant	11.37	TRUE
SF3B1	0.92	1.42	0.004	6.71	0.27	1.17	resistant	12.45	TRUE
MTERFD2	1.02	1.31	0.002	8.50	0.24	1.16	resistant	NA	NA
NUP205	1.37	0.92	0.004	6.89	0.26	1.14	resistant	11.66	TRUE
FLCN	1.09	1.19	0.001	9.81	0.22	1.14	resistant	8.52	TRUE
RNMTL1	1.04	1.23	0.001	9.20	0.22	1.13	resistant	NA	NA
EEFSEC	1.26	0.97	0.002	8.20	0.25	1.12	resistant	-4.59	FALSE
PPP2R4	0.89	1.32	0.004	6.89	0.26	1.10	resistant	NA	NA
NDUFAF3	0.84	1.34	0.005	6.26	0.29	1.09	resistant	-2.74	FALSE
LSM12	1.03	1.12	0.001	9.34	0.22	1.08	resistant	8.18	FALSE
MED16	1.01	1.15	0.001	9.05	0.23	1.08	resistant	-14.37	FALSE
DDX28	0.84	1.29	0.004	6.53	0.28	1.07	resistant	-8.22	FALSE
GET4	1.08	0.99	0.001	8.99	0.23	1.04	resistant	1.82	FALSE
NDUFA11	0.90	1.15	0.002	7.81	0.25	1.03	resistant	-1.82	FALSE
NKTR	0.91	1.11	0.002	8.10	0.25	1.01	resistant	-0.82	FALSE
MIOS	0.95	1.08	0.002	8.58	0.24	1.01	resistant	4.26	TRUE
DDI2	1.09	0.93	0.002	8.34	0.24	1.01	resistant	-1.84	FALSE
SPEN	1.03	0.95	0.002	8.63	0.24	0.99	resistant	4.90	TRUE
NDUFC1	0.86	1.11	0.003	7.50	0.25	0.99	resistant	-3.28	FALSE
MRRF	0.90	1.06	0.002	8.09	0.25	0.98	resistant	-17.84	FALSE
PPAT	1.10	0.83	0.003	7.24	0.26	0.97	resistant	12.06	TRUE
ENSG0000027 8662	1.04	0.85	0.003	7.62	0.25	0.94	resistant	NA	NA
PTP4A1	1.04	0.84	0.003	7.56	0.25	0.94	resistant	-7.79	FALSE
MVD	1.10	0.77	0.004	6.55	0.28	0.93	resistant	9.86	TRUE
MRPL33	0.97	0.87	0.002	7.91	0.25	0.92	resistant	3.91	FALSE
SNRNP27	0.76	1.07	0.004	6.54	0.28	0.91	resistant	13.35	TRUE
CHD1	0.94	0.88	0.002	7.98	0.25	0.91	resistant	12.89	TRUE
GADD45GIP1	0.80	1.02	0.003	7.13	0.26	0.91	resistant	6.93	TRUE
TOMM20	0.90	0.91	0.002	8.01	0.25	0.90	resistant	14.16	TRUE
CDC73	0.90	0.89	0.002	7.91	0.25	0.89	resistant	5.20	FALSE
UBR4	0.83	0.95	0.003	7.63	0.25	0.89	resistant	6.44	TRUE
ALDH18A1	0.89	0.87	0.002	7.78	0.25	0.88	resistant	-4.19	FALSE
SUPT4H1	0.81	0.94	0.003	7.45	0.26	0.88	resistant	10.54	TRUE

Gene Name	D19	D20	p-val	tstat	FDR	Mean FC	Type	BF	Essential
FCF1	0.79	0.96	0.003	7.15	0.26	0.87	resistant	20.81	TRUE
MRPL3	0.79	0.91	0.003	7.23	0.26	0.85	resistant	-0.26	FALSE
RTF1	0.79	0.92	0.003	7.20	0.26	0.85	resistant	12.12	TRUE
TIMM13	0.72	0.98	0.004	6.48	0.28	0.85	resistant	3.05	FALSE
NDUFV2	0.77	0.92	0.003	7.06	0.26	0.85	resistant	-1.00	FALSE
MIDN	0.75	0.94	0.004	6.85	0.27	0.85	resistant	5.90	TRUE
DPH1	0.73	0.95	0.004	6.64	0.27	0.84	resistant	-9.41	FALSE
NDUFA9	0.70	0.98	0.005	6.17	0.29	0.84	resistant	-3.80	FALSE
MRPL44	0.92	0.74	0.004	6.74	0.27	0.83	resistant	5.39	FALSE
RPE	0.82	0.83	0.003	7.30	0.26	0.82	resistant	14.13	TRUE
PNPT1	0.83	0.82	0.003	7.30	0.26	0.82	resistant	4.35	FALSE
TAF8	0.69	0.96	0.005	6.17	0.29	0.82	resistant	8.83	TRUE
SREBF1	0.74	0.91	0.004	6.76	0.27	0.82	resistant	2.62	FALSE
UQCC2	0.68	0.95	0.005	6.12	0.29	0.82	resistant	0.02	FALSE
ALYREF	0.91	0.71	0.004	6.54	0.28	0.81	resistant	10.06	NA
FOXRED1	0.67	0.94	0.006	6.06	0.30	0.81	resistant	-3.40	FALSE
SCAF4	0.70	0.91	0.005	6.38	0.29	0.81	resistant	-1.86	FALSE
FPGS	0.81	0.80	0.003	7.12	0.26	0.80	resistant	2.83	FALSE
MESDC2	0.78	0.79	0.003	6.99	0.26	0.79	resistant	8.07	FALSE
CTPS1	0.83	0.73	0.004	6.73	0.27	0.78	resistant	10.53	TRUE
RPUSD3	0.88	0.67	0.005	6.16	0.29	0.78	resistant	-6.57	FALSE
COX5B	0.75	0.79	0.004	6.78	0.27	0.77	resistant	-0.71	FALSE
SHMT2	0.69	0.84	0.005	6.42	0.29	0.77	resistant	-4.17	FALSE
FAM60A	0.81	0.68	0.005	6.32	0.29	0.75	resistant	16.64	TRUE
GJA1	0.70	0.69	0.005	6.18	0.29	0.70	resistant	-9.90	FALSE
GUCY2D	-0.66	-0.72	0.006	-6.06	0.30	-0.69	sensitizing	-8.68	FALSE
FUBP3	-0.69	-0.70	0.005	-6.14	0.29	-0.69	sensitizing	-13.35	FALSE
KLHL35	-0.72	-0.67	0.005	-6.12	0.29	-0.70	sensitizing	-7.37	FALSE
ADIPOR2	-0.72	-0.68	0.005	-6.16	0.29	-0.70	sensitizing	-11.79	FALSE
MYH9	-0.69	-0.72	0.005	-6.20	0.29	-0.70	sensitizing	-10.68	FALSE
PRAMEF9	-0.66	-0.76	0.005	-6.10	0.29	-0.71	sensitizing	NA	NA
ELF3	-0.72	-0.70	0.005	-6.29	0.29	-0.71	sensitizing	-3.74	FALSE
ATRIP	-0.75	-0.67	0.005	-6.21	0.29	-0.71	sensitizing	6.55	FALSE
MED1	-0.67	-0.76	0.005	-6.21	0.29	-0.72	sensitizing	-4.44	FALSE
PTTG1	-0.72	-0.71	0.005	-6.36	0.29	-0.72	sensitizing	-1.48	FALSE
EFCAB12	-0.70	-0.74	0.005	-6.35	0.29	-0.72	sensitizing	-10.19	FALSE
DCAF15	-0.68	-0.78	0.005	-6.26	0.29	-0.73	sensitizing	-10.80	FALSE
ZMAT5	-0.71	-0.76	0.004	-6.46	0.28	-0.73	sensitizing	14.06	TRUE
MON2	-0.76	-0.70	0.005	-6.45	0.28	-0.73	sensitizing	-14.50	FALSE
CEP63	-0.80	-0.68	0.005	-6.31	0.29	-0.74	sensitizing	-4.65	FALSE
TBCB	-0.82	-0.67	0.005	-6.21	0.29	-0.74	sensitizing	13.09	TRUE
SRGAP2C	-0.73	-0.76	0.004	-6.58	0.28	-0.74	sensitizing	6.61	NA
ENSG0000028 4461	-0.71	-0.79	0.004	-6.49	0.28	-0.75	sensitizing	NA	NA
PPP6R3	-0.75	-0.81	0.004	-6.83	0.27	-0.78	sensitizing	4.28	FALSE
PIANP	-0.75	-0.80	0.004	-6.85	0.27	-0.78	sensitizing	-8.99	FALSE

Gene Name	D19	D20	p-val	tstat	FDR	Mean FC	Type	BF	Essential
HELZ	-0.87	-0.69	0.005	-6.40	0.29	-0.78	sensitizing	-6.59	FALSE
UFSP2	-0.73	-0.83	0.004	-6.75	0.27	-0.78	sensitizing	-6.08	FALSE
FZR1	-0.70	-0.89	0.005	-6.39	0.29	-0.79	sensitizing	-8.69	FALSE
WDR91	-0.85	-0.74	0.004	-6.80	0.27	-0.79	sensitizing	-6.96	FALSE
ALG8	-0.91	-0.69	0.005	-6.28	0.29	-0.80	sensitizing	-9.94	FALSE
SETDB1	-0.73	-0.87	0.004	-6.69	0.27	-0.80	sensitizing	-0.50	FALSE
CCBE1	-0.81	-0.79	0.003	-7.07	0.26	-0.80	sensitizing	-11.61	FALSE
TUBA1B	-0.73	-0.87	0.004	-6.76	0.27	-0.80	sensitizing	12.97	TRUE
CPSF7	-0.79	-0.82	0.003	-7.09	0.26	-0.80	sensitizing	-8.60	FALSE
MKLN1	-0.75	-0.87	0.004	-6.90	0.26	-0.81	sensitizing	-9.43	FALSE
NFRKB	-0.80	-0.82	0.003	-7.17	0.26	-0.81	sensitizing	2.11	FALSE
C1QTNF9B	-0.79	-0.83	0.003	-7.17	0.26	-0.81	sensitizing	-3.03	FALSE
TBCK	-0.83	-0.80	0.003	-7.19	0.26	-0.82	sensitizing	-12.84	FALSE
PDDC1	-0.87	-0.77	0.003	-7.03	0.26	-0.82	sensitizing	NA	NA
OLFML2A	-0.84	-0.81	0.003	-7.28	0.26	-0.82	sensitizing	-13.51	FALSE
ARIH1	-0.72	-0.93	0.004	-6.58	0.28	-0.83	sensitizing	10.54	NA
FEM1B	-0.71	-0.94	0.004	-6.46	0.28	-0.83	sensitizing	-4.84	FALSE
DIDO1	-0.96	-0.70	0.005	-6.29	0.29	-0.83	sensitizing	14.62	TRUE
COPS8	-0.77	-0.89	0.003	-7.11	0.26	-0.83	sensitizing	0.23	FALSE
METTL14	-0.96	-0.70	0.005	-6.29	0.29	-0.83	sensitizing	9.10	TRUE
FRMD8	-0.94	-0.73	0.004	-6.62	0.27	-0.83	sensitizing	-10.96	FALSE
NPRL3	-0.71	-0.96	0.005	-6.37	0.29	-0.84	sensitizing	-7.35	FALSE
GSS	-0.76	-0.91	0.003	-7.00	0.26	-0.84	sensitizing	-12.61	FALSE
DDX10	-0.81	-0.87	0.003	-7.36	0.26	-0.84	sensitizing	17.42	TRUE
NAMPT	-0.84	-0.86	0.003	-7.55	0.25	-0.85	sensitizing	-13.72	FALSE
RAD51C	-0.94	-0.76	0.003	-6.98	0.26	-0.85	sensitizing	12.82	TRUE
YTHDC1	-0.85	-0.86	0.003	-7.56	0.25	-0.85	sensitizing	2.74	FALSE
NCAPG	-0.88	-0.83	0.003	-7.55	0.25	-0.86	sensitizing	14.07	TRUE
SBNO1	-0.98	-0.77	0.003	-6.97	0.26	-0.87	sensitizing	7.45	TRUE
PSAP	-1.03	-0.73	0.005	-6.33	0.29	-0.88	sensitizing	-15.04	FALSE
LEMD2	-0.86	-0.89	0.002	-7.74	0.25	-0.88	sensitizing	-3.17	FALSE
BTG1	-0.80	-0.96	0.003	-7.30	0.26	-0.88	sensitizing	-14.03	FALSE
DEPDC5	-0.93	-0.83	0.003	-7.61	0.25	-0.88	sensitizing	-18.42	FALSE
COPS3	-0.95	-0.83	0.003	-7.55	0.25	-0.89	sensitizing	9.69	TRUE
NAA25	-0.80	-0.98	0.003	-7.30	0.26	-0.89	sensitizing	11.26	TRUE
ATP8B3	-0.84	-0.94	0.002	-7.70	0.25	-0.89	sensitizing	-6.19	FALSE
C12orf44	-0.78	-1.01	0.003	-6.97	0.26	-0.90	sensitizing	NA	NA
PCBP1	-0.73	-1.07	0.005	-6.23	0.29	-0.90	sensitizing	19.25	TRUE
LRRD1	-0.97	-0.86	0.002	-7.85	0.25	-0.91	sensitizing	-12.94	FALSE
MPHOSPH8	-0.94	-0.90	0.002	-8.13	0.25	-0.92	sensitizing	-8.25	FALSE
EI24	-0.81	-1.03	0.003	-7.27	0.26	-0.92	sensitizing	-0.92	FALSE
NUCB1	-0.96	-0.90	0.002	-8.19	0.25	-0.93	sensitizing	-3.28	FALSE
POP7	-1.00	-0.88	0.002	-8.01	0.25	-0.94	sensitizing	12.90	TRUE
ZNHIT2	-1.10	-0.78	0.004	-6.62	0.27	-0.94	sensitizing	15.27	TRUE
USP9X	-0.88	-1.00	0.002	-8.05	0.25	-0.94	sensitizing	-8.87	FALSE
AC253572.1	-0.82	-1.08	0.003	-7.15	0.26	-0.95	sensitizing	NA	NA

Gene Name	D19	D20	p-val	tstat	FDR	Mean FC	Type	BF	Essential
KRTAP10-1	-1.09	-0.83	0.003	-7.26	0.26	-0.96	sensitizing	0.52	FALSE
SESN2	-0.93	-1.00	0.002	-8.41	0.24	-0.96	sensitizing	-11.45	FALSE
RNMT	-1.00	-0.94	0.002	-8.50	0.24	-0.97	sensitizing	10.55	TRUE
RUVBL2	-1.00	-0.94	0.002	-8.53	0.24	-0.97	sensitizing	19.27	TRUE
FAM204A	-1.07	-0.88	0.002	-7.90	0.25	-0.98	sensitizing	-0.26	FALSE
DDB1	-0.83	-1.15	0.003	-6.97	0.26	-0.99	sensitizing	16.68	TRUE
USP33	-0.94	-1.05	0.002	-8.53	0.24	-0.99	sensitizing	-5.11	FALSE
UCHL5	-1.13	-0.86	0.003	-7.43	0.26	-0.99	sensitizing	-1.24	FALSE
RRP7A	-1.13	-0.86	0.003	-7.47	0.26	-1.00	sensitizing	13.50	TRUE
GOLGA6L9	-0.86	-1.13	0.003	-7.44	0.26	-1.00	sensitizing	17.03	TRUE
RAB7A	-1.04	-0.95	0.002	-8.64	0.24	-1.00	sensitizing	-7.56	FALSE
FIBP	-1.00	-1.00	0.002	-8.86	0.24	-1.00	sensitizing	-9.23	FALSE
GNPTAB	-0.95	-1.07	0.002	-8.57	0.24	-1.01	sensitizing	-7.39	FALSE
TRIM43	-0.82	-1.20	0.004	-6.62	0.27	-1.01	sensitizing	0.18	FALSE
ITPK1	-1.13	-0.90	0.002	-7.92	0.25	-1.01	sensitizing	1.63	FALSE
PTBP1	-0.96	-1.08	0.002	-8.74	0.24	-1.02	sensitizing	-4.03	FALSE
ALG13	-0.88	-1.17	0.003	-7.51	0.25	-1.03	sensitizing	13.21	TRUE
GCN1L1	-0.86	-1.20	0.003	-7.07	0.26	-1.03	sensitizing	NA	NA
ALG5	-1.26	-0.80	0.005	-6.19	0.29	-1.03	sensitizing	-1.44	FALSE
CCNB1	-0.80	-1.27	0.005	-6.15	0.29	-1.03	sensitizing	7.47	TRUE
PSMA7	-1.00	-1.07	0.001	-9.06	0.23	-1.04	sensitizing	20.90	TRUE
HNRNPA2B1	-0.93	-1.15	0.002	-8.22	0.25	-1.04	sensitizing	-2.09	FALSE
IPPK	-1.06	-1.04	0.001	-9.29	0.22	-1.05	sensitizing	4.46	FALSE
ZSWIM1	-1.04	-1.06	0.001	-9.30	0.22	-1.05	sensitizing	-8.19	FALSE
RAP1B	-0.92	-1.20	0.002	-7.78	0.25	-1.06	sensitizing	6.92	TRUE
GINS4	-0.99	-1.14	0.002	-8.85	0.24	-1.06	sensitizing	16.84	TRUE
ZKSCAN1	-0.91	-1.25	0.003	-7.52	0.25	-1.08	sensitizing	-11.83	FALSE
RPS29	-1.13	-1.04	0.001	-9.39	0.22	-1.08	sensitizing	21.28	TRUE
NPRL2	-1.08	-1.10	0.001	-9.63	0.22	-1.09	sensitizing	-10.64	FALSE
PPP1CB	-1.31	-0.88	0.004	-6.78	0.27	-1.09	sensitizing	-11.90	FALSE
PUF60	-0.92	-1.27	0.003	-7.52	0.25	-1.10	sensitizing	14.54	TRUE
MYBL2	-1.16	-1.04	0.001	-9.36	0.22	-1.10	sensitizing	4.49	FALSE
EPG5	-1.17	-1.05	0.001	-9.46	0.22	-1.11	sensitizing	-11.32	FALSE
SRP68	-1.03	-1.19	0.001	-9.15	0.22	-1.11	sensitizing	5.76	TRUE
FRYL	-0.96	-1.26	0.002	-7.98	0.25	-1.11	sensitizing	-17.29	FALSE
PAFAH1B1	-1.00	-1.25	0.002	-8.63	0.24	-1.12	sensitizing	13.59	TRUE
USB1	-0.96	-1.29	0.002	-7.93	0.25	-1.13	sensitizing	-6.36	FALSE
CPSF3	-1.00	-1.25	0.002	-8.59	0.24	-1.13	sensitizing	16.54	TRUE
PMVK	-1.00	-1.25	0.002	-8.59	0.24	-1.13	sensitizing	4.23	FALSE
TAF13	-0.87	-1.39	0.005	-6.32	0.29	-1.13	sensitizing	6.78	TRUE
SRRT	-0.89	-1.38	0.004	-6.61	0.27	-1.14	sensitizing	9.76	TRUE
CNOT4	-1.15	-1.13	0.001	-10.10	0.20	-1.14	sensitizing	-16.14	FALSE
STRAP	-1.00	-1.29	0.002	-8.40	0.24	-1.15	sensitizing	13.89	TRUE
VPS36	-0.93	-1.37	0.003	-7.09	0.26	-1.15	sensitizing	-11.66	FALSE
WIPI2	-1.14	-1.17	0.001	-10.22	0.20	-1.16	sensitizing	-12.81	FALSE
ALG3	-1.20	-1.15	0.001	-10.31	0.20	-1.17	sensitizing	-14.21	FALSE

Gene Name	D19	D20	p-val	tstat	FDR	Mean FC	Type	BF	Essential
ORC6	-0.90	-1.45	0.005	-6.37	0.29	-1.18	sensitizing	17.79	TRUE
ZMPSTE24	-0.93	-1.43	0.004	-6.77	0.27	-1.18	sensitizing	-10.37	FALSE
SMG6	-0.91	-1.46	0.004	-6.46	0.28	-1.19	sensitizing	6.62	FALSE
POLR2B	-1.00	-1.40	0.002	-7.76	0.25	-1.20	sensitizing	20.81	TRUE
CSDE1	-1.27	-1.16	0.001	-10.44	0.20	-1.22	sensitizing	4.42	FALSE
AMBRA1	-1.40	-1.05	0.002	-8.31	0.24	-1.23	sensitizing	-14.79	FALSE
SMNDC1	-1.13	-1.33	0.001	-9.88	0.22	-1.23	sensitizing	7.70	TRUE
ATP6V1C1	-1.00	-1.47	0.003	-7.35	0.26	-1.24	sensitizing	13.29	TRUE
KIN	-1.42	-1.06	0.002	-8.33	0.24	-1.24	sensitizing	12.54	TRUE
CRIPT	-1.33	-1.16	0.001	-10.17	0.20	-1.24	sensitizing	-7.93	FALSE
ACO2	-1.00	-1.49	0.003	-7.22	0.26	-1.25	sensitizing	14.37	TRUE
CDS2	-1.52	-0.99	0.004	-6.93	0.26	-1.25	sensitizing	-3.75	FALSE
CFL1	-1.14	-1.41	0.001	-9.49	0.22	-1.28	sensitizing	1.65	FALSE
GOLGA7	-1.00	-1.55	0.004	-6.89	0.26	-1.28	sensitizing	-18.18	FALSE
ERCC4	-1.18	-1.40	0.001	-10.16	0.20	-1.29	sensitizing	-2.95	FALSE
BCL2L1	-1.00	-1.59	0.004	-6.71	0.27	-1.30	sensitizing	-12.44	FALSE
RNF31	-1.17	-1.47	0.001	-9.50	0.22	-1.32	sensitizing	-13.00	FALSE
PPHLN1	-1.11	-1.57	0.002	-8.13	0.25	-1.34	sensitizing	-6.31	FALSE
UBE2F	-1.02	-1.68	0.005	-6.42	0.29	-1.35	sensitizing	-20.22	FALSE
STAG1	-1.11	-1.61	0.002	-7.82	0.25	-1.36	sensitizing	-12.58	FALSE
ZNF217	-1.18	-1.54	0.001	-9.23	0.22	-1.36	sensitizing	-15.02	FALSE
ATG3	-1.03	-1.74	0.005	-6.31	0.29	-1.39	sensitizing	-16.73	FALSE
TIAL1	-1.15	-1.64	0.002	-8.13	0.25	-1.40	sensitizing	-12.72	FALSE
RBCK1	-1.48	-1.40	0.000	-12.56	0.17	-1.44	sensitizing	-10.26	FALSE
DHRSX	-1.51	-1.41	0.000	-12.58	0.17	-1.46	sensitizing	-10.29	FALSE
SMG7	-1.10	-1.84	0.004	-6.53	0.28	-1.47	sensitizing	6.42	TRUE
TRAF2	-1.44	-1.51	0.000	-12.89	0.17	-1.48	sensitizing	1.11	FALSE
PGS1	-1.20	-1.75	0.002	-7.98	0.25	-1.48	sensitizing	9.51	TRUE
TADA1	-1.40	-1.56	0.000	-12.31	0.17	-1.48	sensitizing	-7.48	FALSE
RB1CC1	-1.34	-1.67	0.001	-10.55	0.20	-1.51	sensitizing	-11.04	FALSE
ATG10	-1.25	-1.82	0.002	-8.11	0.25	-1.53	sensitizing	-11.15	FALSE
KRR1	-1.17	-1.93	0.004	-6.71	0.27	-1.55	sensitizing	4.51	FALSE
EEF1G	-1.47	-1.64	0.000	-12.75	0.17	-1.55	sensitizing	18.27	TRUE
ATP6V1H	-1.26	-1.89	0.002	-7.73	0.25	-1.57	sensitizing	8.11	FALSE
ATP6V0B	-1.67	-1.50	0.000	-13.04	0.17	-1.59	sensitizing	15.29	TRUE
TSC1	-1.71	-1.50	0.000	-12.76	0.17	-1.61	sensitizing	-6.85	FALSE
SUPT20H	-1.59	-1.68	0.000	-14.12	0.17	-1.63	sensitizing	-17.42	FALSE
ZNF638	-1.47	-1.80	0.001	-11.35	0.20	-1.63	sensitizing	-11.55	FALSE
GTF3C4	-1.71	-1.62	0.000	-14.44	0.17	-1.66	sensitizing	11.66	TRUE
IPMK	-1.52	-1.89	0.001	-11.33	0.20	-1.70	sensitizing	-6.54	FALSE
PSMG2	-1.61	-1.84	0.000	-13.40	0.17	-1.72	sensitizing	16.09	TRUE
EPRS	-1.97	-1.52	0.001	-10.60	0.20	-1.75	sensitizing	17.26	TRUE
TBCA	-1.63	-1.89	0.000	-13.22	0.17	-1.76	sensitizing	15.55	TRUE
PTPN23	-1.87	-1.64	0.000	-13.71	0.17	-1.76	sensitizing	10.98	TRUE
VPS37A	-1.88	-1.74	0.000	-15.21	0.17	-1.81	sensitizing	2.25	FALSE
SIN3A	-1.32	-2.34	0.005	-6.21	0.29	-1.83	sensitizing	9.90	TRUE

Gene Name	D19	D20	p-val	tstat	FDR	Mean FC	Type	BF	Essential
ATP6AP1	-1.88	-1.79	0.000	-15.86	0.17	-1.83	sensitizing	12.19	TRUE
RAD21	-1.34	-2.34	0.005	-6.37	0.29	-1.84	sensitizing	12.79	TRUE
MIB2	-1.40	-2.30	0.003	-6.98	0.26	-1.85	sensitizing	-9.24	FALSE
PPA1	-2.15	-1.62	0.001	-10.45	0.20	-1.89	sensitizing	11.91	TRUE
HCFC1	-1.48	-2.37	0.003	-7.33	0.26	-1.92	sensitizing	17.07	TRUE
UBE2M	-1.62	-2.24	0.001	-9.73	0.22	-1.93	sensitizing	12.53	TRUE
WDR43	-2.29	-1.62	0.001	-9.28	0.22	-1.96	sensitizing	21.15	TRUE
CHMP4B	-2.50	-1.54	0.003	-7.21	0.26	-2.02	sensitizing	17.46	TRUE
CFLAR	-2.45	-1.64	0.002	-8.47	0.24	-2.05	sensitizing	-13.15	FALSE
TAF5L	-1.55	-2.59	0.004	-6.95	0.26	-2.07	sensitizing	-8.55	FALSE
SUPT7L	-1.74	-2.61	0.002	-8.48	0.24	-2.18	sensitizing	-13.76	FALSE
CTAGE9	-1.75	-2.62	0.002	-8.51	0.24	-2.19	sensitizing	8.40	TRUE
PTPN2	-2.03	-2.50	0.000	-13.51	0.17	-2.27	sensitizing	-10.50	FALSE
TSC2	-2.97	-1.74	0.004	-6.79	0.27	-2.36	sensitizing	-8.14	FALSE
RIPK1	-1.77	-2.96	0.003	-7.04	0.26	-2.36	sensitizing	-13.51	FALSE
PMPCA	-2.00	-2.77	0.001	-10.24	0.20	-2.39	sensitizing	17.11	TRUE
EIF2AK4	-1.70	-3.09	0.005	-6.21	0.29	-2.40	sensitizing	-3.99	FALSE
TAF6L	-1.89	-2.92	0.002	-8.17	0.25	-2.41	sensitizing	-12.92	FALSE
RBM14-RBM4	-3.06	-2.21	0.001	-10.52	0.20	-2.64	sensitizing	11.79	TRUE
TARS2	-3.20	-2.08	0.002	-8.29	0.24	-2.64	sensitizing	13.73	TRUE
AHR	-2.28	-3.08	0.001	-11.14	0.20	-2.68	sensitizing	-7.22	FALSE
SLC3A2	-2.50	-2.93	0.000	-16.90	0.17	-2.72	sensitizing	-1.83	FALSE
USP39	-3.32	-2.68	0.000	-14.66	0.17	-3.00	sensitizing	12.49	TRUE
ATG9A	-2.73	-3.28	0.000	-16.08	0.17	-3.00	sensitizing	-12.90	FALSE
MPI	-2.74	-3.36	0.000	-15.26	0.17	-3.05	sensitizing	-7.58	FALSE
HGS	-2.91	-3.26	0.000	-21.01	0.17	-3.08	sensitizing	9.37	TRUE
TADA2B	-3.79	-2.54	0.001	-9.00	0.23	-3.16	sensitizing	-14.88	FALSE
ENSG00000280789	-2.93	-5.36	0.005	-6.31	0.29	-4.14	sensitizing	NA	NA
SLC7A5	-4.91	-5.70	0.000	-22.25	0.17	-5.30	sensitizing	-4.55	FALSE
PAXIP1	-4.35	-6.45	0.001	-9.48	0.22	-5.40	sensitizing	-11.26	FALSE
HINT1	-5.27	-9.19	0.004	-6.90	0.26	-7.23	sensitizing	-7.87	FALSE

Supp. Table 4. Candidates of ROR1 CAR screen.

Gene Name	D21	D22	D23	p-val	tstat	FDR	Mean FC	Type	BF	Essential
POLR2I	1.49	1.78	1.74	0.000	15.64	0.01	1.67	resistant	22.1	TRUE
TOP2A	1.98	1.12	0.58	0.001	5.23	0.16	1.22	resistant	18.4	TRUE
POLR2E	1.52	0.27	1.67	0.002	4.58	0.20	1.15	resistant	17.9	TRUE
EIF3D	1.26	1.68	0.50	0.001	5.58	0.14	1.15	resistant	16.4	TRUE
RAD51C	0.79	1.70	0.30	0.005	3.95	0.28	0.93	resistant	12.8	TRUE
ATP6V1H	1.51	0.73	0.53	0.001	5.00	0.18	0.92	resistant	8.1	FALSE
MTRF1	0.85	0.72	1.16	0.000	7.77	0.04	0.91	resistant	-7.5	FALSE
BID	0.96	0.69	1.03	0.000	8.16	0.04	0.89	resistant	-5.5	FALSE
GRWD1	1.31	1.18	0.16	0.004	4.14	0.25	0.88	resistant	15.2	TRUE

Gene Name	D21	D22	D23	p-val	tstat	FDR	Mean FC	Type	BF	Essential
TOPBP1	0.74	1.54	0.28	0.005	3.94	0.28	0.85	resistant	13.1	TRUE
ELAVL1	0.62	1.33	0.59	0.001	5.33	0.15	0.85	resistant	4.8	FALSE
SART3	0.81	0.84	0.89	0.000	8.78	0.04	0.85	resistant	14.5	TRUE
MFAP1	0.66	0.72	1.11	0.000	6.83	0.07	0.83	resistant	15.2	TRUE
RBM6	0.60	1.49	0.37	0.005	4.03	0.27	0.82	resistant	-7.4	FALSE
RPS28	0.78	0.66	1.02	0.000	7.41	0.05	0.82	resistant	22.7	TRUE
PTPMT1	0.80	1.36	0.28	0.003	4.27	0.24	0.81	resistant	13.4	TRUE
ZFAT	1.37	0.18	0.83	0.006	3.88	0.29	0.79	resistant	-9.0	FALSE
URB1	0.48	1.32	0.55	0.002	4.59	0.20	0.79	resistant	16.1	TRUE
ISCA1	0.68	1.01	0.65	0.000	6.92	0.07	0.78	resistant	11.5	TRUE
WDR43	1.19	0.71	0.39	0.001	4.96	0.18	0.77	resistant	21.1	TRUE
SPDL1	1.27	0.80	0.18	0.005	3.93	0.28	0.75	resistant	16.7	TRUE
RPS29	0.47	1.32	0.42	0.004	4.08	0.26	0.74	resistant	21.3	TRUE
CEP95	1.01	0.47	0.72	0.001	5.79	0.12	0.73	resistant	-8.1	FALSE
SPEN	0.83	0.59	0.76	0.000	7.10	0.06	0.73	resistant	4.9	TRUE
FAS	0.87	0.66	0.64	0.000	7.01	0.06	0.72	resistant	-9.2	FALSE
PSMA1	1.25	0.27	0.63	0.005	4.04	0.27	0.72	resistant	17.2	TRUE
FADD	0.64	0.79	0.71	0.000	7.23	0.06	0.71	resistant	-8.7	FALSE
PPAT	0.82	0.78	0.53	0.000	6.63	0.07	0.71	resistant	12.1	TRUE
PMAIP1	0.63	0.71	0.77	0.000	7.17	0.06	0.70	resistant	-10.1	FALSE
CASP8	0.78	0.62	0.69	0.000	7.05	0.06	0.70	resistant	-14.0	FALSE
ROR1	0.91	0.82	0.35	0.001	5.22	0.16	0.69	resistant	-5.4	FALSE
DENR	0.50	0.53	1.05	0.001	5.21	0.16	0.69	resistant	13.4	TRUE
COPS6	0.73	0.45	0.83	0.000	5.95	0.11	0.67	resistant	10.6	TRUE
MRPL51	0.44	0.50	1.06	0.002	4.71	0.19	0.67	resistant	8.8	TRUE
KIF11	0.89	0.75	0.36	0.001	5.24	0.16	0.67	resistant	22.0	TRUE
TUBB	0.92	0.79	0.24	0.003	4.44	0.22	0.65	resistant	21.8	TRUE
ATP6V0B	0.79	0.86	0.29	0.002	4.80	0.18	0.64	resistant	15.3	TRUE
INTS12	0.51	0.81	0.61	0.000	6.05	0.10	0.64	resistant	6.8	TRUE
DYNC2LI1	0.97	0.35	0.59	0.002	4.75	0.19	0.64	resistant	-12.4	FALSE
FAM60A	0.34	1.12	0.44	0.005	3.94	0.28	0.63	resistant	16.6	TRUE
GTF2E2	0.82	0.65	0.42	0.001	5.53	0.14	0.63	resistant	12.2	TRUE
DNAJC17	0.16	1.01	0.71	0.006	3.88	0.29	0.63	resistant	11.6	TRUE
KHDRBS1	0.59	0.66	0.60	0.000	6.42	0.09	0.62	resistant	-3.4	FALSE
RPS4X	0.33	1.05	0.47	0.004	4.10	0.26	0.62	resistant	23.5	TRUE
EIF3B	0.73	0.79	0.32	0.001	5.00	0.18	0.62	resistant	18.6	TRUE
CTU2	0.97	0.63	0.24	0.004	4.21	0.25	0.61	resistant	14.6	TRUE
RPP30	0.33	1.00	0.51	0.003	4.31	0.24	0.61	resistant	17.5	TRUE
ECT2	0.77	0.70	0.37	0.001	5.31	0.15	0.61	resistant	14.5	TRUE
CHORDC1	0.73	0.29	0.80	0.002	4.80	0.18	0.61	resistant	12.8	TRUE
BRF2	0.62	1.00	0.21	0.005	3.95	0.28	0.61	resistant	19.3	TRUE
MOGS	0.28	0.71	0.81	0.002	4.71	0.19	0.60	resistant	2.3	FALSE
HORMAD1	0.95	0.63	0.23	0.004	4.13	0.25	0.60	resistant	-1.7	FALSE
RPL23	0.89	0.45	0.45	0.002	4.87	0.18	0.60	resistant	18.5	TRUE
MYC	0.34	0.61	0.84	0.002	4.86	0.18	0.60	resistant	12.6	TRUE
CCT8	0.71	0.78	0.26	0.002	4.58	0.20	0.58	resistant	16.5	TRUE

Gene Name	D21	D22	D23	p-val	tstat	FDR	Mean FC	Type	BF	Essential
ATP6AP1	0.67	0.23	0.80	0.003	4.30	0.24	0.57	resistant	12.2	TRUE
DUSP10	0.44	0.93	0.31	0.004	4.07	0.27	0.56	resistant	-7.5	FALSE
URB2	0.24	0.85	0.60	0.004	4.20	0.25	0.56	resistant	11.4	TRUE
PIAS1	0.75	0.51	0.42	0.001	5.14	0.16	0.56	resistant	-0.1	FALSE
WDR33	0.41	0.53	0.70	0.001	5.17	0.16	0.55	resistant	13.7	TRUE
HDAC3	0.64	0.83	0.17	0.005	3.90	0.29	0.55	resistant	16.5	TRUE
TERF2	0.91	0.32	0.41	0.005	4.02	0.27	0.54	resistant	16.4	TRUE
PPP4C	0.68	0.19	0.75	0.005	4.04	0.27	0.54	resistant	17.9	TRUE
EIF3G	0.42	0.45	0.74	0.002	4.91	0.18	0.54	resistant	16.1	TRUE
ACTR3	0.49	0.66	0.44	0.001	5.18	0.16	0.53	resistant	6.2	TRUE
HEXIM1	0.58	0.70	0.28	0.002	4.52	0.21	0.52	resistant	-8.0	FALSE
ATP6V1C1	0.60	0.72	0.24	0.003	4.26	0.24	0.52	resistant	13.3	TRUE
MUC12	0.60	0.46	0.48	0.001	5.26	0.16	0.52	resistant	-11.9	FALSE
MOCS3	0.64	0.50	0.38	0.002	4.90	0.18	0.51	resistant	13.1	TRUE
THAP11	0.46	0.37	0.68	0.002	4.67	0.19	0.50	resistant	-5.3	FALSE
HSF1	0.53	0.74	0.23	0.004	4.09	0.26	0.50	resistant	-2.3	FALSE
TBCA	0.42	0.26	0.82	0.006	3.87	0.29	0.50	resistant	15.5	TRUE
MPHOSPH6	0.39	0.46	0.65	0.002	4.80	0.18	0.50	resistant	-2.2	FALSE
SLC22A18	0.60	0.50	0.39	0.002	4.92	0.18	0.50	resistant	-16.9	FALSE
PCYT2	0.52	0.68	0.29	0.003	4.40	0.23	0.49	resistant	-6.4	FALSE
DCST1	0.59	0.63	0.27	0.003	4.38	0.23	0.49	resistant	-3.9	FALSE
PPP5C	0.35	0.44	0.69	0.003	4.49	0.21	0.49	resistant	-7.8	FALSE
AC244394.1	0.51	0.64	0.32	0.002	4.56	0.20	0.49	resistant	NA	NA
FBXL17	0.51	0.61	0.35	0.002	4.71	0.19	0.49	resistant	-5.9	FALSE
IWS1	0.61	0.53	0.33	0.002	4.64	0.20	0.49	resistant	-3.8	FALSE
FBXL14	0.38	0.72	0.34	0.004	4.19	0.25	0.48	resistant	-9.7	FALSE
OR12D3	0.55	0.45	0.44	0.002	4.93	0.18	0.48	resistant	-11.3	FALSE
RND2	0.28	0.75	0.39	0.005	3.92	0.28	0.47	resistant	-8.8	FALSE
MBNL1	0.44	0.46	0.52	0.002	4.89	0.18	0.47	resistant	-14.1	FALSE
DNAJC11	0.45	0.67	0.28	0.004	4.18	0.25	0.47	resistant	8.4	FALSE
CLIC3	0.59	0.44	0.38	0.002	4.64	0.20	0.47	resistant	-8.2	FALSE
TRAF3	0.45	0.44	0.51	0.002	4.86	0.18	0.47	resistant	-10.9	FALSE
PFAS	0.34	0.54	0.52	0.002	4.62	0.20	0.47	resistant	7.6	FALSE
IMPDH1	0.42	0.65	0.30	0.004	4.18	0.25	0.46	resistant	-7.0	FALSE
DSTYK	0.47	0.47	0.42	0.002	4.73	0.19	0.45	resistant	-7.9	FALSE
METAP2	0.39	0.54	0.44	0.002	4.62	0.20	0.45	resistant	12.0	TRUE
BAZ1B	0.71	0.39	0.26	0.006	3.85	0.29	0.45	resistant	-3.3	FALSE
KRTAP1-3	0.51	0.51	0.33	0.003	4.45	0.22	0.45	resistant	-10.5	FALSE
MORF4L1	0.33	0.69	0.33	0.005	3.90	0.29	0.45	resistant	3.5	FALSE
STIP1	0.66	0.43	0.24	0.006	3.89	0.29	0.45	resistant	-2.0	FALSE
GTF3C3	0.31	0.64	0.39	0.004	4.08	0.26	0.44	resistant	9.0	TRUE
FCN2	0.41	0.65	0.26	0.005	3.93	0.28	0.44	resistant	-1.2	FALSE
ATRX	0.35	0.56	0.41	0.003	4.38	0.23	0.44	resistant	-3.3	FALSE
PSMB5	0.26	0.40	0.66	0.006	3.86	0.29	0.44	resistant	20.1	TRUE
RBFOX2	0.35	0.58	0.38	0.004	4.24	0.24	0.44	resistant	-19.9	FALSE
RPUSD4	0.47	0.46	0.39	0.002	4.53	0.21	0.44	resistant	3.6	FALSE

Gene Name	D21	D22	D23	p-val	tstat	FDR	Mean FC	Type	BF	Essential
RPS2	0.24	0.65	0.42	0.006	3.83	0.29	0.44	resistant	20.5	TRUE
NR2C2AP	0.49	0.50	0.32	0.003	4.33	0.24	0.44	resistant	10.4	TRUE
NDUFS5	0.59	0.21	0.50	0.006	3.84	0.29	0.43	resistant	1.5	FALSE
TIMM23B	0.29	0.39	0.62	0.005	4.02	0.27	0.43	resistant	NA	NA
KRTCAP3	0.53	0.23	0.54	0.005	3.95	0.28	0.43	resistant	-5.0	FALSE
ANKS3	0.50	0.50	0.29	0.004	4.21	0.25	0.43	resistant	-7.5	FALSE
LAMP3	0.53	0.41	0.35	0.003	4.33	0.24	0.43	resistant	-11.9	FALSE
C1D	0.49	0.28	0.52	0.004	4.15	0.25	0.43	resistant	-2.9	FALSE
CREBBP	0.32	0.43	0.54	0.004	4.20	0.25	0.43	resistant	1.4	FALSE
DEFB135	0.52	0.33	0.42	0.003	4.25	0.24	0.42	resistant	-14.5	FALSE
OR10J3	0.33	0.62	0.32	0.006	3.89	0.29	0.42	resistant	-9.9	FALSE
WASL	0.49	0.50	0.29	0.004	4.14	0.25	0.42	resistant	-6.1	FALSE
SLC4A7	0.34	0.51	0.42	0.003	4.27	0.24	0.42	resistant	5.8	TRUE
EMC1	0.27	0.56	0.43	0.005	3.98	0.28	0.42	resistant	9.0	FALSE
SETD2	0.37	0.56	0.33	0.004	4.09	0.26	0.42	resistant	4.9	FALSE
LMTK3	0.54	0.40	0.31	0.004	4.07	0.27	0.41	resistant	-15.9	FALSE
CRADD	0.48	0.53	0.23	0.006	3.84	0.29	0.41	resistant	-14.3	FALSE
LYRM2	0.51	0.43	0.30	0.004	4.06	0.27	0.41	resistant	-6.3	FALSE
MTRNR2L3	0.26	0.51	0.42	0.006	3.83	0.29	0.40	resistant	4.0	FALSE
UBE2R2	0.47	0.29	0.42	0.005	3.94	0.28	0.39	resistant	-15.7	FALSE
TRHR	0.42	0.32	0.42	0.005	4.00	0.27	0.39	resistant	-10.9	FALSE
KTI12	0.37	0.29	0.50	0.006	3.81	0.30	0.38	resistant	5.2	NA
MSL1	0.35	0.36	0.45	0.005	3.94	0.28	0.38	resistant	-3.8	FALSE
TEAD4	0.37	0.38	0.38	0.005	3.94	0.28	0.38	resistant	-5.1	FALSE
ARNT	-0.34	-0.36	-0.40	0.006	-3.81	0.30	-0.37	sensitizing	-3.7	FALSE
ZNF19	-0.36	-0.41	-0.34	0.006	-3.85	0.29	-0.37	sensitizing	-12.8	FALSE
ACTR8	-0.44	-0.29	-0.41	0.006	-3.87	0.29	-0.38	sensitizing	13.9	TRUE
SPNS1	-0.50	-0.30	-0.36	0.006	-3.81	0.30	-0.38	sensitizing	-13.3	FALSE
RP11-347C12.3	-0.34	-0.41	-0.41	0.005	-4.01	0.27	-0.39	sensitizing	NA	NA
DHX35	-0.46	-0.26	-0.44	0.006	-3.84	0.29	-0.39	sensitizing	-6.1	FALSE
SRRD	-0.38	-0.45	-0.34	0.005	-4.00	0.27	-0.39	sensitizing	-10.1	FALSE
CFL1	-0.31	-0.33	-0.54	0.006	-3.83	0.29	-0.39	sensitizing	1.6	FALSE
HCFC2	-0.38	-0.50	-0.31	0.005	-3.95	0.28	-0.39	sensitizing	-16.3	FALSE
CD274	-0.30	-0.46	-0.43	0.005	-4.00	0.27	-0.40	sensitizing	-15.5	FALSE
SIGLEC6	-0.44	-0.46	-0.29	0.005	-3.97	0.28	-0.40	sensitizing	-7.7	FALSE
FEZ1	-0.48	-0.37	-0.34	0.005	-4.03	0.27	-0.40	sensitizing	-13.9	FALSE
VCP	-0.29	-0.40	-0.51	0.005	-3.97	0.28	-0.40	sensitizing	13.7	TRUE
TCERG1	-0.52	-0.36	-0.32	0.005	-4.00	0.27	-0.40	sensitizing	-0.8	FALSE
KCNK9	-0.40	-0.29	-0.54	0.005	-3.99	0.27	-0.41	sensitizing	-11.5	FALSE
DDX39B	-0.33	-0.48	-0.42	0.004	-4.18	0.25	-0.41	sensitizing	-8.4	FALSE
JUND	-0.41	-0.37	-0.46	0.003	-4.25	0.24	-0.41	sensitizing	-3.3	FALSE
PNPLA8	-0.44	-0.41	-0.38	0.003	-4.29	0.24	-0.41	sensitizing	-5.2	FALSE
NUP50	-0.51	-0.41	-0.33	0.004	-4.17	0.25	-0.41	sensitizing	10.7	TRUE
FAM172A	-0.58	-0.41	-0.26	0.006	-3.88	0.29	-0.42	sensitizing	-8.3	FALSE
C11orf95	-0.31	-0.52	-0.42	0.004	-4.13	0.25	-0.42	sensitizing	-11.6	FALSE

Gene Name	D21	D22	D23	p-val	tstat	FDR	Mean FC	Type	BF	Essential
TTC33	-0.29	-0.58	-0.38	0.005	-3.95	0.28	-0.42	sensitizing	-6.8	FALSE
NR2F6	-0.35	-0.36	-0.54	0.004	-4.13	0.25	-0.42	sensitizing	-7.2	FALSE
ANKRD17	-0.47	-0.45	-0.34	0.003	-4.28	0.24	-0.42	sensitizing	-5.1	FALSE
SPOP	-0.39	-0.41	-0.46	0.003	-4.36	0.24	-0.42	sensitizing	-11.9	FALSE
RBMS2	-0.48	-0.42	-0.37	0.003	-4.34	0.24	-0.42	sensitizing	-11.2	FALSE
C19orf24	-0.52	-0.45	-0.30	0.004	-4.17	0.25	-0.42	sensitizing	-3.4	FALSE
CHMP1A	-0.37	-0.31	-0.60	0.005	-4.00	0.27	-0.42	sensitizing	-6.4	FALSE
TNRC6A	-0.52	-0.35	-0.40	0.003	-4.30	0.24	-0.43	sensitizing	-9.3	FALSE
RP11-302B13.5	-0.37	-0.60	-0.31	0.005	-4.00	0.27	-0.43	sensitizing	NA	NA
ROCK1	-0.25	-0.53	-0.50	0.005	-4.02	0.27	-0.43	sensitizing	-10.2	FALSE
EXTL3	-0.59	-0.44	-0.25	0.005	-3.94	0.28	-0.43	sensitizing	-18.1	FALSE
STT3A	-0.64	-0.29	-0.36	0.006	-3.89	0.29	-0.43	sensitizing	1.7	FALSE
ISYNA1	-0.28	-0.52	-0.50	0.004	-4.19	0.25	-0.44	sensitizing	-2.8	FALSE
DSCC1	-0.27	-0.61	-0.43	0.005	-4.04	0.27	-0.44	sensitizing	7.2	TRUE
PPAN-P2RY11	-0.53	-0.49	-0.29	0.004	-4.23	0.25	-0.44	sensitizing	NA	NA
APOB	-0.37	-0.61	-0.34	0.004	-4.17	0.25	-0.44	sensitizing	-11.8	FALSE
CHTOP	-0.49	-0.48	-0.36	0.003	-4.51	0.21	-0.44	sensitizing	5.2	FALSE
ZBTB10	-0.51	-0.42	-0.40	0.002	-4.56	0.20	-0.44	sensitizing	-10.7	FALSE
RNF144B	-0.39	-0.60	-0.35	0.003	-4.28	0.24	-0.45	sensitizing	-14.0	FALSE
WNT1	-0.36	-0.34	-0.65	0.004	-4.12	0.26	-0.45	sensitizing	-7.3	FALSE
ACSL3	-0.44	-0.60	-0.31	0.003	-4.29	0.24	-0.45	sensitizing	12.2	TRUE
PTPN2	-0.43	-0.64	-0.29	0.004	-4.11	0.26	-0.45	sensitizing	-10.5	FALSE
SNX32	-0.47	-0.22	-0.66	0.006	-3.89	0.29	-0.45	sensitizing	-2.7	FALSE
DDA1	-0.70	-0.28	-0.39	0.005	-3.91	0.29	-0.46	sensitizing	-2.5	FALSE
RNMT	-0.53	-0.50	-0.34	0.002	-4.57	0.20	-0.46	sensitizing	10.5	TRUE
MT2A	-0.44	-0.30	-0.63	0.003	-4.26	0.24	-0.46	sensitizing	2.9	FALSE
FAM204A	-0.72	-0.24	-0.43	0.006	-3.84	0.29	-0.46	sensitizing	-0.3	FALSE
U2AF2	-0.30	-0.46	-0.63	0.003	-4.30	0.24	-0.46	sensitizing	9.1	TRUE
IKZF2	-0.53	-0.52	-0.34	0.002	-4.61	0.20	-0.46	sensitizing	-19.2	FALSE
IMP3	-0.72	-0.23	-0.45	0.006	-3.82	0.29	-0.47	sensitizing	17.5	TRUE
SIN3A	-0.56	-0.43	-0.41	0.002	-4.73	0.19	-0.47	sensitizing	9.9	TRUE
TGS1	-0.30	-0.75	-0.35	0.006	-3.84	0.29	-0.47	sensitizing	2.7	FALSE
ERCC4	-0.50	-0.42	-0.49	0.002	-4.85	0.18	-0.47	sensitizing	-3.0	FALSE
CUL5	-0.54	-0.55	-0.32	0.002	-4.52	0.21	-0.47	sensitizing	-20.0	FALSE
FOXD1	-0.50	-0.51	-0.40	0.002	-4.83	0.18	-0.47	sensitizing	-5.8	FALSE
LPHN1	-0.23	-0.58	-0.59	0.004	-4.13	0.25	-0.47	sensitizing	NA	NA
IPO13	-0.46	-0.22	-0.73	0.006	-3.83	0.29	-0.47	sensitizing	9.5	TRUE
ECEL1	-0.56	-0.47	-0.39	0.002	-4.78	0.18	-0.47	sensitizing	-13.9	FALSE
COPS3	-0.24	-0.74	-0.44	0.006	-3.85	0.29	-0.47	sensitizing	9.7	TRUE
LIMS1	-0.47	-0.74	-0.22	0.006	-3.84	0.29	-0.48	sensitizing	10.2	TRUE
MCM6	-0.59	-0.57	-0.27	0.003	-4.32	0.24	-0.48	sensitizing	13.6	TRUE
CNOT4	-0.57	-0.49	-0.37	0.002	-4.74	0.19	-0.48	sensitizing	-16.1	FALSE
GPS1	-0.40	-0.51	-0.52	0.002	-4.90	0.18	-0.48	sensitizing	12.0	TRUE
N4BP2	-0.57	-0.62	-0.25	0.003	-4.25	0.24	-0.48	sensitizing	-15.0	FALSE
ARL8B	-0.53	-0.65	-0.27	0.003	-4.33	0.24	-0.48	sensitizing	1.4	FALSE

Gene Name	D21	D22	D23	p-val	tstat	FDR	Mean FC	Type	BF	Essential
MPI	-0.41	-0.62	-0.43	0.002	-4.77	0.18	-0.48	sensitizing	-7.6	FALSE
KANSL1	-0.71	-0.43	-0.33	0.003	-4.33	0.24	-0.49	sensitizing	0.0	FALSE
CHUK	-0.46	-0.68	-0.33	0.003	-4.45	0.22	-0.49	sensitizing	-13.6	FALSE
ENSG00000276966	-0.61	-0.56	-0.29	0.003	-4.50	0.21	-0.49	sensitizing	NA	NA
KLHL9	-0.42	-0.46	-0.59	0.002	-4.93	0.18	-0.49	sensitizing	-9.9	FALSE
IFNGR2	-0.51	-0.65	-0.32	0.002	-4.56	0.20	-0.49	sensitizing	-17.7	FALSE
ING1	-0.59	-0.49	-0.40	0.002	-4.93	0.18	-0.49	sensitizing	-7.0	FALSE
GALE	-0.55	-0.69	-0.24	0.004	-4.16	0.25	-0.49	sensitizing	-6.7	FALSE
ZNF800	-0.65	-0.61	-0.23	0.004	-4.17	0.25	-0.50	sensitizing	-17.8	FALSE
ZNF219	-0.34	-0.72	-0.44	0.003	-4.42	0.23	-0.50	sensitizing	-14.9	FALSE
PCF11	-0.76	-0.42	-0.32	0.004	-4.22	0.25	-0.50	sensitizing	7.6	TRUE
FMN2	-0.74	-0.33	-0.43	0.003	-4.35	0.24	-0.50	sensitizing	-8.0	FALSE
PGM3	-0.50	-0.59	-0.43	0.001	-5.11	0.16	-0.50	sensitizing	-3.3	FALSE
DPH1	-0.40	-0.56	-0.57	0.001	-5.11	0.16	-0.51	sensitizing	-9.4	FALSE
WDR81	-0.46	-0.29	-0.78	0.004	-4.18	0.25	-0.51	sensitizing	-15.1	FALSE
SF3B3	-0.73	-0.37	-0.43	0.002	-4.59	0.20	-0.51	sensitizing	18.7	TRUE
CHD9	-0.47	-0.30	-0.78	0.003	-4.27	0.24	-0.52	sensitizing	-12.3	FALSE
NUP37	-0.77	-0.55	-0.23	0.004	-4.09	0.26	-0.52	sensitizing	-1.0	FALSE
RTCB	-0.70	-0.56	-0.31	0.002	-4.61	0.20	-0.52	sensitizing	16.6	TRUE
TMEM41B	-0.52	-0.58	-0.47	0.001	-5.40	0.15	-0.52	sensitizing	-3.6	FALSE
TMEM161A	-0.75	-0.59	-0.24	0.004	-4.23	0.25	-0.53	sensitizing	-7.2	FALSE
PHF21A	-0.69	-0.51	-0.38	0.001	-4.95	0.18	-0.53	sensitizing	-7.0	FALSE
MAPK14	-0.62	-0.58	-0.40	0.001	-5.22	0.16	-0.53	sensitizing	-11.3	FALSE
CTC-429P9.4	-0.75	-0.57	-0.30	0.002	-4.55	0.20	-0.54	sensitizing	NA	NA
KCMF1	-0.81	-0.30	-0.50	0.003	-4.36	0.24	-0.54	sensitizing	0.0	FALSE
VPS16	-0.61	-0.41	-0.60	0.001	-5.30	0.15	-0.54	sensitizing	-3.0	FALSE
ATG14	-0.53	-0.77	-0.32	0.002	-4.60	0.20	-0.54	sensitizing	-14.1	FALSE
BTG1	-0.40	-0.47	-0.77	0.002	-4.83	0.18	-0.54	sensitizing	-14.0	FALSE
RBCK1	-0.65	-0.62	-0.37	0.001	-5.12	0.16	-0.55	sensitizing	-10.3	FALSE
ZSWIM6	-0.77	-0.56	-0.30	0.002	-4.56	0.20	-0.55	sensitizing	-16.1	FALSE
SLC35A2	-0.77	-0.35	-0.52	0.002	-4.79	0.18	-0.55	sensitizing	-11.3	FALSE
ETV6	-0.80	-0.70	-0.15	0.006	-3.86	0.29	-0.55	sensitizing	-19.1	FALSE
THAP1	-0.81	-0.48	-0.37	0.002	-4.65	0.20	-0.55	sensitizing	19.6	TRUE
ACTR5	-0.44	-0.72	-0.50	0.001	-5.24	0.16	-0.55	sensitizing	-3.0	FALSE
CAND1	-0.68	-0.42	-0.56	0.001	-5.36	0.15	-0.56	sensitizing	-8.6	FALSE
XPO4	-0.63	-0.62	-0.43	0.001	-5.50	0.14	-0.56	sensitizing	-9.1	FALSE
C12orf44	-0.83	-0.26	-0.59	0.003	-4.35	0.24	-0.56	sensitizing	NA	NA
LAMTOR2	-0.65	-0.41	-0.63	0.001	-5.43	0.15	-0.56	sensitizing	11.9	TRUE
SRP68	-0.57	-0.28	-0.84	0.003	-4.40	0.23	-0.56	sensitizing	5.8	TRUE
POLR3F	-0.75	-0.41	-0.53	0.001	-5.16	0.16	-0.56	sensitizing	9.2	TRUE
RYBP	-0.55	-0.90	-0.24	0.004	-4.07	0.26	-0.56	sensitizing	-6.7	FALSE
JMJD1C	-0.42	-0.52	-0.76	0.001	-5.17	0.16	-0.56	sensitizing	-17.6	FALSE
TAB2	-0.55	-0.56	-0.58	0.001	-5.90	0.11	-0.57	sensitizing	-18.2	FALSE
DCPS	-0.48	-0.78	-0.44	0.001	-5.12	0.16	-0.57	sensitizing	4.4	FALSE
ZNF639	-0.83	-0.45	-0.43	0.002	-4.84	0.18	-0.57	sensitizing	-15.6	FALSE

Gene Name	D21	D22	D23	p-val	tstat	FDR	Mean FC	Type	BF	Essential
PDS5B	-0.75	-0.32	-0.64	0.002	-4.85	0.18	-0.57	sensitizing	-11.7	FALSE
MAT2A	-0.24	-0.56	-0.91	0.004	-4.12	0.26	-0.57	sensitizing	12.9	TRUE
VPS41	-0.63	-0.41	-0.68	0.001	-5.48	0.14	-0.58	sensitizing	4.7	FALSE
KMT2D	-0.38	-0.83	-0.53	0.002	-4.87	0.18	-0.58	sensitizing	-6.2	FALSE
RANBP9	-0.99	-0.43	-0.31	0.005	-3.96	0.28	-0.58	sensitizing	-10.4	FALSE
PGAM1	-0.60	-0.69	-0.45	0.001	-5.67	0.13	-0.58	sensitizing	18.5	TRUE
RUNX1	-0.96	-0.51	-0.27	0.004	-4.09	0.26	-0.58	sensitizing	-19.3	FALSE
RNF31	-0.38	-0.76	-0.62	0.001	-5.25	0.16	-0.59	sensitizing	-13.0	FALSE
FBRS	-0.89	-0.64	-0.24	0.003	-4.29	0.24	-0.59	sensitizing	-6.9	FALSE
ACTR6	-1.02	-0.38	-0.38	0.005	-4.01	0.27	-0.59	sensitizing	5.2	NA
WDR3	-0.54	-0.64	-0.61	0.000	-6.13	0.10	-0.60	sensitizing	12.8	TRUE
SUDS3	-0.41	-0.89	-0.48	0.002	-4.81	0.18	-0.60	sensitizing	6.3	TRUE
SERBP1	-0.84	-0.27	-0.68	0.002	-4.55	0.20	-0.60	sensitizing	11.9	TRUE
POLD1	-0.48	-0.40	-0.91	0.002	-4.74	0.19	-0.60	sensitizing	12.5	TRUE
PABPN1	-0.95	-0.16	-0.70	0.006	-3.87	0.29	-0.60	sensitizing	12.7	TRUE
ROCK2	-0.78	-0.68	-0.36	0.001	-5.21	0.16	-0.61	sensitizing	-8.4	FALSE
UBE2F	-0.65	-0.66	-0.52	0.000	-6.18	0.10	-0.61	sensitizing	-20.2	FALSE
PSMF1	-0.82	-0.50	-0.52	0.001	-5.58	0.14	-0.61	sensitizing	-7.7	FALSE
MLLT1	-0.80	-0.48	-0.56	0.001	-5.68	0.13	-0.61	sensitizing	-18.2	FALSE
PIK3R4	-0.43	-0.85	-0.57	0.001	-5.33	0.15	-0.62	sensitizing	3.8	FALSE
WIBG	-0.54	-0.76	-0.56	0.000	-6.04	0.10	-0.62	sensitizing	NA	NA
PAXBP1	-0.77	-0.71	-0.39	0.001	-5.44	0.15	-0.62	sensitizing	6.9	TRUE
RPL27A	-0.84	-0.55	-0.48	0.001	-5.55	0.14	-0.62	sensitizing	17.8	TRUE
EIF3L	-0.82	-0.78	-0.27	0.002	-4.65	0.20	-0.62	sensitizing	-2.2	FALSE
GTF3C4	-0.36	-0.73	-0.81	0.001	-5.30	0.15	-0.63	sensitizing	11.7	TRUE
METTL16	-0.86	-0.70	-0.35	0.001	-5.16	0.16	-0.64	sensitizing	5.1	TRUE
CDK8	-0.89	-0.47	-0.57	0.001	-5.50	0.14	-0.64	sensitizing	-17.7	FALSE
RELA	-0.99	-0.38	-0.57	0.002	-4.82	0.18	-0.65	sensitizing	-4.2	FALSE
ZNF217	-0.82	-0.67	-0.45	0.001	-5.83	0.11	-0.65	sensitizing	-15.0	FALSE
EIF2AK4	-0.26	-0.57	-1.12	0.005	-3.98	0.28	-0.65	sensitizing	-4.0	FALSE
HDAC2	-0.98	-0.63	-0.35	0.002	-4.82	0.18	-0.65	sensitizing	-10.2	FALSE
PHF3	-1.02	-0.55	-0.38	0.002	-4.70	0.19	-0.65	sensitizing	-11.8	FALSE
TAF5L	-0.68	-0.87	-0.42	0.001	-5.54	0.14	-0.65	sensitizing	-8.6	FALSE
CHMP6	-0.84	-0.67	-0.45	0.001	-5.81	0.11	-0.65	sensitizing	16.5	TRUE
AP3B1	-0.63	-0.92	-0.42	0.001	-5.38	0.15	-0.66	sensitizing	-4.8	FALSE
TSC1	-0.76	-0.70	-0.54	0.000	-6.54	0.08	-0.67	sensitizing	-6.8	FALSE
NXT1	-0.73	-0.27	-1.03	0.003	-4.49	0.21	-0.68	sensitizing	11.7	TRUE
DROSHA	-0.36	-0.71	-0.96	0.001	-5.13	0.16	-0.68	sensitizing	2.9	FALSE
RBM10	-0.62	-0.53	-0.89	0.000	-6.10	0.10	-0.68	sensitizing	-7.1	FALSE
SUPT7L	-0.60	-0.68	-0.76	0.000	-6.86	0.07	-0.68	sensitizing	-13.8	FALSE
ECD	-0.80	-0.63	-0.62	0.000	-6.79	0.07	-0.68	sensitizing	17.2	TRUE
TXNDC17	-1.02	-0.51	-0.52	0.001	-5.25	0.16	-0.68	sensitizing	-4.8	FALSE
ALG1	-0.26	-0.91	-0.90	0.002	-4.63	0.20	-0.69	sensitizing	12.4	TRUE
NCOA5	-0.44	-1.09	-0.53	0.002	-4.79	0.18	-0.69	sensitizing	-13.0	FALSE
EXOSC6	-0.97	-0.20	-0.91	0.003	-4.30	0.24	-0.69	sensitizing	15.8	TRUE
NAA20	-1.05	-0.55	-0.49	0.001	-5.16	0.16	-0.70	sensitizing	8.6	TRUE

Gene Name	D21	D22	D23	p-val	tstat	FDR	Mean FC	Type	BF	Essential
LRR1	-0.91	-0.57	-0.61	0.000	-6.24	0.10	-0.70	sensitizing	20.3	TRUE
DNAJC13	-0.71	-0.65	-0.74	0.000	-7.25	0.06	-0.70	sensitizing	-7.9	FALSE
CTPS1	-0.43	-1.06	-0.62	0.001	-5.13	0.16	-0.70	sensitizing	10.5	TRUE
MDM2	-0.60	-1.26	-0.26	0.006	-3.89	0.29	-0.71	sensitizing	18.1	TRUE
SUV420H1	-0.74	-0.85	-0.54	0.000	-6.62	0.07	-0.71	sensitizing	NA	NA
NUP133	-0.51	-0.49	-1.13	0.002	-4.86	0.18	-0.71	sensitizing	19.2	TRUE
PTBP1	-0.68	-0.88	-0.58	0.000	-6.69	0.07	-0.71	sensitizing	-4.0	FALSE
TLN1	-0.43	-1.07	-0.64	0.001	-5.20	0.16	-0.71	sensitizing	8.4	TRUE
CTDNEP1	-0.24	-0.63	-1.28	0.006	-3.87	0.29	-0.72	sensitizing	5.8	NA
CALR	-0.15	-1.11	-0.91	0.005	-4.00	0.27	-0.72	sensitizing	-1.0	FALSE
TXNRD1	-0.65	-1.09	-0.44	0.001	-5.22	0.16	-0.73	sensitizing	-3.5	FALSE
POLA2	-0.77	-0.17	-1.25	0.006	-3.84	0.29	-0.73	sensitizing	18.4	TRUE
EIF2B5	-1.25	-0.70	-0.26	0.004	-4.15	0.25	-0.74	sensitizing	17.1	TRUE
CBWD2	-0.91	-0.79	-0.52	0.000	-6.58	0.08	-0.74	sensitizing	14.2	TRUE
THOC3	-0.42	-0.46	-1.36	0.005	-3.96	0.28	-0.74	sensitizing	16.9	TRUE
MBD3	-1.06	-0.89	-0.29	0.002	-4.80	0.18	-0.74	sensitizing	-11.9	FALSE
ADAT3	-0.79	-1.15	-0.30	0.002	-4.62	0.20	-0.74	sensitizing	3.3	FALSE
SUPT20H	-0.99	-1.03	-0.23	0.003	-4.48	0.21	-0.75	sensitizing	-17.4	FALSE
CCNT1	-0.58	-1.23	-0.45	0.002	-4.73	0.19	-0.75	sensitizing	11.7	TRUE
NUS1	-0.92	-1.08	-0.30	0.002	-4.85	0.18	-0.77	sensitizing	18.2	TRUE
PTK2	-1.23	-0.40	-0.68	0.002	-4.82	0.18	-0.77	sensitizing	9.6	TRUE
HSP90AB1	-0.75	-1.05	-0.51	0.000	-6.13	0.10	-0.77	sensitizing	2.2	FALSE
VPS29	-0.43	-0.64	-1.26	0.002	-4.79	0.18	-0.78	sensitizing	7.7	TRUE
MMS22L	-0.48	-0.77	-1.09	0.001	-5.85	0.11	-0.78	sensitizing	18.5	TRUE
MARS	-1.42	-0.63	-0.30	0.005	-3.93	0.28	-0.78	sensitizing	17.0	TRUE
FARSA	-0.66	-0.66	-1.02	0.000	-6.79	0.07	-0.78	sensitizing	10.6	TRUE
ZBTB7A	-0.95	-0.98	-0.43	0.001	-5.85	0.11	-0.78	sensitizing	-20.8	FALSE
VPS33A	-0.86	-0.81	-0.69	0.000	-7.92	0.04	-0.79	sensitizing	6.1	TRUE
TMEM165	-0.76	-0.91	-0.70	0.000	-7.78	0.04	-0.79	sensitizing	-7.6	FALSE
RPL3	-0.67	-0.90	-0.81	0.000	-7.75	0.04	-0.79	sensitizing	21.6	TRUE
PRKRIR	-0.75	-1.10	-0.53	0.000	-6.11	0.10	-0.79	sensitizing	NA	NA
GMPPB	-1.40	-0.58	-0.42	0.003	-4.29	0.24	-0.80	sensitizing	14.8	TRUE
RPL23A	-0.68	-1.23	-0.51	0.001	-5.42	0.15	-0.81	sensitizing	21.3	TRUE
TOX4	-0.85	-0.92	-0.69	0.000	-8.07	0.04	-0.82	sensitizing	-10.8	FALSE
RBM14-RBM4	-0.39	-1.05	-1.05	0.001	-5.54	0.14	-0.83	sensitizing	11.8	TRUE
SNRPF	-1.08	-0.49	-0.96	0.000	-6.31	0.09	-0.84	sensitizing	20.6	TRUE
CSE1L	-0.76	-0.76	-1.03	0.000	-7.94	0.04	-0.85	sensitizing	14.6	TRUE
CCAR1	-1.08	-0.89	-0.57	0.000	-6.85	0.07	-0.85	sensitizing	6.7	FALSE
SRSF11	-0.82	-0.94	-0.79	0.000	-8.61	0.04	-0.85	sensitizing	12.0	TRUE
MED15	-0.72	-0.99	-0.85	0.000	-8.18	0.04	-0.85	sensitizing	-17.2	FALSE
CMTR1	-0.58	-1.29	-0.70	0.001	-5.70	0.13	-0.85	sensitizing	5.5	TRUE
CCDC130	-1.27	-1.13	-0.19	0.003	-4.27	0.24	-0.86	sensitizing	10.0	TRUE
R3HCC1L	-0.88	-1.42	-0.30	0.003	-4.46	0.22	-0.87	sensitizing	-8.0	FALSE
NCBP1	-1.27	-0.41	-0.94	0.001	-5.34	0.15	-0.87	sensitizing	10.4	TRUE
UBR5	-1.62	-0.66	-0.35	0.005	-3.95	0.28	-0.88	sensitizing	-14.2	FALSE
TADA2B	-0.83	-0.72	-1.09	0.000	-7.87	0.04	-0.88	sensitizing	-14.9	FALSE

Gene Name	D21	D22	D23	p-val	tstat	FDR	Mean FC	Type	BF	Essential
AMBRA1	-1.12	-0.81	-0.71	0.000	-7.60	0.05	-0.88	sensitizing	-14.8	FALSE
LSM7	-1.14	-0.48	-1.04	0.000	-6.14	0.10	-0.89	sensitizing	15.7	TRUE
RIPK1	-1.24	-0.87	-0.54	0.000	-6.18	0.10	-0.89	sensitizing	-13.5	FALSE
CD2BP2	-0.94	-0.77	-0.99	0.000	-8.84	0.04	-0.90	sensitizing	-6.3	FALSE
RBM25	-1.68	-0.32	-0.73	0.005	-3.90	0.29	-0.91	sensitizing	16.4	TRUE
TSEN54	-1.15	-0.95	-0.64	0.000	-7.37	0.05	-0.91	sensitizing	7.0	TRUE
CDCA8	-0.97	-1.58	-0.25	0.004	-4.17	0.25	-0.93	sensitizing	22.1	TRUE
THOC6	-1.30	-0.95	-0.56	0.000	-6.32	0.09	-0.93	sensitizing	0.0	FALSE
STAG2	-0.92	-1.03	-0.86	0.000	-9.43	0.03	-0.93	sensitizing	-18.3	FALSE
STAT1	-1.16	-1.06	-0.60	0.000	-7.16	0.06	-0.94	sensitizing	-15.4	FALSE
VPS39	-1.00	-0.92	-0.90	0.000	-9.69	0.03	-0.94	sensitizing	4.7	FALSE
IKBKG	-1.53	-0.69	-0.60	0.001	-5.17	0.16	-0.94	sensitizing	-11.6	FALSE
SENP6	-1.59	-0.62	-0.63	0.002	-4.90	0.18	-0.95	sensitizing	11.8	TRUE
FOSL1	-0.66	-0.90	-1.30	0.000	-6.98	0.07	-0.95	sensitizing	0.2	FALSE
ANKRD52	-1.25	-0.77	-0.85	0.000	-7.79	0.04	-0.96	sensitizing	-2.0	FALSE
PYROXD1	-1.01	-1.59	-0.29	0.003	-4.40	0.23	-0.97	sensitizing	10.4	TRUE
AHR	-0.94	-1.41	-0.55	0.000	-5.96	0.11	-0.97	sensitizing	-7.2	FALSE
TRIP12	-1.17	-0.79	-0.98	0.000	-8.82	0.04	-0.98	sensitizing	-18.6	FALSE
IRF1	-0.67	-1.58	-0.70	0.001	-5.35	0.15	-0.98	sensitizing	-11.9	FALSE
CUL3	-1.27	-1.23	-0.47	0.001	-5.90	0.11	-0.99	sensitizing	-19.5	FALSE
SRSF10	-0.71	-1.29	-0.98	0.000	-7.70	0.04	-1.00	sensitizing	-4.5	FALSE
MAP3K7	-1.38	-1.12	-0.51	0.000	-6.05	0.10	-1.00	sensitizing	-9.0	FALSE
PCBP2	-0.54	-0.80	-1.76	0.002	-4.75	0.19	-1.03	sensitizing	9.1	FALSE
IFNGR1	-1.19	-0.75	-1.19	0.000	-8.51	0.04	-1.04	sensitizing	-15.7	FALSE
XPO5	-0.88	-0.75	-1.52	0.000	-6.69	0.07	-1.05	sensitizing	11.4	TRUE
MTA2	-0.78	-0.86	-1.51	0.000	-6.80	0.07	-1.05	sensitizing	-4.9	FALSE
ARID4B	-1.53	-1.09	-0.56	0.000	-6.01	0.10	-1.06	sensitizing	-9.6	FALSE
MED24	-0.97	-0.93	-1.31	0.000	-9.33	0.03	-1.07	sensitizing	-11.6	FALSE
LSM3	-0.53	-0.86	-1.84	0.002	-4.73	0.19	-1.08	sensitizing	18.8	TRUE
PPP6C	-2.06	-0.41	-0.78	0.006	-3.87	0.29	-1.08	sensitizing	19.5	TRUE
FLCN	-1.10	-1.18	-1.03	0.000	-11.19	0.02	-1.10	sensitizing	8.5	TRUE
RRM1	-1.28	-0.98	-1.12	0.000	-10.63	0.02	-1.13	sensitizing	22.0	TRUE
TYMS	-1.07	-1.50	-0.82	0.000	-7.98	0.04	-1.13	sensitizing	10.0	TRUE
SLC3A2	-1.34	-0.64	-1.46	0.000	-6.92	0.07	-1.15	sensitizing	-1.8	FALSE
ITPK1	-1.17	-1.68	-0.62	0.000	-6.16	0.10	-1.16	sensitizing	1.6	FALSE
SLC7A5	-0.97	-1.09	-1.43	0.000	-9.72	0.03	-1.16	sensitizing	-4.6	FALSE
NF2	-1.65	-1.40	-0.50	0.001	-5.75	0.12	-1.18	sensitizing	-21.7	FALSE
ENSG00002 80789	-1.26	-1.28	-1.05	0.000	-11.60	0.02	-1.20	sensitizing	NA	NA
RB1CC1	-1.58	-1.12	-0.90	0.000	-8.48	0.04	-1.20	sensitizing	-11.0	FALSE
VPS35	-1.01	-1.94	-0.79	0.000	-6.00	0.10	-1.25	sensitizing	2.9	FALSE
MED16	-1.66	-0.79	-1.38	0.000	-7.76	0.04	-1.28	sensitizing	-14.4	FALSE
PAXIP1	-1.53	-1.76	-0.63	0.000	-6.40	0.09	-1.31	sensitizing	-11.3	FALSE
KPNB1	-1.47	-1.24	-1.22	0.000	-12.48	0.01	-1.31	sensitizing	20.9	TRUE
GSPT1	-2.25	-1.16	-0.61	0.001	-4.95	0.18	-1.34	sensitizing	16.5	TRUE
HNRNPU	-1.85	-0.89	-1.28	0.000	-7.70	0.04	-1.34	sensitizing	21.2	TRUE

Gene Name	D21	D22	D23	p-val	tstat	FDR	Mean FC	Type	BF	Essential
OTUD5	-1.41	-1.58	-1.05	0.000	-10.63	0.02	-1.35	sensitizing	-20.0	FALSE
TADA1	-0.66	-1.32	-2.19	0.001	-5.54	0.14	-1.39	sensitizing	-7.5	FALSE
UBIAD1	-1.18	-2.12	-0.90	0.000	-6.49	0.08	-1.40	sensitizing	14.1	TRUE
PSMC3	-2.47	-1.64	-0.14	0.006	-3.82	0.30	-1.42	sensitizing	20.0	TRUE
SACM1L	-1.71	-1.44	-1.10	0.000	-10.67	0.02	-1.42	sensitizing	15.9	TRUE
DUSP28	-2.40	-0.88	-1.02	0.001	-5.26	0.16	-1.43	sensitizing	-1.9	FALSE
KEAP1	-1.87	-1.26	-1.19	0.000	-9.73	0.03	-1.44	sensitizing	-13.4	FALSE
ATG9A	-1.59	-1.83	-0.93	0.000	-8.50	0.04	-1.45	sensitizing	-12.9	FALSE
JUNB	-2.08	-1.30	-0.99	0.000	-7.47	0.05	-1.45	sensitizing	-12.0	FALSE
CCNC	-1.46	-1.48	-1.51	0.000	-15.43	0.01	-1.48	sensitizing	-15.9	FALSE
JAK1	-1.68	-1.81	-0.99	0.000	-9.03	0.04	-1.49	sensitizing	-17.6	FALSE
TSC2	-1.99	-1.41	-1.22	0.000	-9.95	0.03	-1.54	sensitizing	-8.1	FALSE
MED23	-1.58	-1.63	-1.59	0.000	-16.64	0.01	-1.60	sensitizing	-14.7	FALSE
UROD	-2.25	-2.22	-0.34	0.002	-4.64	0.20	-1.60	sensitizing	6.6	FALSE
CBFB	-2.34	-1.63	-1.07	0.000	-7.80	0.04	-1.68	sensitizing	-14.3	FALSE
SOD1	-1.01	-2.17	-1.96	0.000	-8.15	0.04	-1.71	sensitizing	18.6	TRUE

Supp. Table 5. Median overall survival of melanoma patients.

Gene	Cohort	n	Events	Median	95% lower CI	95% upper CI	Function
CHUK	High Expression	165	95	50.9	34.3	71.7	NF-κB signaling
CHUK	Low Expression	161	85	39.5	28.8	59.4	NF-κB signaling
CHUK	Moderate Expression	318	144	85	65.8	148.1	NF-κB signaling
COX10	High Expression	163	90	50.9	35.2	66.7	OXPHOS
COX10	Low Expression	161	67	105	63.3	204.5	OXPHOS
COX10	Moderate Expression	320	167	61	44.1	79.5	OXPHOS
COX17	High Expression	162	64	66.6	58.5	167.6	OXPHOS
COX17	Low Expression	181	112	42.7	32.8	63	OXPHOS
COX17	Moderate Expression	301	148	65.9	48.9	96.2	OXPHOS
DEPDC5	High Expression	163	87	49.5	34.8	65.8	mTOR signaling
DEPDC5	Low Expression	164	91	65.4	44.1	98.3	mTOR signaling
DEPDC5	Moderate Expression	317	146	66.7	50.9	105	mTOR signaling
IFNGR1	High Expression	163	77	80.6	53.2	148.1	IFN response
IFNGR1	Low Expression	161	92	46.9	28.8	66.4	IFN response
IFNGR1	Moderate Expression	320	155	61.2	48.9	96.2	IFN response
IKBKG	High Expression	250	120	55.6	33.5	78.9	NF-κB signaling
IKBKG	Low Expression	132	75	63.3	47.2	102	NF-κB signaling
IKBKG	Moderate Expression	262	129	65.8	50.9	103.2	NF-κB signaling
IRF1	High Expression	163	53	162	103.2	NA	IFN response
IRF1	Low Expression	164	104	34.8	27	49.5	IFN response
IRF1	Moderate Expression	317	167	61	47.3	74.6	IFN response
ISYNA1	High Expression	163	84	50.1	35.9	81.1	IP metabolism

Gene	Cohort	n	Events	Median	95% lower CI	95% upper CI	Function
ISYNA1	Low Expression	163	74	103.1	69	216.5	IP metabolism
ISYNA1	Moderate Expression	318	166	53.9	46.4	66.4	IP metabolism
JAK1	High Expression	163	83	72	53.5	117.8	IFN response
JAK1	Low Expression	163	90	41.6	28.8	61.1	IFN response
JAK1	Moderate Expression	318	151	65.9	50.7	96.2	IFN response
JUNB	High Expression	162	77	60.2	43.8	103.2	NF-κB signaling
JUNB	Low Expression	164	103	37.9	28.8	54.4	NF-κB signaling
JUNB	Moderate Expression	318	144	74.6	61.2	113.4	NF-κB signaling
MAP3K7	High Expression	164	98	48.9	37.9	65.4	NF-κB signaling
MAP3K7	Low Expression	160	78	44.1	34.8	64.4	NF-κB signaling
MAP3K7	Moderate Expression	320	148	94.9	66.4	117.8	NF-κB signaling
MAPK14	High Expression	163	102	47.2	35.4	68.1	NF-κB signaling
MAPK14	Low Expression	160	78	55.6	35.2	103	NF-κB signaling
MAPK14	Moderate Expression	321	144	71.7	61.1	112.5	NF-κB signaling
MED15	High Expression	162	88	43.2	32.3	54.4	Mediator complex
MED15	Low Expression	161	92	60.2	43.8	103.2	Mediator complex
MED15	Moderate Expression	321	144	78.9	61.5	113.4	Mediator complex
MED20	High Expression	163	98	43.2	33.7	62.7	Mediator complex
MED20	Low Expression	163	76	66.7	48.9	127.1	Mediator complex
MED20	Moderate Expression	318	150	65.4	50.9	105	Mediator complex
MED23	High Expression	163	88	61	48	103.1	Mediator complex
MED23	Low Expression	161	86	43.4	28.8	61.2	Mediator complex
MED23	Moderate Expression	320	150	72	59.4	117.1	Mediator complex
NPRL3	High Expression	161	84	50.1	43.2	68.1	mTOR signaling
NPRL3	Low Expression	165	90	53.5	36	103.1	mTOR signaling
NPRL3	Moderate Expression	318	150	65.8	54.4	127.1	mTOR signaling
PGM3	High Expression	163	91	64.4	47.5	121	Msc. Metabolism
PGM3	Low Expression	160	82	44.1	28.2	65.9	Msc. Metabolism
PGM3	Moderate Expression	321	151	65.8	53.2	96.2	Msc. Metabolism
PIK3R4	High Expression	164	96	41.6	33.5	68.1	Unknown
PIK3R4	Low Expression	160	76	63	44.1	112.5	Unknown
PIK3R4	Moderate Expression	320	152	66.6	59.4	103.2	Unknown
PSAP	High Expression	160	73	74.6	55.6	107.1	Msc. Metabolism
PSAP	Low Expression	162	100	34.8	27.6	66.4	Msc. Metabolism
PSAP	Moderate Expression	322	151	61.5	49.5	94.9	Msc. Metabolism
SLC3A2	High Expression	159	82	48	32.4	68.1	AA transporter
SLC3A2	Low Expression	163	80	98.3	63.3	168.1	AA transporter
SLC3A2	Moderate Expression	322	162	54.4	48.6	74.6	AA transporter
SLC7A5	High Expression	162	85	47.5	32.3	66.6	AA transporter
SLC7A5	Low Expression	162	71	81.1	60.2	162	AA transporter
SLC7A5	Moderate Expression	320	168	62.7	48	80.6	AA transporter
STAT1	High Expression	164	64	148.1	96.2	297.7	IFN response
STAT1	Low Expression	163	103	28.2	25.9	44.5	IFN response

Gene	Cohort	n	Events	Median	95% lower CI	95% upper CI	Function
STAT1	Moderate Expression	317	157	61.1	48.6	69	IFN response
TAB2	High Expression	163	91	61.5	47.2	103.1	mTOR signaling
TAB2	Low Expression	159	80	35.2	28.7	58.5	mTOR signaling
TAB2	Moderate Expression	322	153	79.5	60.2	117.1	mTOR signaling

Supp. Table 6. Statistics of identified essential genes in meta-analysis.

Sample	log2FC	Number
A375+CD8CAR	-3.79	2199
A375+CD8CTRL	-3.7	2260
A375+GDCTRL	-4.22	1896
A375+GDTcell	-5.09	2022
A375+NKCTRL	-4.59	2062
A375+NKcell	-4.67	1966
A375CD19	-4.57	1718
A375CD33	-4.47	1372

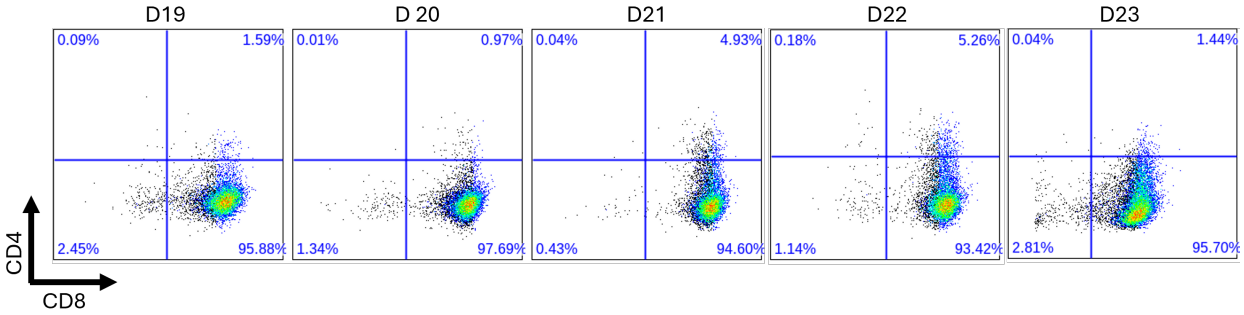

Supp. Figure 1. Purity of primary CD8⁺ T cells.

Dot plots of CD4 and CD8 surface marker expression on CD8⁺ T cells purified from the buffy coat of the 5 healthy donors (D19 – D23) included in the screen.

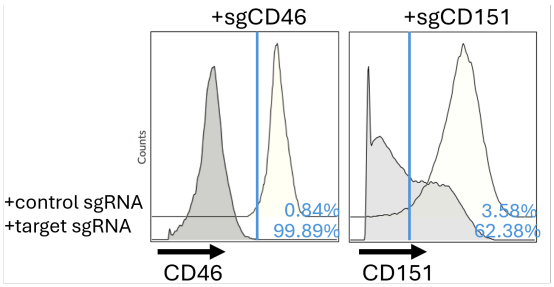

Supp. Figure 2. Cas9 KO efficiency of A375-ROR1^{high}-Cas9 cells

A375-Cas9-ROR1^{high} cells were transduced to express CD46-/CD151-targeting sgRNAs or control sgRNAs. After selection in 2 µg/mL Puro selection for 48 hours, the A375 clones were stained for surface CD46 and CD151 protein and fixed in 4% PFA, before analyzing with a flow cytometer. Number represents the percentage of cells with a loss on CD46 and CD151 expression.

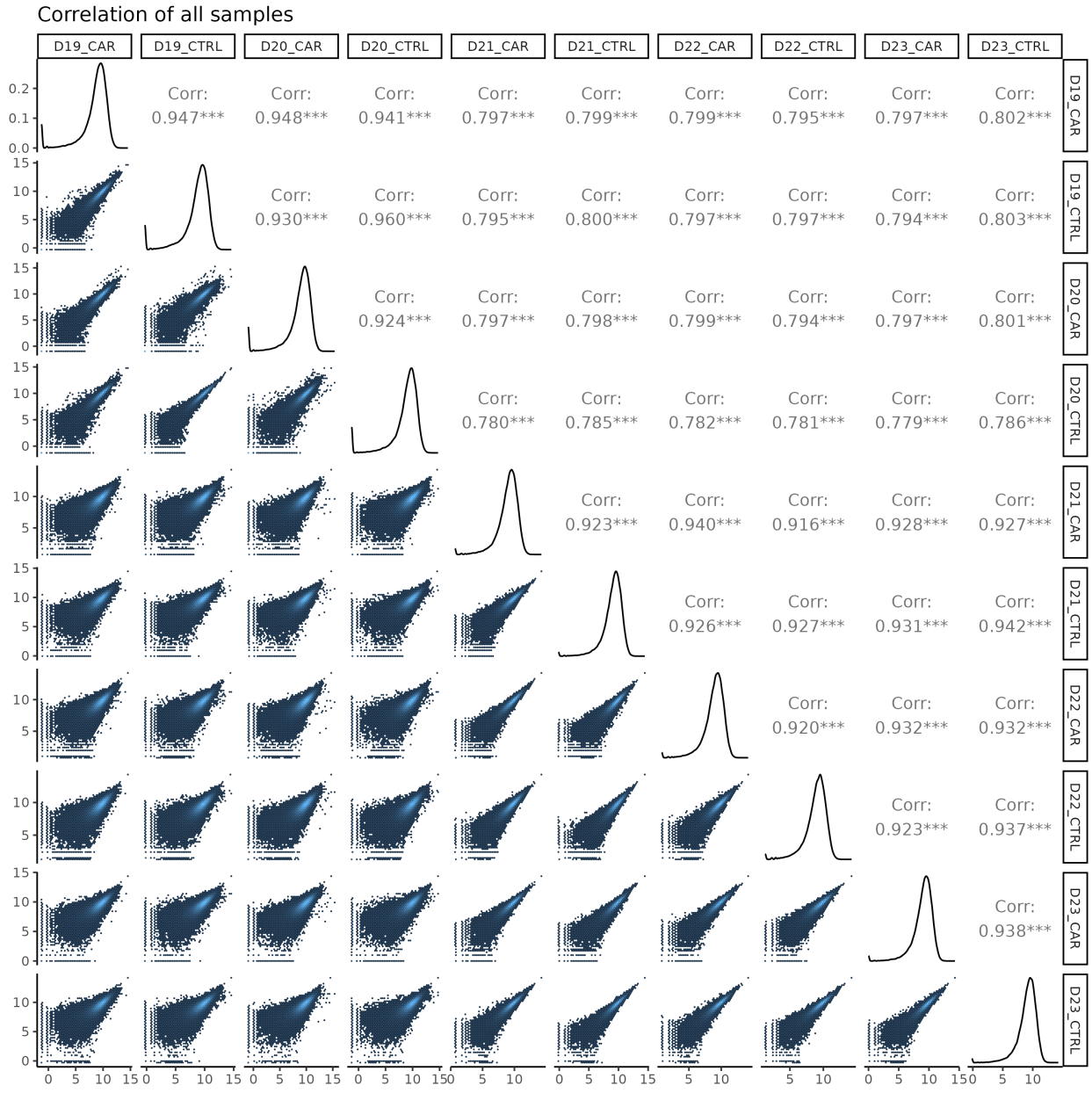

Supp. Figure 3. Correlation of all co-culture screen samples on normalized sgRNA counts.

sgRNAs from all samples were plotted against each other. Pearson correlation coefficients were calculated which were indicated by the numbers. Asterisks denote significance level. sgRNA count distributions were plotted on the diagonal.

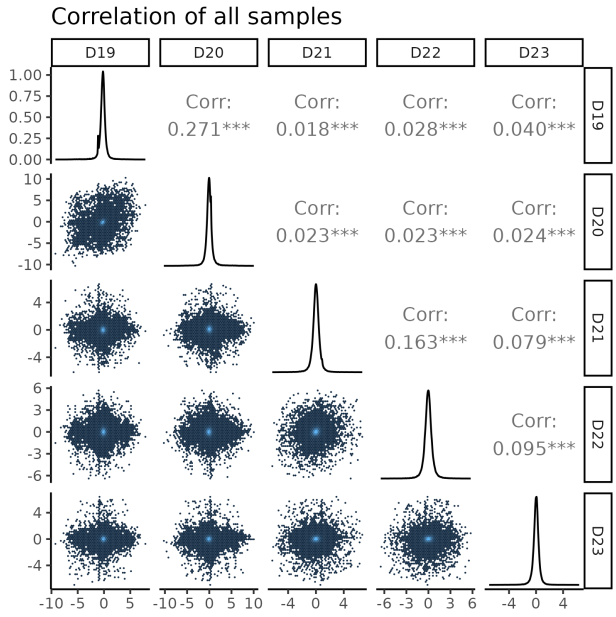

Supp. Figure 4. Correlation of all co-culture screen samples on log_2 fold-change level

sgRNAs from all samples were plotted against each other. Pearson correlation coefficients were calculated which were indicated by the numbers. Asterisks denote significance level. sgRNA count distributions were plotted on the diagonal.

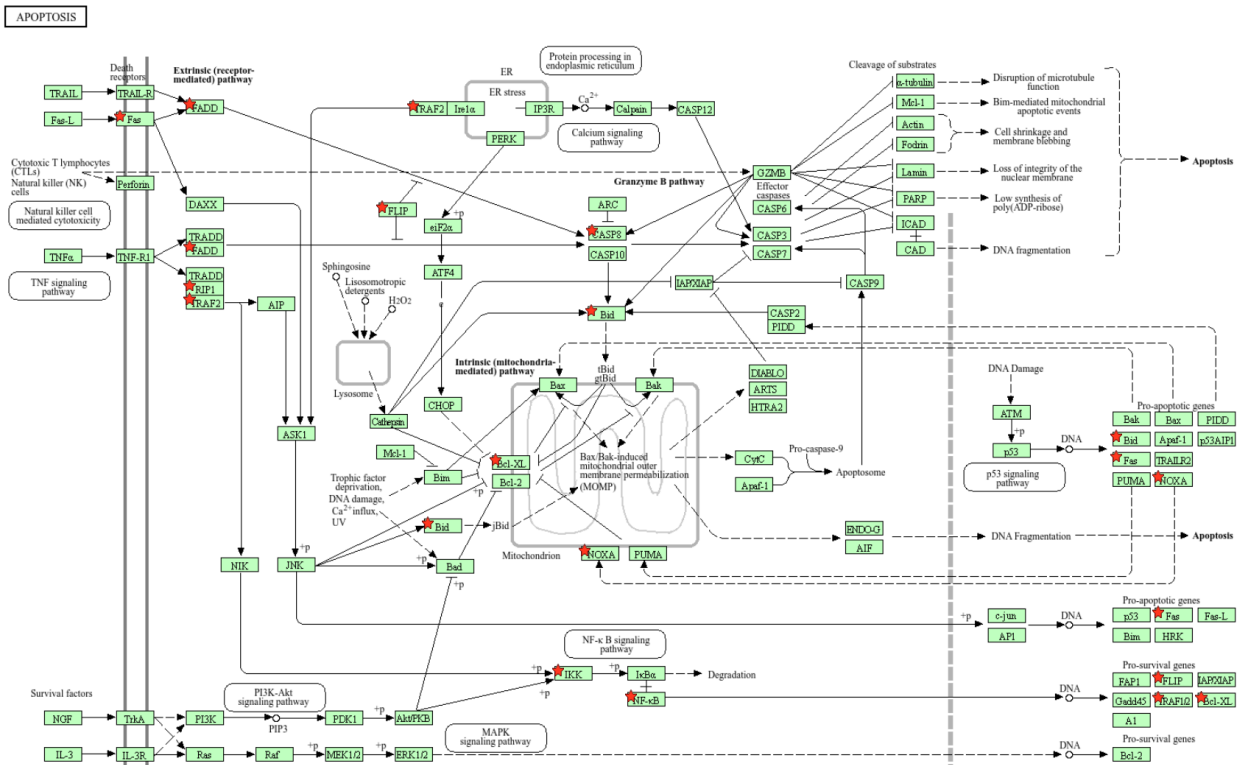

Supp. Figure 5. Co-culture screen hits mapped to KEGG Apoptosis pathway.

KEGG Apoptosis was identified from pathway enrichment analysis using statistically significant genes candidates of the screens. Red stars indicate the hits assigned to this pathway.

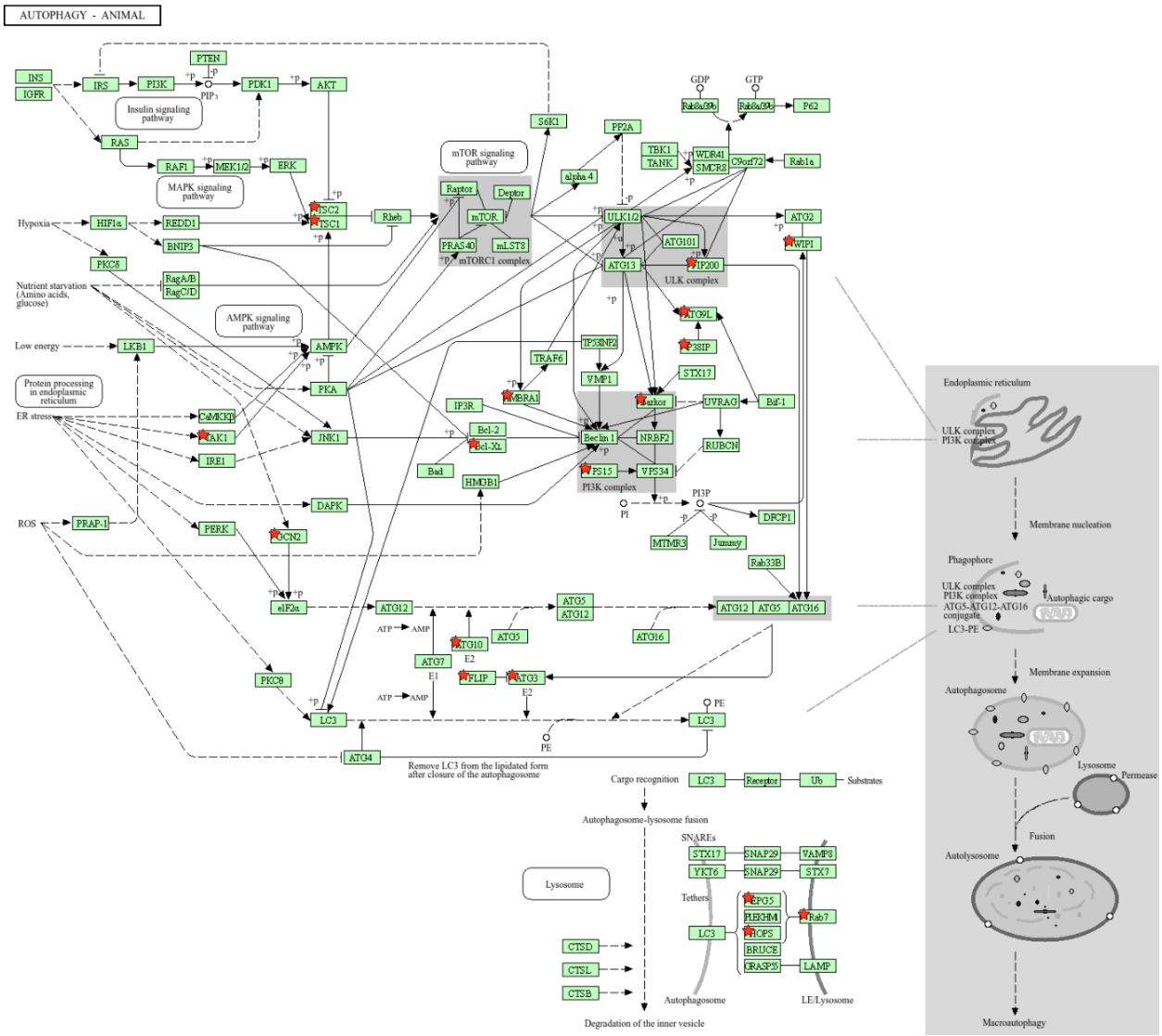

Supp. Figure 6. Co-culture screen hits mapped to KEGG Autophagy – animal pathway.

KEGG Autophagy Animal pathway was identified from pathway enrichment analysis using statistically significant genes candidates of the screens. Red stars indicate the hits assigned to this pathway.

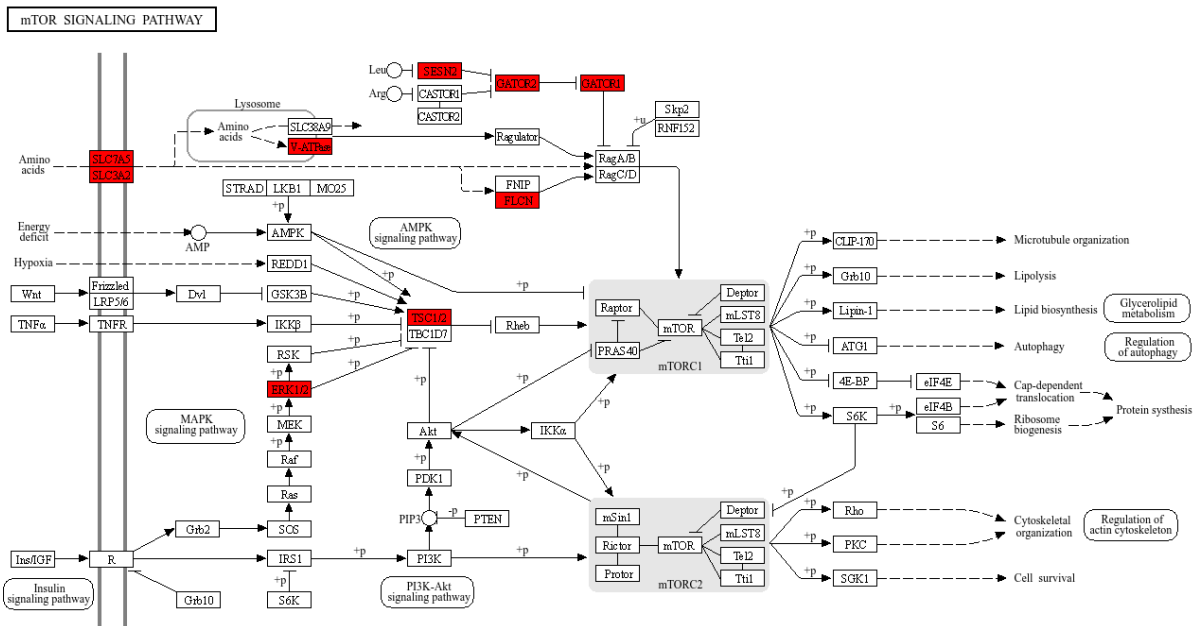

Supp. Figure 7. Co-culture screen hits mapped to KEGG mTOR signaling pathway.

KEGG mTOR signaling pathway was identified from pathway enrichment analysis by DAVID using statistically significant genes candidates of the screens. Red labels indicated the hits included in mapping process.

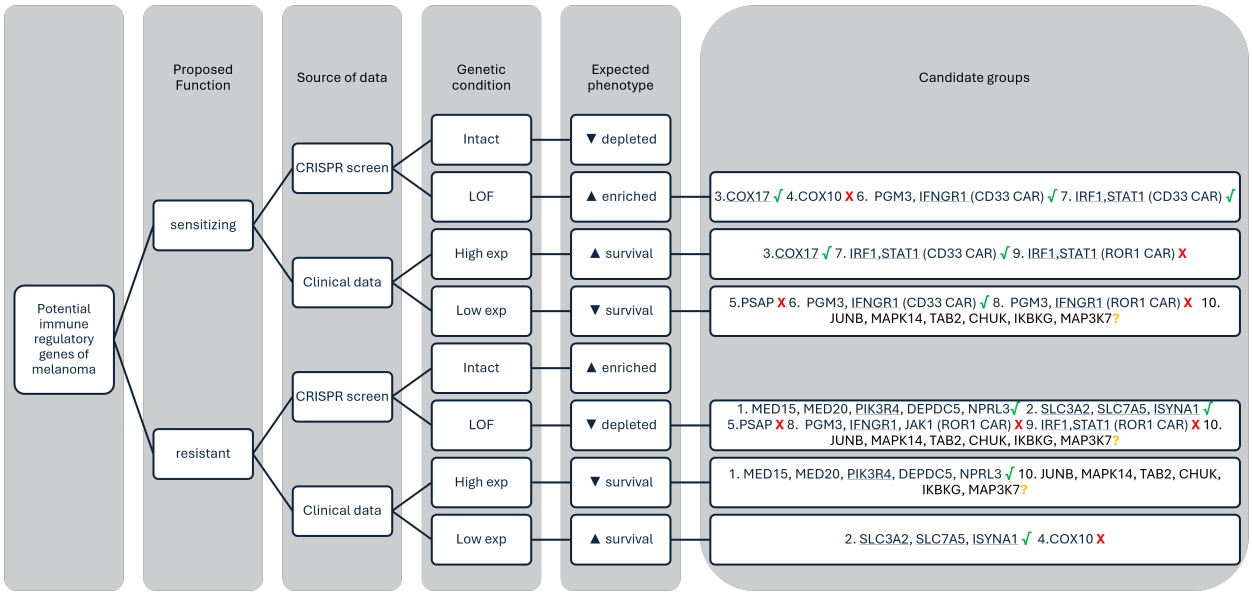

Supp. Figure 8. Summary of gene function deduction.

The graph illustrates the deduction rationale of the potential gene functions from the observed phenotype from survival analysis and co-culture screen data. Genes are grouped by their presented phenotype in both survival analysis and co-culture screen result, as indicated by the preceding number. Green ticks represent genes with matched phenotypes in both clinical data and screen data, and red crosses for mismatches. Question marks

denote uncertain observations. Underlines indicate the genes with appropriate correlation with cytolytic scores.

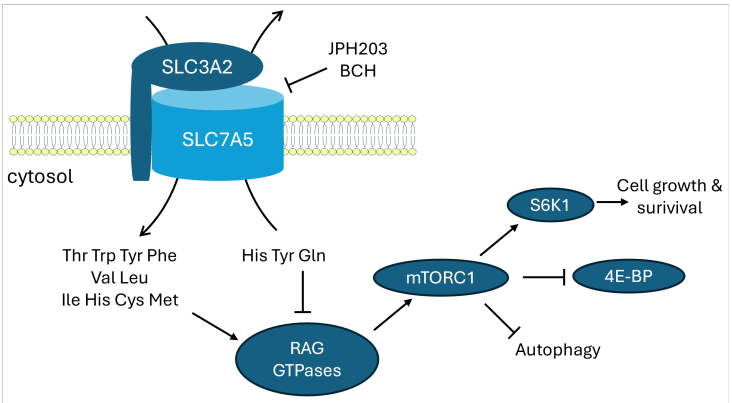

Supp. Figure 9. Function and structure of CD98 transporter.

CD98 is a heterodimeric transmembrane amino acid transporter that preferentially uptake large neutral amino acids. The transporter comprises of SLC3A2 (heavy chain) and SLC7A5 (light chain). With continuous amino acid uptake, mTOR signaling pathway will be triggered to regulate autophagy, protein synthesis and cell growth.

10. Abbreviations

AA	Amino acid
ACT	Adoptive cell transfer
AML	Acute myeloid leukemia
ANOVA	Analysis of variance
APC	Antigen-presenting cell
AUC	Area-under-curve
BAGEL	Bayesian analysis of gene essentiality
BF	Bayes factor
CAR	Chimeric antigen receptor
CI	Confidence interval
CRISPR	Clustered regularly interspaced short palindromic repeats
CTRL	Control
DcR1	Decoy receptor 1
DcR2	Decoy receptor 2
E:T	Effector to target
ECL	Enhanced chemiluminescence
ER	Endoplasmic reticulum
ERAPs	Aminopeptidases
FACS	Fluorescence-activated cell sorting
FBS	Fetal bovine serum
FDA	Food and Drug Administration
FDR	False discovery rate
FPKM	Fragments per kilobase million
GD	γδ
GO	Gene ontology
HLA	Human leukocyte antigen
ICB	Immune checkpoint blocker
IFN	Interferon
IFNGR	Interferon-γ receptor
IP	Inositol phosphate
KO	Knockout
LNAA	Large neutral amino acids
LOF	Loss-of-function
log2FC	Log_2 fold-change
MHC	Major histocompatibility complex
MOI	Multiplicity of infection
NGS	Next-generation sequencing
NK	Natural killer
OPG	Osteoprotegerin
OS	Overall survival
OXPHOS	Oxidative phosphorylation
PBMCs	Peripheral blood mononuclear cells
PCA	Principal component analysis
PCR	Polymerase chain reaction

PR	Precision-recall
PURO	Puromycin
R	Pearson correlation coefficient
ROS	Reactive oxygen species
sd	Standard deviation
sgRNA	Single-guide RNA
shRNA	Short hairpin
T0	Time zero
TCGA	Cancer genome atlas program
TCR	T cell receptor
TIL	Tumor-infiltrating lymphocyte
TMB	Tumor mutational burden
TME	Tumor microenvironment
TRAIL-R1	TRAIL receptor 1
TRAIL-R2	TRAIL receptor 2
WT	Wild type

11. List of figures

12. List of tables

13. Acknowledgments

I would like to begin by expressing my deepest and most sincere gratitude to everyone who has guided and supported me throughout this journey. Completing this dissertation has been one of the most challenging and rewarding experiences of my life, and it would not have been possible without the unwavering encouragement, patience, and kindness of so many people who stood by me through the inevitable ups and downs.

My foremost gratitude belongs to my primary supervisor, Michael Boutros, for his invaluable guidance, endless patience, and unwavering support throughout the course of this dissertation. His insightful advice and critical feedback have been instrumental in shaping my research and my development as a scientist. I am deeply grateful for the opportunities, resources, and freedom he provided, without which this work would not have been possible.

I am equally thankful to my TAC members and co-supervisors, Aurelio Teleman and Adelheid Cerwenka, for generously sharing their expertise and for their invaluable suggestions that have enriched my work in so many ways. Their support and perspective have broadened my scientific horizons immeasurably.

I wish to acknowledge RTG2099 for their initial financial support, as well as for the inspiring opportunities to visit London, where I could connect with leading melanoma researchers and strengthen my network in this field.

My heartfelt thanks go to Florian Heigwer and Kim Boonekamp, whose unconditional support and wise counsel were constant sources of strength throughout my PhD. They are always there through highs and lows, ready with encouragement, guidance on project direction, and their extensive knowledge in bioinformatics and systems biology. I simply could not have navigated the countless challenges without them.

Many wonderful collaborations have shaped this dissertation into something greater than I could have achieved alone. I am grateful to Tianzuo Zhan, Tomáš Hofman, De-en

Sun, and Helen Stark who brought fresh ideas, different perspectives, and helped put our scientific tools to good use.

Overcoming hurdles along the way would not have been possible without the generosity and expertise of many others. I would like to thank Tomáš Hofman once more for sharing his deep knowledge of immunology, which greatly helped with experimental design. My sincere thanks also go to Dominique Kranz for her advice on TRAIL signaling experiments and Luisa Henkel for passing on her expertise on the Heidelberg CRISPR sgRNA library. I deeply appreciate the invaluable organizational support from Ulrike Hardeland, Felicitas Olschowsky, Angelika Manz, and Caroline, as well as the exceptional technical assistance from Barbara Schmitt, Thilo Miersch, Svenja Leible, David Ibberson, Claudia Blaß, for the exceptional technical support. I am thankful to Erica Valentini and Jan Gerwin whose IT support always came to the rescue just when needed. I would like to extend my thanks to the DKFZ Core Facilities, specifically the microscopy, flow cytometry, and NGS Core Facilities. All these professional support I received have elevated the quality of my research and provided momentum that kept my work moving forward.

I also want thank my brilliant and supportive colleagues - Fillip Port, Jan Michaela Holzem, Antonia Schubert, Bojana Pavlovic, Christian Scheeder, Christian Galata, Alena Ivanova, Giulia Ambrosi, Diego Aponte, Jun Zhou, Jan Gleixner, Katharina Imkeller, Siamak Redhai, Shiv Bahuguna, Javed Iqbal, Vaishali Grewal, Pradhipa Manivannan, Cornelia Redel-Smirnov, Oksana Voloshanenko, Alessio Falzone, Leo Bamberg, Christian Maercker, Martina Zowada, Büsra Kocamese, Philipp Albrecht, Lucrezia Tondo, Saskia Reuter, Tianyu Wang, Nadine Winkler, Mona Stricker, Claudia Strein, Revekka Dimou, Ralitsa Karadzhova, Zhenchong Li - thank you for creating a warm, supportive atmosphere filled with meaningful conversations and laughters that made every day in the lab so much brighter.

Last, but certainly never least, I owe my deepest gratitude to my family and friends for their unconditional love, constant patience, and unwavering belief in me. Their

encouragement has carried me through the toughest days and reminded me of what truly matters. I am endlessly grateful to have you by my side.

14. Reference

Abizanda-Campo, S., Virumbrales-Muñoz, M., Humayun, M., Marmol, I., Beebe, D. J., Ochoa, I., Oliván, S., & Ayuso, J. M. (2023). Microphysiological systems for solid tumor immunotherapy: Opportunities and challenges. *Microsystems & Nanoengineering*, *9*(1), 1–30. https://doi.org/10.1038/s41378-023-00616-x

Aggarwal, P., Knabel, P., & Fleischer, A. B. (2021). United States burden of melanoma and non-melanoma skin cancer from 1990 to 2019. *Journal of the American Academy of Dermatology*, *85*(2), 388–395. https://doi.org/10.1016/j.jaad.2021.03.109

Ahn, E., Araki, K., Hashimoto, M., Li, W., Riley, J. L., Cheung, J., Sharpe, A. H., Freeman, G. J., Irving, B. A., & Ahmed, R. (2018). Role of PD-1 during effector CD8 T cell differentiation. *Proceedings of the National Academy of Sciences*, *115*(18), 4749–4754. https://doi.org/10.1073/pnas.1718217115

Alberts, B., Johnson, A., Lewis, J., Raff, M., Roberts, K., & Walter, P. (2007). The Adaptive Immune System. In *Molecular Biology of the Cell* (5th ed.). W.W. Norton & Company.

Alduaij, W., Ivanov, A., Honeychurch, J., Cheadle, E. J., Potluri, S., Lim, S. H., Shimada, K., Chan, C. H. T., Tutt, A., Beers, S. A., Glennie, M. J., Cragg, M. S., & Illidge, T. M. (2011). Novel type II anti-CD20 monoclonal antibody (GA101) evokes homotypic adhesion and actin-dependent, lysosome-mediated cell death in B-cell malignancies. *Blood*, *117*(17), 4519–4529. https://doi.org/10.1182/blood-2010-07-296913

Ashburner, M., Ball, C. A., Blake, J. A., Botstein, D., Butler, H., Cherry, J. M., Davis, A. P., Dolinski, K., Dwight, S. S., Eppig, J. T., Harris, M. A., Hill, D. P., Issel-Tarver, L., Kasarskis, A., Lewis, S., Matese, J. C., Richardson, J. E., Ringwald, M., Rubin, G. M., & Sherlock, G. (2000). Gene Ontology: Tool for the unification of biology. *Nature Genetics*, *25*(1), 25–29. https://doi.org/10.1038/75556

Badovinac, V. P., Tvinnereim, A. R., & Harty, J. T. (2000). Regulation of Antigen-Specific CD8+ T Cell Homeostasis by Perforin and Interferon-γ. *Science*, *290*(5495), 1354–1357. https://doi.org/10.1126/science.290.5495.1354

Bellail, A. C., Olson, J. J., Yang, X., Chen, Z. J., & Hao, C. (2012). A20 Ubiquitin Ligase–Mediated Polyubiquitination of RIP1 Inhibits Caspase-8 Cleavage and TRAIL-Induced Apoptosis in Glioblastoma. *Cancer Discovery*, *2*(2), 140–155. https://doi.org/10.1158/2159-8290.CD-11-0172

Berraondo, P., Sanmamed, M. F., Ochoa, M. C., Etxeberria, I., Aznar, M. A., Pérez-Gracia, J. L., Rodríguez-Ruiz, M. E., Ponz-Sarvise, M., Castañón, E., & Melero, I. (2019). Cytokines in clinical cancer immunotherapy. *British Journal of Cancer*, *120*(1), 6–15. https://doi.org/10.1038/s41416-018-0328-y

Besser, M. J., Shapira-Frommer, R., Treves, A. J., Zippel, D., Itzhaki, O., Hershkovitz, L., Levy, D., Kubi, A., Hovav, E., Chermoshniuk, N., Shalmon, B., Hardan, I., Catane, R., Markel, G., Apter, S., Ben-Nun, A., Kuchuk, I., Shimoni, A., Nagler, A., & Schachter, J. (2010). Clinical responses in a phase II study using adoptive transfer of short-term cultured tumor infiltration lymphocytes in metastatic melanoma patients. *Clinical Cancer Research: An Official Journal of the American Association for Cancer Research*, *16*(9), 2646–2655. https://doi.org/10.1158/1078-0432.CCR-10-0041

Betts, M. R., & Koup, R. A. (2004). Detection of T-Cell Degranulation: CD107a and b. In *Methods in Cell Biology* (Vol. 75, pp. 497–512). Academic Press. https://doi.org/10.1016/S0091-679X(04)75020-7

Bhat, P., Leggatt, G., Waterhouse, N., & Frazer, I. H. (2017). Interferon-γ derived from cytotoxic lymphocytes directly enhances their motility and cytotoxicity. *Cell Death & Disease*, *8*(6), e2836–e2836. https://doi.org/10.1038/cddis.2017.67

Biswas, S. K. (2015). Metabolic Reprogramming of Immune Cells in Cancer Progression. *Immunity*, *43*(3), 435–449. https://doi.org/10.1016/j.immuni.2015.09.001

Boucher, M. J., Morisset, J., Vachon, P. H., Reed, J. C., Lainé, J., & Rivard, N. (2000). MEK/ERK signaling pathway regulates the expression of Bcl-2, Bcl-X(L), and Mcl-1 and promotes survival of human pancreatic cancer cells. *Journal of Cellular Biochemistry*, *79*(3), 355–369. https://doi.org/10.1002/1097-4644(20001201)79:3<355::aid-jcb20>3.0.co;2-0

Braendstrup, P., Levine, B. L., & Ruella, M. (2020). The Long Road to the First FDA Approved Gene Therapy: Chimeric Antigen Receptor T Cells Targeting CD19. *Cytotherapy*, *22*(2), 57–69. https://doi.org/10.1016/j.jcyt.2019.12.004

Bristol-Myers Squibb. (2021). *A Phase 3, Randomized Study of Adjuvant Immunotherapy With Nivolumab Combined With Ipilimumab Versus Nivolumab Monotherapy After Complete Resection of Stage IIIb/c/d or Stage IV Melanoma* (Clinical Trial Registration No. NCT03068455). clinicaltrials.gov. https://clinicaltrials.gov/study/NCT03068455

Bristol-Myers Squibb. (2024). *A Randomized, Multicenter, Open-Label, Phase 3 Study of Nivolumab Plus Ipilimumab or Nivolumab in Combination With Oxaliplatin Plus Fluoropyrimidine Versus Oxaliplatin Plus Fluoropyrimidine in Subjects*

With Previously Untreated Advanced or Metastatic Gastric or Gastroesophageal Junction Cancer (Clinical Trial Registration No. NCT02872116). clinicaltrials.gov. https://clinicaltrials.gov/study/NCT02872116

Cappell, K. M., Sherry, R. M., Yang, J. C., Goff, S. L., Vanasse, D. A., McIntyre, L., Rosenberg, S. A., & Kochenderfer, J. N. (2020). Long-Term Follow-Up of Anti-CD19 Chimeric Antigen Receptor T-Cell Therapy. *Journal of Clinical Oncology*, *38*(32), 3805–3815. https://doi.org/10.1200/JCO.20.01467

Cemerski, S., Cantagrel, A., Meerwijk, J. P. M. van, & Romagnoli, P. (2002). Reactive Oxygen Species Differentially Affect T Cell Receptor-signaling Pathways*. *Journal of Biological Chemistry*, *277*(22), 19585–19593. https://doi.org/10.1074/jbc.M111451200

Ceolin, V., Brivio, E., van Tinteren, H., Rheingold, S. R., Leahy, A., Vormoor, B., O'Brien, M. M., Rubinstein, J. D., Kalwak, K., De Moerloose, B., Jacoby, E., Bader, P., López-Duarte, M., Goemans, B. F., Locatelli, F., Hoogerbrugge, P., Calkoen, F. G., & Zwaan, C. M. (2023). Outcome of chimeric antigen receptor T-cell therapy following treatment with inotuzumab ozogamicin in children with relapsed or refractory acute lymphoblastic leukemia. *Leukemia*, *37*(1), 53–60. https://doi.org/10.1038/s41375-022-01740-9

Cerami, E., Gao, J., Dogrusoz, U., Gross, B. E., Sumer, S. O., Aksoy, B. A., Jacobsen, A., Byrne, C. J., Heuer, M. L., Larsson, E., Antipin, Y., Reva, B., Goldberg, A. P., Sander, C., & Schultz, N. (2012). The cBio Cancer Genomics Portal: An Open Platform for Exploring Multidimensional Cancer Genomics Data. *Cancer Discovery*, *2*(5), 401–404. https://doi.org/10.1158/2159-8290.CD-12-0095

Chalmers, Z. R., Connelly, C. F., Fabrizio, D., Gay, L., Ali, S. M., Ennis, R., Schrock, A., Campbell, B., Shlien, A., Chmielecki, J., Huang, F., He, Y., Sun, J., Tabori, U., Kennedy, M., Lieber, D. S., Roels, S., White, J., Otto, G. A., … Frampton, G. M. (2017). Analysis of 100,000 human cancer genomes reveals the landscape of tumor mutational burden. *Genome Medicine*, *9*(1), 34. https://doi.org/10.1186/s13073-017-0424-2

Chaudhary, P. M., Eby, M., Jasmin, A., Bookwalter, A., Murray, J., & Hood, L. (1997). Death Receptor 5, a New Member of the TNFR Family, and DR4 Induce FADD-Dependent Apoptosis and Activate the NF-κB Pathway. *Immunity*, *7*(6), 821–830. https://doi.org/10.1016/S1074-7613(00)80400-8

Chinnaiyan, A. M., O'Rourke, K., Tewari, M., & Dixit, V. M. (1995). FADD, a novel death domain-containing protein, interacts with the death domain of fas and initiates apoptosis. *Cell*, *81*(4), 505–512. https://doi.org/10.1016/0092-8674(95)90071-3

Chulanov, V., Kostyusheva, A., Brezgin, S., Ponomareva, N., Gegechkori, V., Volchkova, E., Pimenov, N., & Kostyushev, D. (2021). CRISPR Screening: Molecular Tools for Studying Virus–Host Interactions. *Viruses*, *13*(11), Article 11. https://doi.org/10.3390/v13112258

Clement, L. T. (1992). Isoforms of the CD45 common leukocyte antigen family: Markers for human T-cell differentiation. *Journal of Clinical Immunology*, *12*(1), 1–10. https://doi.org/10.1007/BF00918266

Crespo, J., Sun, H., Welling, T. H., Tian, Z., & Zou, W. (2013). T cell anergy, exhaustion, senescence, and stemness in the tumor microenvironment. *Current Opinion in Immunology*, *25*(2), 214–221. https://doi.org/10.1016/j.coi.2012.12.003

Curtsinger, J. M., Agarwal, P., Lins, D. C., & Mescher, M. F. (2012). Autocrine IFN-γ Promotes Naive CD8 T Cell Differentiation and Synergizes with IFN-α To Stimulate Strong Function. *The Journal of Immunology*, *189*(2), 659–668. https://doi.org/10.4049/jimmunol.1102727

D'Angelo, S. P., Araujo, D. M., Razak, A. R. A., Agulnik, M., Attia, S., Blay, J.-Y., Garcia, I. C., Charlson, J. A., Choy, E., Demetri, G. D., Druta, M., Forcade, E., Ganjoo, K. N., Glod, J., Keedy, V. L., Cesne, A. L., Liebner, D. A., Moreno, V., Pollack, S. M., … Tine, B. A. V. (2024). Afamitresgene autoleucel for advanced synovial sarcoma and myxoid round cell liposarcoma (SPEARHEAD-1): An international, open-label, phase 2 trial. *The Lancet*, *403*(10435), 1460–1471. https://doi.org/10.1016/S0140-6736(24)00319-2

de Bruijn, I., Kundra, R., Mastrogiacomo, B., Tran, T. N., Sikina, L., Mazor, T., Li, X., Ochoa, A., Zhao, G., Lai, B., Abeshouse, A., Baiceanu, D., Ciftci, E., Dogrusoz, U., Dufilie, A., Erkoc, Z., Garcia Lara, E., Fu, Z., Gross, B., … Schultz, N. (2023). Analysis and Visualization of Longitudinal Genomic and Clinical Data from the AACR Project GENIE Biopharma Collaborative in cBioPortal. *Cancer Research*, *83*(23), 3861–3867. https://doi.org/10.1158/0008-5472.CAN-23-0816

DepMap, B. (2023). *DepMap 23Q4 Public* (p. 21888030738 Bytes) [Dataset]. Figshare+. https://doi.org/10.25452/FIGSHARE.PLUS.24667905.V2

Dufour, F., Rattier, T., Shirley, S., Picarda, G., Constantinescu, A. A., Morlé, A., Zakaria, A. B., Marcion, G., Causse, S., Szegezdi, E., Zajonc, D. M., Seigneuric, R., Guichard, G., Gharbi, T., Picaud, F., Herlem, G., Garrido, C., Schneider, P., Benedict, C. A., & Micheau, O. (2017). N-glycosylation of mouse TRAIL-R and human TRAIL-R1 enhances TRAIL-induced death. *Cell Death & Differentiation*, *24*(3), 500–510. https://doi.org/10.1038/cdd.2016.150

Duggan, M. C., Jochems, C., Donahue, R. N., Richards, J., Karpa, V., Foust, E., Paul, B., Brooks, T., Tridandapani, S., Olencki, T., Pan, X., Lesinski, G. B., Schlom, J., & Carson III, W. E. (2016). A phase I study of recombinant (r) vaccinia-CEA(6D)-TRICOM and rFowlpox-CEA(6D)-TRICOM vaccines with GM-CSF and IFN-α-2b in patients with CEA-expressing carcinomas. *Cancer Immunology, Immunotherapy*, *65*(11), 1353–1364. https://doi.org/10.1007/s00262-016-1893-7

Fagerberg, L., Hallström, B. M., Oksvold, P., Kampf, C., Djureinovic, D., Odeberg, J., Habuka, M., Tahmasebpoor, S., Danielsson, A., Edlund, K., Asplund, A., Sjöstedt, E., Lundberg, E., Szigyarto, C. A.-K., Skogs, M., Takanen, J. O., Berling, H., Tegel, H., Mulder, J., … Uhlén, M. (2014). Analysis of the Human Tissue-specific Expression by Genome-wide Integration of Transcriptomics and Antibody-based Proteomics*. *Molecular & Cellular Proteomics*, *13*(2), 397–406. https://doi.org/10.1074/mcp.M113.035600

Feng, X., Yang, C., Huang, Y., Su, D., Wang, C., Wilson, L. L., Yin, L., Tang, M., Li, S., Chen, Z., Zhu, D., Wang, S., Zhang, S., Zhang, J., Zhang, H., Nie, L., Huang, M., Park, J.-I., Hart, T., … Chen, J. (2024). In vivo CRISPR screens identify Mga as an immunotherapy target in triple-negative breast cancer. *Proceedings of the National Academy of Sciences*, *121*(39), e2406325121. https://doi.org/10.1073/pnas.2406325121

Franco, A. V., Zhang, X. D., Van Berkel, E., Sanders, J. E., Zhang, X. Y., Thomas, W. D., Nguyen, T., & Hersey, P. (2001). The Role of NF-κB in TNF-Related Apoptosis-Inducing Ligand (TRAIL)-Induced Apoptosis of Melanoma Cells1. *The Journal of Immunology*, *166*(9), 5337–5345. https://doi.org/10.4049/jimmunol.166.9.5337

Gao, J., Aksoy, B. A., Dogrusoz, U., Dresdner, G., Gross, B., Sumer, S. O., Sun, Y., Jacobsen, A., Sinha, R., Larsson, E., Cerami, E., Sander, C., & Schultz, N. (2013). Integrative Analysis of Complex Cancer Genomics and Clinical Profiles Using the cBioPortal. *Science Signaling*, *6*(269), pl1–pl1. https://doi.org/10.1126/scisignal.2004088

Geldres, C., Savoldo, B., Hoyos, V., Caruana, I., Zhang, M., Yvon, E., Del Vecchio, M., Creighton, C. J., Ittmann, M., Ferrone, S., & Dotti, G. (2014). T Lymphocytes Redirected against the Chondroitin Sulfate Proteoglycan-4 Control the Growth of Multiple Solid Tumors both In Vitro and In Vivo. *Clinical Cancer Research*, *20*(4), 962–971. https://doi.org/10.1158/1078-0432.CCR-13-2218

Ginaldi, L., Martinis, M. D., Matutes, E., Farahat, N., Morilla, R., & Catovsky, D. (1998). Levels of expression of CD19 and CD20 in chronic B cell leukaemias. *Journal of Clinical Pathology*, *51*(5), 364–369. https://doi.org/10.1136/jcp.51.5.364

Griss, J., Viteri, G., Sidiropoulos, K., Nguyen, V., Fabregat, A., & Hermjakob, H. (2020). ReactomeGSA - Efficient Multi-Omics Comparative Pathway Analysis. *Molecular & Cellular Proteomics*, *19*(12), 2115–2125. https://doi.org/10.1074/mcp.TIR120.002155

Groettrup, M., Kirk, C. J., & Basler, M. (2010). Proteasomes in immune cells: More than peptide producers? *Nature Reviews Immunology*, *10*(1), 73–78. https://doi.org/10.1038/nri2687

Harlin, H., Meng, Y., Peterson, A. C., Zha, Y., Tretiakova, M., Slingluff, C., McKee, M., & Gajewski, T. F. (2009). Chemokine Expression in Melanoma Metastases Associated with CD8+ T-Cell Recruitment. *Cancer Research*, *69*(7), 10.1158/0008-5472.CAN-08–2281. https://doi.org/10.1158/0008-5472.CAN-08-2281

Hart, T., Brown, K. R., Sircoulomb, F., Rottapel, R., & Moffat, J. (2014). Measuring error rates in genomic perturbation screens: Gold standards for human functional genomics. *Molecular Systems Biology*, *10*(7), 733. https://doi.org/10.15252/msb.20145216

Hart, T., Chandrashekhar, M., Aregger, M., Steinhart, Z., Brown, K. R., MacLeod, G., Mis, M., Zimmermann, M., Fradet-Turcotte, A., Sun, S., Mero, P., Dirks, P., Sidhu, S., Roth, F. P., Rissland, O. S., Durocher, D., Angers, S., & Moffat, J. (2015). High-Resolution CRISPR Screens Reveal Fitness Genes and Genotype-Specific Cancer Liabilities. *Cell*, *163*(6), 1515–1526. https://doi.org/10.1016/j.cell.2015.11.015

Hart, T., & Moffat, J. (2016). BAGEL: A computational framework for identifying essential genes from pooled library screens. *BMC Bioinformatics*, *17*(1), 164. https://doi.org/10.1186/s12859-016-1015-8

Hayes, G. M., Chinn, L., Cantor, J. M., Cairns, B., Levashova, Z., Tran, H., Velilla, T., Duey, D., Lippincott, J., Zachwieja, J., Ginsberg, M. H., & H. van der Horst, E. (2015). Antitumor activity of an anti-CD98 antibody. *International Journal of Cancer*, *137*(3), 710–720. https://doi.org/10.1002/ijc.29415

Hellwig, C. T., Delgado, M. E., Skoko, J., Dyck, L., Hanna, C., Wentges, A., Langlais, C., Hagenlocher, C., Mack, A., Dinsdale, D., Cain, K., MacFarlane, M., & Rehm, M. (2022). Proteasome inhibition triggers the formation of TRAIL receptor 2 platforms for caspase-8 activation that accumulate in the cytosol. *Cell Death & Differentiation*, *29*(1), 147–155. https://doi.org/10.1038/s41418-021-00843-7

Henkel, L., Rauscher, B., Schmitt, B., Winter, J., & Boutros, M. (2020). Genome-scale CRISPR screening at high sensitivity with an empirically designed sgRNA library. *BMC Biology*, *18*(1), 174. https://doi.org/10.1186/s12915-020-00905-1

Hirayama, A. V., Gauthier, J., Hay, K. A., Voutsinas, J. M., Wu, Q., Pender, B. S., Hawkins, R. M., Vakil, A., Steinmetz, R. N., Riddell, S. R., Maloney, D. G., & Turtle, C. J. (2019). High rate of durable complete remission in follicular lymphoma after CD19 CAR-T cell immunotherapy. *Blood*, *134*(7), 636–640. https://doi.org/10.1182/blood.2019000905

Hou, B., Tang, Y., Li, W., Zeng, Q., & Chang, D. (2019). Efficiency of CAR-T Therapy for Treatment of Solid Tumor in Clinical Trials: A Meta-Analysis. *Disease Markers*, *2019*(1), 3425291. https://doi.org/10.1155/2019/3425291

Hu, W.-H., Johnson, H., & Shu, H.-B. (1999). Tumor Necrosis Factor-related Apoptosis-inducing Ligand Receptors Signal NF-κB and JNK Activation and Apoptosis through Distinct Pathways *. *Journal of Biological Chemistry*, *274*(43), 30603–30610. https://doi.org/10.1074/jbc.274.43.30603

Huang, D. W., Sherman, B. T., & Lempicki, R. A. (2009). Systematic and integrative analysis of large gene lists using DAVID bioinformatics resources. *Nature Protocols*, *4*(1), 44–57. https://doi.org/10.1038/nprot.2008.211

Hudecek, M., Lupo-Stanghellini, M.-T., Kosasih, P. L., Sommermeyer, D., Jensen, M. C., Rader, C., & Riddell, S. R. (2013). Receptor Affinity and Extracellular Domain Modifications Affect Tumor Recognition by ROR1-Specific Chimeric Antigen Receptor T Cells. *Clinical Cancer Research*, *19*(12), 3153–3164. https://doi.org/10.1158/1078-0432.CCR-13-0330

Incyte Corporation. (2022). *A Phase 2, Randomized, Double-Blind Study of Pembrolizumab (MK-3475) Plus Epacadostat (INCB024360) Versus Pembrolizumab Plus Placebo as First-Line Treatment in Patients With Metastatic Non-Small Cell Lung Cancer Expressing High Levels of PD-L1* (Clinical Trial Registration No. NCT03322540). clinicaltrials.gov. https://clinicaltrials.gov/study/NCT03322540

Irmler, M., Thome, M., Hahne, M., Schneider, P., Hofmann, K., Steiner, V., Bodmer, J.-L., Schröter, M., Burns, K., Mattmann, C., Rimoldi, D., French, L. E., & Tschopp, J. (1997). Inhibition of death receptor signals by cellular FLIP. *Nature*, *388*(6638), 190–195. https://doi.org/10.1038/40657

Ishizuka, J. J., Manguso, R. T., Cheruiyot, C. K., Bi, K., Panda, A., Iracheta-Vellve, A., Miller, B. C., Du, P. P., Yates, K. B., Dubrot, J., Buchumenski, I., Comstock, D. E., Brown, F. D., Ayer, A., Kohnle, I. C., Pope, H. W., Zimmer, M. D., Sen, D. R., Lane-Reticker, S. K., … Haining, W. N. (2019). Loss of ADAR1 in tumours overcomes resistance to immune checkpoint blockade. *Nature*, *565*(7737), 43–48. https://doi.org/10.1038/s41586-018-0768-9

Jeremias, I., Kupatt, C., Baumann, B., Herr, I., Wirth, T., & Debatin, K. M. (1998). Inhibition of Nuclear Factor κB Activation Attenuates Apoptosis Resistance in Lymphoid Cells. *Blood*, *91*(12), 4624–4631. https://doi.org/10.1182/blood.V91.12.4624

Johnson, L. A., Morgan, R. A., Dudley, M. E., Cassard, L., Yang, J. C., Hughes, M. S., Kammula, U. S., Royal, R. E., Sherry, R. M., Wunderlich, J. R., Lee, C.-C. R., Restifo, N. P., Schwarz, S. L., Cogdill, A. P., Bishop, R. J., Kim, H., Brewer, C. C., Rudy, S. F., VanWaes, C., … Rosenberg, S. A. (2009). Gene therapy with human and mouse T-cell receptors mediates cancer regression and targets normal tissues expressing cognate antigen. *Blood*, *114*(3), 535–546. https://doi.org/10.1182/blood-2009-03-211714

Jost, P. J., Grabow, S., Gray, D., McKenzie, M. D., Nachbur, U., Huang, D. C. S., Bouillet, P., Thomas, H. E., Borner, C., Silke, J., Strasser, A., & Kaufmann, T. (2009). XIAP discriminates between type I and type II FAS-induced apoptosis. *Nature*, *460*(7258), 1035–1039. https://doi.org/10.1038/nature08229

Kaech, S. M., & Cui, W. (2012). Transcriptional control of effector and memory CD8+ T cell differentiation. *Nature Reviews Immunology*, *12*(11), 749–761. https://doi.org/10.1038/nri3307

Kamiński, M. M., Sauer, S. W., Kamiński, M., Opp, S., Ruppert, T., Grigaravičius, P., Grudnik, P., Gröne, H.-J., Krammer, P. H., & Gülow, K. (2012). T cell Activation Is Driven by an ADP-Dependent Glucokinase Linking Enhanced Glycolysis with Mitochondrial Reactive Oxygen Species Generation. *Cell Reports*, *2*(5), 1300–1315. https://doi.org/10.1016/j.celrep.2012.10.009

Kanehisa, M. (2019). Toward understanding the origin and evolution of cellular organisms. *Protein Science*, *28*(11), 1947–1951. https://doi.org/10.1002/pro.3715

Karbowniczek, M., Spittle, C. S., Morrison, T., Wu, H., & Henske, E. P. (2008). mTOR Is Activated in the Majority of Malignant Melanomas. *Journal of Investigative Dermatology*, *128*(4), 980–987. https://doi.org/10.1038/sj.jid.5701074

Karin, M., & Greten, F. R. (2005). NF-κB: Linking inflammation and immunity to cancer development and progression. *Nature Reviews Immunology*, *5*(10), 749–759. https://doi.org/10.1038/nri1703

Kawai, T., & Akira, S. (2007). Signaling to NF-κB by Toll-like receptors. *Trends in Molecular Medicine*, *13*(11), 460–469. https://doi.org/10.1016/j.molmed.2007.09.002

Kenderian, S. S., Ruella, M., Shestova, O., Klichinsky, M., Aikawa, V., Morrissette, J. J. D., Scholler, J., Song, D., Porter, D. L., Carroll, M., June, C. H., & Gill, S. (2015). CD33-specific chimeric antigen receptor T cells exhibit potent preclinical activity against human acute myeloid leukemia. *Leukemia*, *29*(8), 1637–1647. https://doi.org/10.1038/leu.2015.52

Khoshnan, A., Tindell, C., Laux, I., Bae, D., Bennett, B., & Nel, A. E. (2000). The NF-κB Cascade Is Important in Bcl-xL Expression and for the Anti-Apoptotic Effects of the CD28 Receptor in Primary Human CD4+ Lymphocytes1. *The Journal of Immunology*, *165*(4), 1743–1754. https://doi.org/10.4049/jimmunol.165.4.1743

Kingwell, K. (2017). CAR T therapies drive into new terrain. *Nature Reviews Drug Discovery*, *16*(5), 301–304. https://doi.org/10.1038/nrd.2017.84

Kleppe, M., Lahortiga, I., El Chaar, T., De Keersmaecker, K., Mentens, N., Graux, C., Van Roosbroeck, K., Ferrando, A. A., Langerak, A. W., Meijerink, J. P. P., Sigaux, F., Haferlach, T., Wlodarska, I., Vandenberghe, P., Soulier, J., & Cools, J. (2010). Deletion of the protein tyrosine phosphatase gene PTPN2 in T-cell acute lymphoblastic leukemia. *Nature Genetics*, *42*(6), 530–535. https://doi.org/10.1038/ng.587

Kleppe, M., Soulier, J., Asnafi, V., Mentens, N., Hornakova, T., Knoops, L., Constantinescu, S., Sigaux, F., Meijerink, J. P., Vandenberghe, P., Tartaglia, M., Foa, R., Macintyre, E., Haferlach, T., & Cools, J. (2011). PTPN2 negatively regulates oncogenic JAK1 in T-cell acute lymphoblastic leukemia. *Blood*, *117*(26), 7090–7098. https://doi.org/10.1182/blood-2010-10-314286

Kochenderfer, J. N., Dudley, M. E., Feldman, S. A., Wilson, W. H., Spaner, D. E., Maric, I., Stetler-Stevenson, M., Phan, G. Q., Hughes, M. S., Sherry, R. M., Yang, J. C., Kammula, U. S., Devillier, L., Carpenter, R., Nathan, D.-A. N., Morgan, R. A., Laurencot, C., & Rosenberg, S. A. (2012). B-cell depletion and remissions of malignancy along with cytokine-associated toxicity in a clinical trial of anti-CD19 chimeric-antigen-receptor–transduced T cells. *Blood*, *119*(12), 2709–2720. https://doi.org/10.1182/blood-2011-10-384388

Kreutmair, S., Pfeifer, D., Waterhouse, M., Takács, F., Graessel, L., Döhner, K., Duyster, J., Illert, A. L., Frey, A.-V., Schmitt, M., & Lübbert, M. (2022). First-in-human study of WT1 recombinant protein vaccination in elderly patients with AML in remission: A single-center experience. *Cancer Immunology, Immunotherapy : CII*, *71*(12), 2913–2928. https://doi.org/10.1007/s00262-022-03202-8

Krummel, M. F., & Allison, J. P. (1995). CD28 and CTLA-4 have opposing effects on the response of T cells to stimulation. *Journal of Experimental Medicine*, *182*(2), 459–465. https://doi.org/10.1084/jem.182.2.459

Lane-Reticker, S. K., Kessler, E. A., Muscato, A. J., Kim, S. Y., Doench, J. G., Yates, K. B., Manguso, R. T., & Dubrot, J. (2023). Protocol for *in vivo* CRISPR screening using selective CRISPR antigen removal lentiviral vectors. *STAR Protocols*, *4*(1), 102082. https://doi.org/10.1016/j.xpro.2023.102082

Larkin, J., Chiarion-Sileni, V., Gonzalez, R., Grob, J.-J., Rutkowski, P., Lao, C. D., Cowey, C. L., Schadendorf, D., Wagstaff, J., Dummer, R., Ferrucci, P. F., Smylie, M., Hogg, D., Hill, A., Márquez-Rodas, I., Haanen, J., Guidoboni, M., Maio, M., Schöffski, P., … Wolchok, J. D. (2019). Five-Year Survival with Combined Nivolumab and Ipilimumab in Advanced Melanoma. *New England Journal of Medicine*, *381*(16), 1535–1546. https://doi.org/10.1056/NEJMoa1910836

Lawson, K. A., Sousa, C. M., Zhang, X., Kim, E., Akthar, R., Caumanns, J. J., Yao, Y., Mikolajewicz, N., Ross, C., Brown, K. R., Zid, A. A., Fan, Z. P., Hui, S., Krall, J. A., Simons, D. M., Slater, C. J., De Jesus, V., Tang, L., Singh, R., … Moffat, J. (2020). Functional genomic landscape of cancer-intrinsic evasion of killing by T cells. *Nature*, *586*(7827), 120–126. https://doi.org/10.1038/s41586-020-2746-2

Lennerz, V., Fatho, M., Gentilini, C., Frye, R. A., Lifke, A., Ferel, D., Wölfel, C., Huber, C., & Wölfel, T. (2005). The response of autologous T cells to a human melanoma is dominated by mutated neoantigens. *Proceedings of the National Academy of Sciences*, *102*(44), 16013–16018. https://doi.org/10.1073/pnas.0500090102

Li, W., Xu, H., Xiao, T., Cong, L., Love, M. I., Zhang, F., Irizarry, R. A., Liu, J. S., Brown, M., & Liu, X. S. (2014). MAGeCK enables robust identification of essential genes from genome-scale CRISPR/Cas9 knockout screens. *Genome Biology*, *15*(12), 554. https://doi.org/10.1186/s13059-014-0554-4

Liu, D., Schilling, B., Liu, D., Sucker, A., Livingstone, E., Jerby-Arnon, L., Zimmer, L., Gutzmer, R., Satzger, I., Loquai, C., Grabbe, S., Vokes, N., Margolis, C. A., Conway, J., He, M. X., Elmarakeby, H., Dietlein, F., Miao, D., Tracy, A., … Schadendorf, D. (2019). Integrative molecular and clinical modeling of clinical outcomes to PD1 blockade in patients with metastatic melanoma. *Nature Medicine*, *25*(12), 1916–1927. https://doi.org/10.1038/s41591-019-0654-5

Liu, T., Zhang, L., Joo, D., & Sun, S.-C. (2017). NF-κB signaling in inflammation. *Signal Transduction and Targeted Therapy*, *2*(1), 1–9. https://doi.org/10.1038/sigtrans.2017.23

Lizio, M., Abugessaisa, I., Noguchi, S., Kondo, A., Hasegawa, A., Hon, C. C., de Hoon, M., Severin, J., Oki, S., Hayashizaki, Y., Carninci, P., Kasukawa, T., & Kawaji, H. (2019). Update of the FANTOM web resource: Expansion to provide additional transcriptome atlases. *Nucleic Acids Research*, *47*(D1), D752–D758. https://doi.org/10.1093/nar/gky1099

Lonsdale, J., Thomas, J., Salvatore, M., Phillips, R., Lo, E., Shad, S., Hasz, R., Walters, G., Garcia, F., Young, N., Foster, B., Moser, M., Karasik, E., Gillard, B., Ramsey, K., Sullivan, S., Bridge, J., Magazine, H., Syron, J., … Moore, H. F. (2013). The Genotype-Tissue Expression (GTEx) project. *Nature Genetics*, *45*(6), 580–585. https://doi.org/10.1038/ng.2653

Luo, X., Budihardjo, I., Zou, H., Slaughter, C., & Wang, X. (1998). Bid, a Bcl2 Interacting Protein, Mediates Cytochrome c Release from Mitochondria in Response to Activation of Cell Surface Death Receptors. *Cell*, *94*(4), 481–490. https://doi.org/10.1016/S0092-8674(00)81589-5

Lupetti, R., Pisarra, P., Verrecchia, A., Farina, C., Nicolini, G., Anichini, A., Bordignon, C., Sensi, M., Parmiani, G., & Traversari, C. (1998). Translation of a Retained Intron in Tyrosinase-related Protein (TRP) 2 mRNA Generates a New Cytotoxic T Lymphocyte (CTL)-defined and Shared Human Melanoma Antigen Not Expressed in Normal Cells of the Melanocytic Lineage. *Journal of Experimental Medicine*, *188*(6), 1005–1016. https://doi.org/10.1084/jem.188.6.1005

Manguso, R. T., Pope, H. W., Zimmer, M. D., Brown, F. D., Yates, K. B., Miller, B. C., Collins, N. B., Bi, K., LaFleur, M. W., Juneja, V. R., Weiss, S. A., Lo, J., Fisher, D. E., Miao, D., Van Allen, E., Root, D. E., Sharpe, A. H., Doench, J. G., & Haining, W. N. (2017). In vivo CRISPR screening identifies Ptpn2 as a cancer immunotherapy target. *Nature*, *547*(7664), 413–418. https://doi.org/10.1038/nature23270

Marabelle, A., Fakih, M., Lopez, J., Shah, M., Shapira-Frommer, R., Nakagawa, K., Chung, H. C., Kindler, H. L., Lopez-Martin, J. A., Miller, W. H., Italiano, A., Kao, S., Piha-Paul, S. A., Delord, J.-P., McWilliams, R. R., Fabrizio, D. A., Aurora-Garg, D., Xu, L., Jin, F., … Bang, Y.-J. (2020). Association of tumour mutational burden with outcomes in patients with advanced solid tumours treated with pembrolizumab: Prospective biomarker analysis of the multicohort, open-label, phase 2 KEYNOTE-158 study. *The Lancet Oncology*, *21*(10), 1353–1365. https://doi.org/10.1016/S1470-2045(20)30445-9

Mayo, M. W., & Baldwin, A. S. (2000). The transcription factor NF-κB: Control of oncogenesis and cancer therapy resistance. *Biochimica et Biophysica Acta (BBA) - Reviews on Cancer*, *1470*(2), M55–M62. https://doi.org/10.1016/S0304-419X(00)00002-0

Monin, L., & Gaffen, S. L. (2018). Interleukin 17 Family Cytokines: Signaling Mechanisms, Biological Activities, and Therapeutic Implications. *Cold Spring Harbor Perspectives in Biology*, *10*(4), a028522. https://doi.org/10.1101/cshperspect.a028522

Mueller, S. N., & Mackay, L. K. (2016). Tissue-resident memory T cells: Local specialists in immune defence. *Nature Reviews Immunology*, *16*(2), 79–89. https://doi.org/10.1038/nri.2015.3

Mumm, J. B., Emmerich, J., Zhang, X., Chan, I., Wu, L., Mauze, S., Blaisdell, S., Basham, B., Dai, J., Grein, J., Sheppard, C., Hong, K., Cutler, C., Turner, S., LaFace, D., Kleinschek, M., Judo, M., Ayanoglu, G., Langowski, J., … Oft, M. (2011). IL-10 Elicits IFNγ-Dependent Tumor Immune Surveillance. *Cancer Cell*, *20*(6), 781–796. https://doi.org/10.1016/j.ccr.2011.11.003

Munshi, N. C., Anderson, L. D., Shah, N., Madduri, D., Berdeja, J., Lonial, S., Raje, N., Lin, Y., Siegel, D., Oriol, A., Moreau, P., Yakoub-Agha, I., Delforge, M., Cavo, M., Einsele, H., Goldschmidt, H., Weisel, K., Rambaldi, A., Reece, D., … San-Miguel, J. (2021). Idecabtagene Vicleucel in Relapsed and Refractory Multiple Myeloma. *New England Journal of Medicine*, *384*(8), 705–716. https://doi.org/10.1056/NEJMoa2024850

Nagaraj, S., Schrum, A. G., Cho, H.-I., Celis, E., & Gabrilovich, D. I. (2010). Mechanism of T-cell tolerance induced by myeloid-derived suppressor cells. *Journal of Immunology (Baltimore, Md. : 1950)*, *184*(6), 3106. https://doi.org/10.4049/jimmunol.0902661

Nicklin, P., Bergman, P., Zhang, B., Triantafellow, E., Wang, H., Nyfeler, B., Yang, H., Hild, M., Kung, C., Wilson, C., Myer, V. E., MacKeigan, J. P., Porter, J. A., Wang, Y. K., Cantley, L. C., Finan, P. M., & Murphy, L. O. (2009). Bidirectional Transport of Amino Acids Regulates mTOR and Autophagy. *Cell*, *136*(3), 521–534. https://doi.org/10.1016/j.cell.2008.11.044

Nishimura, D. (2001). BioCarta. *Biotech Software & Internet Report*, *2*(3), 117–120. https://doi.org/10.1089/152791601750294344

Oda, E., Ohki, R., Murasawa, H., Nemoto, J., Shibue, T., Yamashita, T., Tokino, T., Taniguchi, T., & Tanaka, † Nobuyuki. (2000). Noxa, a BH3-Only Member of the Bcl-2 Family and Candidate Mediator of p53-Induced Apoptosis. *Science*. https://doi.org/10.1126/science.288.5468.1053

Overmeire, E. V., Laoui, D., Keirsse, J., Ginderachter, J. A. V., & Sarukhan, A. (2014). Mechanisms Driving Macrophage Diversity and Specialization in Distinct Tumor Microenvironments and Parallelisms with Other Tissues. *Frontiers in Immunology*, *5*, 127. https://doi.org/10.3389/fimmu.2014.00127

Pan, D., Kobayashi, A., Jiang, P., Ferrari de Andrade, L., Tay, R. E., Luoma, A. M., Tsoucas, D., Qiu, X., Lim, K., Rao, P., Long, H. W., Yuan, G.-C., Doench, J., Brown, M., Liu, X. S., & Wucherpfennig, K. W. (2018). A major chromatin regulator determines resistance of tumor cells to T cell–mediated killing. *Science*, *359*(6377), 770–775. https://doi.org/10.1126/science.aao1710

Panner, A., James ,C. David, Berger ,Mitchel S., & and Pieper, R. O. (2005). mTOR Controls FLIPS Translation and TRAIL Sensitivity in Glioblastoma Multiforme Cells. *Molecular and Cellular Biology*, *25*(20), 8809–8823. https://doi.org/10.1128/MCB.25.20.8809-8823.2005

Patel, S. J., Sanjana, N. E., Kishton, R. J., Eidizadeh, A., Vodnala, S. K., Cam, M., Gartner, J. J., Jia, L., Steinberg, S. M., Yamamoto, T. N., Merchant, A. S., Mehta, G. U., Chichura, A., Shalem, O., Tran, E., Eil, R., Sukumar, M., Guijarro, E. P., Day, C.-P., … Restifo, N. P. (2017). Identification of essential genes for cancer immunotherapy. *Nature*, *548*(7669), 537–542. https://doi.org/10.1038/nature23477

Payne, R., Glenn, L., Hoen, H., Richards, B., Smith, J. W., Lufkin, R., Crocenzi, T. S., Urba, W. J., & Curti, B. D. (2014). Durable responses and reversible toxicity of high-dose interleukin-2 treatment of melanoma and renal cancer in a Community Hospital Biotherapy Program. *Journal for ImmunoTherapy of Cancer*, *2*(1), 13. https://doi.org/10.1186/2051-1426-2-13

Porter, D. L., Levine, B. L., Kalos, M., Bagg, A., & June, C. H. (2011). Chimeric Antigen Receptor–Modified T Cells in Chronic Lymphoid Leukemia. *New England Journal of Medicine*, *365*(8), 725–733. https://doi.org/10.1056/NEJMoa1103849

Prasad, P. D., Wang, H., Huang, W., Kekuda, R., Rajan, D. P., Leibach, F. H., & Ganapathy, V. (1999). Human LAT1, a Subunit of System L Amino Acid Transporter: Molecular Cloning and Transport Function. *Biochemical and Biophysical Research Communications*, *255*(2), 283–288. https://doi.org/10.1006/bbrc.1999.0206

Reck, M., Rodríguez-Abreu, D., Robinson, A. G., Hui, R., Csőszi, T., Fülöp, A., Gottfried, M., Peled, N., Tafreshi, A., Cuffe, S., O'Brien, M., Rao, S., Hotta, K., Leiby, M. A., Lubiniecki, G. M., Shentu, Y., Rangwala, R., & Brahmer, J. R. (2016). Pembrolizumab versus Chemotherapy for PD-L1–Positive Non–Small-Cell Lung Cancer. *New England Journal of Medicine*, *375*(19), 1823–1833. https://doi.org/10.1056/NEJMoa1606774

Reynolds, S. M., Miller, M., Lee, P., Leinonen, K., Paquette, S. M., Rodebaugh, Z., Hahn, A., Gibbs, D. L., Slagel, J., Longabaugh, W. J., Dhankani, V., Reyes, M., Pihl, T., Backus, M., Bookman, M., Deflaux, N., Bingham, J., Pot, D., & Shmulevich, I. (2017). The ISB Cancer Genomics Cloud: A Flexible Cloud-Based Platform for Cancer Genomics Research. *Cancer Research*, *77*(21), e7–e10. https://doi.org/10.1158/0008-5472.CAN-17-0617

Rooney, M. S., Shukla, S. A., Wu, C. J., Getz, G., & Hacohen, N. (2015). Molecular and Genetic Properties of Tumors Associated with Local Immune Cytolytic Activity. *Cell*, *160*(1), 48–61. https://doi.org/10.1016/j.cell.2014.12.033

Rosenberg, S. A., Yang, J. C., Sherry, R. M., Kammula, U. S., Hughes, M. S., Phan, G. Q., Citrin, D. E., Restifo, N. P., Robbins, P. F., Wunderlich, J. R., Morton, K. E., Laurencot, C. M., Steinberg, S. M., White, D. E., & Dudley, M. E. (2011a). Durable Complete Responses in Heavily Pretreated Patients with Metastatic Melanoma Using T Cell Transfer Immunotherapy. *Clinical Cancer Research : An Official Journal of the American Association for Cancer Research*, *17*(13), 4550–4557. https://doi.org/10.1158/1078-0432.CCR-11-0116

Rosenberg, S. A., Yang, J. C., Sherry, R. M., Kammula, U. S., Hughes, M. S., Phan, G. Q., Citrin, D. E., Restifo, N. P., Robbins, P. F., Wunderlich, J. R., Morton, K. E., Laurencot, C. M., Steinberg, S. M., White, D. E., & Dudley, M. E. (2011b). Durable complete responses in heavily pretreated patients with metastatic melanoma using T-cell transfer immunotherapy. *Clinical Cancer Research: An Official Journal of the American Association for Cancer Research*, *17*(13), 4550–4557. https://doi.org/10.1158/1078-0432.CCR-11-0116

Rudin, C. M., Poirier, J. T., Senzer, N. N., Stephenson, J., Loesch, D., Burroughs, K. D., Reddy, P. S., Hann, C. L., & Hallenbeck, P. L. (2011). Phase I Clinical Study of Seneca Valley Virus (SVV-001), a Replication-Competent Picornavirus, in Advanced Solid Tumors with Neuroendocrine Features. *Clinical Cancer Research : An Official Journal of the American Association for Cancer Research*, *17*(4), 888–895. https://doi.org/10.1158/1078-0432.CCR-10-1706

Santarpia, M., & Karachaliou, N. (2015). Tumor immune microenvironment characterization and response to anti-PD-1 therapy. *Cancer Biology & Medicine*, *12*(2), 74–78. https://doi.org/10.7497/j.issn.2095-3941.2015.0022

Sarkar, T., Dhar, S., & Sa, G. (2021). Tumor-infiltrating T-regulatory cells adapt to altered metabolism to promote tumor-immune escape. *Current Research in Immunology*, *2*, 132–141. https://doi.org/10.1016/j.crimmu.2021.08.002

Scheidmann, M. C., Castro-Giner, F., Strittmatter, K., Krol, I., Paasinen-Sohns, A., Scherrer, R., Donato, C., Gkountela, S., Szczerba, B. M., Diamantopoulou, Z., Muenst, S., Vlajnic, T., Kunz, L., Vetter, M., Rochlitz, C., Taylor, V., Giachino, C., Schroeder, T., Platt, R. J., & Aceto, N. (2022). An In Vivo CRISPR Screen Identifies Stepwise Genetic Dependencies of Metastatic Progression. *Cancer Research*, *82*(4), 681–694. https://doi.org/10.1158/0008-5472.CAN-21-3908

Schubert, K. M., & Duronio, V. (2001). Distinct roles for extracellular-signal-regulated protein kinase (ERK) mitogen-activated protein kinases and phosphatidylinositol 3-kinase in the regulation of Mcl-1 synthesis. *Biochemical Journal*, *356*(Pt 2), 473–480. https://doi.org/10.1042/0264-6021:3560473

Segawa, H., Fukasawa, Y., Miyamoto, K., Takeda, E., Endou, H., & Kanai, Y. (1999). Identification and Functional Characterization of a Na+-independent Neutral Amino Acid Transporter with Broad Substrate Selectivity *. *Journal of Biological Chemistry*, *274*(28), 19745–19751. https://doi.org/10.1074/jbc.274.28.19745

Sena, L. A., Li, S., Jairaman, A., Prakriya, M., Ezponda, T., Hildeman, D. A., Wang, C.-R., Schumacker, P. T., Licht, J. D., Perlman, H., Bryce, P. J., & Chandel, N. S. (2013). Mitochondria Are Required for Antigen-Specific T Cell Activation through Reactive Oxygen Species Signaling. *Immunity*, *38*(2), 225–236. https://doi.org/10.1016/j.immuni.2012.10.020

Serrone, L., Zeuli, M., Sega, F. M., & Cognetti, F. (2000). Dacarbazine-based chemotherapy for metastatic melanoma: Thirty-year experience overview. *Journal of Experimental & Clinical Cancer Research*, *19*(1), 21–34.

Sha, H., Wang, D., Yan, D., Hu, Y., Yang, S., Liu, S., & Feng, J. (2017). Chimaeric antigen receptor T-cell therapy for tumour immunotherapy. *Bioscience Reports*, *37*(1), BSR20160332. https://doi.org/10.1042/BSR20160332

Sherman, B. T., Hao, M., Qiu, J., Jiao, X., Baseler, M. W., Lane, H. C., Imamichi, T., & Chang, W. (2022). DAVID: A web server for functional enrichment analysis and functional annotation of gene lists (2021 update). *Nucleic Acids Research*, *50*(W1), W216–W221. https://doi.org/10.1093/nar/gkac194

Shin, S., Lee, Y., Kim, W., Ko, H., Choi, H., & Kim, K. (2005). Caspase-2 primes cancer cells for TRAIL-mediated apoptosis by processing procaspase-8. *The EMBO Journal*, *24*(20), 3532–3542. https://doi.org/10.1038/sj.emboj.7600827

Shu, H.-B., Halpin, D. R., & Goeddel, D. V. (1997). Casper Is a FADD- and Caspase-Related Inducer of Apoptosis. *Immunity*, *6*(6), 751–763. https://doi.org/10.1016/S1074-7613(00)80450-1

Shustov, A., Nguyen, P., Finkelman, F., Elkon, K. B., & Via, C. S. (1998). Differential Expression of Fas and Fas Ligand in Acute and Chronic Graft-Versus-Host Disease: Up-Regulation of Fas and Fas Ligand Requires CD8+ T Cell Activation and IFN-γ Production. *The Journal of Immunology*, *161*(6), 2848–2855. https://doi.org/10.4049/jimmunol.161.6.2848

Silva-Santos, B., Mensurado, S., & Coffelt, S. B. (2019). γδ T cells: Pleiotropic immune effectors with therapeutic potential in cancer. *Nature Reviews Cancer*, *19*(7), 392–404. https://doi.org/10.1038/s41568-019-0153-5

Snyder, A., Makarov, V., Merghoub, T., Yuan, J., Zaretsky, J. M., Desrichard, A., Walsh, L. A., Postow, M. A., Wong, P., Ho, T. S., Hollmann, T. J., Bruggeman, C., Kannan, K., Li, Y., Elipenahli, C., Liu, C., Harbison, C. T., Wang, L., Ribas, A., … Chan, T. A. (2014). Genetic Basis for Clinical Response to CTLA-4 Blockade in Melanoma. *New England Journal of Medicine*, *371*(23), 2189–2199. https://doi.org/10.1056/NEJMoa1406498

Sorokin, M., Kholodenko, I., Kalinovsky, D., Shamanskaya, T., Doronin, I., Konovalov, D., Mironov, A., Kuzmin, D., Nikitin, D., Deyev, S., Buzdin, A., & Kholodenko, R. (2020). RNA Sequencing-Based Identification of Ganglioside GD2-Positive Cancer Phenotype. *Biomedicines*, *8*(6), 142. https://doi.org/10.3390/biomedicines8060142

Straathof, K., Flutter, B., Wallace, R., Jain, N., Loka, T., Depani, S., Wright, G., Thomas, S., Cheung, G. W.-K., Gileadi, T., Stafford, S., Kokalaki, E., Barton, J., Marriott, C., Rampling, D., Ogunbiyi, O., Akarca, A. U., Marafioti, T., Inglott, S., … Anderson, J. (2020). Antitumor activity without on-target off-tumor toxicity of GD2–chimeric antigen receptor T cells in patients with neuroblastoma. *Science Translational Medicine*, *12*(571), eabd6169. https://doi.org/10.1126/scitranslmed.abd6169

Strioga, M., Pasukoniene, V., & Characiejus, D. (2011). CD8+ CD28− and CD8+ CD57+ T cells and their role in health and disease. *Immunology*, *134*(1), 17–32. https://doi.org/10.1111/j.1365-2567.2011.03470.x

Svedman, F. C., Pillas, D., Taylor, A., Kaur, M., Linder, R., & Hansson, J. (2016). Stage-specific survival and recurrence in patients with cutaneous malignant melanoma in Europe – a systematic review of the literature. *Clinical Epidemiology*, *8*, 109–122. https://doi.org/10.2147/CLEP.S99021

Tinhofer, I., Marschitz, I., Kos, M., Henn, T., Egle, A., Villunger, A., & Greil, R. (1998). Differential Sensitivity of CD4+ and CD8+T Lymphocytes to the Killing Efficacy of Fas (Apo-1/CD95) Ligand+ Tumor Cells in B Chronic Lymphocytic Leukemia. *Blood*, *91*(11), 4273–4281. https://doi.org/10.1182/blood.V91.11.4273

Tran, S. E. F., Holmström, T. H., Ahonen, M., Kähäri, V.-M., & Eriksson, J. E. (2001). MAPK/ERK Overrides the Apoptotic Signaling from Fas, TNF, and TRAIL Receptors *. *Journal of Biological Chemistry*, *276*(19), 16484–16490. https://doi.org/10.1074/jbc.M010384200

Uhlén, M., Fagerberg, L., Hallström, B. M., Lindskog, C., Oksvold, P., Mardinoglu, A., Sivertsson, Å., Kampf, C., Sjöstedt, E., Asplund, A., Olsson, I., Edlund, K., Lundberg, E., Navani, S., Szigyarto, C. A.-K., Odeberg, J., Djureinovic, D., Takanen, J. O., Hober, S., … Pontén, F. (2015). Tissue-based map of the human proteome. *Science*, *347*(6220), 1260419. https://doi.org/10.1126/science.1260419

Van Allen, E. M., Miao, D., Schilling, B., Shukla, S. A., Blank, C., Zimmer, L., Sucker, A., Hillen, U., Geukes Foppen, M. H., Goldinger, S. M., Utikal, J., Hassel, J. C., Weide, B., Kaehler, K. C., Loquai, C., Mohr, P., Gutzmer, R., Dummer, R., Gabriel, S., … Garraway, L. A. (2015). Genomic correlates of response to CTLA-4 blockade in metastatic melanoma. *Science*, *350*(6257), 207–211. https://doi.org/10.1126/science.aad0095

Villunger, A., O'Reilly, L. A., Holler, N., Adams, J., & Strasser, A. (2000). FAS Ligand, Bcl-2, Granulocyte Colony-Stimulating Factor, and p38 Mitogen-Activated Protein Kinase: Regulators of Distinct Cell Death and Survival Pathways in Granulocytes. *Journal of Experimental Medicine*, *192*(5), 647–658. https://doi.org/10.1084/jem.192.5.647

Vivier, E., Raulet, D. H., Moretta, A., Caligiuri, M. A., Zitvogel, L., Lanier, L. L., Yokoyama, W. M., & Ugolini, S. (2011). Innate or Adaptive Immunity? The Example of Natural Killer Cells. *Science*, *331*(6013), 44–49. https://doi.org/10.1126/science.1198687

Voest, E. E., Kenyon, B. M., O'Reilly, M. S., Truitt, G., D'Amato, R. J., & Folkman, J. (1995). Inhibition of Angiogenesis In Vivo by Interleukin 12. *JNCI: Journal of the National Cancer Institute*, *87*(8), 581–586. https://doi.org/10.1093/jnci/87.8.581

Vredevoogd, D. W., Kuilman, T., Ligtenberg, M. A., Boshuizen, J., Stecker, K. E., Bruijn, B. de, Krijgsman, O., Huang, X., Kenski, J. C. N., Lacroix, R., Mezzadra, R., Gomez-Eerland, R., Yildiz, M., Dagidir, I., Apriamashvili, G., Zandhuis, N., Noort, V. van der, Visser, N. L., Blank, C. U., … Peeper, D. S. (2019). Augmenting Immunotherapy Impact by Lowering Tumor TNF Cytotoxicity Threshold. *Cell*, *178*(3), 585-599.e15. https://doi.org/10.1016/j.cell.2019.06.014

Waldman, A. D., Fritz, J. M., & Lenardo, M. J. (2020). A guide to cancer immunotherapy: From T cell basic science to clinical practice. *Nature Reviews Immunology*, *20*(11), 651–668. https://doi.org/10.1038/s41577-020-0306-5

Wang, C.-Y., Mayo, M. W., Korneluk, R. G., Goeddel, D. V., & Baldwin, A. S. (1998). NF-κB Antiapoptosis: Induction of TRAF1 and TRAF2 and c-IAP1 and c-IAP2 to Suppress Caspase-8 Activation. *Science*, *281*(5383), 1680–1683. https://doi.org/10.1126/science.281.5383.1680

Wang, M., Munoz, J., Goy, A., Locke, F. L., Jacobson, C. A., Hill, B. T., Timmerman, J. M., Holmes, H., Jaglowski, S., Flinn, I. W., McSweeney, P. A., Miklos, D. B., Pagel, J. M., Kersten, M.-J., Milpied, N., Fung, H., Topp, M. S., Houot, R., Beitinjaneh, A., … Reagan, P. M. (2020). KTE-X19 CAR T-Cell Therapy in Relapsed or Refractory Mantle-Cell Lymphoma. *New England Journal of Medicine*, *382*(14), 1331–1342. https://doi.org/10.1056/NEJMoa1914347

Wang, S., & El-Deiry, W. S. (2003). TRAIL and apoptosis induction by TNF-family death receptors. *Oncogene*, *22*(53), 8628–8633. https://doi.org/10.1038/sj.onc.1207232

Wang, X., Tokheim, C., Gu, S. S., Wang, B., Tang, Q., Li, Y., Traugh, N., Zeng, Z., Zhang, Y., Li, Z., Zhang, B., Fu, J., Xiao, T., Li, W., Meyer, C. A., Chu, J., Jiang, P., Cejas, P., Lim, K., … Liu, X. S. (2021). In vivo CRISPR screens identify the E3 ligase Cop1 as a modulator of macrophage infiltration and cancer immunotherapy target. *Cell*, *184*(21), 5357-5374.e22. https://doi.org/10.1016/j.cell.2021.09.006

Whitmire, J. K., Tan, J. T., & Whitton, J. L. (2005). Interferon-γ acts directly on CD8+ T cells to increase their abundance during virus infection. *Journal of Experimental Medicine*, *201*(7), 1053–1059. https://doi.org/10.1084/jem.20041463

Yan, R., Li, Y., Müller, J., Zhang, Y., Singer, S., Xia, L., Zhong, X., Gertsch, J., Altmann, K.-H., & Zhou, Q. (2021). Mechanism of substrate transport and inhibition of the human LAT1-4F2hc amino acid transporter. *Cell Discovery*, *7*(1), 1–8. https://doi.org/10.1038/s41421-021-00247-4

Ying, Z., Huang, X. F., Xiang, X., Liu, Y., Kang, X., Song, Y., Guo, X., Liu, H., Ding, N., Zhang, T., Duan, P., Lin, Y., Zheng, W., Wang, X., Lin, N., Tu, M., Xie, Y., Zhang, C., Liu, W., … Chen, S.-Y. (2019). A safe and potent anti-CD19 CAR T cell therapy. *Nature Medicine*, *25*(6), 947–953. https://doi.org/10.1038/s41591-019-0421-7

Zeng, G., Touloukian, C. E., Wang, X., Restifo, N. P., Rosenberg, S. A., & Wang, R.-F. (2000). Identification of CD4+ T Cell Epitopes from NY-ESO-1 Presented by HLA-DR Molecules. *Journal of Immunology (Baltimore, Md. : 1950)*, *165*(2), 1153–1159. https://doi.org/10.4049/jimmunol.165.2.1153

Zhang, S. Q., Kovalenko, A., Cantarella, G., & Wallach, D. (2000). Recruitment of the IKK Signalosome to the p55 TNF Receptor: RIP and A20 Bind to NEMO (IKKγ) upon Receptor Stimulation. *Immunity*, *12*(3), 301–311. https://doi.org/10.1016/S1074-7613(00)80183-1

Zhang, Z., Liu, X., Chen, D., & Yu, J. (2022). Radiotherapy combined with immunotherapy: The dawn of cancer treatment. *Signal Transduction and Targeted Therapy*, *7*(1), 1–34. https://doi.org/10.1038/s41392-022-01102-y

Zhou, P., Shaffer, D. R., Arias, D. A. A., Nakazaki, Y., Pos, W., Torres, A. J., Cremasco, V., Dougan, S. K., Cowley, G. S., Elpek, K., Brogdon, J., Lamb, J., Turley, S., Ploegh, H. L., Root, D. E., Love, J. C., Dranoff, G., Hacohen, N., Cantor, H., & Wucherpfennig, K. W. (2014). In vivo Discovery of Immunotherapy Targets in the Tumor Microenvironment. *Nature*, *506*(7486), 52–57. https://doi.org/10.1038/nature12988

Zong, W.-X., Edelstein, L. C., Chen, C., Bash, J., & Gélinas, C. (1999). The prosurvival Bcl-2 homolog Bfl-1/A1 is a direct transcriptional target of NF-κB that blocks TNFα-induced apoptosis. *Genes & Development*, *13*(4), 382–387.